Sources and pathways of radiogenic elements in surface media above the Millennium and McArthur River uranium deposits in the Athabasca Basin, Saskatchewan, Canada

By: Mary Cecilia Devine

A thesis submitted to the Faculty of Graduate and Postdoctoral Studies in partial fulfillment of the requirements for a Master of Science degree in Earth Sciences.

Department of Earth Sciences
Faculty of Science
University of Ottawa

Abstract

This thesis examines the abundance of radionuclides within soil, groundwater, and fractures in shallow sandstones above two deeply buried U deposits in an effort to investigate the mechanisms that concentrate He, Rn, Ra and U within surficial material. Two high-grade, unconformity-associated, monometallic U deposits in the eastern margin of the Athabasca Basin, Saskatchewan, Canada were used as case studies; the Millennium deposit (750 m deep) and the McArthur River deposit (approx. 500 m deep). Extensive glacial sediments up to 100 m thick cover both deposits.

Groundwater was sampled from diamond drill-holes and monitoring wells, and surface water was sampled from lakes, and analyzed for the abundance of ^{3}H, minor elements (Cl, Br, F, N, S, U, Th, Pb), stable isotope composition ($^{13}C/^{12}C$, $^{2}H/H$, $^{18}O/^{16}O$, $^{3}He/^{4}He$), dissolved organic and inorganic carbon content, pH, conductivity and oxidation-reduction potential. B and C-horizon soil samples were collected and leached by ammonium acetate at pH 5 to identify elements adsorbed or co-precipitated on secondary minerals such as carbonates, Fe-Mn-oxy-hydroxides, and clays. Soils were also leached with $HF\text{-}HNO_3\text{-}HClO_4$ and measured by ICP-MS for major, trace and rare-earth elements. Rn in soil was measured from 30 cm - 80 cm deep within undisturbed soils at both sites. Coatings on drill-core fracture surfaces were leached sequentially with different strengths of nitric acid to determine the concentrations of P, Mn, Fe, Ni, Cu, As, Zr, Ba, Pb, Th, U and Ca. The Ra content of fracture coatings and soil from McArthur River was determined by γ-ray spectrometry, and the mineralogy was determined by powder X-ray diffraction (XRD) and sequential leach geochemistry.

All groundwater (down to 50 m depth) at Millennium and McArthur River is <20-year old meteoric water, based on ^{3}H results. Groundwater has undergone minor evaporation, which is

evident from the greater abundance of ^{2}H and ^{18}O than the local meteoric water line, and is representative of Saskatchewan precipitation. The negative $\delta^{13}C$ signature of DIC in groundwater suggests that potential sources of inorganic carbon are dissolved non-marine carbonates, the oxidation of DOC, and soil-derived CO_2. The organic carbon signature is similar to that of terrestrial C3 plants ($\delta^{13}C$ DOC = -24 to -27 ‰). Radiogenic ^{4}He in groundwater is reported to be up to 100 times the expected value in equilibrium with the atmospheric at the Millennium deposit (Power, 2014), but is atmospheric near the McArthur River deposit. Rn radioactivity in groundwater has a similar range at both deposits; from 44 – 5342 cpm (approx. 2- 232 Bq/L) at McArthur River, and from 0.8 – 278 Bq/L at Millennium. These values are within the range of Rn radioactivity throughout the Athabasca Basin reported by Earle and Drever (1983).

Drill-core fracture coatings contain Ra (≤ 32.2 pg/g) and the dominant mineral phases determined by XRD are illite, kaolin and quartz. Fe-Mn oxy-hydroxides are evident from sequential leach geochemistry. Ra is less abundant in B-horizon soils (≤ 0.220 pg/g) than fracture coatings and Ra in B-horizon soils is highest near the surface projection of the McArthur River deposit, where Rn in soil gas is also highest (6.3 kBq/m^3) near drill-hole MC-251.

The abundance of Ra adsorbed to secondary minerals on core fracture coatings is likely impacted by groundwater flow and the Fe and Mn concentration of fracture surfaces. Secondly, Rn in groundwater above Millennium and McArthur River U deposits is a decay product primarily from local Ra on fracture surfaces, and less so from Ra in B-horizon soils. Additionally, Rn in soil gas correlates with Ra in soils; however, Rn does not correlate with U in groundwater, soil or coatings along fractures. Furthermore, Rn in soil gas is at background levels of <10 kBq/m^3 above both deposits, and therefore not an indication of U mineralization in these glaciated terrains.

This study's findings suggest that the concentration of Rn in groundwater is controlled by radon's 3.82-day half-life, the mobility of U^{6+} in oxidized conditions, and radium's affinity for Mn-oxy-hydroxides. Rn within young groundwater above the two deeply buried U deposits is a decay product from local Ra on fracture surfaces. Rn gas in oxidized, shallow groundwater does not correlate with the concentration of U in nearby soil, groundwater, or core fracture coatings.

Acknowledgements

I would like to thank Dr. Keiko Hattori for giving me the opportunity to complete my Master's project in surficial geochemistry. Your unlimited energy and persistent encouragement are much appreciated. Thank you for providing the opportunity to complete fieldwork and present my research at several national conferences. I would also like to thank Dr. Jack Cornett for opening my eyes to the world of radiochemistry. Your kind demeanour and dedication to your work are inspirational.

Further thanks are extended to the Canadian Mining Innovation Council Footprints Project for funding of this project and the in-kind support from all members. Specific thanks are extended to Dr. Tom Kotzer (Cameco Corporation) for assisting with fieldwork and for your considerations on all results presented throughout the project. Further thanks to Kaitlyn Browne (Cameco Corporation), for helping with fieldwork in 2014. Gratitude is also extended to Shannon Guffey and Nicholas Joyce for their collaboration throughout the footprints project and to everyone else in the CMIC-U group. I have so much appreciation for the members of the Hattori research group, including Erin Adlakha, Shishi (Chris) Chen, Lilianne Page, Michael Power, Ian O'Connel and Nick Dudek. Thank you for your assistance with fieldwork, GIS, chemistry and general camaraderie.

Additional thanks to all of my friends in Ottawa for making it feel like a second home. To David and Ginley, you boys are like my brothers and I cherish the true friendship we have formed over countless beers and various excursions. Thanks as well to the Duff and Warren families for the copious Sunday dinners, pool parties and much needed distractions. Last but not least I would like to thank my St. John's family and friends for their limitless support and encouragement.

List of Contents

List of Figures

Figure 1: Map of Canada with inset location of the Athabasca Basin 5

Figure 2: Satellite imagery from ArcGIS World Imagery of the Athabasca Basin region, with larger scale maps of the Millennium and McArthur River 6

Figure 3: Geological setting and major unconformity-associated uranium mines and deposits within the Athabasca Basin, Saskatchewan, Canada. 8

Figure 4: Lithostratigraphic cross section of the Athabasca Basin 8

Figure 5: Regional ice-flow direction and their relative ages in the Athabasca Basin 11

Figure 6: Surface projection of the (750 m deep) Millennium deposit and drill-hole locations. . 31

Figure 7: Plan view map of DDH sampled for various surficial geochemical media relative to the McArthur River deposit 32

Figure 8: In-situ dissolved gas (He) sampler 35

Figure 9: Photograph of ionization chambers and the electrometer used to measure Rn in soil gas. 36

Figure 10: Photograph of Rn in soil gas sampling equipment (250 cc plastic syringe, rubber tubing and 1.1 m x 1 cm metal pipe. 37

Figure 11: Comparison of two methods of Rn analysis; Rn in water direct method (Bq/L) and Rn in oil extraction method (counts per minute). 40

Figure 12: Bar graph of tritium contents (in tritium units) of DDH groundwater at Millennium collected in 2014 42

Figure 13: Tritium content expressed in tritium units 43

Figure 14: Schematic geological cross section of the Millennium deposit, depicting the vertical distance from soil and groundwater sampling locations to mineralization and faults 49

Figure 15: Scatterplot showing the lack of correlation between pH and depth of sampling. 50

Figure 16: Scatterplot comparing conductivity to water depth (m from surface) in 12 drill-holes sampled in 2013. 51

Figure 17: Bar graph comparing Cl content in groundwater taken from the same depth (m below surface) in 2014 and 2013 55

Figure 18: Bar graph comparing fluorine content in groundwater taken from the same depth (m below surface) in 2014 and 2013.. 56

Figure 19: O and H isotope compositions of 14 shallow groundwater samples from 12 DDH at Millennium, compared to Saskatoon precipitation and the global meteoric water line..... 58

Figure 20: Ratio of dissolved inorganic carbon (DIC) to dissolved organic carbon (DOC) of groundwater taken at varying depths and locations at Millennium. 60

Figure 21: Plan view map of 2013 groundwater sampling locations and Rn radioactivity (counts per minute) 62

Figure 22: Bar graph comparing Rn activity (Bq/L) from 4 locations in 2014 and 2013 63

Figure 23: Scatterplot showing Rn activity (counts per minute) with water depth (m) at three Millennium drill holes..... 64

Figure 24: Plan view map of Rn activity in soil (kBq/m^3) at Millennium..... 66

Figure 26: Bar graph illustrating the mean Rn activity (cpm) in water taken from various geological materials including till, sandstone and the boundary between the two. 69

Figure 27: Plan view map of the Millennium site indicating locations of drill-holes, soil samples and the surface projection of the U deposit 71

Figure 28: Percent dissolution of Ca, Fe, and Mg of B-horizon soils in AA5 from Millennium, collected in 2014. 72

Figure 29: Percent of dissolution of Ca, Fe, and Mg in B-Horizon soils from Millennium collected in 2013. 73

Figure 30: Line graph of percent of dissolution of trace elements of three soil samples at Millennium collected in 2014. Ammonium acetate leach (pH = 5) chemistry, normalized with multi acid digestion concentrations, and converted to percent. 74

Figure 31: Line graph of trace elements of B-horizon soil samples from Millennium. Ammonium acetate leach (pH = 5) chemistry is normalized with multi acid leach chemistry, and converted to percent. 75

Figure 32: Line graph of trace element chemistry of C-horizon soil samples from Millennium collected in 2013. Fractions of elements dissolved in ammonium acetate leach (pH = 5) relative to multi acid leach in percent. 76

Figure 33: Line graph of the abundance of rare earth elements and Y of B-horizon soil samples from Millennium collected in 2013. Fractions of elements dissolved in ammonium acetate leach (pH = 5) relative to multi acid leach in percent. 77

Figure 34: Line graph of rare earth elements abundances in C-horizon soil samples from Millennium collected in 2013. Fractions of elements dissolved in ammonium acetate leach (pH = 5) relative to multi acid leach in percent. 78

Figure 35: Line graph of rare earth elements in B and C-horizon soil samples from Millennium collected in 2014. Fractions of elements dissolved in ammonium acetate leach (pH = 5) relative to multi acid leach in percent. 79

Figure 36: Line graph of concentrations of major elements in multi-acid digestion in three Millennium soils, collected in 2014. 80

Figure 37: Line graph of concentrations of trace elements in multi-acid digestion in three Millennium soils, collected in 2014. 80

Figure 38: Line graph of REE from multi-acid digestion of B and C-horizon soils. Concentrations are normalized to North American Shale Composite 82

Figure 39: Scatterplot showing trends of pH vs. EC (µS/cm) 84

Figure 40: Depth profiles of Rn, conductivity, Cl and pH in the drill-hole with the highest Rn activity (CX-40) 86

Figure 41: Radon (counts per minute) compared to dissolved organic carbon (mg/L C) and dissolved inorganic carbon (mg/L carbon) in groundwater throughout the Millennium site 87

Figure 42: Rn activity (counts per minute) and water chemistry parameters 89

Figure 43: Scatterplot showing ^{4}He and Rn in groundwater 90

Figure 44: XY plot of Rn in soil gas at Millennium versus depth of sampling 91

Figure 45: Schematic cross Section of general geology, P2 fault and mineralization at McArthur River, with DDH trace to >500 m depth. 98

Figure 46: Plan view map of drill-hole locations relative to the surficial projection of the McArthur River deposit 99

Figure 47: Scatter plot of $\delta^{18}O$ and $\delta^{2}H$ values from 14 shallow groundwater samples from McArthur River, Saskatoon precipitation and the Global Meteoric Water Line. 102

Figure 48: Ratio of dissolved inorganic carbon (DIC) and dissolved organic carbon (DOC) by sample site. 104

Figure 49: Tritum contents (in tritium units) of DDH groundwater at McArthur River and a nearby fresh water source (Slush Lake) in 2014. 105

Figure 50: Plan view map of DDH sampled for Rn in groundwater at McArthur River 106

Figure 51: Plan view map of Rn activity in soil at McArthur River. Activity increases from grey to red 110

Figure 52: Plan view map indicating the surficial expression of the McArthur River uranium deposit 111

Figure 53: Line graph of major element chemistry of B-horizon soil samples from McArthur River collected in 2014. Ammonium acetate leach (pH = 5) chemistry, normalized with multi acid leach chemistry, and converted to percent. 112

Figure 54: Plan view map of uranium concentrations leached from B-horizon soils near McArthur River. Values are divided into quartiles, and given in parts per billion (ppb). 114

Figure 55: Line graph of trace element chemistry of B-horizon soil samples from McArthur River collected in 2014. Ammonium acetate leach (pH = 5) chemistry, normalized with multi acid leach chemistry, and converted to percent. 115

Figure 56: Line graph of rare earth element chemistry of B-horizon soil samples from McArthur River collected in 2014. Ammonium acetate leach (pH = 5) chemistry, normalized with multi acid leach chemistry, and converted to percent. 116

Figure 57: Major elements dissolved by multi-acid digestion of McArthur River soil samples; concentrations are in percent. 118

Figure 58: Scatterplot of trace elements dissolved by multi-acid digestion of McArthur River soil samples; concentrations are in parts per million. 119

Figure 59: Line graph of REE from multi-acid digestion of B-horizon soils. Concentrations are normalized to North American Shale Composite 120

Figure 60: Plan view map illustrating the location of the McArthur River U deposit in red, and the location of drill-holes sampled for core fracture samples 122

Figure 61: Concentrations (ppm) of water-leached elements from three fractures taken at 13.4 m (black), 86.2 m (light grey) and 86.5 m (dark grey) within drill-hole MC-208 123

Figure 62: Concentrations (ppm) of water-leached elements from three fractures taken at 21.7 m (black) within drill-hole MC-252, and at 75 m (light grey) and 78 m (dark grey) within drill-hole MC-253. 124

Figure 63: Concentrations (ppm) of water-leached elements from four fractures taken at 101.7 m (black), 24.1 m (light grey) and 37.0 m (medium grey), and 47.2 m (dark grey) within drill-hole MC-255. 124

Figure 64: Concentrations (ppm) of water-leached elements from two fractures taken at 19.15 m (black), 64.6 m (light grey) within drill-hole MC-338. 125

Figure 65: Concentrations (ppm) of water-leached elements from three fractures taken at 73.6 m (black) from drill-hole MC-413, and two fractures at 80.4 m (light grey) and 82.9 m (dark grey) within drill-hole MC-415. 125

Figure 66: Concentrations (ppm) of water-leached elements from two fractures taken at 24.2 m (black) and 9.0 m (light grey) within drill-hole MC-434..... 126

Figure 67: Concentrations (ppm) of elements leached in 0.05 N HNO3 from three fractures taken at 13.4 m (black), 86.2 m (light grey) and 86.5 m (dark grey) within drill-hole MC-208..... 126

Figure 68: Concentrations (ppm) of elements leached in 0.05 N HNO_3 from two fractures taken at 53 m (black) and at 71.8 m (light grey) within drill-hole MC-246..... 126

Figure 69: Concentrations (ppm) of elements leached in 0.05 N HNO_3 from three fractures taken at 21.7 m (black) within drill-hole MC-252, and at 75 m (light grey) and 78 m (dark grey) within drill-hole MC-253. 127

Figure 70: Concentrations (ppm) of elements leached in 0.05 N HNO_3 from four fractures taken at 101.7 m (black), 24.1 m (light grey) and 37.0 m (medium grey), and 47.2 m (dark grey) within drill-hole MC-255. 127

Figure 71: Concentrations (ppm) of elements leached in 0.05 N HNO_3 from two fractures taken at 19.15 m (black), 64.6 m (light grey) within drill-hole MC-338. 128

Figure 72: Concentrations (ppm) of elements leached in 0.05 N HNO_3 from three fractures taken at 73.6 m (black) from drill-hole MC-413, and two fractures at 80.4 m (light grey) and 82.9 m (dark grey) within drill-hole MC-415. 128

Figure 73: Concentrations (ppm) of elements leached in 0.05 N HNO_3 from two fractures taken at 24.2 m (black) and 9.0 m (light grey) within drill-hole MC-434..... 128

Figure 74: Concentrations (ppm) of elements leached in 0.1 N HNO_3 from three fractures taken at 13.4 m (black), 86.2 m (light grey) and 86.5 m (dark grey) within drill-hole MC-208..... 129

Figure 75: Concentrations (ppm) of elements leached in 0.1 N HNO_3 from two fractures taken at 53 m (black) and at 71.8 m (light grey) within drill-hole MC-246..... 129

Figure 76: Concentrations (ppm) of elements leached in 0.1 N HNO_3 from three fractures taken at 21.7 m (black) within drill-hole MC-252, and at 75 m (light grey) and 78 m (dark grey) within drill-hole MC-253 130

Figure 77: Concentrations (ppm) of elements leached in 0.1 N HNO_3 from four fractures taken at 101.7 m (black), 24.1 m (light grey) and 37.0 m (medium grey), and 47.2 m (dark grey) within drill-hole MC-255 130

Figure 78: Concentrations (ppm) of elements leached in 0.1 N HNO_3 from two fractures taken at 19.15 m (black) and 64.6 m (light grey) within drill-hole MC-338 130

Figure 79: Concentrations (ppm) of elements leached in 0.1 N HNO_3 from three fractures taken at 73.6 m (black) from drill-hole MC-413, and two fractures at 80.4 m (light grey) and 82.9 m (dark grey) within drill-hole MC-415 131

Figure 80: Concentrations (ppm) of elements leached in 0.1 N HNO_3 from two fractures taken at 24.2 m (black) and 9.0 m (light grey) within drill-hole MC-434 131

Figure 81: Concentrations (ppm) of elements leached in 0.5 N HNO_3 from two fractures taken at 13.4 m (black), 86.2 m (light grey) and 86.5 m (dark grey) within drill-hole MC-208 131

Figure 82: Concentrations (ppm) of elements leached in 0.5 N HNO_3 from two fractures taken at 53 m (black) and at 71.8 m (light grey) within drill-hole MC-246..... 132

Figure 83: Concentrations (ppm) of elements leached in 0.5 N HNO_3 from three fractures taken at 21.7 m (black) within drill-hole MC-252, and at 75 m (light grey) and 78 m (dark grey) within drill-hole MC-253 132

Figure 84: Concentrations (ppm) of elements leached in 0.5 N HNO_3 from four fractures taken at 101.7 m (black), 24.1 m (light grey) and 37.0 m (medium grey), and 47.2 m (dark grey) within drill-hole MC-255 132

Figure 85: Concentrations (ppm) of elements leached in 0.5 N HNO_3 from two fractures taken at 19.15 m (black), 64.6 m (light grey) within drill-hole MC-338. 133

Figure 86: Concentrations (ppm) of elements leached in 0.5 N HNO_3 from three fracture taken at 73.6 m (black) from drill-hole MC-413, and two fractures at 80.4 m (light grey) and 82.9 m (dark grey) within drill-hole MC-415 133

Figure 87: Concentrations (ppm) of elements leached in 0.5 N HNO_3 from two fractures taken at 24.2 m (black) and 9.0 m (light grey) within drill-hole MC-434 133

Figure 88: Concentrations (ppm) of elements leached in 2 N HNO_3 from three fractures taken at 13.4 m (black), 86.2 m (light grey) and 86.5 m (dark grey) within drill-hole MC-208 134

Figure 89: Concentrations (ppm) of elements leached in 2 N HNO_3 from two fractures taken at 53 m (black) and at 71.8 m (light grey) within drill-hole MC-246..... 134

Figure 90: Concentrations (ppm) of elements leached in 2 N HNO_3 from three fractures taken at 21.7 m (black) within drill-hole MC-252, and at 75 m (light grey) and 78 m (dark grey) within drill-hole MC-253 135

Figure 91: Concentrations (ppm) of elements leached in 2 N HNO_3 from four fractures taken at 101.7 m (black), 24.1 m (light grey) and 37.0 m (medium grey), and 47.2 m (dark grey) within drill-hole MC-255 135

Figure 92: Concentrations (ppm) of elements leached in 2 N HNO_3 from two fractures taken at 19.15 m (black), 64.6 m (light grey) within drill-hole MC-338 135

Figure 93: Concentrations (ppm) of elements leached in 2 N HNO_3 from three fractures taken at 73.6 m (black) from drill-hole MC-413, and two fractures at 80.4 m (light grey) and 82.9 m (dark grey) within drill-hole MC-415 136

Figure 94: Concentrations (ppm) of elements leached in 2 N HNO_3 from two fractures taken at 24.2 m (black) and 9.0 m (light grey) within drill-hole MC-434 136

Figure 95: Box and whisker plots of P, Mn, Fe, Ca, Ni and Cu sequential leach results..... 138

Figure 96: Box and whisker plots of As, Zr, Pb, U, Th and Ba sequential leach results..... 139

Figure 97: X-ray diffraction spectra of core fracture material at 85 m depth from drill-hole MC-415 at McArthur River..... 141

Figure 98: X-ray diffraction spectra of core fracture material at 82.9 m depth in drill-hole MC-415 at McArthur River..... 142

Figure 99: X-ray diffraction spectra of core fracture material at 24 m depth in drill-hole MC-434 at McArthur River..... 143

Figure 100: Map of the McArthur River site with Ra (fg/g) and radon in soil (kBq/m^3) content. 145

Figure 101: Tritium values from 1953 to 2014 from Ottawa, ON, Fort Smith, AB, Churchill, MB, McArthur River and Millennium (IAEA GNIP). 147

Figure 102: Rn activity (counts per minute) and dissolved ions in groundwater at McArthur River..... 148

Figure 103: Geological cross section of six McArthur River diamond drill-holes (DDH) with partial uranium concentration 152

Figure 104: XY plots of alkali earth metals Ba (ppm) and Ca (%) compared to Ra (fg/g). 153

Figure 105: XY plot showing the correlation between total Ca (ppm) and Ba (ppm) within soils at McArthur River 154

Figure 106: XY plot of calcium and barium against potassium concentration (ppm) after a multi acid leach of B-horizon soils from McArthur River 154

Figure 107: XY plot of radium concentration (fg/g) compared to trace element partial concentrations (ppm) after the sequential leach 156

Figure 108: XY plot of radium concentration (fg/g) compared to trace element partial concentrations (ppm) after the sequential leach 157

List of Tables

Table 1: List of nuclides in the U-238 decay series, their decay type and half-lives 22

Table 2: Isotope composition of three internal standards and one blind standard used to normalise O and H data. 41

Table 3: General groundwater characteristics 51

Table 4: Minor ion concentrations of groundwater. 54

Table 5: Table of $\delta^{2}H$- $\delta^{18}O$ values (‰) reported in $^{2}H/1H$ and $^{18}O/^{16}O$ relative to Vienna Standard Mean Ocean Water (VSMOW) 58

Table 6: $\delta^{13}C$ sources and values in ‰ compared to PDB standard from Faure (1988) and *Palmer (2001) 59

Table 7: Concentration of dissolved organic carbon (DOC) and dissolved inorganic carbon (DIC), and their $\delta^{13}C$ values 59

Table 8: Rn activity in soil with GPS coordinates and depth in meters 67

Table 9: List of samples and their corresponding lithology at the sample depth 67

Table 10: Concentration of major elements leached by ammonium acetate from B-horizon soils. 71

Table 11: Concentration of elements leached by ammonium acetate from C-horizon soils 71

Table 12: Concentration of elements leached by ammonium acetate from B-horizon soils 73

Table 13: Concentration of trace elements leached by ammonium acetate from C-horizon soils. 73

Table 14: Concentration of rare earth elements and Y leached by ammonium acetate from B-horizon soils 76

Table 15: Concentration of rare earth elements leached by ammonium acetate from C-horizon soils 77

Table 16: Concentration of major elements dissolved by multi-acid digestion from three soil samples at Millennium. 79

Table 17: Concentration of trace elements dissolved by multi-acid digestion from three soil samples at Millennium 80

Table 18: Concentration of rare earth elements and Y dissolved by multi-acid digestion from three soil samples at Millennium 81

Table 19: Groundwater characteristics from McArthur River 99

Table 20: Groundwater chemistry by sample 100

Table 21: $\delta^{2}H$- $\delta^{18}O$ values (‰) reported in $^{2}H/^{1}H$ and $^{18}O/^{16}O$ relative to Vienna Standard Mean Ocean Water (VSMOW) 102

Table 22: Concentration of dissolved organic carbon (DOC) and dissolved inorganic carbon (DIC), and their $\delta^{13}C$ (‰) values 103

Table 23: Rn activity (counts per minute) from groundwater at 6 locations above the McArthur River deposit. 105

Table 24: Groundwater Rn activity and the depth to overburden in six McArthur River drill-holes 107

Table 25: Noble gas abundance data from three McArthur River drill-holes, including depth of the water table, depth of sampling, and $^{4}He/^{20}Ne$ normalized to air saturated water (ASW) 107

Table 26: Rn activity in soil with GPS coordinates and depth in meters 108

Table 27: Concentration of major elements leached by ammonium acetate from B-horizon soils at McArthur River 111

Table 28: Concentration of trace elements leached by ammonium acetate from B-horizon soils at McArthur River 113

Table 29: Concentration of rare earth elements and Y leached by ammonium acetate from B-horizon soils at McArthur River 116

Table 30: Major element concentrations of McArthur River B-horizon soils after multi-acid digestion 117

Table 31: Trace element concentrations in ppm (Ag in ppb) of McArthur River B-horizon soils dissolved by multi-acid digestion 118

Table 32: Rare earth element (REE) concentrations in ppm of McArthur River B-horizon soils dissolved by multi-acid digestion 119

Table 33: McArthur River fracture coating samples listed by drill-hole ID and sample depth.. 121

Table 34: γ-ray spectroscopy results of Ra activity of fracture coating material in DDH, and location based on mineralized zones..... 144

Table 35: Radium concentration of 8 soil samples taken near DDH at McArthur River. Concentration is reported in pg per gram of soil. 144

List of Equations

Equation 1: Conversion equation from counts per minute to activity (Bq/L) 38

Equation 2: Radioactive decay equation..... 39

Equation 3: Extraction volume correction equation 39

List of Appendices

Appendix A: Complete data set

Appendix B: Core fracture photographs

Appendix C: Conference abstracts, posters and presentations

Table of Contents

Abstract ii
Acknowledgements v
List of Contents vi
List of Figures vi
List of Tables xiii
List of Equations xv
List of Appendices xv

CHAPTER 1: Grand Introduction 1
1.1 Introduction 1
1.1.1 Thesis Objectives and Hypotheses 1
1.1.2 Thesis Outline 2
1.1.3 Contributions 3
1.1.4 Project Area 4
1.1.5 Regional Geology of the Athabasca Basin 7
1.1.6 Quaternary Geology 10
1.1.7 Regional Climate and Ecoregion 12
1.2 Previous Research 13
1.2.1 Exploration Methods in the Athabasca Basin 13
1.2.2 Surficial Geochemistry 16
1.2.3 Radionuclides in Uranium Exploration 22
1.2.4 Groundwater Hydrogeochemistry 25
CHAPTER 2: Grand Conclusion 27
CHAPTER 3: Methods 30
3.1 Field Methods 30
3.1.1 Water Sampling 32
3.1.2 Helium Sampling 34
3.1.3 Soil Gas Sample Collection 35
3.1.4 Soil Sampling Procedure 37
3.1.5 Collection of Drill Core Fracture Coatings 37
3.2 Laboratory Methods 38
3.2.1 Radon in Water Analyses 38

3.2.2 Water Chemistry **40**
3.2.3 Stable Isotope Compositions **40**
3.2.4 Tritium **41**
3.2.5 Helium **43**
3.2.6 Soil **43**
3.2.7 Core Fractures **44**
3.2.8 Powder X-ray Diffraction **44**
3.2.9 γ-ray Spectrometry **44**
3.2.10 Sequential Leach Experiment **45**
CHAPTER 4: Examining radiogenic elements in soil and groundwater above the deeply buried Millennium Uranium Deposit, Saskatchewan **47**
4.1 Introduction **47**
4.2 Geologic Setting **48**
4.3 Results **49**
4.3.1 General Groundwater Characteristics **49**
4.3.2 Groundwater Chemistry **53**
4.3.3 Stable Isotope Characteristics **57**
4.3.4 Tritium **60**
4.3.5 Radon in groundwater **61**
4.3.7 Rn in Soil **64**
4.3.8 Soil Geochemistry **69**
4. 4 Discussion **82**
4.5 Conclusions **92**
CHAPTER 5: Examining the surficial expression of the McArthur River uranium deposit in groundwater, shallow sandstone fracture coatings and soils. **96**
5.1 Introduction **96**
5.2 Geologic Setting **96**
5.3 Results **98**
5.3.1 General groundwater characteristics **98**
5.3.2 Groundwater Chemistry **100**
5.3.3 Stable Isotope Compositions **101**

5.3.4 Tritium **104**
5.3.5 Rn in groundwater **105**
5.3.6 Rn in Soil **108**
5.3.7 Soil Geochemistry **110**
5.3.8 Fracture Sequential Leach **120**
5.3.9 X-ray Diffraction: Fracture Minerals **140**
5.3.10 Radium **143**
5.4 Discussion **146**
5.5 Conclusions **157**
CHAPTER 6: Recommendations for future work **159**
REFERENCES **161**

CHAPTER 1: Grand Introduction

1.1 Introduction

1.1.1 Thesis Objectives and Hypotheses

Uranium ore is essential for maintaining the world's energy needs and is a large part of Canada's energy sector; roughly 15% of Canada's electricity (World Nuclear Association, 2015) and 57% of Ontario's electricity (Ottawa Hydro, 2014) is generated by nuclear power. Hydro-geochemistry has been used to explore for uranium (U) deposits since the late 1950s, and requires an understanding of the geology, hydrology and water chemistry of the area of interest (Dyck and Tan, 1978). Typically, U and three of its radiogenic decay products; radon (^{222}Rn), radium (^{226}Ra) and lead (Pb) are used to determine the proximity of both surficial and deeply buried U deposits.

As part of the Canadian Mining Innovation Council Uranium Footprints Project, this research focuses on the occurrence of ^{238}U decay chain nuclides above the Millennium and the McArthur River U deposits in the Athabasca Basin, Saskatchewan, Canada. The primary objectives of this thesis are to 1) Examine geochemical signatures of water and soil above the Millennium and McArthur River deposits and 2) Determine the source(s) of radiogenic gases and the secondary geochemical processes involved in their movement throughout soil and groundwater. This study's initial hypothesis was that the chemistry, physical conditions, residence age and source of groundwater would contribute to the variance in Rn radioactivity within groundwater. It was hypothesized that groundwater with more dissolved organic carbon would have higher radon radioactivity. Carbon isotopes were measured to determine the sources of carbon in the groundwater. It was also hypothesized that the Ra content of local soil and shallow sandstone fractures would contribute to the Rn radioactivity of groundwater.

1.1.2 Thesis Outline

This thesis is a traditional monograph-style thesis divided into six chapters. Chapter 1 is a grand introduction to the project. It summarizes previous research about bedrock geology, Quaternary geology, climate and ecoregion, U exploration methods, and groundwater hydro-geochemistry within the Athabasca Basin. It also reviews the use of radionuclides in U exploration. Chapter 2 serves as a grand conclusion of the main outcomes of the thesis, and is placed at the beginning of the thesis to summarize the study's findings to the reader up-front.

Chapter 3 details the field and laboratory methods used for this study. Field methods include sampling procedures for groundwater, gas, soil and fracture coatings of sandstones. The laboratory methods section explains the procedures involved in analyzing groundwater for Rn, anions, cations, stable isotopes, ^{3}H and He. Chapter 3 also describes the digestions performed by ACME Analytical Laboratories on soil samples. Additionally, it outlines the analytical methods used for fracture coatings of sandstones, including X-ray diffraction, γ-ray spectrometry, and sequential leach geochemistry.

The remainder of the thesis presents results, discussions and conclusions about radiogenic elements above the Millennium and McArthur River U deposits. Chapter 4 is the first of two case studies and outlines the occurrence of U decay products within groundwater and soil above the Millennium U deposit. Chapter 5 is the second case study, and discusses the movement of U decay products within groundwater, soil and core fractures above the McArthur River U deposit. Chapter 6 outlines recommendations for future work, and methodological innovations.

1.1.3 Contributions

The author completed fieldwork in the summers of 2013 (Millennium) and 2014 (Millennium and McArthur River) to collect samples from two study sites. Water and soil sample collection was completed with support from Dr. Tom Kotzer and Kaitlyn Browne of Cameco Corporation and Dr. Keiko Hattori, University of Ottawa. Core sample collection was completed in tandem with fellow Canadian Mining Innovation Council (CMIC) – Uranium Project members, Shannon Guffey and Nicholas Joyce. Fieldwork was funded by Cameco and Areva Resources as an in-kind contribution to the Footprints project. Mary Devine completed all radiochemical work (Rn in water, Rn in soil, Ra in core and soil) with great assistance from Dr. Jack Cornet, University of Ottawa. Mary Devine also completed ^{3}H, Rn and He laboratory analyses with great assistance from Monika Wilk, University of Ottawa. Sequential leach digestions and water chemistry samples were prepared by Mary Devine and analysed by ICP-MS/ES by Nimal de Silva, University of Ottawa. Dionex analyses for halogen content of water were analysed by Pingqing Zhang, University of Ottawa. Stable isotope analyses (O, H and C) were completed at the G.G. Hatch Stable Isotope Laboratory at the University of Ottawa. Soil geochemistry was analysed by ACME Analytical Laboratories in Vancouver, B.C. Mary Devine wrote the work presented in this thesis with crucial input and critical review by Dr. Keiko Hattori. Funding and in-kind support for this study was provided by the NSERC Collaborative Research and Development Grant with the Canadian Mining Innovation Council, and the Society of Economic Geologists' Graduate Student Fellowship.

The author presented portions of this work in poster format at the Saskatchewan Geological Survey Open House (Saskatoon, 2013) and the Canadian Mining Innovation Council's Minerals Colloquium (Toronto, 2014). Oral presentations of this work were presented

by the author at the Joint Annual Meeting of the Geological Association of Canada and Mineralogical Association of Canada (Fredericton, 2014), and at the Advances in Earth Science Research Conference (Ottawa, 2014). Additionally, the content of this thesis was presented in CMIC quarterly reports and annual meeting presentations throughout 2013-2015. These presentations and abstracts are available online at www.cmic-footprints.ca/home/publications.

1.1.4 Project Area

Two field sites were chosen for this project as case studies to determine the sources and pathways of radiogenic elements above deeply buried U deposits. Both Millennium and McArthur River occur within the eastern margin of the Athabasca Basin, Canada (Figures 1 and 2) and are mono-metallic, high-grade U deposits. They are 70% and 67% owned by Cameco Corporation respectively (Cameco Corporation, 2014).

Figure 1: Map of Canada with inset location of the Athabasca Basin (after Chen et al., 2015). Provincial and territorial boundaries are represented by black lines.

Mineralization at McArthur River and Millennium ranges from 500 – 650 m and approximately 750 m depth from the current surface, respectively. Within the top 100 m of the Manitou Falls Formation (MFd Member) sandstone there is no perched mineralization, however there are some instances where the sandstone has anomalous (>2.5 ppm) concentrations of U, most notably at McArthur River. This makes them applicable case studies for determining the surficial footprint of radiogenic decay products above deeply buried U mineralization (Figure 2).

Three surficial materials were tested for Rn, Ra and U in order to determine the source for Rn in groundwater: 1) glacial till and soil, 2) groundwater, and 3) fracture coatings of upper sandstones.

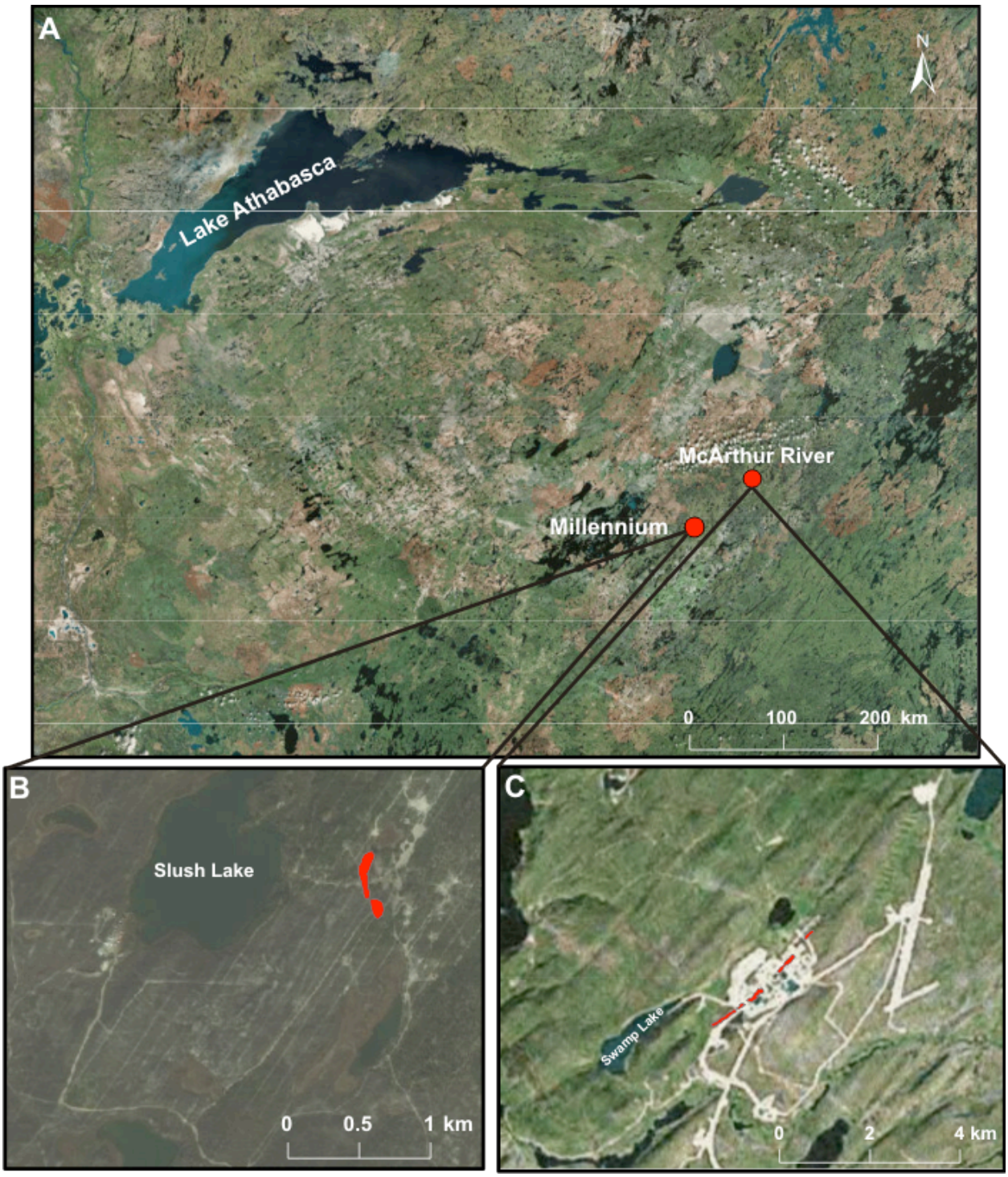

Figure 2: Satellite imagery from ArcGIS World Imagery of the Athabasca Basin region (A), with larger scale maps of the Millennium (B) and McArthur River (C) sites. Red dots (A) indicate deposit locations, and red shapes (B and C) represent U deposits at depth.

1.1.5 Regional Geology of the Athabasca Basin

The Athabasca Basin is located in the southwest of the Churchill Structural Province of the Canadian Shield (Ramaekers, 1981) and hosts several large, high-grade U deposits. The Athabasca Basin is located between the eroded remnants of two major orogenic belts, the Thelon tectonic zone and the trans-Hudson Orogen. These belts accommodated ductile transpression during the convergence of the Slave and Superior provinces (Hoffman, 1983) to form the western portion of the Rae province and the eastern portion of the Hearne province (Figure 3 and 4). The reactivated faults are evidence of transpressional and extensional tectonics that are crucial for ore deposition (Jefferson et al., 2007).

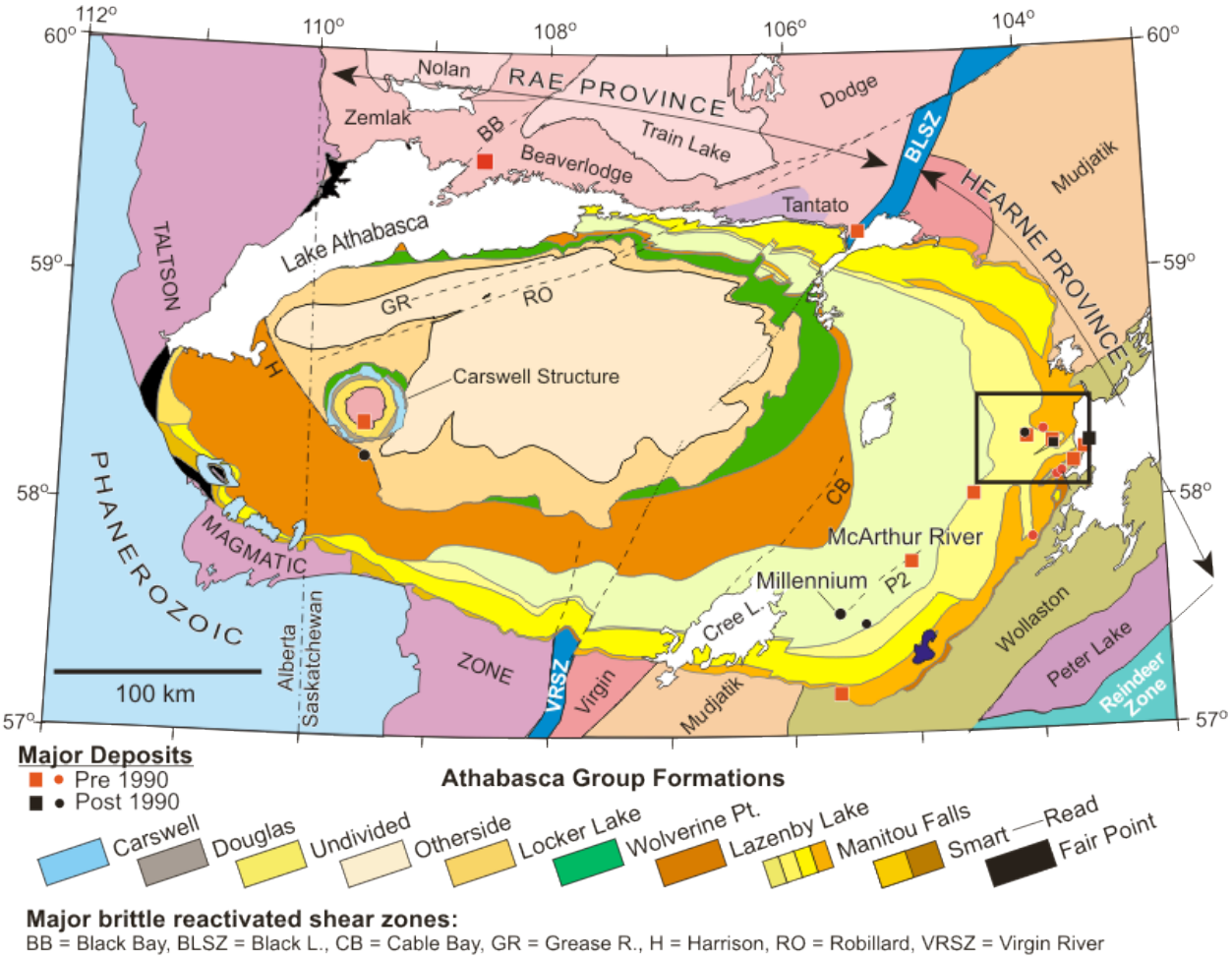

Figure 3: Geological setting and major unconformity-associated uranium mines (red) and deposits (black) within the Athabasca Basin, Saskatchewan, Canada. Modified after Jefferson et al. (2007). Black Box indicates location of International Atomic Energy Association Test Area in IAEA (1989).

An unconformity occurs between Paleo-Mesoproterozoic conglomeratic sandstones and the metamorphosed basement rocks. Above the unconformity, the Athabasca group sandstones consist of reddish quartzose conglomerates, sandstones and mudstones.

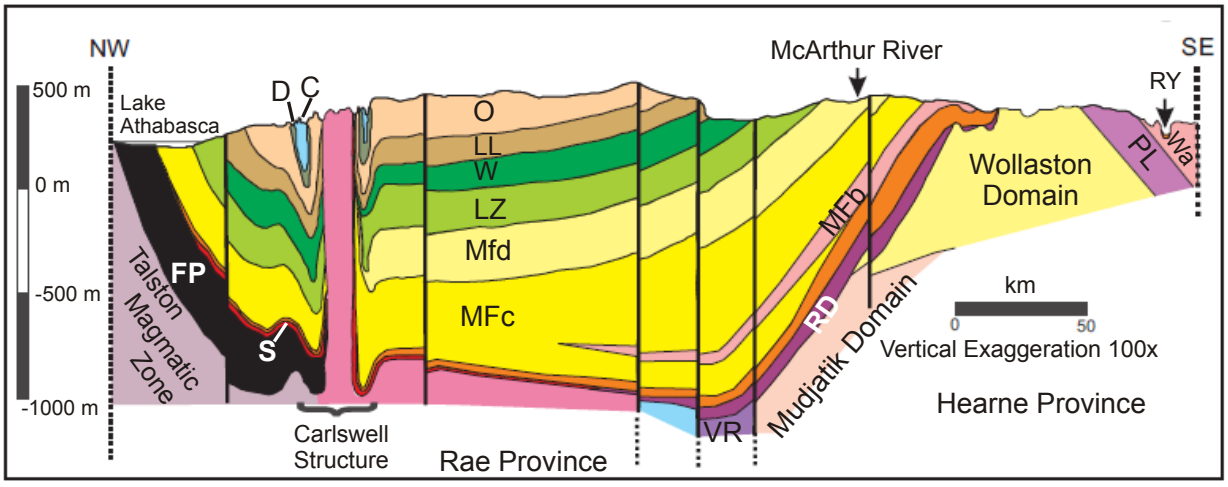

Figure 4: Lithostratigraphic cross section of the Athabasca Basin modified after Jefferson et al. (2007), RD= Read Formation, MFb = Manitou Falls formation (Bird Member), MFc = Manitou Falls formation (Collins Member), MFd = Manitou Fall formation (Dunlop Member) FP = Fair Point Formation, S = Smart Formation, D = Douglas Formation, C = Carswell Formation, O = Otherside Formation, LL= Locker Lake Formation, W = Wolverine Formation, LZ = Lazenby Lake Formation, VR = Virgin River Formation, Wa = Wathaman Batholith, Ry = Reilly Formation, PL = Parker Lake Formation. The McArthur River deposit is indicated above the Mudjatik Domain of the Hearne Province.

The Athabasca sedimentary strata are Proterozoic (1.8 to <1.55 Ga), mainly fluvial to shallow marine in origin, and are overall flat-lying and unmetamorphosed (Ramaekers et al., 2007). The maximum thickness of the Athabasca group is about 1 500 m. There are four sandstone units of the Athabasca group within the Manitou Falls Formation that occur

throughout the basin. Each unit is separated by unconformities that record repeated deposition and erosion around 200 Ma (Jefferson et al., 2007). In the eastern portion of the basin, where the Millennium and McArthur River Deposits are located, as well as many other high-grade U deposits, the Manitou Falls formation (MF) is the only remaining formation of the Athabasca group, due to erosion. Four sequences defined by Ramaekers listed from youngest to oldest are: Manitou Falls Dunlop (MFd), Manitou Falls Collins (MFc), Manitou Falls Bird (MFb) and Manitou Falls A (MFa, also identified as the Read Formation (RD), and is not present in this study area). MFd is classified as quartz arenite with clay-intraclasts and mudstone interbeds; MFc is classified as quartz arenite with minor quartz pebble beds, mudstone interbeds, conglomerate interbeds and clay intraclasts. MFb is classified as interbedded quartz-pebble conglomerate, pebbly quartz arenite, and thin mudstone with siltstone interbeds.

Below the unconformity is a laterally extensive alteration profile consisting of an upper bleached zone of illite and kaolinite, followed by a middle red zone of hematite and kaolinite and a lower green zone of chlorite alteration and finally fresh basement gneiss (Macdonald 1980, and Tremblay, 1983). In the eastern part of the basin, most mines and prospects are located where the Athabasca group unconformably overlies the transition between Wollaston and eastern Mudjatik basement domains (Figure 4). The basement in this area is made up of pelitic quartzose and arkosic paragneiss that are isoclinally folded and interleaved with Archean orthogneiss and intruded by abundant pegmatite. Other eastern deposits occur at the unconformable contact between the Archean granitoid gneiss and late Paleoproterozoic basal Wollaston Supergroup (Yeo and Delaney, 2007), where it contains graphitic metapelitic gneiss (Annesley et al., 2005). These U-rich granitic pegmatites were created during high-grade metamorphism of

metasedimentary rocks, and contain abundant U-bearing minerals like monazite, zircon and uraninite (Jefferson et al., 2007).

Mineralization of unconformity-associated deposits typically occurs as pods, veins and semi-massive replacement ore and as uraninite (Jefferson et al., 2007). Most mineralization in the basin is dated 1600 to 1350 Ma and located between Proterozoic red-beds and metamorphosed basements rocks, especially gneiss and graphitic metapelite (Jefferson et al., 2007). Millennium and McArthur River are both monometallic U deposits, hosted by basement rocks and sandstones respectively (only Zone 2 at McArthur is basement hosted) and are associated with reactivated fault zones (Jefferson et al., 2007).

1.1.6 Quaternary Geology

Initial exploration in the Athabasca Basin successfully used lake sediment geochemistry and boulder train delineation to discover U deposits, such as Key Lake and Midwest Lake, under extensive glacial cover (Campbell, 2007). Due to these successes, many exploration efforts focused on surficial geochemistry, but often lacked a Quaternary mapping program, which is crucial for properly evaluating the surficial geochemistry of such a heavily glaciated region (Campbell, 2007). Due to the importance of understanding the composition and patterns of glacial drift (Campbell, 2007) in surficial geochemistry studies, this section describes the regional Quaternary geology of the eastern Athabasca Basin. This information is crucial for interpreting the surficial geochemical results of this thesis.

Ice-flow directions within the Athabasca Basin are determined based on linear glacial till features such as drumlins, flutings, crag-and-tail structures and striations (Schreiner, 1983). Relative ages were determined based on cross cutting relationships, which are rarely visible due to the lack of bedrock outcrop. Generally, glacial movement is towards the SW (210-200º)

(Schreiner, 1983), with later stage southern and westward movement due to localized flow from pulsing ice-lobe fronts (Campbell, 1995) as shown in Figure 5.

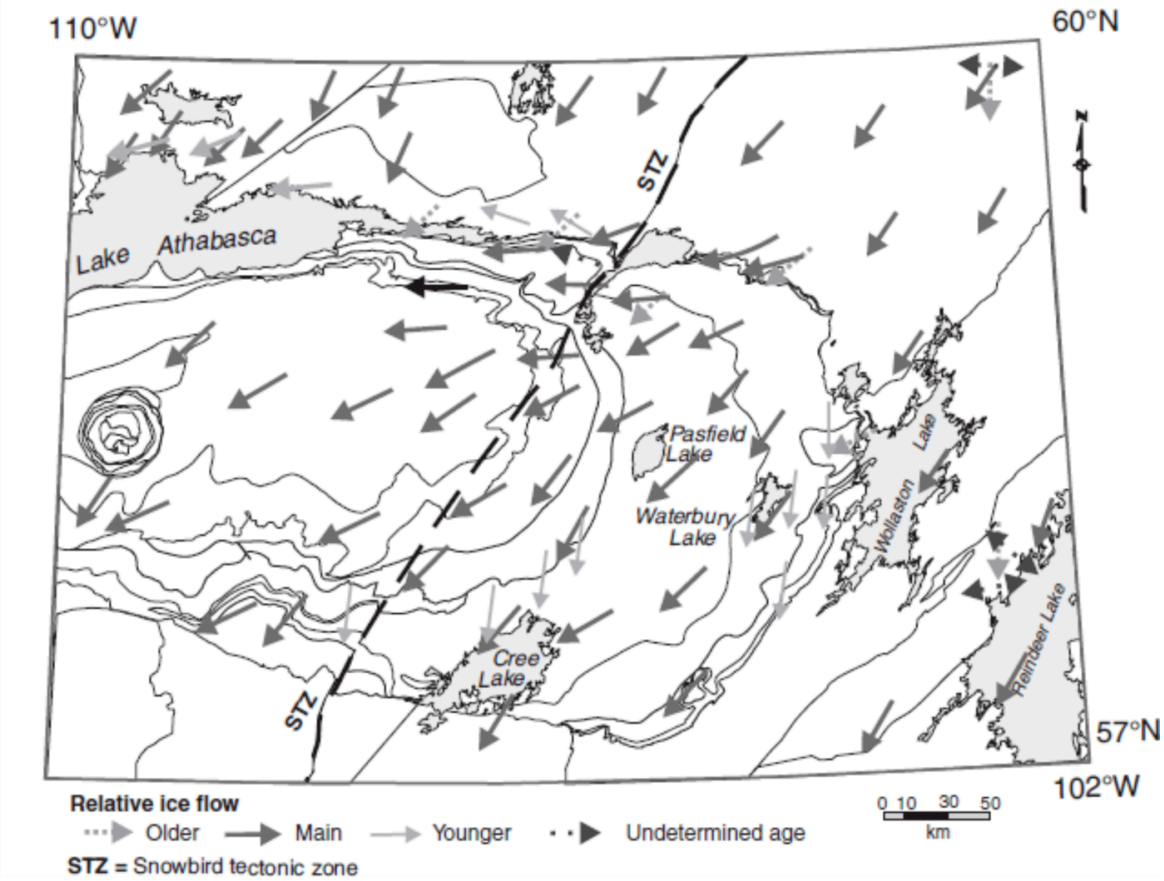

Figure 5: Regional ice-flow direction and their relative ages in the Athabasca Basin from Campbell, 2007.

The Athabasca Basin has been through several glaciations, and is now covered almost completely by glacial till and only 5% by outcropping bedrock (Schreiner, 1983). The thickness of glacial drift ranges from 0-100 m throughout the basin and generally increases from east to west, reaching 100 m thick at McArthur River (Campbell, 1995). The modern day landscape in the eastern margin of the Athabasca Basin is primarily the result of the Wisconsinan glaciation that ended approximately 8 200 years ago (Schreiner, 1983) and is weakly attributed to underlying bedrock topography.

Glacial drift thickness is strongly influenced by bedrock topography (Schreiner, 1983). For example, bedrock valleys have very little surface expression, because they have been filled in with glacial sediments (Campbell, 1995). Alternatively, most bedrock highs have very little glacial drift cover, ranging from only 0-8 m thick. The thickest glacial drift layers occur in bedrock topographic lows, where glacial drumlins have formed.

Tills deposited as terminal and lateral moraines are the most abundant Quaternary deposit in the Athabasca Basin and its composition is greatly influenced by underlying bedrock lithology (Schreiner, 1983). In the eastern portion of the Athabasca Basin, over 90% of cobbles and boulders are derived from Athabasca Group sandstone (Earle et al., 1989). Till is derived from sandstone, intrabasinal deposits, extrabasinal deposits and/or crystalline basement rocks that were eroded throughout glaciation and travelled varying distances. Extrabasinal glacial material is sourced from northeast of the Athabasca Basin, some as far as Nunavut (>100 km) and is the source for the greatest variance in geochemical signature because it includes pebble to boulder size erratics of feldspar, phyllosilicates and heavy minerals. Generally, the thicker the glacial deposit, the greater the proportion of extrabasinal sediments from eskers (Campbell, 1995). Quaternary geology is crucial for the interpretation of surficial geochemistry. The glacial till deposits in the study areas are primarily derived from local bedrock by multiple ice flows.

1.1.7 Regional Climate and Ecoregion

The climate and vegetation cover of the study area is discussed in this section to outline the soil conditions, precipitation amounts and overall climate. The study area of this thesis occurs within the Athabasca Plain Ecoregion (Johnson, 2007) of northern Saskatchewan which experiences short, cool summers (mean temperature = 15ºC) and cold winters (mean temperature = -20.5ºC) (Environment Canada, 2016). This ecozone extends south from Lake Athabasca to

Cree Lake (Figure 5) and follows a similar shape as the occurrence of Athabasca sandstones beneath. Mean annual precipitation ranges from 350-450 mm and the majority of precipitation occurs in the summer as rainfall, with lesser in the winter as snow. This region has a sub-humid, high boreal eco-climate and is home to jack pine, shrubs, and lichen, with lesser spruce, birch, balsam fir, and aspen in the warmer, south facing areas (Environment Canada, 2016).

Forest fires are common in this area, and often result in stunted and young coniferous trees. The Millennium site suffered a forest fire in the summer of 2007, which burned some core storage facilities and parts of the surrounding forest.

More specifically, this region is ecologically defined as the Tiaga Eco-zone, because the bedrock is covered by extensive glacial drift resulting in plains and rolling fluvio-glacial deposits (Environment Canada, 2016). Soil development in this region is mainly brunosolic (has well developed, brownish B-horizon) in areas with well to moderately drained sandy material. The soil is classified by Environment Canada as mostly dystric brunisols due to its acidity (pH = 4.5 – 5.5), developed B-horizon, poorly developed organic Ah-horizon, and the absence of a carbonate layer. Organic soils are less common in this region and only occur in poorly drained areas (Schreiner, 1983). This region has the lowest number of animal species in the province and is dominated by sub-arctic and arctic species (Johnson, 2007).

1.2 Previous Research

1.2.1 Exploration Methods in the Athabasca Basin

Uranium was first discovered in Saskatchewan along the north shore of Lake Athabasca in 1935, followed by several Athabasca-associated U deposits discovered in the late 1960-1980s including Rabbit Lake, Key Lake, Midwest Lake, Dawn Lake and McClean Lake (Jefferson,

2007). Since that time, exploration has transformed from deposits at shallow depths to much deeper (>400 m) deposits such as McArthur River, Millennium, and Phoenix.

Jefferson et al. (2007) outlined the geological exploration criteria for unconformity-associated U-deposits in the Athabasca Basin. They suggest that U-depleted, Paleo/Meso-proterozoic, red-bed basin combined with the underlying U-rich (>5 ppm U) basement complexes are two key components for U mineralization. Other important criteria include the presence of graphitic metapelite, ductile faults, and pre-existing structural complexities within the basement rocks. Graphitic metapelite is considered a crucial source of carbon for reduction of the oxidized U-rich fluids once they enter the basement in order to precipitate U (Jefferson et al., 2007). Ductile faults provide pathways for hydrothermal fluids to travel throughout the basement complex, and structural complexities provide a trap in which to concentrate and precipitate U ore (Jefferson et al., 2007). Features such as paleo-valleys (valleys created due to basement offsets) and intersecting steeply dipping faults (such as the P2 fault at McArthur River) are also favourable for U deposition. The deposit model for U in the Athabasca Basin according to Jefferson et al. (2007) suggests that U was emplaced after the deposition of sedimentary sequences.

Geophysical exploration for U deposits has evolved over the years and was initially used to detect radioactive, near-surface deposits. These methods were responsible for identifying the Rabbit Lake, Key Lake and Cluff Lake deposits (Jefferson et al., 2007). More detailed geophysical surveys now use airborne and ground electro-magnetic (EM) methods to recognize the graphitic faults that are often associated with U deposits. EM methods are the most cost effective tool for locating and characterising basement conductors (Jefferson et al., 2007) and can identify other deposit-related characteristics, such as shallow, low-resistivity alteration zones

(clay-rich) and unconformity fault offsets (Bisset, 2003). As exploration shifted to deeper deposits the geophysical methods changed to natural source audiomagnetotellurics and seismic (Juhojuntti et al., 2012). These more recent methods were employed at McArthur River and Millennium to identify a more accurate location of the unconformity and post-Athabasca fault zones (Juhojuntti et al., 2012). Seismic is used to provide detailed constraints on structures at depth.

Lithogeochemical surveys of upper Athabasca group sandstones and glacial boulders are also effective methods for identifying alteration haloes of U deposits >500 m deep. Earle et al. (1989) used glacial geology and lithogeochemistry to test if potassium, boron and other elemental haloes were detectable within large, angular glacial boulders near the McArthur River deposit. Lithogeochemistry of sandstone boulders was compared to lithogeochemistry of subcropping sandstones, and revealed that the boulders and shallow sandstones show very similar anomalies (Earle et al., 1989). Therefore, correctly sampled boulder trains provide a much less expensive method for determining lithogeochemical anomalies than shallow drilling (Earle et al., 1989). This method is most useful when interpreted with other exploration data, such as electromagnetic geophysical surveys.

The regional lithogeochemistry of the Athabasca basin has also been studied to increase the understanding of U-mineralization processes and background lithogeochemistry of the MF sandstone and basement rocks (Earle and Sopuck, 1987). Overall, there is a stratigraphic control on clay content in Athabasca Group sandstones; MFd has less clay than MFc, MFb, and MFa; which range from 5-20% in clay content. There is no stratigraphic control on illitie/kaolinite ratios throughout the eastern margin of the basin (Earle and Sopuck, 1987), however the lower 10-20 m of sandstone is typically more illite-rich. Earl and Sopuck (1987) determined that

alteration processes have had a larger impact on the lithogeochmical characteristics of the MF sandstones than stratigraphy. The increased understanding of background lithogeochemistry and alteration patterns, increases the likelihood of detecting mineralized zones within the eastern margin of the Athabasca Basin (Earl and Sopuck, 1987).

1.2.2 Surficial Geochemistry

Geochemical mineral exploration often reveals both local and regional mineralogical alteration, and can provide indicators for drilling when used appropriately with geophysics and Quaternary geology. Various media are used in U geochemical exploration including water, soil, till, and lake sediments. The regional background value of U in lake sediments and till in the Athabasca ranges from 1-2 ppm U (Quirt, 1985). U anomalies in lake sediments reach up to 1 500 ppm in the Key Lake area, and the Athabasca group sandstones are defined as anomalous when U is >2.5 ppm (Jefferson et al., 2007). Anomalous sandstones can be found up to 500 m from U mineralization, in areas of heavy clay alteration. Other indicator elements for U exploration include Ni, As, and Co. The movement of these elements is typically tens of meters, making them less useful for green-field exploration, but more useful for pinpointing shallow targets (Jefferson et al., 2007).

It is important to comprehend the mechanisms that control the movement of indicator elements from ore to the surface in order to identify which elements to look for. Some elements move during ore forming process and other elements, such as Rn, move post ore deposition through groundwater and gas. The latter process is termed “secondary dispersion”. Mechanisms of “secondary dispersion” include diffusion, advection, and adsorption among other chemical and physical methods.

Radiometric prospecting and lake-water/sediment/till geochemistry were the main exploration tools used in early U exploration in the Athabasca Basin (Jefferson et al., 2007). Surficial geochemistry has proven to be useful for identifying U deposits close to the surface because pathfinder elements and Rn gas do not travel far from their source. However above deeper U deposits, the measurement of Rn gas within soil and groundwater has been done with mixed results (e.g. Earl and Drever, 1983; Dyck, 1969; Scott, 1983). More recently, the Patterson Lake South U deposit in the south west of the Athabasca Basin was discovered in 2012 by the detection of Rn-in-water (Radonex, 2013) anomalies that outlined successful drilling targets. Biogeochemistry is another common surficial exploration method often used in mineral exploration. For example, the U content of spruce twigs at the McClean and Rabbit Lake deposits revealed a large biogeochemical anomaly formed from tree roots absorbing U from groundwater (Dunn, 1983).

When the necessity for deeper exploration targets increased, geochemical exploration methods began to focus on alteration mineralogy, or primary elemental dispersion rather than secondary dispersion of ore-associated elements (U, Ni, Cu, Mo). Dispersion in this case refers to the general migration of elements throughout bedrock, soil and groundwater, and does not refer to a specific method of element transport in water. Typical alteration haloes include the crystallization of illite, dravitic tourmaline, and quartz dissolution (Adlakha and Hattori, 2015). Illite and dravitic tourmaline are often identified in till and bedrock by lithogeochemistry, potassic alteration (illite) can be identified by short wave infrared spectroscopy (SWIR) and airborne gamma-ray spectrometry (Jefferson et al., 2007).

Lake water and lake sediment surveys have been used to determine the distribution of U and associated elements within the Nuclear Energy Agency/ International Atomic Energy

Agency (NEA/IAEA) Test Area within the Athabasca Basin (Coker and Dunn, 1983). The Test Area is 1 250 km^2 in the eastern margin of the Athabasca Basin near several unconformity-associated U deposits. It is between latitudes 58º07'30''N and 58º22'30" N, and longitudes 103º30'00" W and 104º 15'00" W (Sibbald, 1983, Figure 3). Coker and Dunn (1983) concluded that organic-rich lake sediments, with minor clay minerals, quartz, and Fe-Mn hydroxides reflected subglacial lithologies and there were typically more U in sediments above the Wollaston Domain than the Mudjatik Domain. The parameters that best define U mineralization in lake sediments are U, Ni and As (Coker and Dunn, 1983). Lake water in the NEA/IAEA Test Area has near neutral pH and low conductivity (< 41 S/cm), neither of which correlate to lithology or U mineralization. Cl, PO_4 and less-so F best define U mineralization in lake waters, and NO_3 follows a NE trend with glaciation (Coker and Dunn, 1983). Additionally, there was less than 4 ppb U in lake waters within the NEA/IAEA Test Area (Coker and Dunn, 1983).

Till geochemistry and boulder train analyses can also be useful methods of U exploration where basal till is thin (<10 m) and U mineralization is relatively close to the surface (200 m) (Simpson and Sopuck, 1983). The most effective techniques include sampling U content of boulders, U within the <250-mesh portion of till, and U within the clay-sized particles of till. Geochemical soil surveys and various radiometric techniques are useful for determining boulder trains and underlying shallow mineralization (Dyck and McCorkell, 1983). Rn in soil gas is not usually regionally homogeneous, and can vary by several KBq/m^3 when measured several meters apart, so Rn in soil is likely locally sourced from weathered radioactive boulders or chemically transported and precipitated Ra (Dyck and McCorkell, 1983). Other factors that affect Rn in soil gas concentrations are barometric pressure, soil moisture and sampling depth (Dyck and

McCorkell, 1983) because the diffusion coefficient of Rn increases with decreasing barometric pressure, and decreases with an increase in soil moisture.

Groundwater has been used for exploration since the 1970s (Cameron, 1977; Cameron, 1978; Miller et al., 1982; Earle and Drever, 1983) and more recently by Leybourne and Goodfellow (2003) and Cameron et al. (2004). The range in complexity of groundwater sampling programs for mineral exploration (Au, Cu, U) is outlined by Leybourne and Cameron (2007). Groundwater sampling techniques can range from simple bailers to straddle packer methods, and most require the use of pre-existing drill-holes, or domestic and agricultural wells. Commonly, water is filtered in-situ to either <0.45 μm or <0.20 μm after sample collection, however this does not always remove undissolved metals bound to small colloids. It is also necessary to understand the hydrology and major ion content of groundwater in order to interpret the geochemistry (Leybourne and Cameron, 2007). Major ions indicate the water type, amount of mixing, evaporation, water rock interaction and recharge of the groundwater in question (Leybourne and Cameron, 2007). Major geochemical characteristics of unconformity U deposits include U, Se, Mo, V, Cu, and Pb (Leybourne, 2007). As well, major aqueous geochemical pathfinders for unconformity U deposits include U and Rn in oxidizing conditions and Se, Mo in reducing conditions (Leybourne and Cameron, 2007). Minor aqueous geochemical pathfinders include Se, Mo, As, V, Cu and Pb. Additionally, simple field measurements such as pH, Eh and conductivity can provide in-situ information regarding changes in groundwater sources and redox conditions which can aide in sampling procedures in the field (Leybourne and Cameron, 2007). The main recommendation for U groundwater geochemical exploration is that U is the best indicator for mineralization, and more research is necessary using Pb and U series isotopes (Leybourne and Cameron, 2007).

Another common geochemical exploration method for buried mineral deposits is selective leaching of soil (Cameron et al., 2004), aimed at dissolving only a portion of mobile metals that are presumably derived from ore. Bonham-Carter and Hall (2010) studied surficial geochemical techniques for detection of covered U deposits in the Athabasca Basin above McLean Lake and Cigar Lake. Their work aimed to find the best soil horizon (A, B or C) and the most effective leach method to detect buried U mineralization.

The intense faulting throughout the Athabasca Basin is a likely pathway for metals to migrate from mineralization (Bonham-Carter and Hall, 2010). Geochemical anomalies above the trace of two U deposits are best expressed in U, Co, Ni and REEs, and the most reliable anomalies occur in the A1 humus horizon (Bonham-Carter and Hall, 2010). As well, the anomalies in Bonham-Carter and Hall's study were not affected by pH (of soil leachates), loss on ignition (LOI) or ground elevation. They suggested the most cost effective and reliable leach was aqua-regia decomposition of humus.

Furthermore, significant anomalies were repeatable from year to year; and single point anomalies were less repeatable. With regards to why these anomalies occur where they do, and why within A-horizon soil more so than B and C-horizons, Bonham-Carter and Hall (2010) proposed that dissolved metals move within groundwater from the sandstones to within the Quaternary till, and then concentrate within plant roots. The roots eventually decay and likely produce anomalies within the humus layer.

The soils and till in the Athabasca Basin are relatively young (thousands of years) so mobile elements are likely adsorbed to secondary minerals. Selective leaching is the best geochemical method to assess the anomalies of these secondary minerals because mobile elements reach soils in water-soluble form and adsorb onto secondary minerals such as

carbonates and Fe-Mn oxides (Leybourne and Cameron, 2007). The question of how elements migrate from buried ore to the surface has been a topic of discussion for some time and the commonly discussed mechanisms are diffusion (due to concentration gradients) and advection. Leybourne and Cameron (2007) determined that in arid and semi-arid regions, mass advective transfer of water or air is most likely, because diffusion is orders of magnitude too slow.

Surficial geochemistry of radiogenic noble gases (^{222}Rn and ^{4}He) and soil in the Athabasca Basin has been most recently studied at the Millennium and Phoenix deposits (e.g. Power et al., 2012; Power, 2014; Krahenbil, 2014; Krahenbil et al., 2014; Hattori et al., 2014; Dudek and Hattori, 2015). Concentrations of ^{4}He are extremely high in groundwater close to the surface projection of the Millennium ore body (up to 789 times atmospheric ^{4}He), and are higher at deeper levels (Power, 2014; Krahenbil et al., 2014; Krahenbil, 2014; Hattori et al., 2014). Hattori et al. (2014) suggest that groundwater is likely carrying ^{4}He both laterally and vertically throughout sandstones, and Dudek and Hattori (2015) concluded that Rn in groundwater is likely locally sourced from nearby Ra or U due to its short half-life of 3.82 days.

^{4}He concentrations within groundwater above the Phoenix deposits in the Athabasca Basin are in equilibrium with the atmosphere (Power, 2014; Dudek and Hattori, 2015). Rn in groundwater at Phoenix ranges from 5- 2.04 x 10^{3} Bq/L, and Rn- in soil gas is below the detection limit of 3 Bq/L (Dudek and Hattori, 2015). Dudek and Hattori (2015) concluded that the most likely source of Rn in groundwater at Phoenix is U and Ra in upper sandstones and till, and ruled out other possible sources including drilling-related activity, vertical diffusion, bubbling, and groundwater upwelling.

Power (2014) completed soil geochemical surveys above the Phoenix and Millennium deposits. The study concluded that B-horizon soils leached by ammonium acetate at pH=5,

revealed anomalies of U, Cu, Pb above deposit-hosting shear zones and above mineralization. At the Phoenix deposit, anomalies of U, As and W were found directly above the ore body, as well as above the Hanging Wall shear zone, which hosts the Phoenix deposit (Power, 2014 and Power et al., 2012). Power et al. (2012) also compared the anomalies in soil and humus to the underlying sandstones at the Phoenix deposits, and found that anomalies in soil were mirrored in underlying siliciclastic rocks.

Glacial till geochemistry at the Millennium deposit shows Na_2O concentrations 20 times that of upper MFd sandstones (Power, 2014). This is likely due to the transport of basement lithologies during glaciation, and indicates a basement component within the tills at Millennium (Power, 2014). Repeat collection of humus and B-horizon soils above the Millennium deposit was completed by Krahenbil (2014) and confirmed a three-year repeatability of Cu, U and Pb anomalies in soil above faults, shear zones and U mineralization, previously identified by Power et al., 2012 and Power, 2014.

1.2.3 Radionuclides in Uranium Exploration

The ^{238}U decay chain (Table 1) can be divided by relatively long and short half-lives before and after ^{226}Ra, respectively (Ball et al., 1991). The three main isotopes of interest for this study are ^{238}U, ^{226}Ra and ^{222}Rn.

Table 1: List of nuclides in the U-238 decay series, their decay type and half-lives. After Lederer and Shirley, 1978 and modified from Ball et al., 1991.

Isotope	Decay Type	Half-Life
U-238	α	4.468×10^9 yrs
Th-234	β	24.1 days
Pa-234(m)	β	1.18 min
Pa-234	β	6.7 hrs
U-234	α	2.48×10^5 yrs
Th-234	α	7.52×10^4 yrs

Ra-226	α	1602 yrs
Rn-222	α	3.825 days
Po-218	α	3.05 min
Pb-214	β	26.8 min
At-218	α	2 sec
Bi-214	α	19.7 min
Po-214	α	1.64×10^{-4} sec
Tl-210	β	1.32 min
Pb-210	α	22.3 yes
Bi-210	α	5.02 days
Po-210	α	138.3 days
Tl-206	β	4.19 min
Pb-206	stable	

U is an actinide metal and its isotopes are all radioactive ^{238}U (99.3%) and ^{235}U (0.7%) and ^{234}U (0.0055%). It occurs naturally in concentrations of a few ppm in soil, rocks and water. The average concentration of U in Canadian Shield upper continental crust is 2.45 ppm (Shaw et al., 1986) and 1.0 ppm in Athabasca group sandstones (Quirt, 1985). U readily oxidizes to its hexavalent state in oxidizing conditions, making it highly mobile and creating a diffuse footprint of U throughout surface and groundwater, such as at Key Lake where mineralization occurs near surface (<100 m) (Dyck and Tan, 1978). U concentrations in natural groundwaters range between 0.1 and 10 μg/L however water associated with U ore-deposits can have concentrations as high as 1 mg/L (Hem, 1985). Organics such as the humic layer of soil adsorb and concentrate uranyl ions in soil, while bicarbonate ions in groundwater leach uranyl ions from soil causing a more widespread migration (Dyck and Tan, 1978).

Radium-226 is a decay product of ^{238}U and the parent radionuclide of ^{222}Rn. Radium is more mobile than U under reducing conditions, and its quantities are very low in groundwater (Moore, 1984). In oxidizing conditions, Ra will adsorb with other alkali earth metals; barium (Ba) as $BaSO_4$ and calcium (Ca) as calcite, and also onto Fe^{3+} and Mn^{4+} oxyhydroxides (Dyck

and Tan, 1978). In reducing conditions, there are no hosts for Ba, Ca and Ra salts to adsorb to so they remain in solution.

This study also focuses on the ^{238}U decay product ^{222}Rn, because its radioactivity was expected to be measurable in soil and water above the McArthur and Millennium U deposits. It is a naturally occurring, gaseous, radioactive isotope and is the decay product of ^{226} Ra. ^{222}Rn was originally discovered by Rutherford and described as "radium emanation" before it was declared a radioactive noble gas. It has been researched since the early 1900s; originally as a health benefit at many spas and later for U prospecting in the 1950s and 1960s (Ball et al., 1991), and later as a health hazard in basements above granitic bedrock. Based on Rn's half-life of 3.82 days, diffusion from a deposit must occur within 38.2 days (10 half-lives), or other transport mechanisms known to move gases upwards from mineralized zones such as upwelling of groundwater (Sader et al., 2011), vapour transport (Smee, 1998), or upwelling of water due to seismic activity (Cameron et al., 2002) are occurring. Alternatively, the source of Rn (^{226}Ra) could be local as suggested by Dudek and Hattori (2015).

Based on the ground-water flow rates in the Athabasca Basin, Earle and Drever (1983) determined that Rn could not travel more than a few meters within ten half-lives (40 days). This short travel distance makes diffusion from concentration gradients an unlikely method of transport of Rn from deeply buried U ore (Earle and Drever, 1983). Furthermore, there is often a lack of secular equilibrium between ^{222}Rn in groundwater and ^{238}U in the surrounding rock. Wood et al. (2004) suggested the intermediate nuclide (^{226}Ra) diffuses more rapidly than ^{238}U from crystalline rocks to fracture surfaces. Wood et al. (2004) developed a diffusion/adsorption model whereby ^{226}Ra ions diffuse through the porosity of crystalline rocks to fracture surfaces and adsorb onto weathering products at the rock-water interface. ^{222}Rn is then produced from the

decay of ^{226}Ra and enters the surrounding groundwater by alpha recoil (Wood et al., 2004). Alpha recoil is the process by which a radioactive daughter is mobilized from the position of its parent nuclide by its alpha decay energy (Sun and Semkow, 1998).

Rn is typically measured in Becquerels per cubic meter (Bq/m^3) that equals one disintegration per second (dps) and is extremely mobile as a noble gas. The bulk hydraulic conductivity of MFd sandstones measured during shaft sinking at McArthur River ranges from roughly 20 x 10^{-6} to 280 x10^{-6} cm/sec (Beattie et al., 2008) indicating that at maximum rate of groundwater flow Rn could travel less than 1 m in 40 days. Assuming a generally low hydraulic conductivity throughout the Athabasca Basin it is likely that the source of Rn is proximal to the shallow groundwater sampled at Millennium and McArthur River.

1.2.4 Groundwater Hydrogeochemistry

Groundwater hydrogeochemistry is important for this study because various elements within groundwater can determine its source and history. Frape et al. (1984) studied the chemical and isotopic compositions of groundwater throughout the Canadian Shield, and how they reflect different degrees of water-rock interaction. They concluded that major cation concentrations in shallow, geochemically immature groundwaters of the Canadian Shield are controlled by local rock compositions and that dissolution is the main form of reaction between water and rocks**.** They demonstrated that Cl and Br concentrations change little as major cations increase until total dissolved solids (TDS) reach 3 000-5 000 mg/L, and that the isotopic composition of shallow groundwater reflects local, present day precipitation. Water that occurs above 650 m is fresh or brackish and is dominated by Na-Ca-HCO_3 with local increases of sulfate, with TDS <10 000 mg/L.

Using O and H isotope compositions, Frape et al. (1984) determined that in the Canadian Shield, shallow groundwater falls close to or on the global meteoric water line and local surface waters plot on it or to the right due to surface evaporation (Frape et al., 1984).

CHAPTER 2: Grand Conclusion

The Millennium and McArthur River deposits have very similar groundwater. A major difference however is the abundance of ^{4}He within groundwater at Millennium. It has been reported by previous researchers that ^{4}He is high in groundwater at the Millennium deposit (Power, 2014; Krahenbil, 2014; Krahenbil et al., 2014), and this study found ^{4}He levels are in equilibrium with the atmosphere near the McArthur River deposit. ^{4}He within groundwater at McArthur River is in equilibrium with the atmosphere; potentially due to the large draw down of surface water from mining activity, or due to the absence of groundwater pathways such as faults and fractures from mineralization to the surface. Groundwater at Millennium and McArthur River have short residence ages (<20 yrs) and have O and H isotope values of present day, Saskatchewan precipitation. Groundwater chemistry does not correlate with Rn content, indicating the amount of the noble gas within groundwater is not controlled by the chemical variances of "fresh" groundwater. The physical conditions of the groundwater such as temperature, pH, electrical conductivity and oxidation-reduction potential do not individually correlate to Rn radioactivity, and therefore no connection can be deduced. The abundance of radiogenic nuclides within groundwater (Rn, He) and along fractures (Ra) is likely impacted by groundwater flow.

Rn in groundwater above both deposits ranges from 40 – 5000 cpm (measured with a Perkin Elmer 1220 Quantulus Ultra Low Level Liquid Scintillation Spectrometer) which is equivalent to approximately 1.7 – 217 Bq/L using the estimated conversion factor (1 Bq/L = 23 cpm) described in section 3.2.1. At Millennium, the highest Rn radioactivity was from groundwater in the discovery hole (CX-40), and directly above mineralization. Additionally, the groundwater at Millennium with the least amount of Rn occurred in groundwater farthest from

the deposit, in un-mineralized drill-holes. Groundwater sampling was more restricted at McArthur River because many DDH have been cemented for mine development purposes, making it impossible to sample directly above the ore deposit. There is no correlation between distance from the deposit and Rn radioactivity in McArthur River groundwater, however groundwater with high Rn content between 703 - 5342 cpm (approx. 30-232 Bq/L) is from drill-holes with either heavily fractured bedrock throughout or with >2.5 ppm U in shallow MFd sandstones. There is no perched mineralization in the top 100 m MFd sampled. Additionally, lower levels of Rn exist in groundwater proximal to shallow (< 60 m deep) sandstones with high (>2.5 ppm) U, indicating that Rn in groundwater is not caused by the mere presence of U in nearby sandstones.

At McArthur River Rn in soil gas is highest where concentrations of Ra in soil are also high. As well, replicate Rn in soil gas measurements taken within a 50 m diameter of each other at McArthur River have similar activities. These two findings suggest that Rn in soil can provide a general indication of the amount of Ra and Rn within nearby soil. It varies moderately throughout the region sampled, and is overall very low. Rn radioactivity in soil at Millennium and McArthur River is not anomalous, and is lower than Rn in soil levels throughout the Canadian Shield (Gascoyne et al., 1993). This means that given a blind exploration mission with no previous knowledge of concealed U deposits in the area, Rn in soil gas would not provide any vector towards deeply buried U mineralization, given similar soil conditions.

The abundance of Ra along core fractures provides a likely source for Rn in groundwater. The fracture coatings in the upper MFd sandstones contain Ra (< 32.3 pg/g) (it is less than). Fe-Mn-O-OH on core fracture coatings is likely scavenging the soluble Ra from groundwater based on the positive correlation between the two. Ra may also be adsorbed to carbonate and clay

minerals within upper MFd sandstones. Radium (half-life = 1602 yrs) decays to Rn, which then emanates from the solid phase into the groundwater. Due to the decrease in Rn in groundwater at the overburden/bedrock contact at Millennium, it is hypothesized that a location of higher permeability allows for faster horizontal groundwater flow. This increase in horizontal groundwater flow may dilute the local Rn signature that otherwise exists in slower moving groundwater because Rn would not have a chance to accumulate from nearby Ra.

At McArthur River, B-horizon soil samples contain less Ra (0.058 – 0.22 pg/g) than fracture material. As well, Ra in soil and Rn in soil gas are highest near the surface projection of the U deposit. One un-tested potential source for Rn is Ra within deep (>10 m) glacial till within the saturated zone. The increased surface area of the till compared to consolidated sandstone would likely increase the affinity for Ra to adsorb onto clays and Fe-Mn-oxy-hydroxides, although till contains very little clay and Fe-Mn-oxyhydroxide.

In conclusion, this thesis provides detailed geochemical data of shallow groundwater, B and C-horizon soil and shallow sandstone fractures above two high-grade, unconformity-associated U deposits. The presence of Rn in groundwater and soil is an indication of proximal Ra, which is a decay product of U, on shallow sandstone fractures and soil.

CHAPTER 3: Methods

3.1 Field Methods

The Millennium site was visited in August 2013 and June 2014 (Figure 6). August 2013 sampling consisted of preliminary groundwater collection from 9 diamond drill-holes (DDH) and 3 monitoring wells (MW). Sampling locations were chosen based on accessibility and with a ranging proximity to the surficial projection of the deposit (Figure 6). Soil samples were collected for ammonium acetate leach and near-total digestion with HF-HNO_3-HCl-$HClO_4$. In June 2014, three DDH that had high Rn radioactivity in 2013 were revisited to determine the repeatability of Rn radioactivity in groundwater, and to complete depth profiles. Rn in soil gas measurements were completed in-situ at disturbed and undisturbed areas surrounding DDH to determine if Rn in soil correlated to Rn in groundwater. Nearby Slush Lake was measured for the same parameters that groundwater was measured for, as an indication of local surface water conditions.

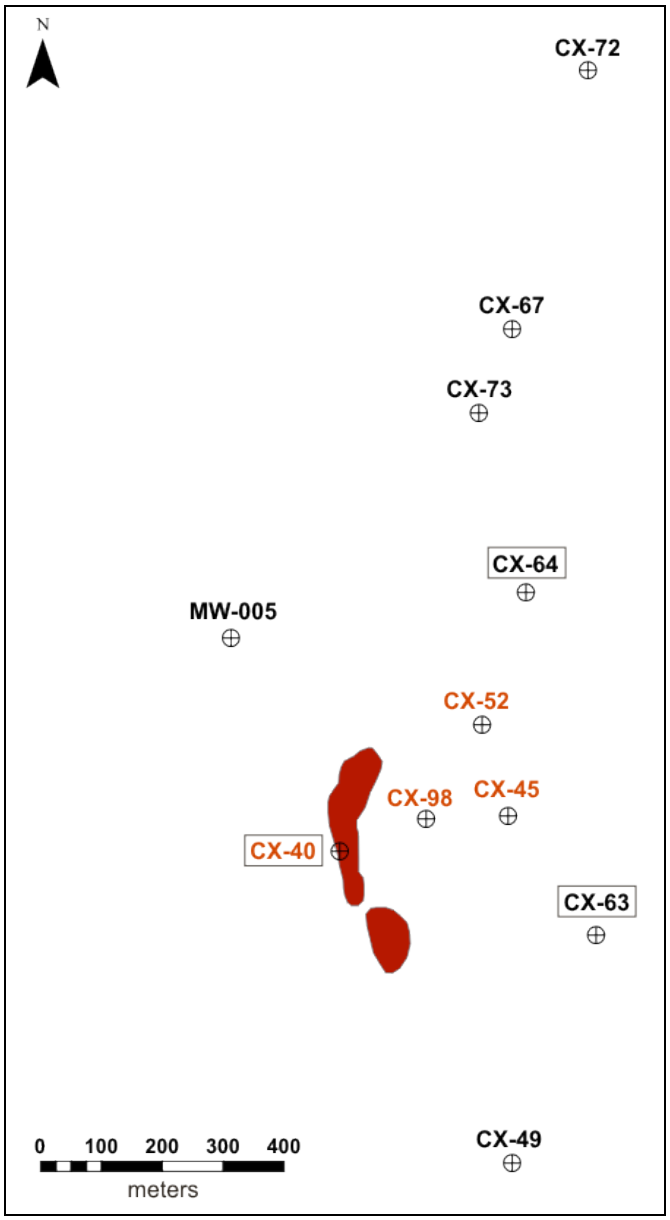

Figure 6: Surface projection of the (750 m deep) Millennium deposit (red) and drill-hole locations. DDH that intersect mineralization are in red, and DDH re-sampled in 2014 are outlined with a black box.

The McArthur River site was visited in August 2014 for sampling of groundwater, Rn in soil gas, B-horizon soil, and core fracture coatings (Figure 7). Shallow groundwater was collected from 6 sites and surface water was collected from nearby "Swamp Lake" and measured in-situ for temperature, pH, conductivity (µS/cm) and oxidation-reduction potential after sample

collection. B-horizon soils were collected surrounding drill holes and Rn in soil was also measured from nearby locations. Lastly, core samples were collected from the top 100 m of MFd sandstone from 13 DDH at McArthur River. Both high and low α-angle fractures were described and photographed and representative samples were collected.

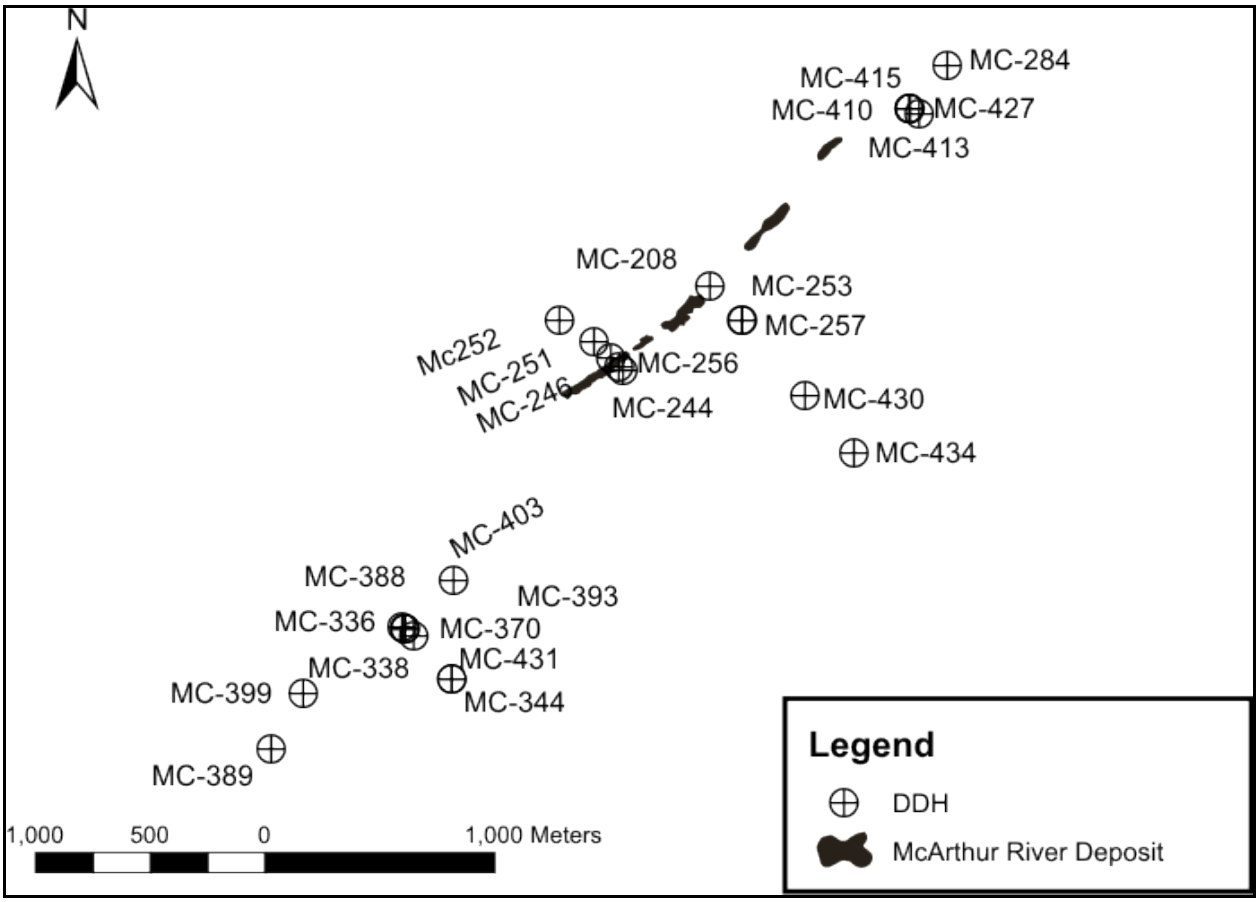

Figure 7: Plan view map of DDH sampled for various surficial geochemical media relative to the McArthur River deposit, represented by a black shape.

3.1.1 Water Sampling

In order to characterize the groundwater at McArthur River and Millennium the abundance of ^{3}H and minor elements (Cl, Br, F, N, S, U, Th, Pb), stable isotope composition ($^{13}C/^{12}C$, $^{2}H/H$, $^{18}O/^{16}O$, $^{3}He/^{4}He$), dissolved organic (DOC) and inorganic carbon (DIC) content, pH, temperature, total dissolved solids (TDS) and oxidation-reduction potential (ORP) of the

groundwater were analyzed. In the field, water samples were collected from un-purged, cased DDH with copper bailers, point source bailers or a Waterra Inertial Pump, depending on the conditions of the borehole and the depth of sampling. For example, copper bailers were used for sampling at the ambient water level, a Waterra Inertial Pump was used in unblocked boreholes at specific depths (up to 20 m), and a Solinst Model 429 Point Source Bailer was used to sample in boreholes at specific depths (up to 60 m). DDH are cased to the depth of the overburden, and most groundwater was sampled from within the casing. In these cases, the groundwater is representative of water from depths below the depth of casing.

Groundwater was bailed from DDH and lakes into 500 ml polyethylene terephthalate (PET) bottles, headspace-free. Water was measured for pH, conductivity, oxidation/reduction potential and temperature at the time of sampling. pH was measured with an Oakton *Waterproof pHTestr 2 Double Junction* pH meter that was calibrated with a pH 7 solution before field work, and rinsed with tap water after every measurement. Conductivity was measured with a Hanna Instruments *HI98129 pH/Conductivity/TDS Tester* with automatic temperature compensation. The probe was one point calibrated with a 1413 µS/cm solution at the start of the field season. ORP was measured with an Extech *ExStik™ Model RE300 Waterproof ORP Meter* that was calibrated with YSI 3682 Zobell Solution before fieldwork, and was rinsed with tap water after every measurement. ORP results are converted to Standard Hydrogen Electrode (SHE) values based on the electrode compensation of 200 mV.

Water was filtered to 0.45µm with Millipore Sterivex™ HV Filter Units. Water sampled for carbon analysis was kept headspace-free in pre-cleaned, 40 ml, amber borosilicate, 0.125" vials with silicone-teflon septa. Water sampled for cation analyses was acidified after filtration with HNO_3^- to keep cations in solution. In 2013, water was not filtered or acidified until a month

after collection, and therefore the U and Pb concentrations represent more than the dissolved portion of metals in the water. Water for all IC and ICP-MS analyses were stored in pre-cleaned, translucent, 40 ml Nalgene bottles after filtration. Water collected for tritium analyses was kept unfiltered in pre-cleaned, translucent, 500 ml Nalgene bottles.

Radon in water was measured using two extraction methods; The Field Extraction Method modified from Leaney and Herczeg (2006) and The Lab Extraction Method, modified from Lefebvre et al. (2013). For field extraction, 30 ml of water was removed from a PET bottle and replaced with 30 ml of *High Efficiency Mineral Oil Scintillator for the detection of radon in water and soil samples* (Perkin Elmer re-order number: 6NE9571). The sample was then shaken for 4 minutes, and left to stand until the water and oil separated. After phase separation, approximately 22 ml of mineral oil was extracted from the PET bottle and pipetted into a Teflon scintillation vial. Time and temperature of extraction were recorded for each extraction. For the Lab Extraction Method, water was collected into 250 ml glass bottles, headspace free, and kept at room temperature until shipped to Université du Québec à Montréal for analysis within 1-2 weeks of sampling.

3.1.2 Helium Sampling

Water-impermeable diffusion samplers made of ¼" Cu tubing and gas-permeable silicon tubing were deployed into several DDH (e.g. Sheldon et al., 2003; Sanford et al., 1996; Hamilton et al., 2005). Diffusion samplers were submerged under the water level at varying depths and left for more than 48 hours to equilibrate gas within the groundwater.

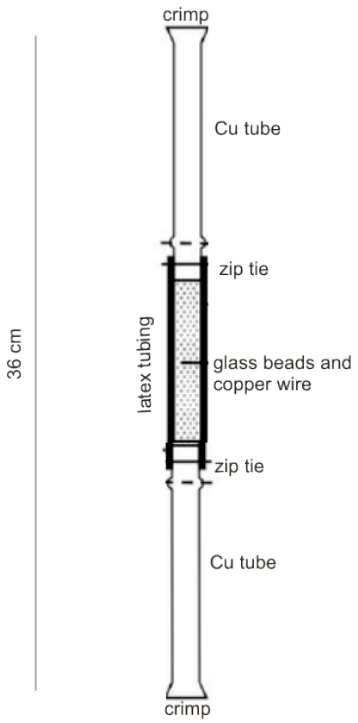

Figure 8: In-situ dissolved gas (He) sampler, modified after Sheldon et al., 2003. Dashed lines represent where the Cu tubes were crimped after retrieval.

The diffusion samplers were then retrieved and the Cu tubing was crimped to trap the diffused gases within the Cu tubing. The sample depth was measured based on the length of fishing line used to lower the sampler into the DDH. The ambient water level and time of deployment and retrieval were recorded. The condition of the sampler was noted upon retrieval in case of leakage or the presence of water within the sampler.

3.1.3 Soil Gas Sample Collection

Radon radioactivity within the pore spaces of soil was measured throughout the Millennium and McArthur River sites. Both disturbed and undisturbed soil was tested, to determine if soil is a source of Rn in groundwater. The portable radon monitoring system consists of a set of 250 ml cylindrical sample ionization chambers, and an electrometer (Figure 9).

Figure 9: Photograph of ionization chambers and the electrometer used to measure Rn in soil gas.

The ionization chambers were cleaned with deionized water-dampened kim wipes and dried before fieldwork, and evacuated with a hand pump prior to sample collection. After a sample location had been chosen based on proximity to the DDH of interest and vegetation cover, a 1.1 m long, 1 cm outer diameter metal pipe with a removable tip was hammered into the soil to a depth of 30-80 cm depending on the compaction and grain size of the till/soil. The soil gas sample was collected by attaching a tightly connected rubber tube to the top of the pipe, with a metal connection valve that attaches to a smaller rubber tube connected to a 250 cc plastic syringe (Figure 10). The 1.1 m metal pipe was evacuated once, then sealed off and the atmospheric air was pumped off. Next, the syringe was reattached and 250 cc of soil gas was sucked into the syringe, and clamped with pliers to prevent the gas from escaping. The narrow rubber tube and syringe were then connected to an evacuated ionization chamber.

Figure 10: Photograph of Rn in soil gas sampling equipment (250 cc plastic syringe, rubber tubing and 1.1 m x 1 cm metal pipe. Hand for scale.

The gas was transferred into the ionization chamber by opening the valve and releasing the pliers on the rubber tubing, allowing the gas to move from the syringe into the evacuated chamber. The chamber valve was then closed and the gas sample was left for 15 minutes to allow secular equilibrium between Rn and its short-lived daughters. The chamber was then connected to the electrometer with an alligator clip and the current produced from the ionization of the alpha particles is converted to kBq/m^3 by the instrument. The ionization chambers were evacuated immediately after each measurement, and an atmospheric sample was taken in between samples to confirm the absence of radioactive progenies deposited on the inside of the ionization chamber. The acceptable background value of an ionization chamber is 0.0 – 0.7 kBq/m^3 and method specific detection limit is 1 kBq/m^3. (www.radon.eu/rm2.html)

3.1.4 Soil Sampling Procedure

Soil samples were collected at the Millennium and McArthur River sites in undisturbed locations with developed vegetation close to the DDH sampled for Rn in water (Figure 23 and 44). Soil was sampled up to 1 m deep with a hand-held Dutch auger. In most locations the B-horizon soil was collected, and in fewer cases C-horizon soil was collected. GPS coordinates of each location were recorded.

3.1.5 Collection of Drill Core Fracture Coatings

Core fracture coatings refer to the minerals present on the surface of open fractures that were exposed to groundwater. The top 100 m of MFd sandstone from 13 DDH at McArthur River were examined for open fractures that appeared to have been a result of natural fracturing/faulting rather than drilling. Fractures that were likely the results of drilling were not

collected and were identified as high angle fractures (90 degrees relative to the core axis) with fresh and jagged fracture surfaces, often occurring at the end and beginning of core boxes. Fractures were collected as 10 cm portions of core containing both sides of the fracture. The depth was recorded and each fracture was photographed in place and open faced to document its color and α-angle (Appendix B).

3.2 Laboratory Methods

3.2.1 Radon in Water Analyses

The measurement of Rn in water by liquid scintillation counting (LSC) requires mixing water with a scintillant to concentrate Rn from the water into the organic phase. As Rn alpha-decays to its daughter products ^{218}Po and ^{214}Po, the energy is absorbed by the scintillant and emitted as light and detected by the photomultiplier tube within the LSC. The energy of the light emitted by the sample identifies the specific radionuclides present in the water and is reported in counts per minute (cpm). Raw cpm is converted to activity (Bq/L) by dividing counts by the efficiency of the extraction and the efficiency of the LSC.

$$Activity\ (\frac{Bq}{L}) = counts\ (cpm) \div (Eff.Extraction * Eff.LSC)$$

Equation 1: Conversion equation from raw counts per minute to activity (Bq/L) by incorporating the efficiency of the radon extraction and the efficiency of the liquid scintillation counter

Rn in water extracted with the Field Extraction Method was measured at the University of Ottawa with a Perkin Elmer 1220 Quantulus Ultra Low Level Liquid Scintillation Spectrometer. 20 ml plastic scintillation vials containing the extracted mineral oil were analyzed and blanks were run every 20 samples. Raw counts were decay corrected to the amount of Rn at the time of collection using the equation below. Counts were also volume corrected based on the ratio of scintillant added to the water and the amount of scintillant extracted.

$$N = No*e^{-\lambda t}$$

Equation 2: Radioactive decay equation, where N = Number of decays counted, No = initial amount of decays, λ

$$\text{Final cpm} = \text{Initial cpm}*(V_{Extracted}/ V_{Added})$$

Equation 3: Extraction volume correction equation where final counts per minute are calculated by multiplying initial counts per minute by the ratio of the volume of scintillant extracted (~22 ml) to the volume of scintillant initially added (~30 ml).

Water collected for the Lab Extraction Method was analyzed on a Hidex 300 SL Automatic TDCR Liquid Scintillation Counter at the Université du Québec à Montréal (UQAM) using the Maxilight scintillant for the Direct Method extraction described by Lefebvre et al., (2013).

Rn radioactivity is reported in both Bq/L and cpm throughout the thesis because two methods of sample collection and measurement were compared to determine the best method for Rn in water analysis. Rn activity ranged from 31 – 5026 cpm and 2 – 278 Bq/L at Millennium in 2013. The two methods are comparable by dividing cpm results by a factor of 23 +/- 9. Cpm values from 2013 are higher than Bq/L values because they are not corrected for efficiency of extraction or spectrometer efficiency.

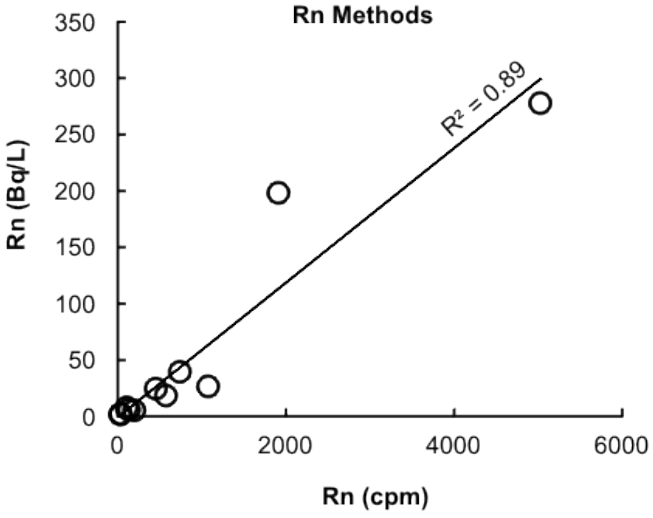

Figure 11: Comparison of two methods of Rn analysis; Rn in water direct method (Bq/L) and Rn in oil extraction method (counts per minute). Relative values correlate well ($R^2 = 0.89$).

3.2.2 Water Chemistry

Water samples were analyzed for Cl^- and F^- using Ion Chromatography (IC) at the University of Ottawa. In 2013, samples were diluted 5x with Milli Q water, and filtered a week after sampling, therefore U and Pb contents are more than the dissolved portion. In 2014 samples were not diluted. Water was also analyzed using Inductively Coupled Plasma Mass Spectrometry/ Emission Spectroscopy (ICP-MS/ES) at the University of Ottawa for Pb, Th, U, Br, SO_4^{2-}, and NO_3^{2-}. Cation aliquots were diluted 5x with 0.5 N $HNO3^-$ and anion aliquots were diluted 5x with 50 µL of NH_3 and the remaining 4.995 mL with Milli Q water.

3.2.3 Stable Isotope Compositions

Water was analyzed for O, H and C isotopes at the G.G. Hatch Stable Isotope Laboratory at the University of Ottawa. The isotopic composition of organic carbon was determined by the analysis of CO_2 produced by combustion on an Elementar Isotope Cube Elemental Analyser followed by "trap and purge" separation and on-line analysis by continuous-flow with a DeltaPlus Advantage isotope ratio mass spectrometer coupled with a ConFlo III (www.isotope.uottawa.ca/techniques/organic-solids.html, 2015). Data was normalised using internal standards, and $\delta^{13}C$ values were calculated relative to Vienna Pee Dee Belemnite (VPDB). The 2σ analytical precision is 2% for C concentrations, and +/- 0.2‰ for C isotopes.

$^2H/^1H$ and $^{18}O/^{16}O$ stable isotope ratios of the DDH water were measured on a Triple Isotope Water Analyzer (TIWA-45EP). Precision for δ^2H is 0.5‰ and for $\delta^{18}O$ is 0.1‰. 1.0 ml of water was pipetted into 2 ml GC septa vials for samples and standards. Each sample and standard was injected 10 times. The data from the first two to four injections were discarded to

minimize memory effect between samples/standards. The other data were averaged provided that there were no flags on the injections. Three internal water standards (Table 2) were run at the beginning and end of each run, as well as after every 10 samples throughout the run. A blind standard (W-20) was run as an unknown. The internal standards are calibrated using Vienna Standard Mean Ocean Water (VSMOW), (Standard Light Antarctic precipitation (SLAP) and Greenland Ice Sheet Precipitation (GISP), and are used to normalise the data.

Table 2: Isotope composition of three internal standards and one blind standard used to calibrate O and H data.

Standard	^{2}H (‰)	^{18}O (‰)
W-7	-198.5	-24.55
W-10	-85.9	-11.84
W-9	11.27	-5.06
W-20	-5.87	-7.34

3.2.4 Tritium

In 2013, 10 ml of groundwater from DDHs was directly measured by LSC for tritium by adding 10 mL of water into 20 ml plastic scintillation vials with 10 ml of Ultima Gold. This method resulted in below detection levels (<0.3 Bq/L) of tritium in most waters. In 2014, water samples were enriched via electrolysis from 250 ml to 25 ml prior to LSC, resulting in detectable levels of tritium.

The tritium enrichment procedure was taken after Plastino et al. (2007). First, 260 ml of sample water was mixed with 1 mg of BIO-RAD AG 501-X8 resin and shaken for 3-4 hours to remove excess ions within the water prior to electrolysis. Once conductivity was < 200 umho/cm, 250 ml of a sample was mixed with 1g of NaOH in a stainless steel anode cell, with the cathode placed inside. Each cell was then connected in series and run with a voltage of 2.2-2.7 V. The cells sat in a cooling bath throughout electrolysis (4-8 ºC) and the volume of sample

reduced from 250 ml to 15 ml. Isotopic fractionation and possible contribution of external source of tritium are prevented within this closed system. After enrichment, the sample was distilled under vacuum to remove any remaining contaminants such as NaOH. After distillation, 10 ml of the sample was transferred to a 20 ml plastic vial with 10 g of Perkin Elmer Ultima Gold fluor. Tritium was analyzed on a Perkin Elmer 1220 Quantulus Ultra Low Level Liquid Scintillation Spectrometer at the University of Ottawa.

Figure 12 and Figure 13 show the importance of electrolytic enrichment for precision with tritium analysis. Figure 12 shows precise tritium values, after electrolytic enrichment and distillation, with error ranging from 1.7 – 2.5 TU. Figure 13 shows un-enriched tritium results with error greater than the tritium result. Blanks were put through the same enrichment procedure and ranged between 0.0 – 0.2 TU.

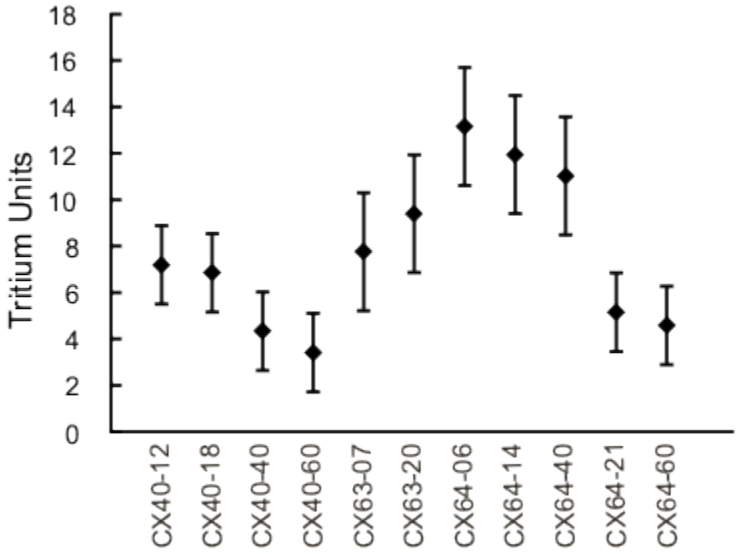

Figure 12: Bar graph of tritium contents (in tritium units) of DDH groundwater at Millennium collected in 2014. Error bars represent 1 standard deviation. ID numbers represent year (2014) DDH number (CX00) and the depth of sample.

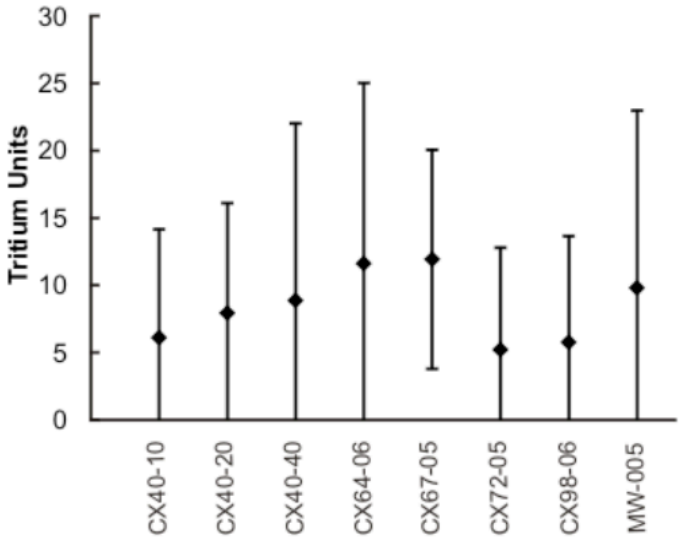

Figure 13: Tritium content expressed in tritium units, with error bars representing +/- 1 standard deviation. ID numbers represent DDH number (CX00) and the depth of sample. As is illustrated by the graph, error exceeds tritium content of these samples indicating the necessity of enrichment for the 2014 samples.

3.2.5 Helium

$^{4}He/^{3}He$ values for Millennium diffusion samplers were analyzed on a quadrupole mass spectrometer at the Noble Gas Laboratory at UQAM (Power, 2014; Krahenbil, 2014; Krahenbil et al., 2014). In 2015, McArthur River samples were analyzed at the University of Ottawa on a Thermo Fisher Scientific Helix SFT mass spectrometer It is suited to simultaneously collect two isotopes of He at mass 3 and 4.

3.2.6 Soil

B and C-horizon soil from Millennium and McArthur River was sent to ACME Labs in Vancouver, BC for geochemical analyses. All soils were dried at 60ºC and screened to -180 microns (-60 mesh). Two geochemical analyses were performed on the soil. First, splits of each soil sample were digested by selective 1M ammonium acetate leach at pH=5 (AA5) and analysed by ICP-MS to determine exchangeable cations absorbed by clay and elements co-precipitated

with carbonates. Secondly, 0.25 g splits of each soil sample underwent a multi-acid digestion with HF-HNO_3-$HClO_4$ and analysed by ICP-MS (Bureau Veritas Mineral Laboratories, 2015).

3.2.7 Core Fractures

Several fractures were chosen for analysis depending on a) the abundance of material coating the fractures, and b) the amount of partial U reported from similar core depths by S. Guffey of Memorial University of Newfoundland. A total of 15 fractures were analyzed from 9 DDH at McArthur River chosen out of the 50 collected. Fracture coatings were scraped off core by hand and then crushed in a ceramic disk mill for 5 minutes. The disk mill was cleaned via silica sand crushing, rinsed with ethanol and water, and dried in between samples.

3.2.8 Powder X-ray Diffraction

Core samples were analyzed on a Philips PW 3020 X'Pert Diffractometer with a copper anode (www.xray.uottawa.ca/en/powder_diffraction.html) to identify the mineralogy of the fracture coatings. Scan speed ranged from 0.25 – 0.4 deg/min, and the scan ranged from 2.0 – 57 degrees.

3.2.9 γ-ray Spectrometry

Prior to γ-ray counting, core and soil samples were weighed and sealed with epoxy in 10 ml glass vials for over 3 weeks to allow for ^{226}Ra to decay and reach secular equilibrium with its daughter products including ^{214}Pb, ^{214}Bi and ^{222}Rn. 13 drill core samples and 10 soil samples were analyzed by γ-ray spectrometry for ^{226}Ra. The ^{226}Ra radioactivity of every sample was measured using an Ortec Gamma-ray Spectrometer with a high-purity germanium crystal and an active well detector (54.6 mm in diameter and 65 mm deep). ^{226}Ra only has one γ-ray energy

peak at 186 KeV, which is coincidence with the ^{235}U peak. Therefore, we used the ^{214}Pb energy peaks at 352 KeV and 295 KeV as a proxy for ^{226}Ra, because ^{214}Pb is a daughter product of ^{226}Ra and a parent isotope to ^{222}Rn. Counting time varied from 3 hrs to 40 hrs depending on the amount of ^{214}Pb within a sample, until there were at least 5000 ^{214}Pb counts. The γ-ray spectra were analyzed with Ortec Maestro 7 Multichannel Analyzer Application Software.

Total ^{214}Pb counts were individually determined using the Maestro software by integrating the peaks and subtracting the background radioactivity to give a net area count of the peak. The net counts (counts – background) were then divided by the time (seconds) of counting to give the cps for each sample. The energy of the peak, full width half maximum (FWHM) and error of the peak were recorded to monitor drift in the detector and detector resolution. Detector resolution was determined from the FWHM based on an expected Gaussian distribution of each peak at a specific energy. The FWHM of the 352 Kev ^{214}Pb peaks ranged between 1.62% and 2.71%. The net cps was then divided by the relative intensity of the 352 Kev γ-ray peak (37.6%), the detector efficiency (0.064%), and the mass of the sample in grams to calculate the Bq/g for each sample. The impact of the density of the sample matrix was not taken into consideration because the main goal of this experiment was to determine the relative radioactivity of core fractures compared to soil and its relation to the Rn in groundwater. These samples were all the same sample matrix and therefore would have a similar impact on detector efficiency. ^{226}Ra concentrations should be considered a minimum due to the assumptions listed above (Appendix A).

3.2.10 Sequential Leach Experiment

Fracture coatings were sequentially leached with increasing concentrations of HNO_3^- to determine the potential mineralogical hosts of different elements. Acid concentrations ranged

from Milli-Q water to 0.05 N, 0.1 N, 0.5 N and 2 N nitric acid. Fracture coatings were weighed to 0.5 g and diluted with 10 ml of Milli-Q and left over night. Samples were then centrifuged to separate the water from the fracture fillings. 2 mL of the leachate was then removed and acidified with 0.5 N HNO_3^- to prepare for ICP-MS analysis. For the second leach, the remaining water-leach samples were acidified to 0.05 N and left overnight. Again, samples were centrifuged after leaching to separate acid from fracture coatings, and 2 ml of the leachate was transferred and diluted with 0.1 N HNO_3^- for ICP-MS purposes. For the third leach, the remaining second-leach samples were acidified to 0.1 N and left for 3 hours. The samples were then centrifuged and 2 ml of the leachate was separated and diluted with 0.1 N nitric acid for ICP-MS purposes. The same procedure was followed for the remaining two leaches, where samples were acidified to 0.5 N and finally 2 N HNO_3^- . All 5 leachates were analyzed via ICP-MS at the University of Ottawa for P, Ca, Fe, Mn, Ba, Ni, Cu, As, Zr, Th and U.

CHAPTER 4: Examining radiogenic elements in soil and groundwater above the deeply buried Millennium Uranium Deposit, Saskatchewan

4.1 Introduction

The Millennium deposit was discovered in 2000 by Cameco Corporation and is part of the Cree Lake Extension project within the southeastern portion of the Athabasca Basin. Located 35 km north of the Key Lake mill (Figure 2) the Millennium deposit was initially discovered by electromagnetic and gravity geophysical surveys, and further defined by diamond drilling (Robertson, 2006). Cameco's Millennium project was chosen for this research as part of the Canadian Mining Innovation Council's Footprints project because it is a high-grade (2.39 % U_3O_8) basement-hosted U deposit, which has 75.9 M lbs indicated resource at a depth of approximately 750 m as of December 31, 2014 (Cameco Corporation, 2014). Millennium is deeply buried under glacial till and bedrock making it significantly harder to discover than a high-grade U deposit closer to the surface.

This portion of the study examines Rn gas within groundwater and soil above the Millennium deposit. The objective is to determine if there is a surficial gaseous footprint of Rn above the deposit, and if it would be a useful tool for future U exploration. It further aims to identify the source(s) of said surficial Rn footprint.

The first site visit for this study was completed in August 2013, and groundwater (n=32) was collected from cased and cemented diamond drill-holes (DDH) (n=11) and shallow monitoring wells (n = 2) (Figure 6).

Sample locations were chosen based on varying proximity (0 - 700 m) to the vertical projection of the deposit at surface, their proximity to the vertical projection of faults, and the intersection of high-grade U within the drill-hole. The following summer (2014), a more focused sampling strategy was performed to determine the Rn radioactivity at varying depths within three

drill-holes. Rn in soil gas and B and C soil horizons were also collected in 2014 in an attempt to identify a surficial source of Rn.

4.2 Geologic Setting

The Millennium deposit is hosted within the Wollaston Group meta-sediments, roughly 100 m below the unconformity between the Manitou Falls Formation and the basement rocks (Wood et al., 2012; Juhojuntti et al., 2012). Hydrothermal alteration overprints both the lower sandstone units (MFa/Read) and basement lithologies which consist of meta-pelite, meta-semipelite, meta-arkose, calc-sillicate and quartzite (Annesley et al., 2005). The basement alteration from distal to proximal is; chlorite and illite, into increasing argillite with major illite and dravite (Juhojuntti et al., 2012). The main hydrothermal conduit in the area is a North-South striking major fault zone that dips 55º east. This zone occurs at the base of the lower calc-silicate assemblage (Figure 14) and is identified as angular wall rock clasts within a clay/dravite matrix (Juhojuntti et al., 2012). This major fault zone is 10 m thick and is a reverse thrust and is interpreted to be the conduit for oxygenated, U-bearing fluids to travel from the sandstones down into the basement (Juhojuntti et al., 2012). As the U-bearing fluids travelled along structural planes, U precipitated within structural and chemical reducing traps (Juhojuntti et al., 2012).

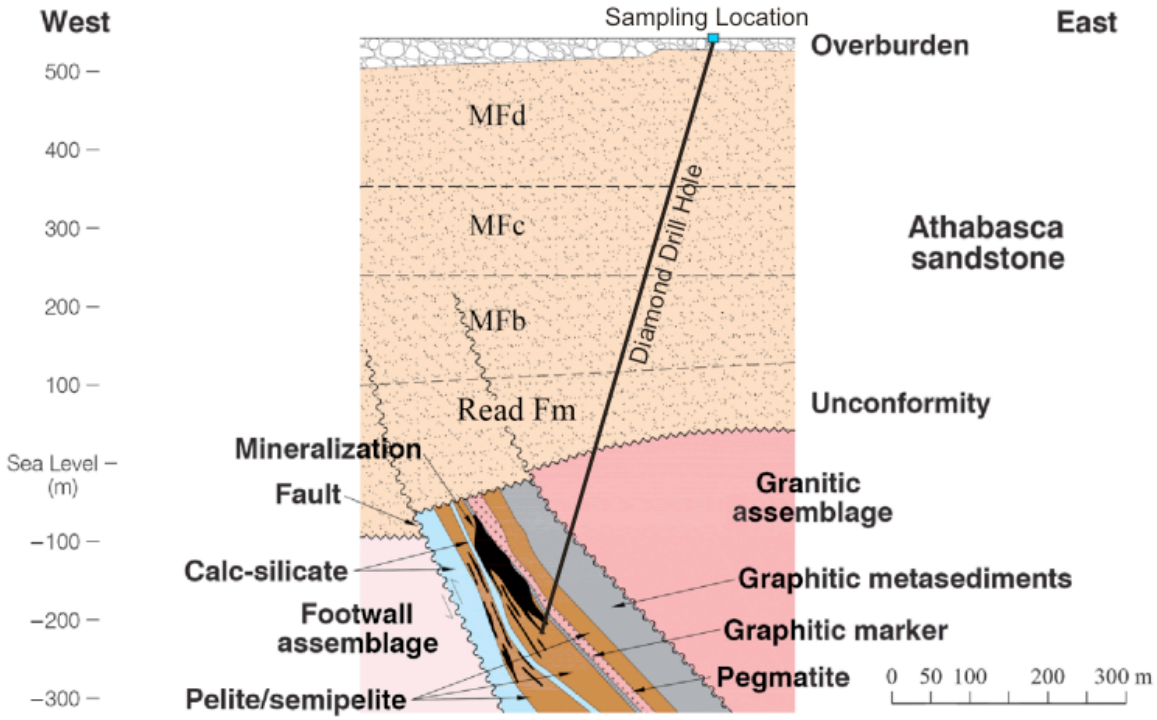

Figure 14: Schematic geological cross section of the Millennium deposit, depicting the vertical distance from soil and groundwater sampling locations to mineralization and faults, modified after Wood et al. (2012).

4.3 Results

4.3.1 General Groundwater Characteristics

Groundwater was collected from drill-holes and measured in-situ for pH and conductivity. Ambient water levels ranged from 0 – 13 m below the surface. pH ranged from 6 - 9.4, and shows no correlation with depth at a given hole (Figure 15). These neutral groundwaters are presumably less reactive with surrounding soil and bedrock than acidic or alkaline waters and therefore the dissolution of non-water-soluble minerals and elements is not extensive.

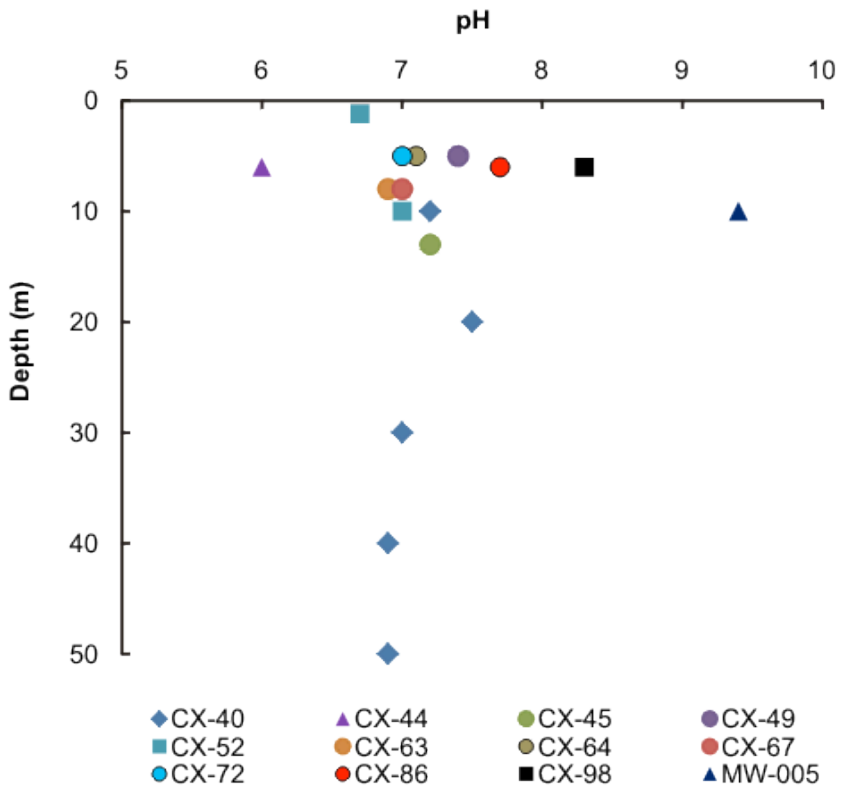

Figure 15: Scatterplot showing the lack of correlation between pH and depth of sampling.

The range from pH 6-9 in groundwater near the water table (10 m depth) and a lack of correlation with depth indicates acidity (hydrogen ion concentration is waters) is relatively stable (Figure 15). It is similar to groundwater measured by Earle and Drever (1983) in the Athabasca Basin, which ranged from pH 5-9. Earl and Drever (1983) found that the majority of their samples had a pH between 6 and 7. In CX-40, pH is near neutral from 10 m - 50 m depth below surface, indicating no change in acidity or alkalinity with depth in that DDH.

Conductivity ranges from 43 – 538 µS/cm, and decreases with increasing depth in the drill-hole closer to mineralization, CX-40 (Figure 16).

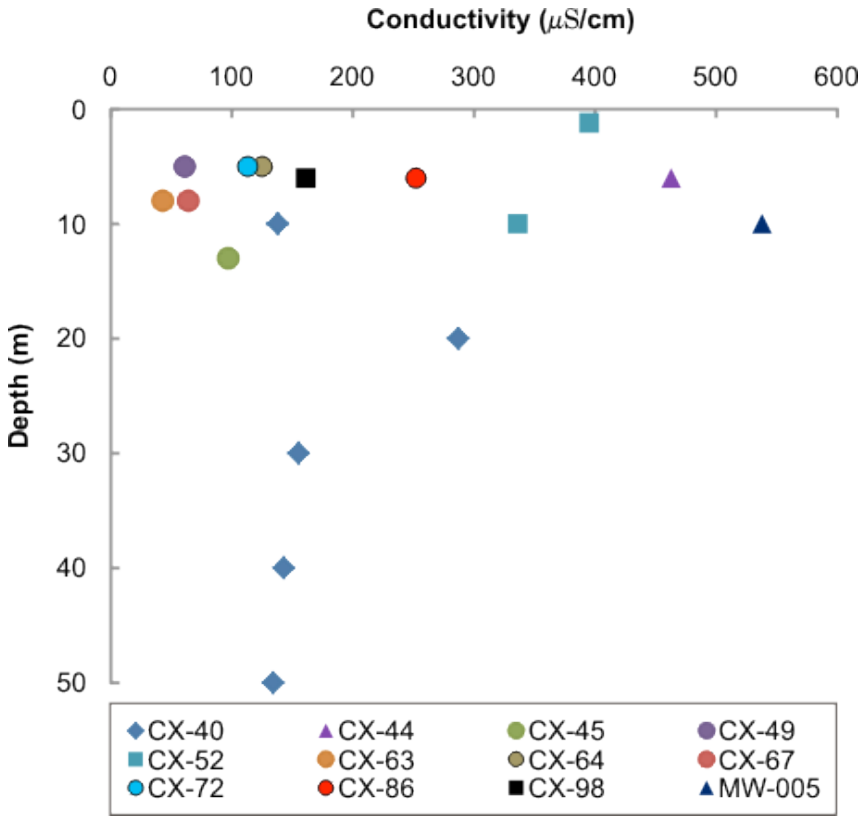

Figure 16: Scatterplot comparing conductivity to water depth (m from surface) in 12 drill-holes sampled in 2013. CX-40 has the largest variance in sample depth and shows a decrease in EC with depth. CX-52 also shows a decrease in EC from 0 to 10 m depth.

The range of conductivity indicates that there is a variance of dissolved salts within the groundwater near surface (Figure 16). The overall range in conductivity indicates fresh water (<1000 mg/L, Freeze and Cherry, 1989). These conductivities are similar to those of groundwater throughout the eastern and southern Athabasca Basin from 100-300 m depth measured by Earl and Drever (1983), which have TDS of <500 mg/L. Samples without a conductivity measurement (Table 3) were unable to be measured in the field, and later laboratory measurements would not be representative of the natural conductivity of the groundwater.

Table 3: General groundwater characteristics are represented in the table below, including pH, EC, ambient water level, depth of sampling, depth to casing, and the date the sample was collected. All depths are in metres below surface.

Drill Hole	pH	Conductivity (µS/cm)	Water Level	Casing Depth	Sample Depth	Sampled below casing?	Date
Slush Lake	-	-	0.0	n/a	0	n/a	June-22-14

13CX-40-10	7.2	138	9.1	21.5	10	No	August-28-13
13CX-40-20	7.5	287	9.1	21.5	20	No	August-27-13
13CX-40-30	7.0	155	9.1	21.5	30	Yes	August-28-13
13CX-40-40	6.9	143	9.1	21.5	40	Yes	August-28-13
13CX-40-50	6.9	134	9.1	21.5	50	Yes	August-28-13
13CX-44-06	6.0	463	5.8		6		August-29-13
13CX-45-13	7.2	97	12.8	21.7	13	No	August-29-13
13CX-49-05	7.4	61	4.8	9.3	5	No	August-28-13
13CX-52-01	6.7	395	1.2	9.2	1	No	August-28-13
13CX-52-10	7.0	336	1.2	9.2	10	Yes	August-27-13
13CX-63-08	6.9	43	7.8	8	8	Yes	August-28-13
13CX-64-05	7.1	125	4.8	13.7	5	No	August-29-13
13CX-67-08	7.0	64	7.5	14.1	8	No	August-29-13
13CX-72-05	7.0	113	4.6	17.4	5	No	August-29-13
13CX-86-06	7.7	252	6.0		6		August-28-13
13CX-98-06	8.3	161	5.8	9.2	6	No	August-29-13
13MW-005-10	9.4	538	9.6	14	10	No	August-29-13
13MW-005-13	6.2	-	9.6	14	13	No	August-29-13
14CX40-12	8.3	-	10.7	21.5	12	No	June-20-14
14CX40-18	7.8	-	10.7	21.5	18	No	June-20-14
14CX40-40	7.3	-	10.7	21.5	40	Yes	June-22-14
14CX40-60	7.2	-	10.7	21.5	60	Yes	June-22-14
14CX63-07	8.0	-	6.8	8	7	No	June-21-14
14CX63-20	7.5	-	6.8	8	20	Yes	June-21-14
14CX64-06	7.3	-	5.7	13.7	6	No	June-21-14
14CX64-06	-	-	5.7	13.7	6	No	June-21-14
14CX64-14	7.7	-	5.7	13.7	14	Yes	June-21-14
14CX64-21	7.6	-	5.7	13.7	21	Yes	June-21-14
14CX64-40	8.2	-	5.7	13.7	40	Yes	June-21-14
Statistical Summary:							
Min	6.0	43	0.0		0		
Max	9.4	538	13.3		60		
Median	7.3	143	6.8		10		
Mean	7.4	206	7.2		16		
SD	0.7	143	3.1		15		

The general groundwater parameters measured in the field at the Millennium deposit (pH, EC) are typical to surface water conditions, or shallow groundwater in the Canadian Shield

(Sanders, 1998) and the eastern Athabasca Basin (Earle and Drever, 1983). All samples are compared as one group when considering further parameters such as water chemistry and radioactivity except for the monitoring well sample MW-005 due to its higher electrical conductivity.

4.3.2 Groundwater Chemistry

Natural groundwater composition is a reflection of solutes derived from the atmosphere, soil, water-rock interactions, and chemical reactions occurring below the land surface (Hem, 1985). It was expected that minor ion concentrations in the shallow groundwater at Millennium will be relatively low, based on the neutral pH and electrical conductivity (a proxy for total dissolved solids) that were measured in the field. In August 2014 groundwater was analyzed for minor anions (F^-, Cl^-, SO_4^{2-}, NO_3^-, Br^-) and cations (U, Pb).

Cramer and Nesbitt (1994) completed a hydrogeochemical study of representative groundwaters around the Cigar Lake U deposit. The range of each analyte determined by that study is used below to compare results from Millennium to other groundwaters in the Athabasca Basin. Fluoride concentrations at Millennium ranged from 0.0094 – 1.7 mg/L (Table 4, Figure 18), and have a wider range than F concentrations at Cigar Lake (<0.25 – 0.54 mg/L). Chloride concentrations ranged from 0.18 – 51 mg/L (Table 4, Figure 17) at Millennium and also had a wider range than at Cigar Lake (0.23-24.9 mg/L). In 2013 F ranged from 0.11 to 3.6 mg/L and Cl^- ranged from 0.31 to 47 mg/L (Table 4). Mean chloride concentration was 12 mg/L in 2013 and 9.7 mg/L in 2014 (Figure 17, Table 5). Sulphate concentrations are much higher in Millennium groundwaters (0.24 – 18 mg/L) (Table 3) than at Cigar Lake (0.17 – 4.88 mg/L). Nitrate is in similar concentrations at Millennium and Cigar Laker and ranged from 0.089 to 1.4 mg/L (Table 4) and <0.65 - 1.44 mg/L, respectively. Lastly, Br is in much lesser concentrations

at Cigar Lake than at Millennium, and ranged from <0.01 - 0.28 mg/L and 0.0049 to 2.7 mg/L (Table 4), respectively. All anion concentrations are reasonable for surficial groundwaters (Faure, 1998), and as expected concentrations of Cl are higher than F, indicating these waters are comparable to surface and shallow groundwater in the Athabasca.

Table 4: Minor ion concentrations of groundwater.

2014 Samples	F (mg/L)	Cl (mg/L)	SO_4 (mg/L)	NO_3 (mg/L)	Br (mg/L)	U (µg/L)	Pb (µg/L)
14CX40-12	0.354	7.57	0.243	0.137	0.391	4.36	<0.022
14CX40-40	0.124	15.1	0.88	<0.032	0.761	<0.002	<0.002
14CX40-18	0.104	7.7	0.533	0.162	0.42	0.299	956
14CX40-60	0.175	16.9	0.28	0.156	0.989	<0.002	<0.002
14CX63-20	0.987	0.395	17.9	1.42	0.005	<0.002	<0.002
14CX63-07	0.218	0.373	1.73	0.118	<0.001	5.58	1.36
14CX64-06	0.134	3.27	0.517	0.139	0.13	4.14	17.7
14CX64-40	0.153	46.4	8.43	0.093	2.44	<0.002	<0.002
14CX64-14	0.053	3.25	0.495	0.089	0.124	1.4	2.47
14CX64-60	0.364	50.5	7.53	<0.032	2.68	<0.002	<0.002
14CX64-21	0.094	3.28	0.806	<0.032	0.09	0.358	<0.022
Slush Lake	0.02	0.797	2.41	<0.032	<0.001	0.405	4.07
LOD	0.0016	0.0071	0.002	0.032	0.001	0.0002	0.022
Min	0.0094	0.176	0.243	<0.032	<0.001	0.299	1.36
Max	1.66	50.5	17.9	1.42	2.68	5.58	956
Mean	0.271	9.7	3.48	0.289	0.803	2.36	196
σ	0.391	14.8	5.34	0.458	0.978	2.26	425
2013 Samples	F (mg/L)	Cl (mg/L)				U (µg/L)	Pb (µg/L)
13BH127-09	0.165	0.313	-	-	-	0.034	0.03
13CX40-10	0.187	6.65	-	-	-	8.66	0.158
13CX40-20	0.204	5.55	-	-	-	22.7	0.297
13CX40-30	0.144	7.75	-	-	-	16.1	12.7
13CX40-40	0.168	6.4	-	-	-	215	0.135
13CX40-50	0.161	7.17	-	-	-	230	0.534
13CX44-06	3.57	31.7	-	-	-	0.301	38.3
13CX49-05	0.239	0.335	-	-	-	0.012	0.043
13CX52-01	0.111	47.2	-	-	-	0.052	0.035
13CX52-60	0.189	46.9	-	-	-	0.03	0.019

13CX53-06	0.223	33.8	-	-	-	0.11	0.144
13CX63-08	0.215	1.49	-	-	-	0.322	4.72
13CX64-05	0.189	1.23	-	-	-	1.39	0.012
13CX67-08	0.294	0.366	-	-	-	0.018	0.023
13CX72-05	0.234	4.94	-	-	-	0.07	4.03
13CX98-06	0.194	1.16	-	-	-	65.6	0.033
13CXMW-05	0.387	1.77	-	-	-	67.5	0.086
13MX005-13	0.227	1.23	-	-	-	1.95	2.85
LOD	0.0014	0.0136	-	-	-	0.0002	0.022
Min	0.111	0.313	-	-	-	0.012	0.012
Max	3.57	47.2	-	-	-	230	38.3
Mean	0.37	12.4	-	-	-	35.0	3.56
σ	0.736	15.7	-	-	-	71.5	9.22

Sample ID represents the year (e.g.14 = 2014) followed by the DDH name (e.g. CX-40) and the depth (m) below surface (e.g. 12). LOD = level of detection, Min = minimum concentration, Max = maximum concentration, Mean = average concentration and σ = standard deviation ($\sqrt{variance}$). 2013 water samples were filtered 3 months after sampling, and therefore the U and Pb content includes those adsorbed on particulates.

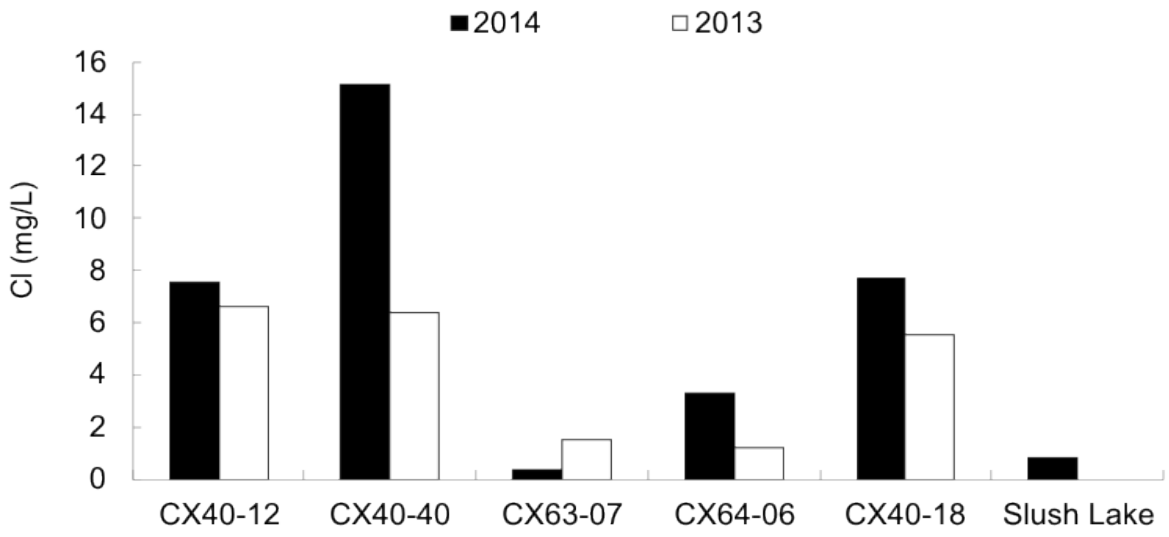

Figure 17: Bar graph comparing Cl content in groundwater taken from the same depth (m below surface) in 2014 (black) and 2013 (white). Level of detection for Cl is 0.0136 in 2013 and 0.071 in 2014. Slush lake Cl content is given for comparison to local fresh water.

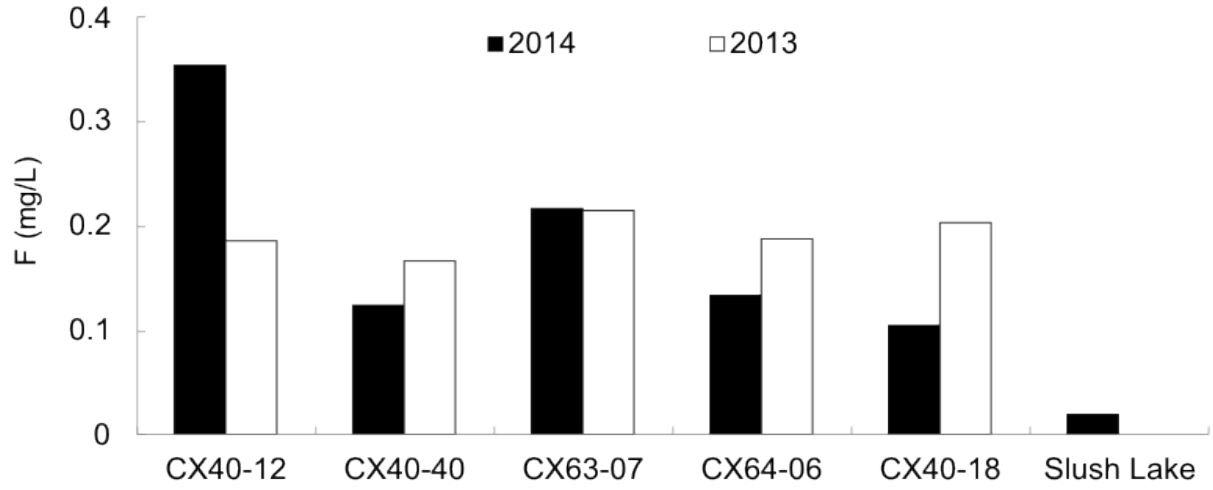

Figure 18: Bar graph comparing fluorine content in groundwater taken from the same depth (m below surface) in 2014 (black) and 2013 (white). Level of detection for F is 0.0014 mg/L in 2013 and 0.0016 mg/L in 2014. Nearby Slush Lake F content is given for comparison to local fresh water.

Cl and F do not correlate in concentration within groundwater samples and there is not a remarkable difference in concentration from the summer of 2013 to summer of 2014 (Figures 17 and 18). Cl concentrations were higher than F both years, as would be expected because Cl is the most abundant halogen in the hydrosphere.

U and Pb concentrations of groundwater were also determined by ICP-MS (Table 4). U concentrations in groundwater from Millennium collected in 2013 and 2014 ranged from 0.012 – 230 μg/L (Table 4). In 2014, samples were filtered and acidified immediately after sampling and result in much lower (<1 - 6 μg/L U) dissolved U concentrations (Table 4). Dissolved U concentrations of filtered groundwater measured by Earl and Drever (1983) in the Athabasca Basin ranged from 0.1 μg/L to >2000 μg/L. They measured to greater depths, and found that elevated U concentrations occurred in DDH that do and do not intersect mineralization (Earle and Drever, 1983).

Pb concentrations of groundwater from Millennium collected in 2013 and 2014 (Table 4) ranged from below the level of detection to 956 μg/L in DDH CX-40 at 18 m depth. Water sampled in 2013 was filtered after 3 months and water sampled in 2014 was filtered and acidified in the field. CX-40 at 18 m has anomalously high Pb concentration (956 μg/L) compared to the other groundwater sampled at Millennium (Table 4). This suggests possible contribution of Pb from surface, or analytical or sampling error. This is by far an extreme outlier, as all other groundwater sampled resulted in Pb concentrations from 38 μg/L to below detection (Table 4).

4.3.3 Stable Isotope Characteristics

Oxygen and H isotopic data collected from 12 DDH at the Millennium site in July 2014 are shown in Figure 19. Overall, values have mid-range $\delta^{18}O$ and low $\delta^{2}H$ compared to GMWL values, and fall within local precipitation from Saskatoon, SK (IAEA GNIP). The $\delta^{2}H$ values reported in Table 5 range from -174 to 137 (+/-0.12) per mil, with an average value of -151 ‰. The $\delta^{18}O$ values reported in Table 7 range from -16.1 to -21.9 (+/- 0.04) per mil with an average of -19.0 ‰.

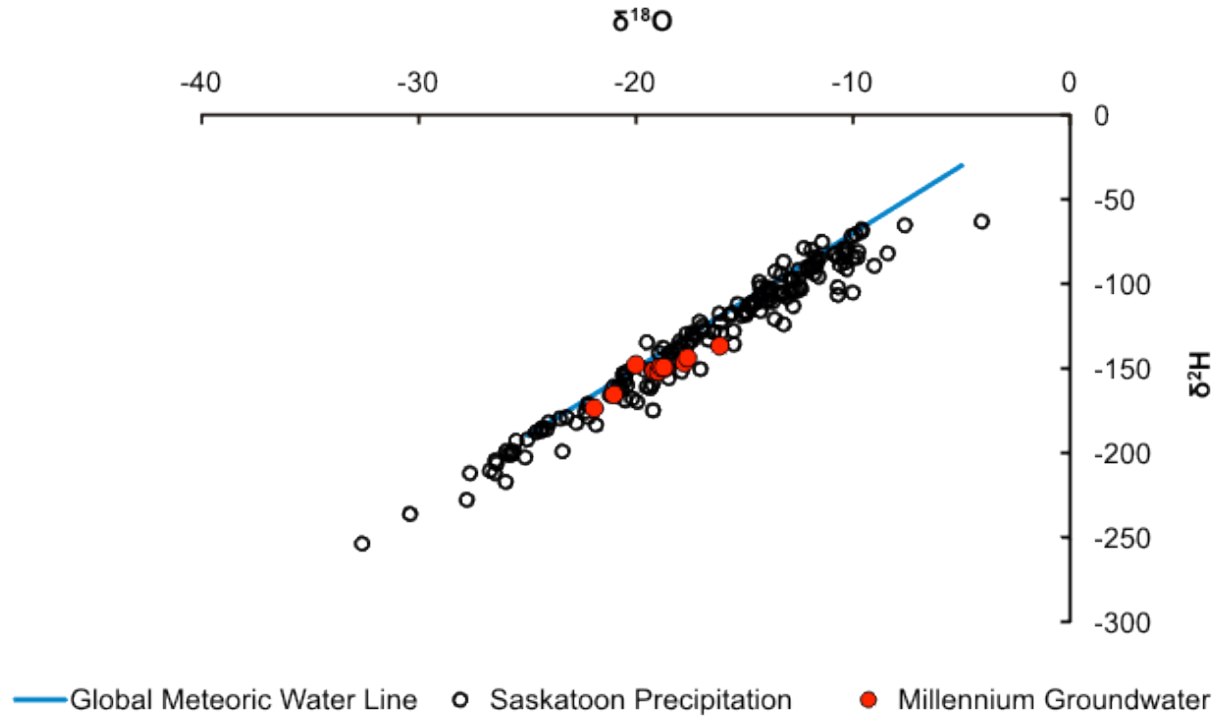

Figure 19: O and H isotope compositions (per mil) of 14 shallow groundwater samples from 12 DDH at Millennium, compared to Saskatoon precipitation (IAEA GNIP) and the global meteoric water line (Craig, 1961).

Table 5: Table of δ^2H- $\delta^{18}O$ values (‰) reported in $^2H/^1H$ and $^{18}O/^{16}O$ relative to Vienna Standard Mean Ocean Water (VSMOW).

Sample ID	δ^2H (VSMOW)	$\delta^{18}O$ (VSMOW)
14CX40-12	-148	-20.0
14CX40-40	-151	-18.9
14CX40-18	-151	-19.2
14CX40-60	-152	-19.0
14CX63-20	-166	-21.0
14CX63-07	-174	-21.9
14CX64-06	-150	-18.7
14CX64-40	-147	-17.8
14CX64-14	-149	-18.7
14CX64-60	-137	-16.1
14CX64-21	-144	-17.6
Slush Lake	-149	-19.0
Min	-174	-21.9
Max	-137	-16.1
Mean	-151	-19.0
Uncertainty	0.3	0..09

Uncertainty determined by analysis of a blind standard (n=6).

Dissolved C concentrations were evaluated because of radon's affinity for organics. The $\delta^{13}C$ DIC data range from -17 to -6.63 ‰, indicating at least two sources with different isotopic signatures. Possible sources of inorganic carbon in these groundwaters are non-marine carbonate dissolution, soil-derived CO_2 produced from the oxidation of organic matter and/or root respiration (Palmer et al., 2001), and the oxidation of DOC (Table 6). $\delta^{13}C$ DOC data range from -24.3 to -26.9 ‰ indicating the source of organic carbon is likely decomposed plants within soil.

Table 6: $\delta^{13}C$ sources and values in ‰ compared to PDB standard from Faure (1988) and *Palmer (2001).

Source	**$\delta^{13}C$ (‰)**
C3 plants	-23 to -34
C4 plants	-6 to -23
Coal	-20 to -30
Methane	-25 to -50
Soil-derived CO_2*	-23 to -28
Marine carbonate	0
Non-marine carbonate	-5

Table 7: Concentration of dissolved organic carbon (DOC) and dissolved inorganic carbon (DIC), and their $\delta^{13}C$ values.

Sample ID	**DOC (mg/L C)**	**$\delta^{13}C$ DOC (‰)**	**DIC (mg/L C)**	**$\delta^{13}C$ DIC (‰)**
14CX40-12	1.12	-25.3	4.65	-
14CX40-18	1.14	-25.4	4.75	-
14CX40-40	0.9	-24.9	5.09	-
14CX40-60	0.89	-24.3	4.82	-
14CX63-07	0.90	-27.8	1.45	-6.76
14CX63-20	0.76	-26.8	1.57	-7.42
14CX64-06	0.90	-25.7	6.05	-10.3
14CX64-14	0.62	-25.7	6.15	-11.5
14CX64-21	0.62	-25.2	6.24	-11.2
14CX64-40	1.56	-26.3	10.0	-17.0
14CX64-60	2.59	-26.6	9.88	-17.0
14SlushLake	2.35	-26.9	1.16	-6.63

Dissolved carbon in groundwater is predominantly inorganic (Figure 20, Table 7); DIC concentrations range from 1.16 – 10.0 mg/L C and DOC concentrations range from 0.62 – 2.59 mg/L C (Figure 20).

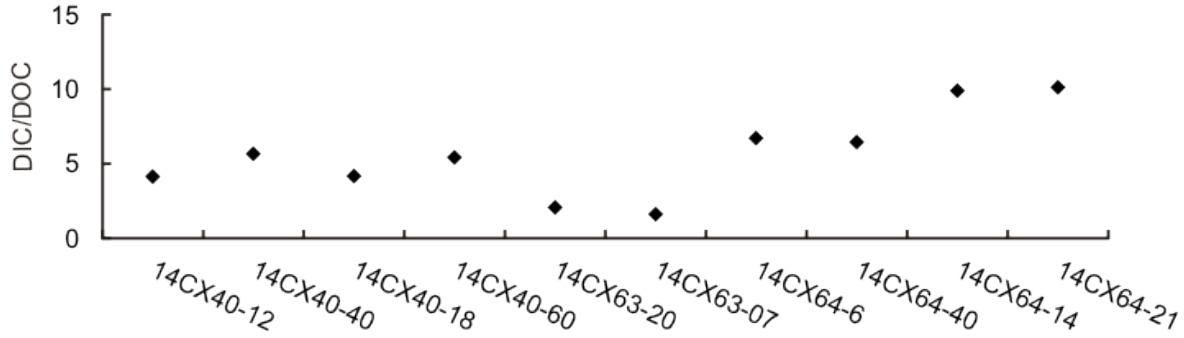

Figure 20: Ratio of dissolved inorganic carbon (DIC) to dissolved organic carbon (DOC) of groundwater taken at varying depths and locations at Millennium.

4.3.4 Tritium

The ^{3}H-^{3}He dating technique has been used since the 1980s to determine the residence age of groundwater in shallow aquifer systems. As rain precipitates, its ^{3}He levels equilibrate with the atmosphere. Once the water infiltrates to the saturated zone, all of the ^{3}He produced is the result of the radioactive decay from ^{3}H (Murphy, 2009). The groundwaters at Millennium were not sampled or analyzed for ^{3}He and therefore the ^{3}H ages must be qualitatively estimated relative to "bomb peak" ^{3}H values and current precipitation values. Mean ^{3}H values in northern hemisphere precipitation and surface waters are currently 5-10 TU, (Plastino et al., 2007) and pre-bomb (before 1952) North American ^{3}H values averaged at 8.2 TU. Tritium in groundwater at Millennium ranges from 3.41-13.2 TU, with a mean value of 7.71 TU. The groundwater is estimated to have a residence age of <20 years (Figure 101) because precipitation in northern Canada has had ^{3}H concentrations consistently below 20 TU since 1993.

4.3.5 Radon in groundwater

All groundwater in a 1.5 km by 1 km area surrounding the Millennium deposit had Rn radioactivity between 0.8 - 278 Bq/L in 2013. The highest Rn radioactivity was at CX-40, the DDH closest to mineralization and the lowest was at CX-44, which is ~300 m from the surface projection of the deposit and upslope of shallow groundwater flow. The DDH with 4th quartile Rn activities are CX-40 and CX-64, and were re-sampled in 2014 to further assess why they had higher Rn radioactivity than others. CX-63 was also re-sampled because it had the next highest radioactivity. Rn radioactivity at Millennium is within the range of previously measured Rn radioactivity in groundwater throughout the Athabasca Basin, which ranged from 2.96 to 7548 Bq/L, and mineralized zones had Rn activity > 92.5 Bq/L (Earle and Drever, 1983).

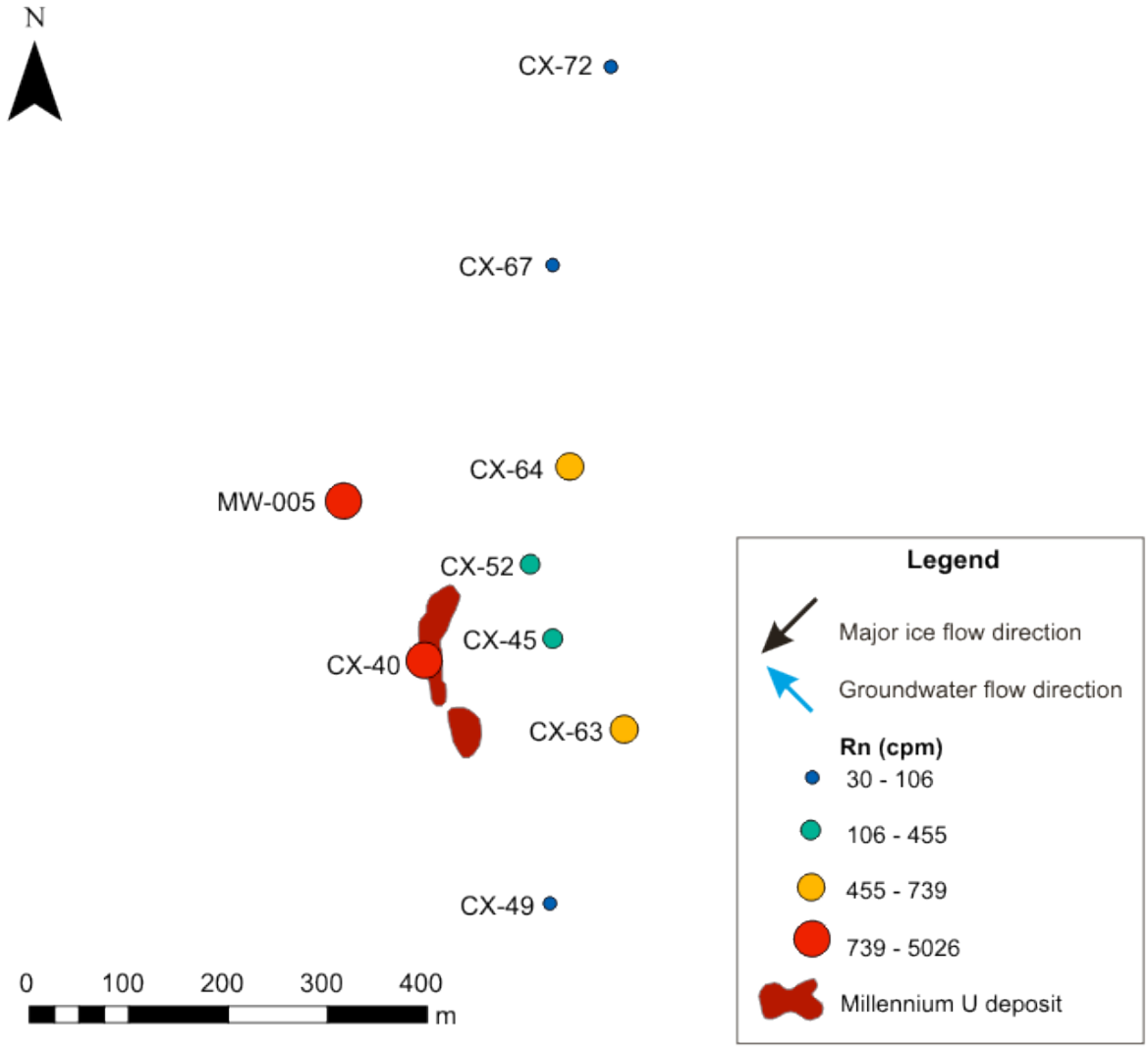

Figure 21: Plan view map of 2013 groundwater sampling locations and Rn radioactivity (counts per minute). Rn radioactivity divided into quartiles increases from blue to red. Major ice flow direction (Schreiner, 1983), and general groundwater flow direction (towards Lake Athabasca) are depicted in the legend.

Water was re-sampled at four locations to determine the repeatability of Rn radioactivity in groundwater from year to year at Millennium (Figure 21 and 22). Overall, the same relative abundances exist between four sample locations; CX-40 (10 m), CX-40 (20 m), CX-64 (5 m) and CX-63 (8 m) listed from highest to lowest, respectively. The largest variance from year to year occurs in CX-40 (10 m), where Rn radioactivity was about five times higher than the previous

year. Rn radioactivity was higher in 2014 than 2013 except for CX-40 (20 m), where Rn levels are almost identical.

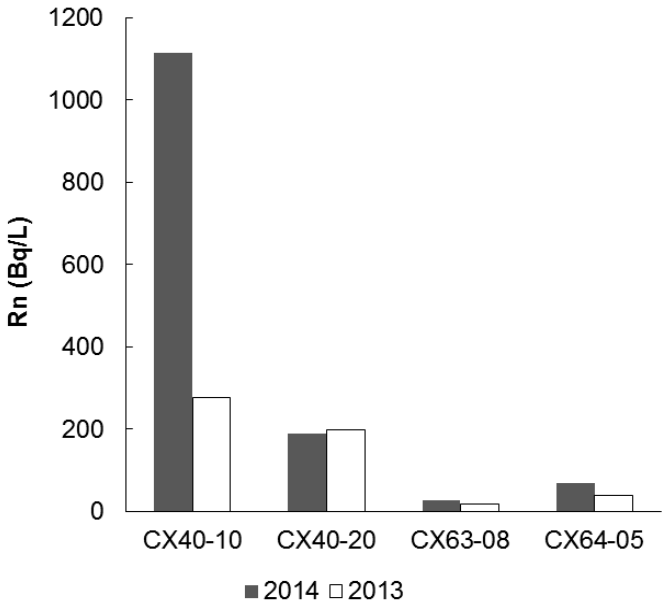

Figure 22: Bar graph comparing Rn activity (Bq/L) from 4 locations in 2014 (grey) and 2013 (white).

Depth profiles of 3 holes were completed in 2014, to determine if there is a correlation with water depth and Rn radioactivity. Rn radioactivity in CX-40 changes drastically between 20 m and 40 m depth but there is no linear increase in Rn with depth (Figure 23) when considering all four depth intervals. CX-63 shows a decrease in Rn from 6 m to 10 m, and then an increase from 10 m to 20 m. Lastly, CX-64 has two data points and Rn radioactivity is the same at both. In summary, there is no trend of Rn with depth, and it appears that Rn is caused by a local source at certain depths in the water column.

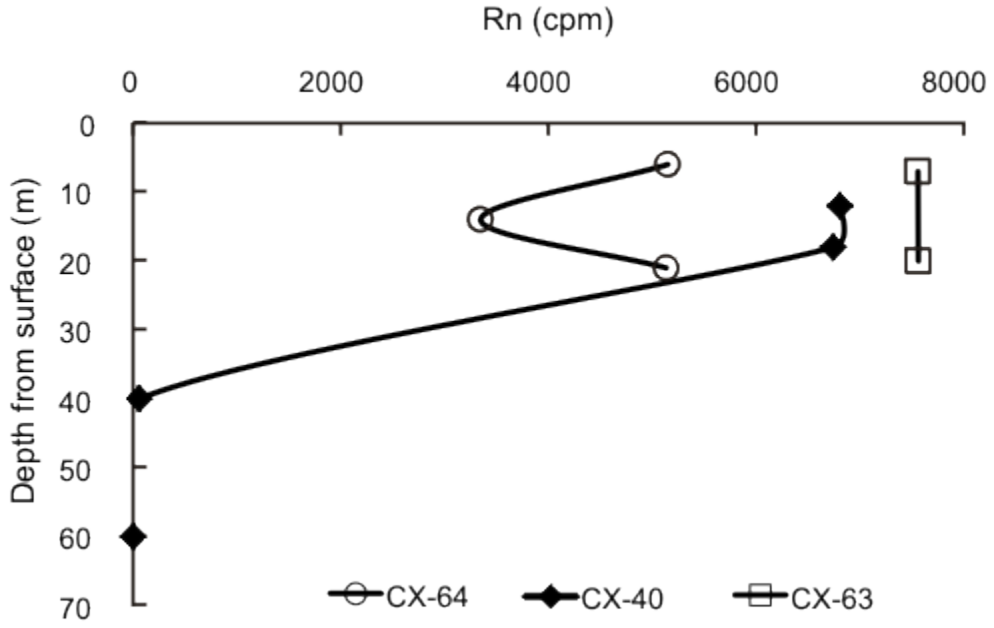

Figure 23: Scatterplot showing Rn activity (counts per minute) with water depth (m) at three Millennium drill holes.

4.3.7 Rn in Soil

Rn in soil results are reported as an average of 5 repeated measurements. Mean values (n = 3) greater than 2σ are considered meaningful, and are presented below. The determined detection limit based on this method is 1 kBq/m^3. Depths range from 30-80 cm below the surface and Rn activity ranges from 1-5.8 kBq/m^3 (Figure 24). Rn radioactivity in soil varies throughout the sampling area, with below detection values directly above the ore body. Three samples within the 4th quartile occur proximal to the surface projection of the ore body; however, there is also a 4th quartile value at the NE corner of the sampling area. Near CX-64, there are four samples with a range of Rn radioactivity within a 50 m^2 area, suggesting that Rn in soil is sourced from a very local source within the till. Rn radioactivity within a 1 km x 0.5 km area surrounding the ore deposit shows background values similar to those throughout the Canadian Shield.

Rn in soil values were collected from above the water table, in the unsaturated portion of the till and soil. Since the partition coefficient from air to water is high, Rn is less abundant within unsaturated soil (Ball et al., 1991) because of the transfer at the soil-atmosphere interface. Saturated lithologies (till, soil or bedrock) that have the capacity to retain large amounts of water, and do not have a disturbance such as a fault or fracture, retain Rn for longer. This prevents the release of Rn into the unsaturated portion of soil and till (Ball et al., 1991) which may be the reason for low values of Rn above the Millennium deposit.

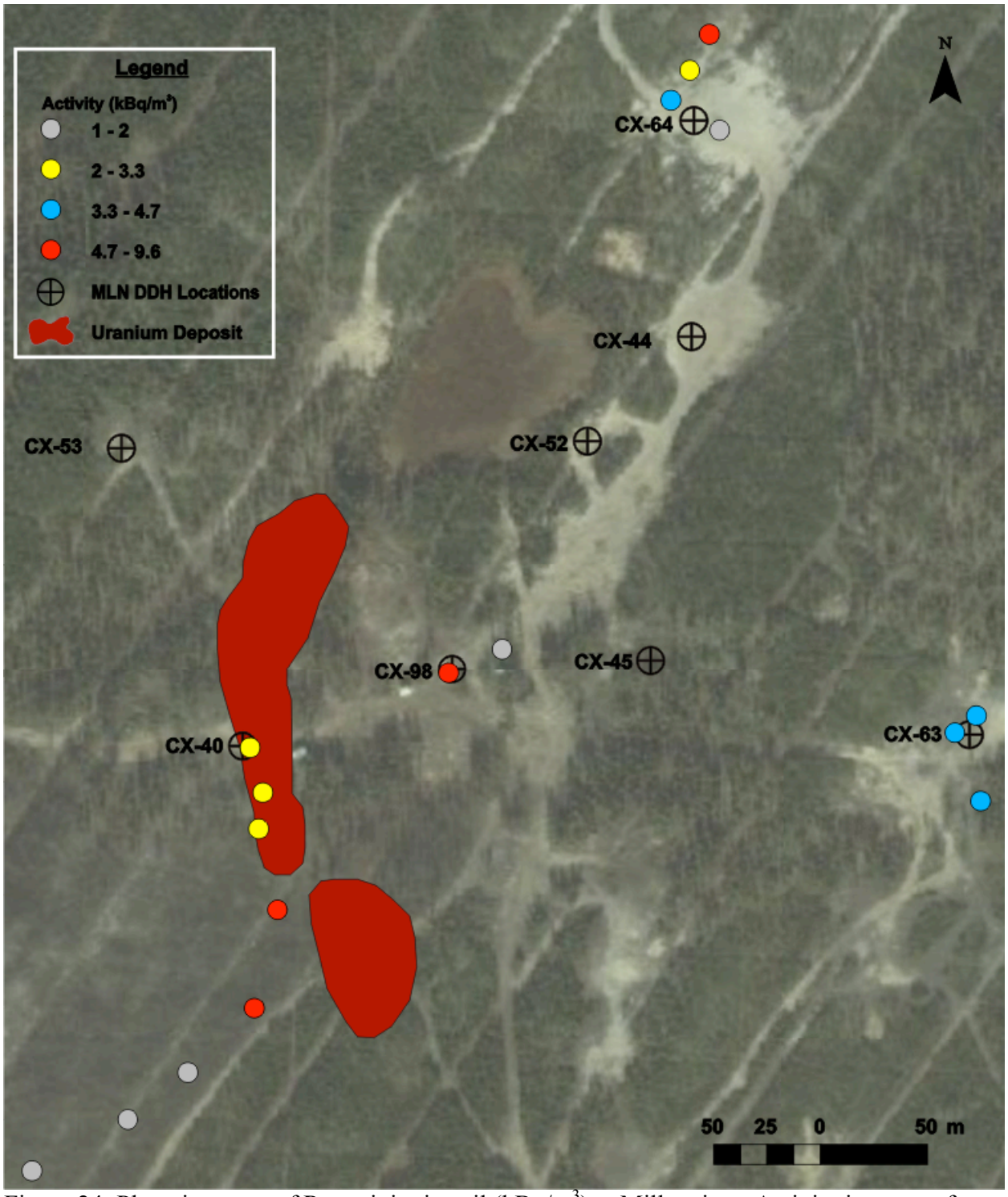

Figure 24: Plan view map of Rn activity in soil (kBq/m^3) at Millennium. Activity increases from grey to red. Drill-holes in the area are represented by a black circle, and the ore body by a red shape.

Rn radioactivity has a lower median value in samples taken < 60 cm deep, and radioactivity was higher at greater depths (Table 8). Overall the range of Rn radioactivity is greater the deeper the sample depth, and radioactivity was lowest between 52-60 cm depth.

Table 8: Table of Rn activity in soil with GPS coordinates and depth in meters.

Easting	Northing	Depth (cm)	Activity (kBq/m^3)
462022	6375744	80	1.9
461999	6375758	80	4.0
462008	6375772	60	3.1
462017	6375789	80	9.6
462142	6375470	60	4.7
461802	6375455	30	3.2
461808	6375434	30	3.3
461806	6375417	80	2.4
461815	6375379	45	5.7
462132	6375462	40	4.6
462144	6375430	40	3.5
461804	6375333	56	5.8
461895	6375490	38	5.7
461920	6375501	45	1.6
461773	6375303	34	1.8
461745	6375281	58	1.0
461700	6375257	52	2.0

GPS coordinates are in Universal Transverse Mercator system, North American Datum 83, Zone 13 North. Activity is the average of three repeated measurements. Detection limit = 1 kBq/m^3.

Overburden thickness varies throughout the Millennium area and was compared to water chemistry because sandstone and till interact with groundwater (Table 9). Figure 26 shows that water sampled from the till horizon (within the casing) does not have a different radioactive signature than water sampled below overburden within the sandstone.

Table 9: List of samples and their corresponding lithology at the sample depth.

Sample	Lithology	Sample	Material
13CX-40-10	Casing	13CX-86-06	Casing
13CX-40-20	Till/SS	13CX-98-06	Casing
13CX-40-30	SS	14CX40-12	Casing

13CX-40-40	SS	14CX40-18	Casing
13CX-40-50	SS	14CX40-40	SS
13CX-44-06	Casing	14CX40-60	SS
13CX-45-13	Casing	14CX63-07	Casing
13CX-52-01	Casing	14CX63-20	SS
13CX-52-10	Till/SS	14CX64-06	Casing
13CX-63-08	Till/SS	14CX64-06	Casing
13CX-64-05	Casing	14CX64-14	Till/SS
13CX-67-08	Casing	14CX64-21	SS
13CX-72-05	Casing	14CX64-40	SS

SS = sandstone and Till/SS represents the boarder of till and sandstone.

The mean Rn radioactivity of water sampled from till and sandstone depths is nearly identical (Figure 25). Water from the boundary between till and sandstone is less varied in Rn radioactivity and shows less radioactivity compared to samples taken within just till or sandstone. The till-sandstone boundary is also the depth where the casing ends in all drill-holes.

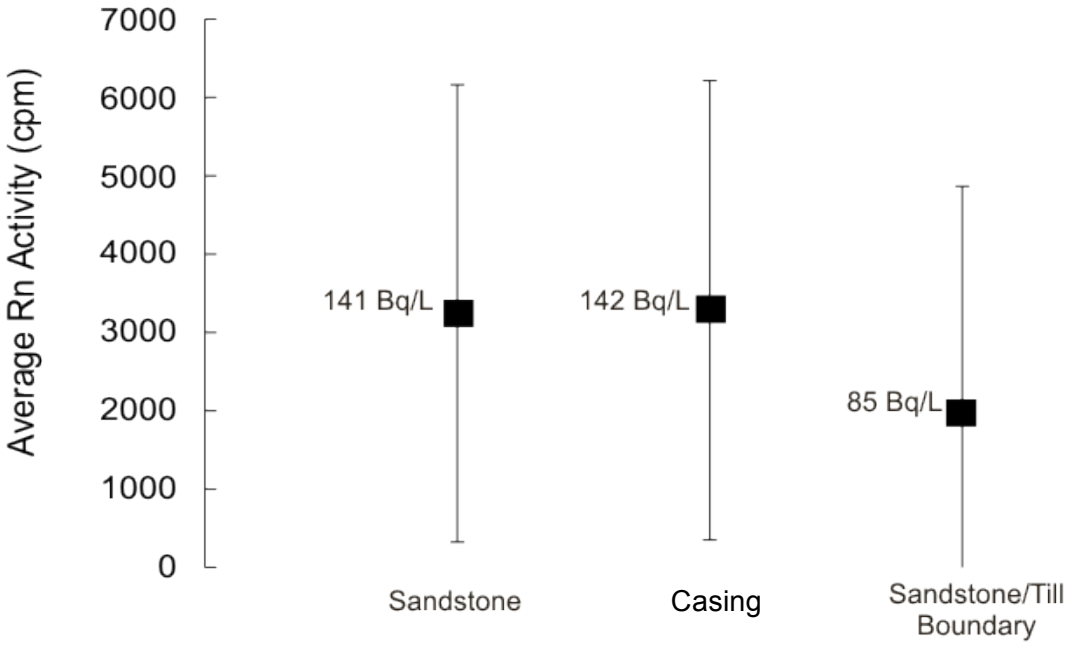

Figure 25: Bar graph illustrating the mean Rn activity (cpm) in water taken from various geological materials including till, sandstone and the boundary between the two. Error bars represent +/- 1 standard deviation. Bq/L values are approximate.

4.3.8 Soil Geochemistry

Soil samples were collected throughout the Millennium site in the summers of 2013 and 2014 from undisturbed locations proximal to drill-holes that were sampled for groundwater (Figure 26). This work follows the soil geochemical survey by Power (2014) and Krahenbil (2014). The objective of analyzing B and C-horizon soils was to identify the major, trace and rare earth element chemistry as well as any anomalies of elements associated with U deposits. The ammonium acetate leach results identify weakly adsorbed or "secondary" elements within the soil. The AA5 leach dissolves minerals co-precipitated with carbonates and elements adsorbed to clay minerals. Multi acid (HNO_3-$HClO_4$-HF-HCl) digestion gives near total values for all elements within each soil sample.

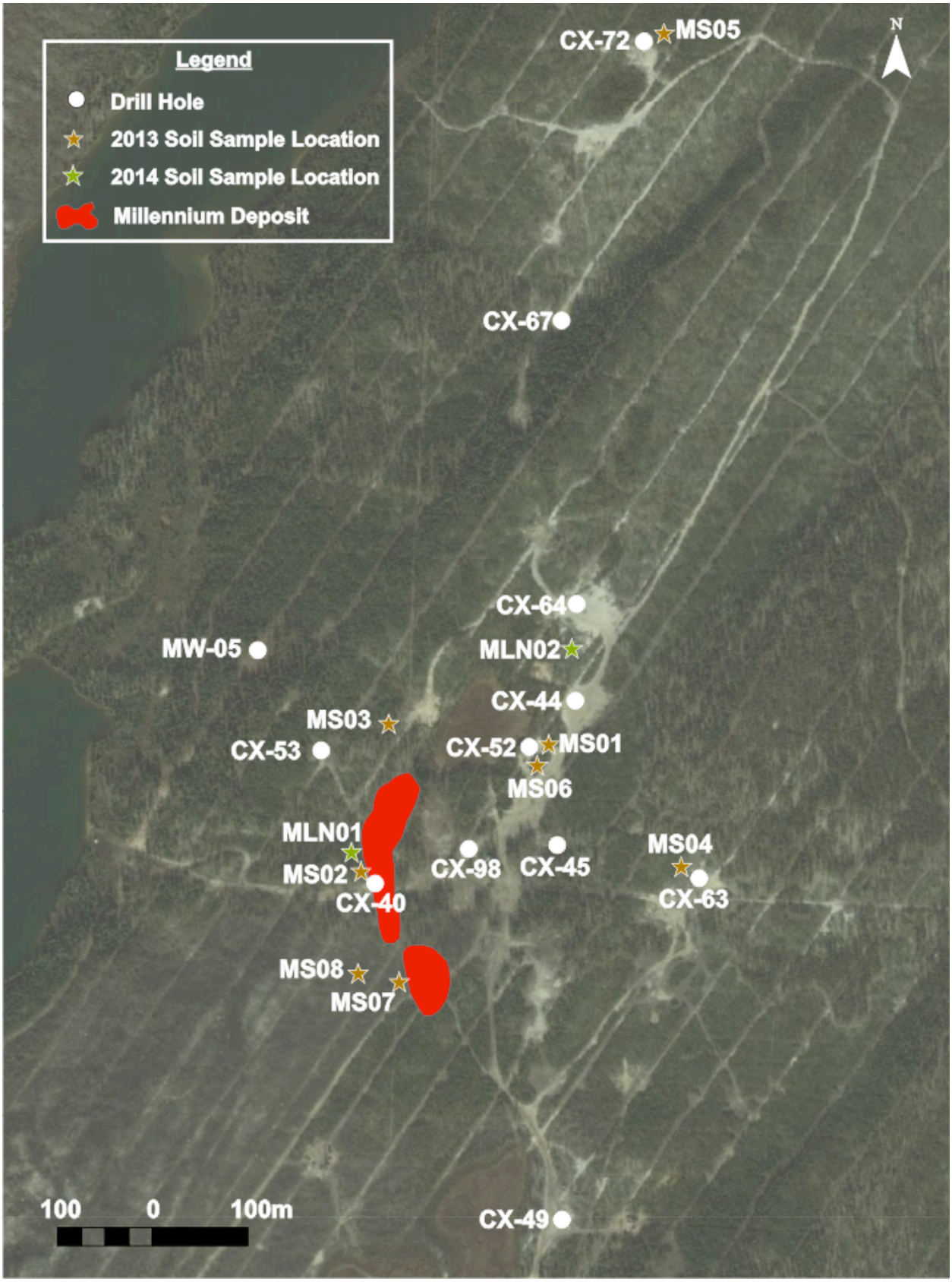
Legend
Drill Hole
2013 Soil Sample Location
2014 Soil Sample Location
Millennium Deposit
N
CX-72
MS05
CX-67
CX-64
MW-05
MLN02
CX-44
MS03
CX-53
CX-52
MS01
MS06
MLN01
MS02
CX-40
CX-98
CX-45
MS04
CX-63
MS08
MS07
CX-49
100
0
100m

Figure 26: Plan view map of the Millennium site indicating locations of drill-holes, soil samples and the surface projection of the U deposit.

Major element results show that Ca (<5 to 57 ppm), Fe (<5 to 40 ppm) and less Mg (<1 to 7 ppm). C-horizon soils (Table 11) leached less Ca, Fe and Mg than B-horizon soils (Table 10).

Table 10: Concentration of major elements leached by ammonium acetate from B-horizon soils. DL = detection limit.

Element	DL	MS02B	MS03B	MS04B	MS05B	MS06B	MS07B	MS08B	MLN01B	MLN02B
Ca (ppm)	5	27	19	39	57	8	16	14	42	22
Fe (ppm)	5	37	33	28	30	14	31	22	14	40
Mg (ppm)	1	5	7	5	7	1	3	6	6	3

Table 11: Concentration of elements leached by ammonium acetate from C-horizon soils. DL = detection limit.

Element	DL	MS01C	MS03C	MS04C	MS05C	MS06C	MS08C	MLN01C	MLN02C
Ca (ppm)	5	<5	<5	11	<5	<5	<5	<5	<5
Fe (ppm)	5	<5	9	11	<5	<5	8	<5	9
Mg (ppm)	1	<1	<1	2	<1	<1	1	<1	1

In order to determine the portion of the major elements that were dissolved in AA5, the results were compared to the near-total digestion data. The AA5 leach dissolved <1% of Ca, Fe and Mg within the soil samples collected in 2014 (Figure 27). Additionally, the B-horizon soil sample MLN02B has a higher proportion of weakly adsorbed Ca, Fe and Mg than the C-horizon soil samples; MLN01C and MLN02C (Fig. 27).

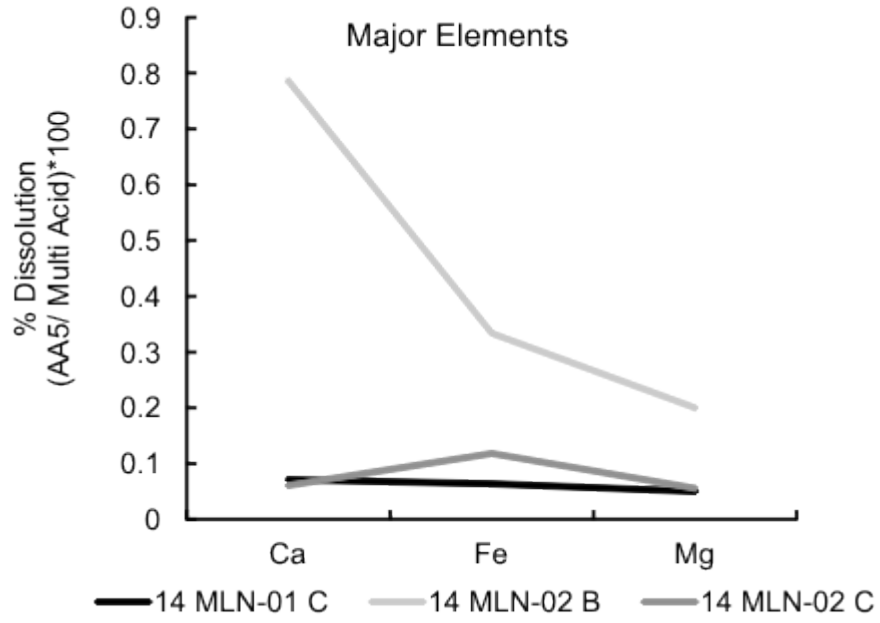

Figure 27: Percent dissolution of Ca, Fe, and Mg of B-horizon soils in AA5 from Millennium, collected in 2014.

The 2013 AA5 results are normalized with MLN02 (B or C) to estimate the percent of weakly adsorbed elements leached by AA5 from each sample (Figure 28, 30, 31, 32, 33). B horizon soils collected in 2013 (Figure 28) show between 0.25 – 2 % dissolution of Ca by AA5 and less than 1 % of the total Fe and Mg in the soils were dissolved by AA5. These data indicate that Ca, Mg and Fe are not easily dissolved by AA5 and less than 2% of their total concentration is from secondary elements.

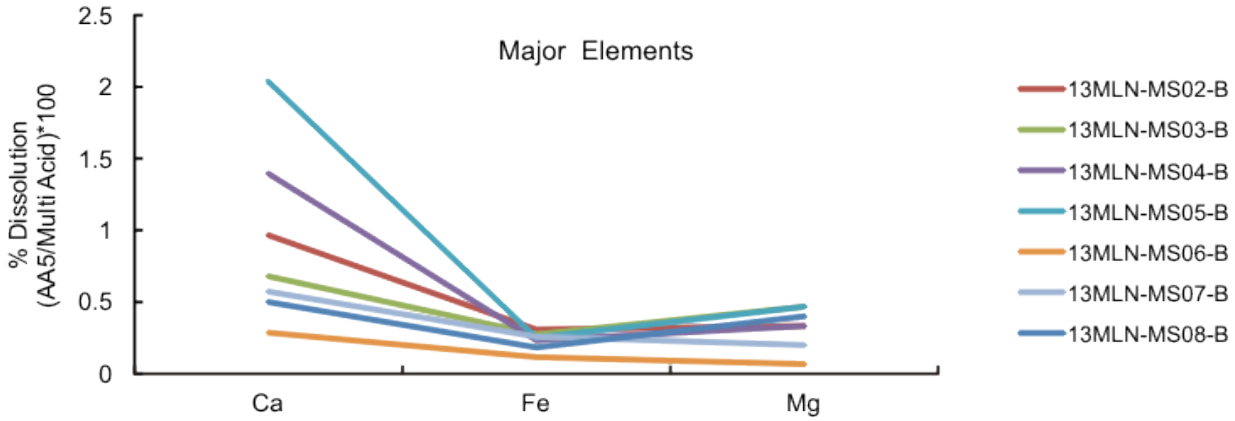

Figure 28: Percent of dissolution of Ca, Fe, and Mg in B-Horizon soils from Millennium collected in 2013.

B and C-horizon soils are also distinguishable by their trace element abundances. AA5 leach results of soil samples collected in 2014 are reported in Figure 29, and combined with 2013 data in Table 12 (B-horizon trace element data) and Table 13 (C-horizon trace elements data).

Table 12: Concentration of elements leached by ammonium acetate from B-horizon soils. DL = detection limit.

Element	DL	MS02B	MS03B	MS04B	MS05B	MS06B	MS07B	MS08B	MLN01B	MLN02B
Ba (ppb)	50	4380	3683	4170	9786	2462	3018	3128	7378	6663
Co (ppb)	20	22	<20	23	34	<20	<20	20	<20	39
Cs (ppb)	5	12	22	14	41	10	19	19	19	27
Cu (ppb)	20	80	44	58	54	34	50	87	82	63
Mn (ppb)	50	1491	3290	2092	3288	1785	1026	1505	675	7645
Ni (ppb)	50	<50	<50	<50	117	<50	99	<50	91	97
Pb (ppb)	20	330	186	219	190	130	225	246	166	342
Sr (ppb)	20	265	204	453	662	120	231	190	360	243
Th (ppb)	20	95	84	44	143	43	65	57	122	116
U (ppb)	5	68	35	21	27	25	35	37	55	42
Zr (ppb)	20	137	96	60	136	48	88	82	112	161

Table 13: Concentration of trace elements leached by ammonium acetate from C-horizon soils. DL = detection limit.

Element	DL	MS01C	MS03C	MS04C	MS05C	MS06C	MS07C	MLN01C	MLN02C

Ba (ppb)	50	384	949	5436	2733	1244	1131	2093	2619
Cs (ppb)	5	<5	8	12	16	<5	17	<5	15
Cu (ppb)	20	<20	36	<20	<20	<20	<20	32	<20
Mn (ppb)	50	349	857	414	210	104	401	343	723
Ni (ppb)	50	<50	<50	<50	<50	<50	79	<50	<50
Pb (ppb)	20	23	21	44	<20	26	46	<20	30
Sr (ppb)	20	23	37	214	71	39	58	84	103
Th (ppb)	20	25	50	113	30	29	26	50	92
U (ppb)	5	<5	11	29	14	7	9	31	26
Zr (ppb)	20	27	50	95	<20	43	26	46	79

Co values were all below detection (DL = 20 ppb)

Figure 29 demonstrates how the percent dissolution of trace elements dissolved by AA5 varies by element. Trace elements are more easily dissolved by AA5 leach than are Fe, Ca and Mg. The most mobile components of the soils sampled in 2014 (based on percent dissolution) are Cu, Pb, U, and Ba.

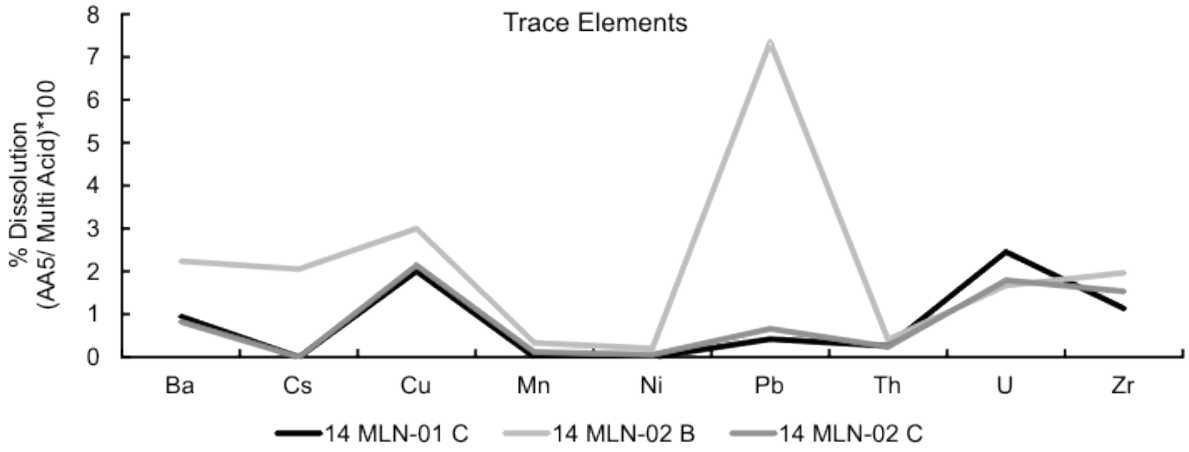

Figure 29: Line graph of percent of dissolution of trace elements of three soil samples at Millennium collected in 2014. Ammonium acetate leach (pH = 5) chemistry, normalized with multi acid digestion concentrations, and converted to percent.

Percent dissolution of 2013 soil samples shows that B-horizon soils have a greater portion of adsorbed secondary minerals than C-horizon soils. B-horizon soils show between 2-8% dissolution of U, with MS02 showing the highest leachable U concentration (Figure 30).

MS02 is the soil sample located closest to the surficial projection of the U deposit and is proximal to the drill hole with the highest Rn in ground water (CX-40). MS02 is also the sample with the highest Pb.

Figure 30 and Figure 31 illustrate 2013 B and C soil horizon trace element geochemistry respectively. B and C-horizons have weakly adsorbed ppb concentrations of Ba (384 to 9786 ppb), Mn (104 to 7645 ppb) and Sr (23 to 662 ppb) and lesser Pb (<20 to 342 ppb). As is typical of C –horizon soils, they have fewer weakly adsorbed trace elements (Fe, Mn) than B-horizon soils because C-horizon does not experience elemental leaching.

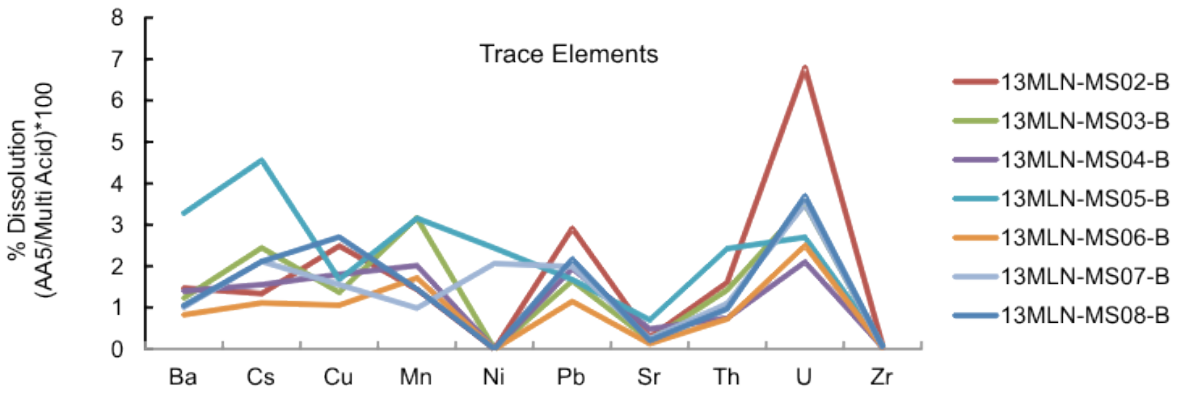

Figure 30: Line graph of trace elements of B-horizon soil samples from Millennium. Ammonium acetate leach (pH = 5) chemistry is normalized with multi acid leach chemistry, and converted to percent.

C-horizon soils (Figure 31) have a smaller portion of weakly adsorbed trace elements than B-horizon soils. The elements leached are Ba, Cs, Mn, Pb and U. MS03 and MS08 show outlying anomalies of Cu and Ni respectively. MS04 shows the highest percent dissolution of all the samples in Ba, Pb and U.

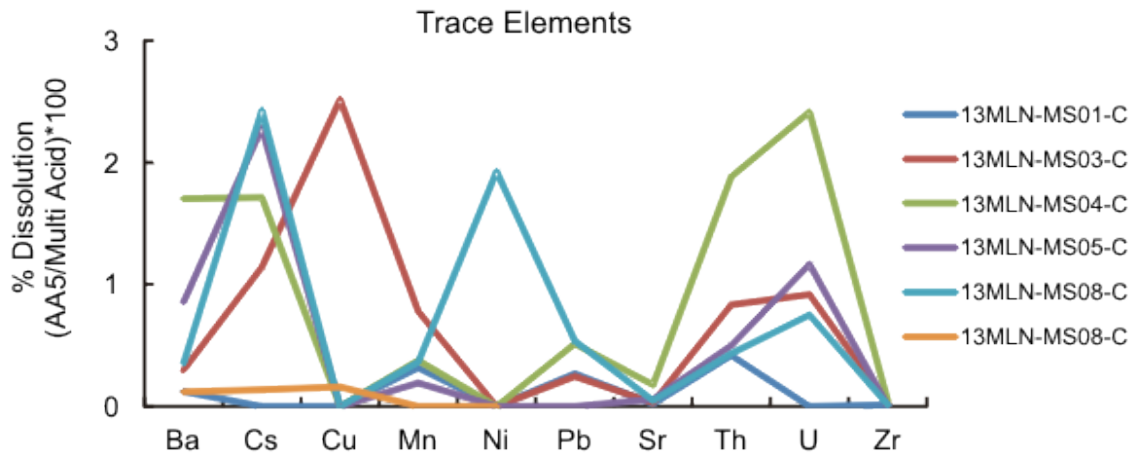

Figure 31: Line graph of trace element chemistry of C-horizon soil samples from Millennium collected in 2013. Fractions of elements dissolved in ammonium acetate leach (pH = 5) relative to multi acid leach in percent.

The percent dissolution of REE within B and C-horizon soils were calculated in order to identify the mobility of the REE within the soil samples (Figures 32-33), and to see if any were co-precipitated with carbonates, or adsorbed onto clays and Fe-Mn oxy-hydroxides. Tables 14 and 15 show the concentration of REE dissolved by AA5. Sediment provenance is the biggest contributor to the REE content of sediments because REE are insoluble and present in very low concentrations within fresh water (Fleet, 1984), and the effects of weathering are minor (Rollinson, 1993). Additionally, the quartz-rich sediments of the Athabasca Basin have a diluting effect on the REE concentrations within the till and soils, and heavy minerals may cause erratic REE patterns in an individual sample (Rollinson, 1993).

Table 14: Concentration of rare earth elements and Y leached by ammonium acetate from B-horizon soils. DL = detection limit.

Element	DL	MS02B	MS03B	MS04B	MS05B	MS06B	MS07B	MS08B	MLN01B	MLN02B
Ce (ppb)	5	140	109	102	181	110	94	121	320	198
La (ppb)	5	66	46	52	98	42	35	47	175	107
Nd (ppb)	5	77	48	55	74	63	43	56	187	82

Pr (ppb)	5	14	12	12	19	12	8	12	44	23
Sm (ppb)	5	20	16	10	10	12	6	19	33	20
Y (ppb)	5	51	42	31	57	35	26	44	118	68

All B-horizon soil samples show similar percent dissolution REE patterns (Figure 32) except for MS05, which shows a much more equal dissolution percent of each REE and a slight positive Y. The percent dissolution patter for all other Millennium B-horizon soils shows that Sm and Nd are more easily dissolved and are likely adsorbed onto clay surfaces, or within carbonates.

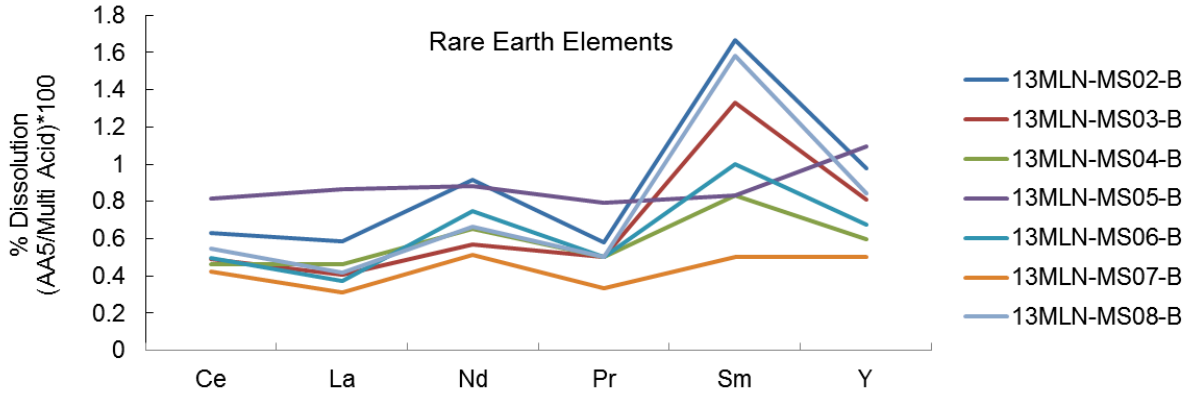

Figure 32: Line graph of the abundance of rare earth elements and Y of B-horizon soil samples from Millennium collected in 2013. Fractions of elements dissolved in ammonium acetate leach (pH = 5) relative to multi acid leach in percent.

C-horizon soils show two groupings of percent dissolution REE patterns (Figure 33). MS04 and MS05 have ~1-2 % higher percent dissolution of Ce, La, Nd, Pr, and Sm than MS01, MS03, MS06.

Table 15: Concentration of rare earth elements leached by ammonium acetate from C-horizon soils. DL = detection limit.

Element	DL	MS01C	MS03C	MS04C	MS05C	MS06C	MS08C	MLN01C	MLN02C
Ce (ppb)	5	65	54	428	259	72	31	144	353
La (ppb)	5	23	25	184	103	30	17	73	172
Nd (ppb)	5	19	22	172	149	24	16	88	148

Pr (ppb)	5	<5	7	40	34	8	<5	23	38
Sm (ppb)	5	11	5	37	20	<5	5	27	34
Y (ppb)	5	13	18	107	103	21	10	62	93

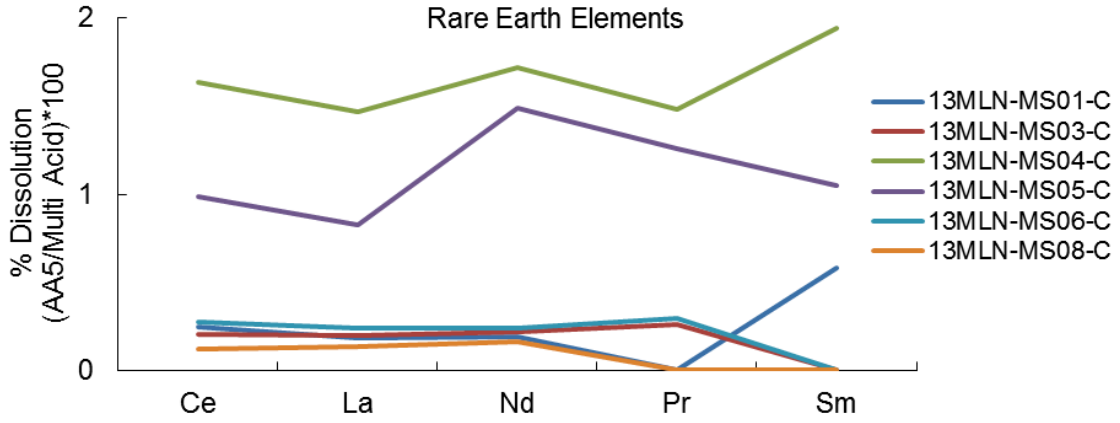

Figure 33: Line graph of rare earth elements abundances in C-horizon soil samples from Millennium collected in 2013. Fractions of elements dissolved in ammonium acetate leach (pH = 5) relative to multi acid leach in percent.

Percent dissolution of REE indicates that about 1% of REE within soils are weakly adsorbed to Fe-Mn oxy-hydroxides or co-precipitated with carbonates (Figure 34). The MLN-01 B sample has a more variable REE pattern than the other two samples controlled by the positive Nd value (Figure 34). This Nd anomaly is most likely an analytical artifact because there is no known mechanism to fractionate Nd within sediments.

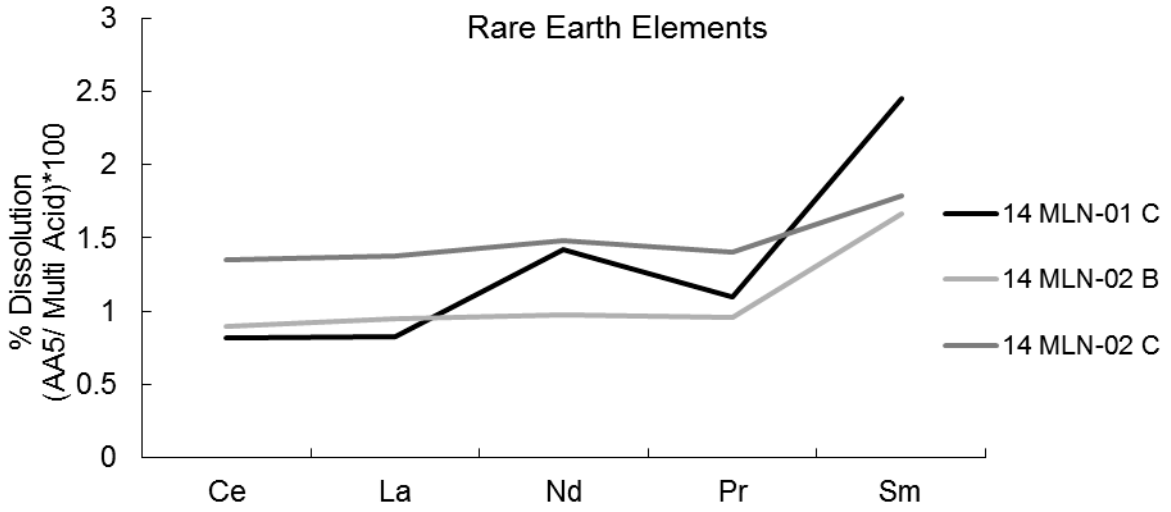

Figure 34: Line graph of rare earth elements in B and C-horizon soil samples from Millennium collected in 2014. Fractions of elements dissolved in ammonium acetate leach (pH = 5) relative to multi acid leach in percent.

A multi-acid digestion was also completed on three Millennium soil samples collected in 2014; two C horizon and one B-horizon. Major element chemistry of B and C-horizon soils (Figure 35, Table 16) shows that Fe, Al, Na and K are the most abundant elements in both soil layers. All major elements have similar relative abundances in each soil sample.

Table 16: Concentration of major elements dissolved by multi-acid digestion from three soil samples at Millennium.

Element	DL	MLN-01C	MLN-02C	MLN-02B
Fe (%)	0.02	0.39	0.76	1.2
Ca (%)	0.02	0.35	0.41	0.28
P (%)	0.001	0.013	0.01	0.043
Mg (%)	0.02	0.1	0.18	0.15
Ti (%)	0.001	0.061	0.11	0.13
Al (%)	0.02	1.86	2.52	3.13
Na (%)	0.002	0.767	1.022	0.763
K (%)	0.02	0.74	1.13	0.95

*S values were all below detection (DL = 0.04%)

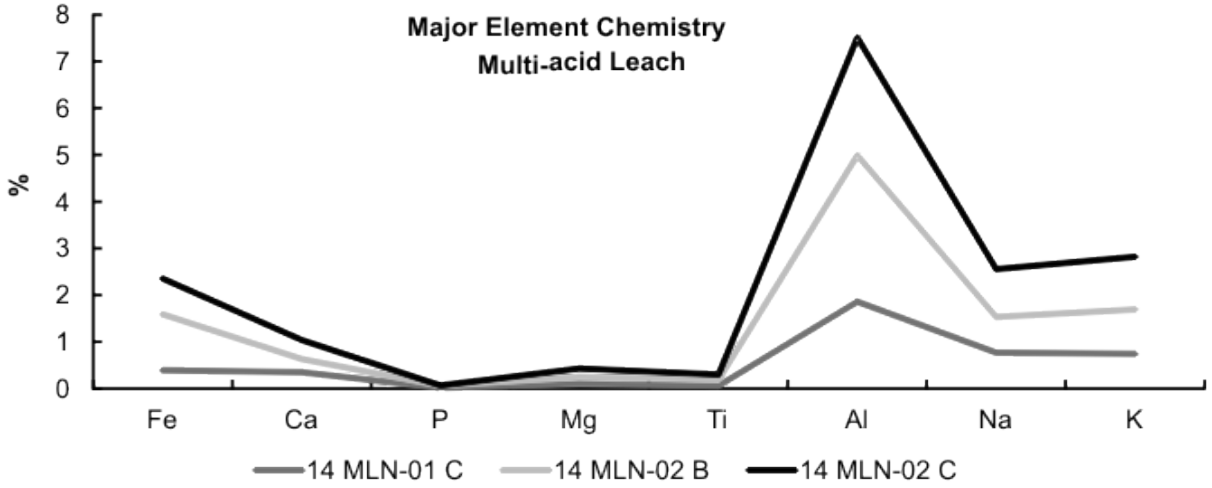

Figure 35: Line graph of concentrations of major elements in multi-acid digestion in three Millennium soils, collected in 2014. Concentrations are in percent.

Multi-acid digestion of B and C horizon soils from Millennium (2014) show similar trace element patterns (Figure 36, Table 17). The most abundant trace elements are Ba (222 – 319 ppm) > Zr (142 – 214 ppm) > Mn (82 – 110 ppm).

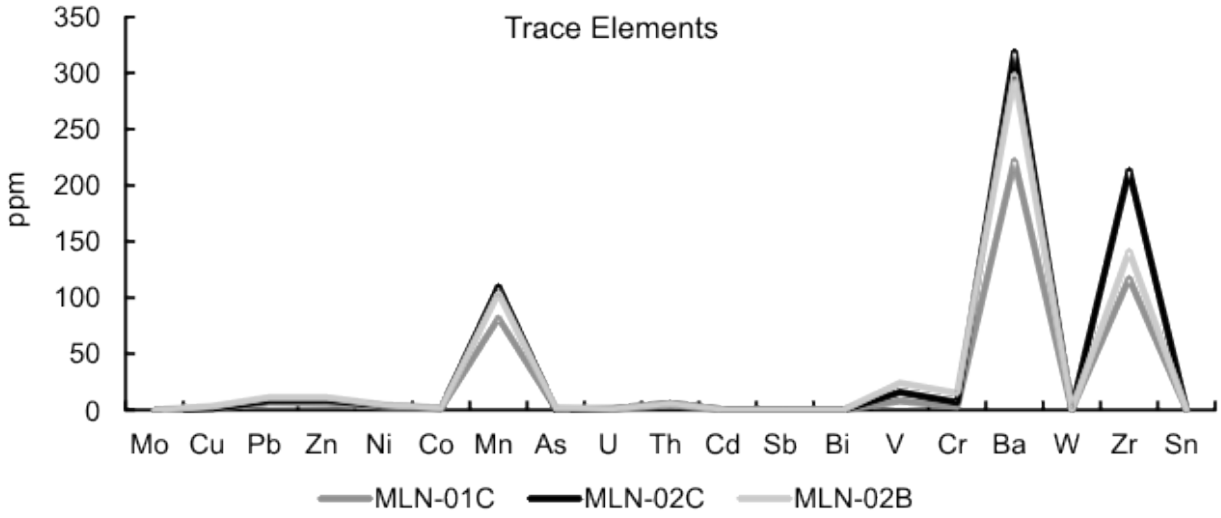

Figure 36: Line graph of concentrations of trace elements in multi-acid digestion in three Millennium soils, collected in 2014. Concentrations are in parts per million (ppm).

Table 17: Concentration of trace elements dissolved by multi-acid digestion from three soil samples at Millennium. DL= detection limit.

Element	DL	MLN-01C	MLN-02C	MLN-02B

Ag (ppb)	20	52	68	39
Mo (ppm)	0.05	0.12	0.11	0.27
Cu (ppm)	0.02	1.45	1.43	3.22
Pb (ppm)	0.02	6.49	8.56	11.31
Zn (ppm)	0.2	6.1	8.8	11.3
Ni (ppm)	0.1	3.1	4.1	4.8
Co (ppm)	0.2	1.3	1.7	1.9
Mn (ppm)	2	82	110	104
As (ppm)	0.2	1.1	0.7	1.9
U (ppm)	0.1	0.8	1.2	1
Th (ppm)	0.1	4.4	6	5.9
Cd (ppm)	0.02	0.06	0.09	0.09
Sb (ppm)	0.02	0.07	0.1	0.13
Bi (ppm)	0.04	0.06	0.07	0.12
V (ppm)	1	8	16	24
Cr (ppm)	1	3	7	15
Ba (ppm)	1	222	319	298
W (ppm)	0.1	0.2	0.3	0.5
Zr (ppm)	0.2	117	214	142
Sn (ppm)	0.1	0.2	0.7	0.7

Rare earth elements from the multi-acid digestion of B and C horizon 2014 soils are normalized to the North American Shale Composite (NASC) (data from Condie, 1993), and show flat lying light rare earth elements, with a general trend from high to low from light to heavy atomic weight. The B-horizon soil (14MLN-02B) shows a slight negative Sm anomaly (Figure 37). Overall, REEs in soils from millennium are depleted compared to the NASC (<1), likely due to dilution caused by the silica-rich Athabasca sandstones from which the tills are partially derived.

Table 18: Concentration of rare earth elements and Y dissolved by multi-acid digestion from three soil samples at Millennium. DL= detection limit.

Element	DL	MLN-01C	MLN-02C	MLN-02B
La (ppm)	0.1	8.8	12.5	11.3
Sc (ppm)	0.1	1.4	2.4	2

Y (ppm)	0.1	3.6	5.9	5.2
Ce (ppm)	0.02	17.6	26.2	22.1
Pr (ppm)	0.1	2.1	2.7	2.4
Nd (ppm)	0.1	6.2	10	8.4
Sm (ppm)	0.1	1.1	1.9	1.2
Eu (ppm)	0.1	0.2	0.3	0.3
Gd (ppm)	0.1	0.9	1.5	1.2
Tb (ppm)	0.1	0.3	<0.1	<0.1
Dy (ppm)	0.1	0.6	0.9	0.9
Ho (ppm)	0.1	0.2	0.2	0.2
Er (ppm)	0.1	0.3	0.6	0.6
Yb (ppm)	0.1	0.5	0.8	0.7

*Tm and Lu values were below detection (1 ppm).

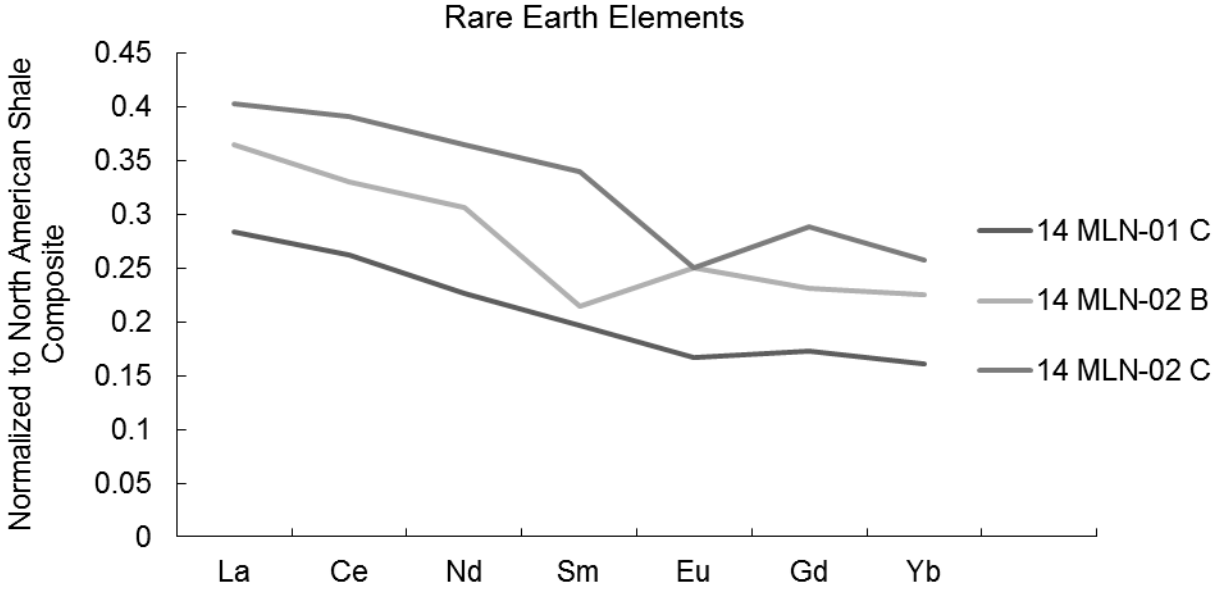

Figure 37: Line graph of REE from multi-acid digestion of B and C-horizon soils. Concentrations are normalized to North American Shale Composite (Condie, 1993).

4. 4 Discussion

There is no correlation between pH and EC with depth in groundwater at the Millennium site, however there is one major outlier MW-005 (Table 3, Figure 38). The outlier has pH=9 and conductivity of 538 µS/cm which likely indicates dissolution of cement used to seal any fractured rocks within the monitoring well. Therefore, groundwater sampled from MW-

005 does not represent the natural groundwater, and is not comparable to other groundwater. All other samples fall within the range of pH and EC in natural groundwaters documented at Cigar Lake by Cramer and Nesbitt (1994). Oxygen and H isotope compositions reveal that the groundwater sampled was meteoric water, and has the same $\delta^{18}O$ and $\delta^{2}H$ as Saskatoon precipitation (IAEA GNIP). ^{3}H content in groundwater at Millennium coincides with that of northern Canadian precipitation (5-20 TU) in 2014. ^{3}H content in northern Canadian precipitation has been <20 TU since 1993 (Figure 100), and therefore only a maximum age of 20 years can be deduced for Millennium groundwater.

The decrease in conductivity with depth seen in DDH CX-40 (Figure 39) could be the result of evaporation in the near surface groundwater, which would cause a relative increase in conductivity near the water-atmosphere interface. Geology can also influence the concentration and content of total dissolved solids in groundwater. For example, Cramer and Nesbitt (1994) indicated that the abundance of dissolved solids within overburden groundwaters was $SiO_{2\,(aq)} > HCO_3^- > Na = K = Ca$ and total dissolved solids amounted to about 30 mg/L. This is an indication that silica is being dissolved within the groundwaters that are within the glacio-fluvial overburden. A further influence on TDS within groundwaters is the abundance of fractures and its influence on groundwater flow. Cramer and Nesbitt (1994) indicated that fracture and fault zones at Cigar Lake span from the MFc and MFd sandstones to the overburden (Cramer and Nesbitt, 1994) in some cases. Fractures and fault zones occur throughout the Athabasca Basin, and are responsible for major groundwater transport that results in late kaolinization (Cramer and Nesbitt, 1994). Kaolinization involves hydration and leaching of K and Si from illite and quartz to form kaolin. The presence of late kaolin along fault and fracture surfaces is reported to indicate considerable movement of groundwater and results in increased TDS (e.g. Kish 1983;

Sibbald et al. 1990; Cramer and Nesbitt, 1994). The most likely influences on the conductivity trend in groundwater at Millennium are evaporation at the water-atmosphere interface and dissolution of solids from overburden materials.

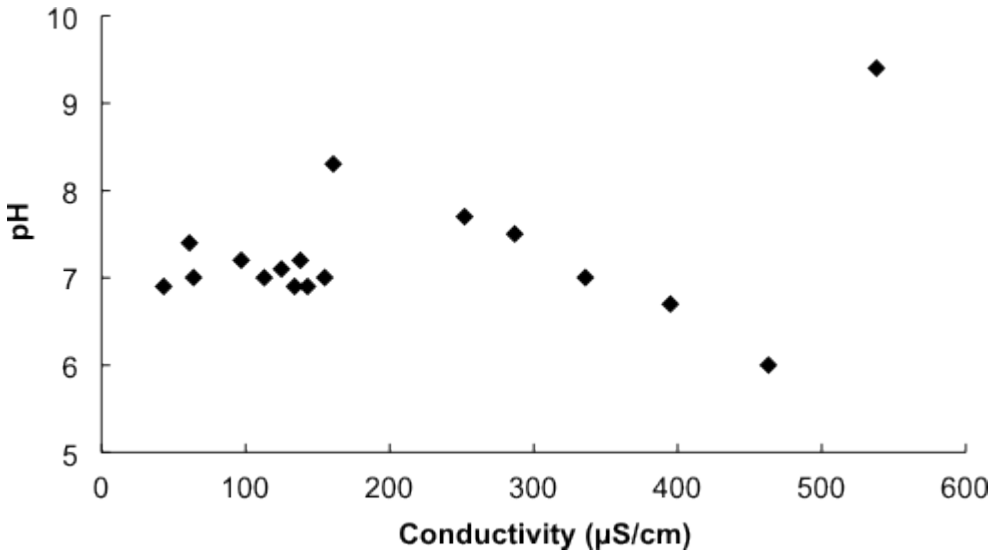

Figure 38: Scatterplot showing trends of pH vs. EC (µS/cm). Samples with low EC have near-neutral pH, samples with >150 µS/cm EC show increased acidity with increased EC, and the major outlier has high pH and conductivity likely due to cementation of the DDH.

In DDH CX-40 Rn radioactivity is highest at the water surface, and decreases with depth until 30 m, and then slightly increases from 30 m to 50 m depth (Figure 39). The ~100 Bq/L range in Rn radioactivity within 40 m depth of the water column indicates a local source of Rn radioactivity at shallow levels, and a lack of vertical mixing within the water column of this drill-hole.

Rn radioactivity was determined in water above (10 m deep) and at the till/sandstone contact (20 m deep) within CX-40. Three other Rn measurements were taken from water samples below the overburden (30 m, 40 m and 50 m deep) within the upper MFd sandstone. A possible reason for the decrease in Rn at 20 m depth is a potential increase in groundwater flow at the overburden-bedrock contact at the end of the casing. The increased permeability and hydraulic conductivity

may dilute the local Rn signature that exists in slower moving groundwater within the till and upper sandstones. Cramer and Nesbitt, (1994) measured the hydraulic conductivity within the overburden ($k = 10^{-4}$ to 10^{-6} m/s) and between the till and upper sandstone ($k = <10^{-8}$ m/s) at Cigar Lake, another high-grade U deposit located in the eastern margin of the Athabasca Basin. Between the till and upper sandstone at Cigar Lake is a thin, highly permeable zone of "Pleistocene conglomerate" and fractured sandstones/rubble. It is likely that a similar zone of higher hydraulic conductivity exists at the Millennium site, and that groundwater flow is higher at the till/sandstone contact (~20 m) within DDH CX-40 than above and below it. An increase in hydraulic conductivity could dilute the local Rn signature and decrease the Rn content at that depth. Additionally, the electrical conductivity of groundwater is higher (>250 µS/cm) in groundwater within the overburden than within the bedrock (<150 µS/cm). This indicates higher dissolved solids within the overburden where Rn radioactivity is highest.

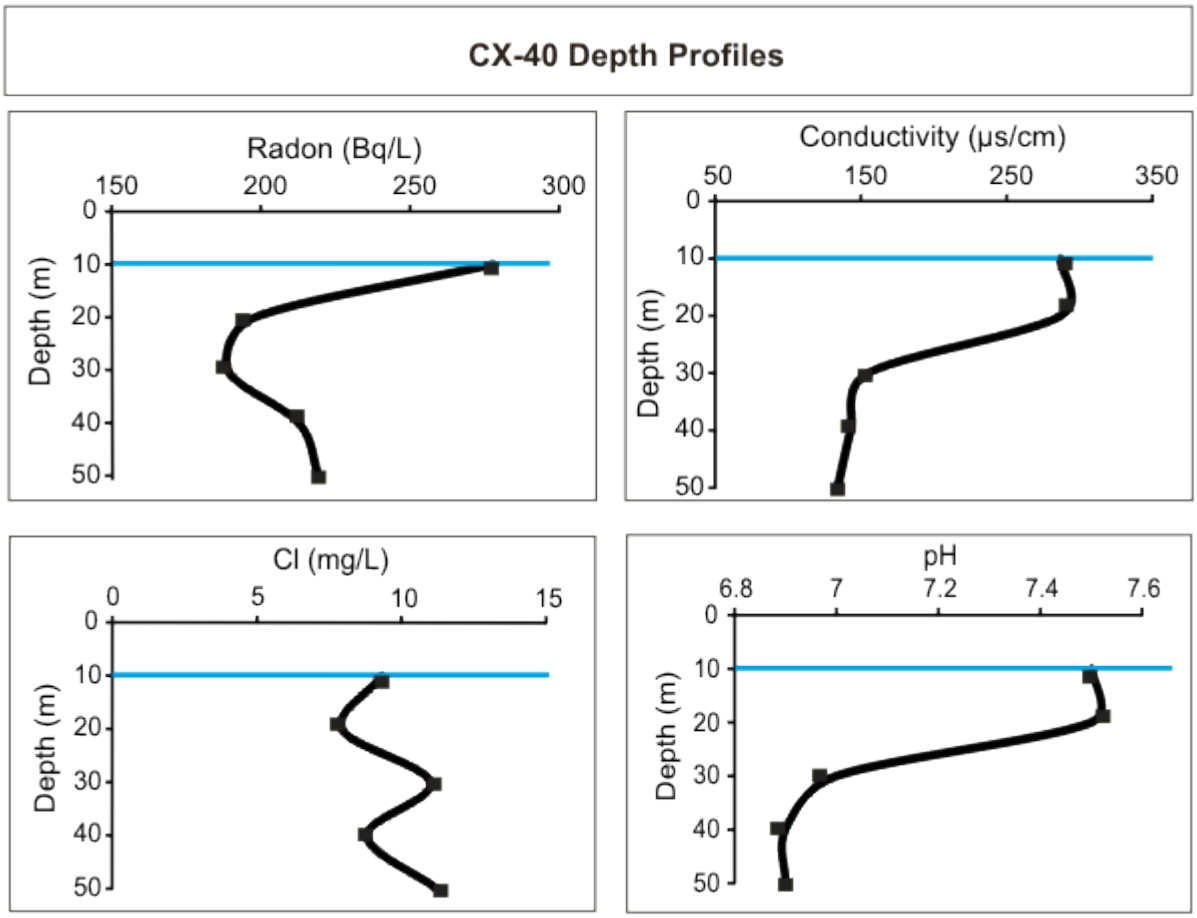

Figure 39: Depth profiles of Rn, conductivity, Cl and pH in the drill-hole with the highest Rn radioactivity (CX-40). The blue line represents the ambient groundwater level (depth below surface, the till/bedrock contact is at 20 m.

The largest variance in groundwater chemistry (anions and cations) from year to year occurred at CX - 40 at 40 m depth where the concentration of Cl^- ranged from 6.5 mg/L in 2013 to 15 mg/L in 2014. However, Rn radioactivity was very similar in 2013 and 2014 in CX-40 at 40 m, indicating that annual variance in Rn radioactivity and Cl concentration do not correlate from year to year at this particular location. Cl is typically a very inert anion that is used as an effective tracer for groundwater (Hem, 1985).

There is also no correlation between DOC and Rn radioactivity (Figure 40). Although Rn has an affinity for organics, in this instance the organic carbon content within the groundwater is

not related to the Rn radioactivity of groundwater. There is a very weak trend between DIC and Rn; groundwater with lower DIC has higher Rn content. The $\delta^{13}C$ values are not in equilibrium with the atmosphere (-7‰) and are more depleted than non-marine (-4.93‰ +/- 2.75) and marine (+0.56 ‰+/- 1.55) carbonate rocks (Faure, 1998). However, the negative $\delta^{13}C$ values are likely due to the oxidation of organic matter into the bicarbonate ion within groundwater (Fauer, 1998) and soil-derived CO_2.

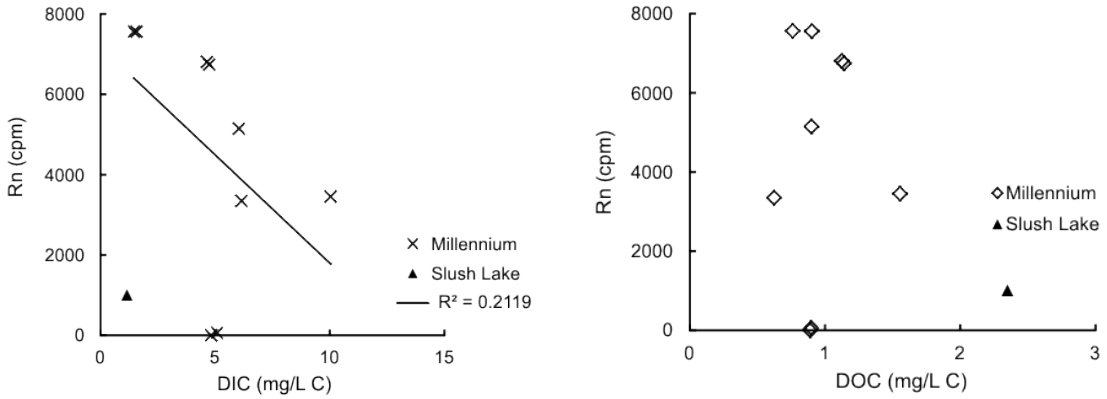

Figure 40: Radon (counts per minute) compared to dissolved organic carbon (mg/L C) and dissolved inorganic carbon (mg/L carbon) in groundwater throughout the Millennium site. DIC weakly correlates to Rn radioactivity ($R^2 = 0.2$).

Rn was compared to dissolved ions (Figure 41). U, SO_4^{2-}, NO_3^-, Br^-, and F^- do not correlate with Rn radioactivity with R^2 values </=0.2, and Cl^- moderately correlates with Rn radioactivity across nine samples from groundwater ($R^2 = 0.7$) (Figure 41). The absence of a relationship between dissolved U and Rn in groundwater at Millennium indicates that the source for Rn in groundwater is not dissolved U within the groundwater.

Cramer and Nesbitt (1994) concluded that a potential source of Cl in groundwater is the leaching of interstitial salts within sandstones. The eastern margin of the Athabasca Basin is primarily fluvial (Ramaekers, 1981) however local marine transgressions also occurred, and provide a source for Cl from seawater within the Manitou Falls formations, including the MFd

upper sandstones (Cramer and Nesbitt, 1994). Cramer and Nesbitt (1994) suggest that the Cl within grain boundaries is leachable along groundwater pathways such as faults and fractures.

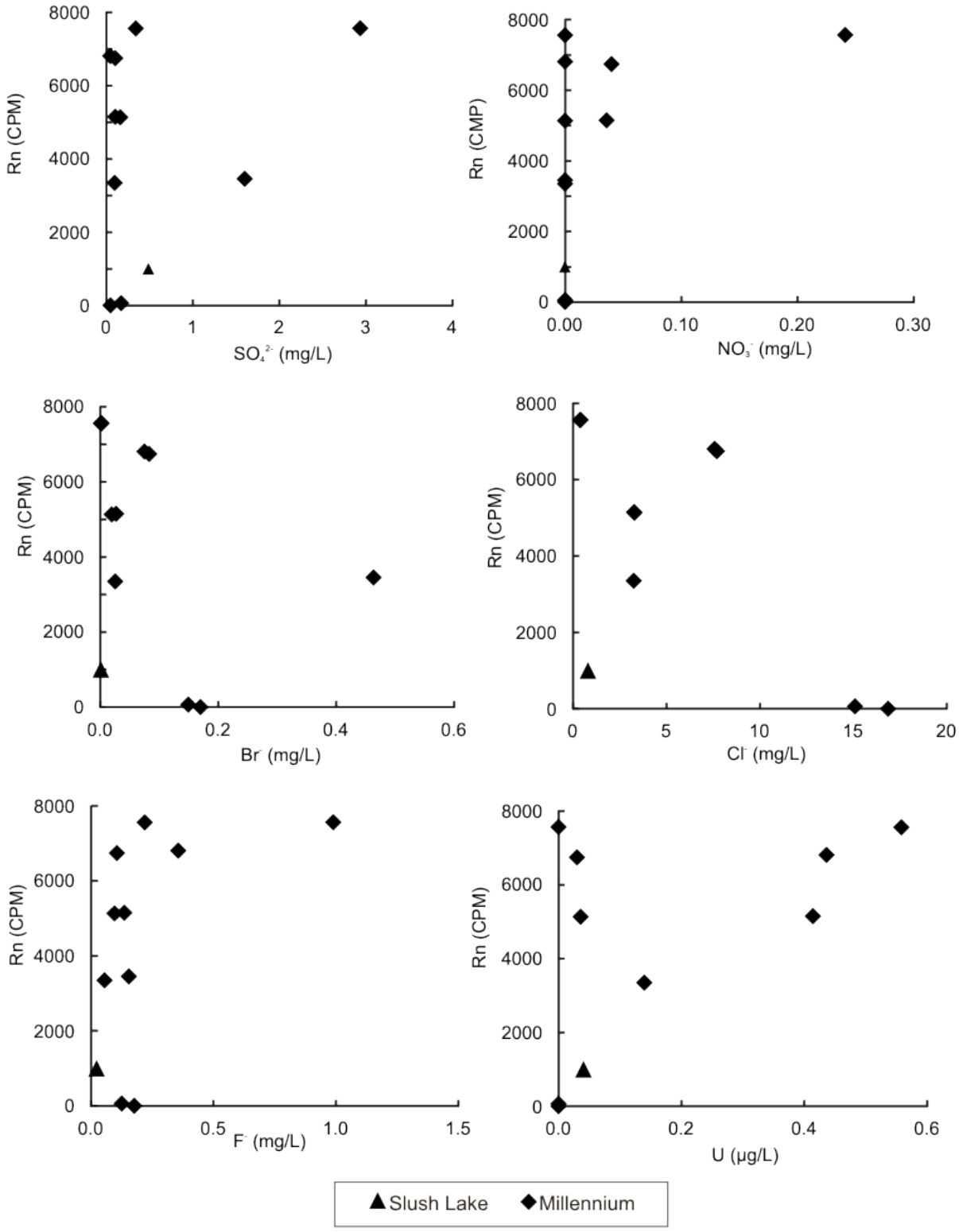

Figure 41: Rn activity (counts per minute) and water chemistry parameters. Limits of detection: U = 0.002 µg/L, SO_4^{2-} = 0.0021 mg/L, NO_3^- = 0.0317 mg/L, Br^- = 0.0011 mg/L, F^- = 0.0016 mg/L, Cl^- = 0.0071 mg/L. R^2 values: U = 0.2, SO_4^{2-} = 0.1, NO_3^- = 0.2, Br^- = 0.2, F^- =0.2, Cl^- = 0.7.

Rn radioactivity was compared to radiogenic ^{4}He/Ar ratios in groundwater obtained by Krahenbil (2014). Figure 42 shows that two DDH close to mineralization have high ^{4}He and Rn and that He and Rn are strongly correlated (R^2=0.94). The ^{4}He content of CX40-10 is higher (10 times atmospheric) than levels found in surface and groundwater throughout the Athabasca Basin above U mineralization (typically 4 times atmospheric) by Dyck and Tan (1978). ^{222}Rn radioactivity from CX-40-10 (approximately 217 Bq/L) is typical of groundwater above U mineralization reported by Earle and Drever (1983) who identified groundwater above U mineralization in the Athabasca Basin had greater than 92.5 Bq/L Rn. Suggesting that there are both local (Rn) and distal (He) sources of radioactivity for this groundwater.

DDH that intersect mineralization (CX-45 and CX-52) and DDH that do not intersect mineralization (CX-49 and CX-63) have low Rn and He contents. This suggests that the source of Rn in groundwater sampled from drill-holes is not residual U or other radiogenic elements that have been brought to the surface during drilling and removal of core from DDH.

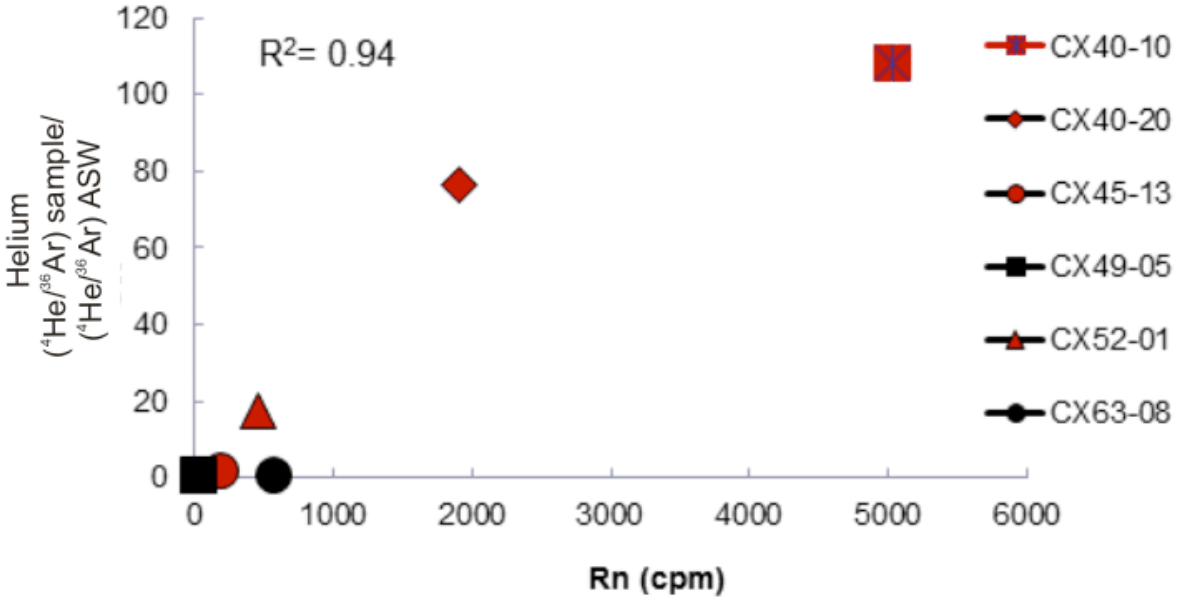

Figure 42: Scatterplot showing ^{4}He and Rn in groundwater. Red shapes represent DDH that intersect mineralization and black shapes represent DDH that do not intersect mineralization. He data obtained from Krahenbil (2014).

Radon in soil was measured near the groundwater sample locations in order to determine if the Rn in water was sourced from radiogenic materials within the soil. Additionally, there is no correlation ($R^2 = 0.03$) between depth below surface and Rn radioactivity in soil (Figure 43). The amount of Rn in soil had greater variation at deeper depths (60-80 cm) compared to shallower depths (Figure 43). This pattern is controlled by one sample, taken at 80 cm below surface which had the highest Rn radioactivity of all the soils tested.

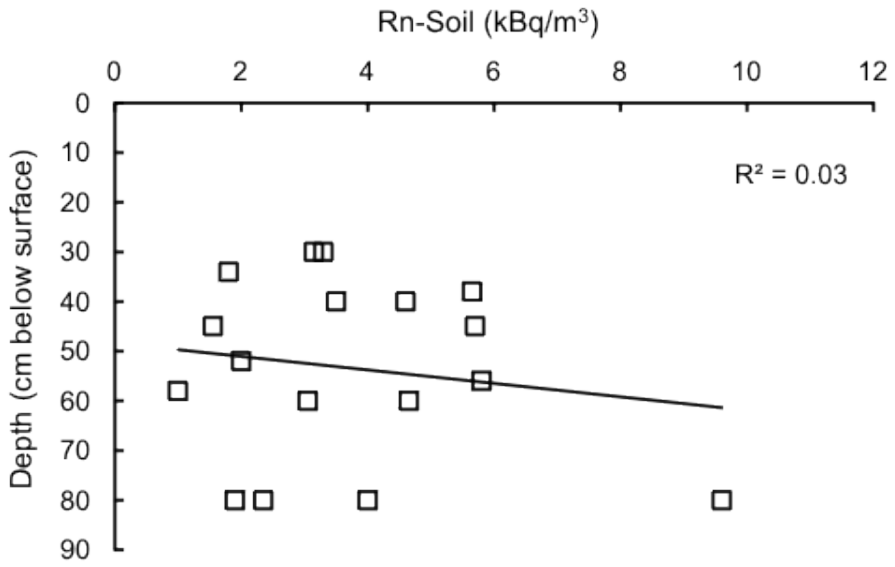

Figure 43: XY plot of Rn in soil gas at Millennium versus depth of sampling. There is no correlation (R^2= 0.03)

The percent dissolution data (Figures 27-34) aimed to identify secondary minerals within soils. Fe and Mn occur within aerated soils and sediments as oxides and hydrous oxides (Chao and Theobald, 1976). In Millennium soils, a greater percentage of Ca was dissolved by AA5 than Fe and Mn, indicating that carbonates are present within soils and are in higher concentration than AA5-soluble Fe-Mn oxyhydroxides. Additionally, between 0-8% of trace elements are dissolved from B-horizon soils by AA5 leach (Figure 29), and more U dissolved than most other trace elements, suggesting that U is present in B-horizon soils adsorbed to Fe-Mn oxides or carbonates.

Ba, Cs and U have the highest percentage of dissolution within C-horizon soils/till (Figure 30), indicating that there is a possibility for Ra to be co-precipitated with Ba because both are alkali earth metals, and that U and Ra are both present within till. Overall, trace elements (Ba, Cs, Cu, Mn, Pb, Th, U) had a higher percent dissolution than Fe, Mg and Ca

within C-horizon soils. This is likely due to the fact that the major elements are more highly concentrated within less-soluble phases.

Bulk REE patterns in three Millennium soil samples indicate that REEs are low in concentration relative to NASC concentrations; this is not due to excess water within soils, because soils were dried before analysis, but rather the large concentration of SiO_2 which causes an overall dilution of REEs within soil. NASC has 64.8 wt % SiO_2 (Condie, 1993) suggesting that REE are less abundant within these soils relative to typical mudstone. Relative to NASC, B-horizon soils at Millennium are more abundant in LREE than HREE. The percent dissolution of REEs was also examined to determine the REE concentration within the secondary mineral phases of Millennium soils. The ~1% dissolution of REEs indicates that almost all are hosted by primary phases.

Typically, minerals that concentrate LREE within rocks include titanite, apatite and monazite (Clarke, 1984). In soils, clay minerals (illite, kaolin etc.) are more likely hosts for REEs than carbonates (Clarke, 1984) because their platy structure provides a larger surface area for REE adsoption. Of the 3 soil samples analyzed for bulk digestions the most abundant trace elements include Zr (zircon) and P (phosphates), in which REEs are likely hosted, and Mn (Mn-oxyhydroxides) and Ba (sulfates).

4.5 Conclusions

Tritium content of groundwater indicates recent (<20 yrs) residence ages for all samples, and does not correlate with varying Rn radioactivity. These waters also have O and H isotope compositions similar to Saskatoon precipitation, indicating that they are meteoric in origin. Rn radioactivity varies throughout groundwater sampled from the Millennium site. Rn is detectable as far as 1 km from the surface projection of the deposit, and is detectable in groundwater from

drill-holes that did and did not intersect mineralization. There is no evidence for a correlation between dissolved elements (U, SO_4^{2-}, NO_3^-, Br^-, F^-) or isotope compositions (O, H, C) and Rn content in shallow groundwater. Elements that positively correlate to Rn in groundwater are ^4He, and Cl^-.

Groundwater sampled from the discovery hole of the Millennium deposit (CX-40) had the highest Rn radioactivity in 2013 and 2014.The depth profile within CX-40 indicates that Rn is higher at shallower depths within till, than within sandstone in this single drill-hole, however it is not known whether this trend would be seen elsewhere above the deposit. This study concludes that groundwater sampled from DDH at Millennium has varying Rn radioactivity, and DDH that intersect mineralization at depth (>500 m) have >106 cpm Rn. As well, the groundwater with the lowest Rn radioactivity occurs in the DDH farthest from the surface projection of the deposit, which does not intersect mineralization. Based on these results, the detection of Rn in groundwater by the bailing and extraction methods is worthwhile. These methods enable a quick perspective into the overall radioactivity of the groundwater in a general area. This study has not found a causative or correlative dissolved ion, or stable isotope that is associated with Rn in groundwater.

The soil and bedrock proximal to groundwater was thought to potentially have an impact on Rn radioactivity in the groundwater. Groundwater sampled within till and upper MFd sandstone have similar quantities of Rn. Groundwater sampled at the till-sandstone contact have a lower mean Rn radioactivity as demonstrated in DDH CX-40 (22 m), CX-64 (14 m). This is likely due to the increased groundwater flow at that contact (Cramer and Nesbitt, 1994), which would increase mixing of Rn-rich and Rn-poor waters. Additionally, a shorter residence time of

the water would prohibit the accumulation of Rn in specific aquifers within Ra-rich soils and rocks.

To determine which elements were weakly adsorbed on Fe-Mn-oxy-hydroxides or co-precipitated with calcite, the ammonium acetate leach was performed on B and C-horizon soils. B-horizon soils have a greater proportion of easily dissolved Ca than Fe and Mg, and the most abundant trace elements within B and C- horizon soils are Ba, Cs, Mn, Pb and U. The majority of REE within soils occur within less-soluble mineral phases-evident from less than 2% dissolution of REE within B and C-horizon soils by AA5. The REE with the highest % dissolution was Sm (relative to Pr and Y) in B-horizon soils. All REE within C-horizon soils have the same % dissolution.

Bulk geochemistry of B and C horizon soils was limited to three samples collected in 2014. These results determined a general geochemistry of the soils. The most abundant major elements and their possible hosts are Al (kaolin, illite, feldspars), Na (feldspars), K (illite) and Fe (ferri-hydrides). The proposed mineral hosts for these elements are based on the literature of common minerals within Athabasca sandstones and soil and were not quantitatively determined. The most abundant trace elements include Mn (Mn-oxyhydroxides), Ba (illite) and Zr (zircon). The LREE enrichment of Millennium soils (Figure 33) indicates that La, Ce, Nd and Sm are more abundant than Eu, Gd and Yb. Overall, REEs are in lower concentration than the NASC.

In conclusion, Rn gas varies throughout surficial groundwater at the Millennium site, and is most abundant within groundwater closest to the deposit. Since there is no correlation between Rn abundance and dissolved ions, ^{3}H, or dissolved C, Rn is likely controlled by groundwater flow. The absence of a spatial correlation between Rn in soil gas and Rn in groundwater at

Millennium suggests that the source for Rn is within the saturated portion of the till/soil or within the upper sandstones. The geochemistry of soil from three locations at the Millennium site confirms that B-horizon soil is derived from mostly sandstone-derived minerals (quartz, illite and kaolin) with a smaller contribution from basement rocks. The AA5 leach indicates that secondary minerals such as Mn-Fe-oxy-hydroxides and carbonate are within B-horizon soils, providing a potential host for adsorbed metals within soils. C-horizon tills are a much less likely host for secondary minerals, because they are not weathered and are therefore less concentrated in Fe and Mn.

CHAPTER 5: Examining the surficial expression of the McArthur River uranium deposit in groundwater, shallow sandstone fracture coatings and soils.

5.1 Introduction

This chapter discusses the occurrence of radionuclides in groundwater, soil and shallow sandstone fractures above the largest high-grade U deposit in the world, McArthur River. Methods were tested and developed during the previous summer of field work at the Millennium site (Chapter 4), allowing for a more in-depth investigation into the Rn content of water and soil at McArthur River, as well as the additional study of the amount of Ra on core fracture coatings and B-horizon soils.

McArthur River was chosen for this study because it occurs at a depth of roughly 500 m and can therefore be used to examine exploration methods for undiscovered, deeply buried, high-grade U deposits. The McArthur River deposit surficial area has been more heavily disturbed than the Millennium site and the natural vegetation and soil have been altered in some places for development of infrastructure. In order to maintain the objective of sampling from un-disturbed areas, the sampling locations for soil and groundwater were selected based on their natural appearance and their distance from the surface projection of the deposit. Core fracture coatings were sampled from DDH in-between the six McArthur River ore lenses in order to determine the occurrence of Ra along fractures within upper sandstones both proximal and distal to the deposit.

5.2 Geologic Setting

The McArthur River U deposit is the world's largest high-grade U deposit. It was discovered in 1990 by Cameco and occurs within the eastern margin of the Athabasca Basin. It is located within the Cree Lake Zone of the Wollaston Domain near the boundary of the Mudjatik

Domain (Ramaekers, 1981). The basement rocks at McArthur River are part of the Aphebian Wollaston Supergroup, and consist of shallow water meta-sedimentary rocks (Lewry and Sibbald, 1980). Overlying the Wollaston group meta-sediments are unmetamorphosed, flat lying Athabasca group sandstones (Ramaekers, 1981). The main structure associated with the McArthur River deposit is the P2 fault (Figure 44) and its accompanying splays. Mineralization at McArthur River is associated with the P2 fault zone series of mostly graphitic thrust faults that are 13 km in strike and have been traced seismically up to 2 km below the unconformity (McGill et al., 1993). Currently, the McArthur River deposit has six main mineralized zones (1, 2, 3, 4, A, B) and current production at the McArthur River mine is from the basement hosted Zone 2 ore body.

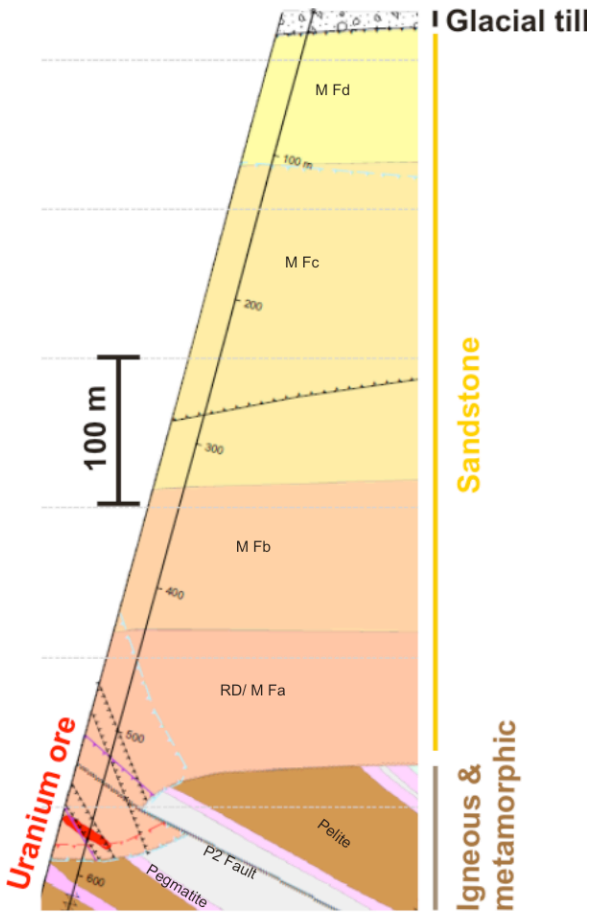

Figure 44: Schematic cross Section of general geology, P2 fault and mineralization at McArthur River, with DDH trace to >500 m depth, modified from Cameco cross section (2014).

Alteration at McArthur River occurs in several stages and includes silica, illite, kaolinite, chlorite and dravite. Alteration occurred both before and after mineralization, which is dated at 1 521 Ma (Marlatt et al., 1992). Glacial till cover is thicker at McArthur than at Millennium, and in places the drumlins have <100 m thick till cover (Tuncer et al., 2006).

5.3 Results

5.3.1 General groundwater characteristics

Groundwater was collected from six McArthur River drill-holes (Figure 45) over a four-day period from July 28 to July 31, 2014. Groundwater was measured for pH, oxidation-reduction potential (ORP) and electrical conductivity (EC) immediately after sample collection in the field (Table 19) and the water table ranged from 0 – 12 meters below the surface. pH ranged from 7 – 12; most groundwater had a near neutral pH, except for water within DDH MC-430 (pH = 12). This MC-430 was recently drilled in 2014 and cemented, which may have increased pH due to the alkaline nature of cement. Earle and Drever (1983) found that 75% of groundwater taken at various depths within drill-holes and piezometers in the Athabasca Basin had a pH between 6 and 7.

Electrical conductivity is useful for estimating the intensity of water-rock interaction. Most of the water at McArthur River is classified as fresh water with conductivity ranging from 47 - 3390 μS/cm, and corresponds to groundwater throughout the eastern and southern Athabasca Basin which typically have TDS of <500 mg/L (Earl and Drever, 1983). MC-430 has anomalously high conductivity (3390 μS/cm), and this combined with its high pH indicates

dissolution of cement used to seal rock fractures. Additionally, there is no correlation with pH and EC in groundwater. Oxidation-reduction potential (ORP) ranged from -47 to 285 mV (standard hydrogen electrode adjusted) at McArthur River.

Table 19: Groundwater characteristics from McArthur River. Parameters include pH, electrical conductivity, ambient water level, the date the sample was collected and the oxidation-reduction potential. All depths are in meters below surface.

Drill Hole	pH	EC (µS/cm)	Water Level	Casing Depth	Sampled below casing?	Date	ORP (mV)
MC-389	7.4	93	0	22.9	No	28/07/2014	-47
MC-399	8.0	65	3	18.2	No	29/07/2014	183
MC-393	6.9	342	5	14.8	No	29/07/2014	252
MC-403	7.1	47	10	16	No	30/07/2014	118
MC-434	8.7	137	12	8.1	Yes	31/07/2014	240
Swamp Lake	7.2	133	0	-	-	30/07/2014	285

See Figure 2 for location of Swamp Lake – located south west of the deposit.

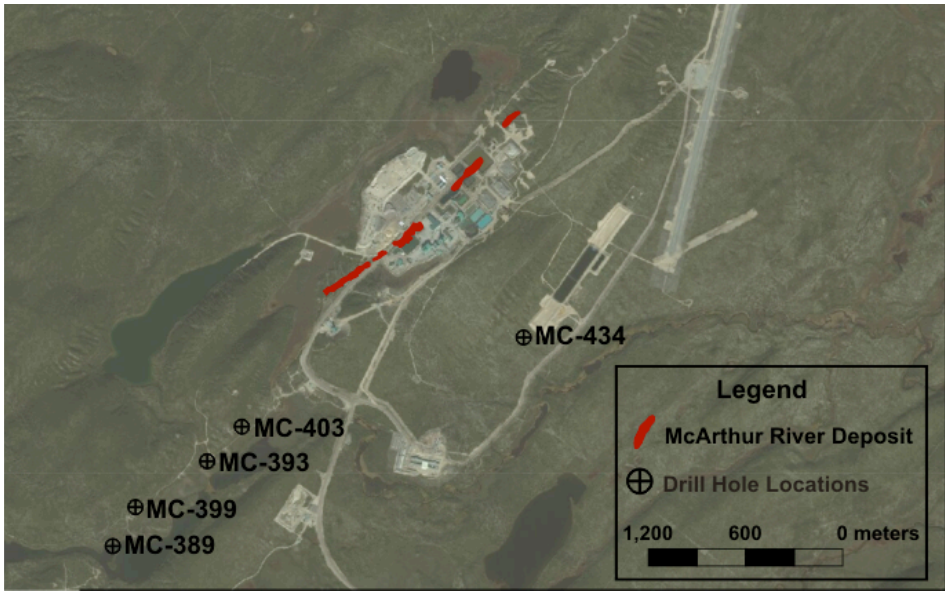

Figure 45: Plan view map of drill-hole locations relative to the surficial projection of the McArthur River deposit, illustrated in red. Groundwater was collected from these drill-holes and analyzed for general groundwater characteristics (pH, temperature, EC, ORP, water level), groundwater chemistry (F^-, Cl^-, SO_4^{2-}, NO_3^-, Br^-, U, Th, Pb), isotopes (D/H, $^{18}O/^{16}O$, DOC, DIC, $\delta^{13}C$ for DOC and DIC), ^3H, and Rn radioactivity.

5.3.2 Groundwater Chemistry

Groundwater was analyzed for major anions (F^-, Cl^-, SO_4^{2-}, NO_3^-, Br^-) and cations (U, Th, Pb). As was done with Millennium, the analyte concentrations at McArthur River will be compared to ranges found within representative groundwaters at Cigar Lake by Cramer and Nesbitt (1994). Fluoride concentrations ranged from 0.009 – 1.7 mg/L, and have a wider range than F concentrations at Cigar Lake (<0.25 – 0.54 mg/L). Chloride concentrations ranged from 0.18 – 24 mg/L and are similar to those of groundwater at Cigar Lake (0.23 – 24.9 mg/L). Sulphate concentrations ranged from 0.49 – 2.7 x 10^3 mg/L in groundwater. MC-430 has the maximum concentration (2.7 x 10^3 mg/L) and is a far outlier with high pH and conductivity. This is due to drilling activity or cement used to seal fractures. Nitrate ranged from below detection to 0.27 mg/L, which is lower than the range determined by Cramer and nesbitt (1994) at Cigar Lake (<0.65 – 1.44 mg/L). Lastly, bromide concentration ranged from below detection to 17 mg/L, and is similar to the range from Cigar Lake (<0.01 – 0.28 mg/L). All anion concentrations are reasonable for surficial groundwater (Faure, 1998) and besides obvious outliers fall near the range of representative samples at Cigar Lake.

Dissolved U and Pb were very minor in McArthur River waters, and below detection for the majority of the water analyzed. The DDH with the highest Pb and U concentration is MC-393 with 0.4 μg/L Pb and 0.24 μg/L U. MC-389 had below detection Pb and 0.155 μg/L U.

Table 20: Groundwater chemistry by sample. Sample ID represents the DDH name. LOD = level of detection, Min = minimum concentration, Max = maximum concentration, Mean = average concentration (with outlier MC-430 removed) and σ = standard deviation. BD means below the level of detection. All values are blank corrected.

Sample	F (mg/L)	Cl (mg/L)	SO_4 (mg/L)	NO_3 (mg/L)	Br (mg/L)	Pb (μg/L)	U (μg/L)
MC-389	0.098	0.64	11	0.27	<0.004	<0.009	0.16
MC-399	0.068	0.36	2.0	<0.025	<0.004	<0.009	<0.0002
MC-393	0.11	0.18	0.49	<0.025	0.005	0.4	0.24
MC-403	0.065	3.2	3.2	0.11	0.13	<0.009	<0.0002

MC-430	1.7	24	2711	<0.025	17	<0.009	<0.0002
MC-434	0.361	0.30	5.3	<0.025	0.006	<0.009	<0.0002
Swamp Lake	0.009	0.40	1.1	<0.025	<0.004	<0.009	<0.0002
LOD	0.002	0.007	0.003	0.025	0.004	0.009	0.0002
Min	0.009	0.18	0.49	0.11	0.005	0.4	0.16
Max	1.7	24	2711	0.27	17	0.4	0.24
Mean	0.34	4.1	3.9	0.19	0.046	<0.009	0.18
σ	0.55	8.1	947	0.081	7.1	<0.009	0.038

Th in all samples was below detection (<0.001 μg/L)

5.3.3 Stable Isotope Compositions

Oxygen and H isotopic data from groundwater collected from 6 sites at McArthur River in July 2014 are shown in Figure 46. These samples show a shift to the right from the global meteoric water line (GMWL) (Craig, 1961); indicating evaporation has impacted these waters. The δ^2H values reported in Table 21 range from -151 to -134 (+/-0.12) per mil, with an average value of 144. The $\delta^{18}O$ values reported in Table 21 range from -19.2 to -16.5 (+/- 0.04) per mil with an average of -18.3 ‰. Overall, values have mid-range $\delta^{18}O$ and low δ^2H compared to the MWL, and fall within local precipitation values recorded in Saskatoon, SK (IAEA GNIP)

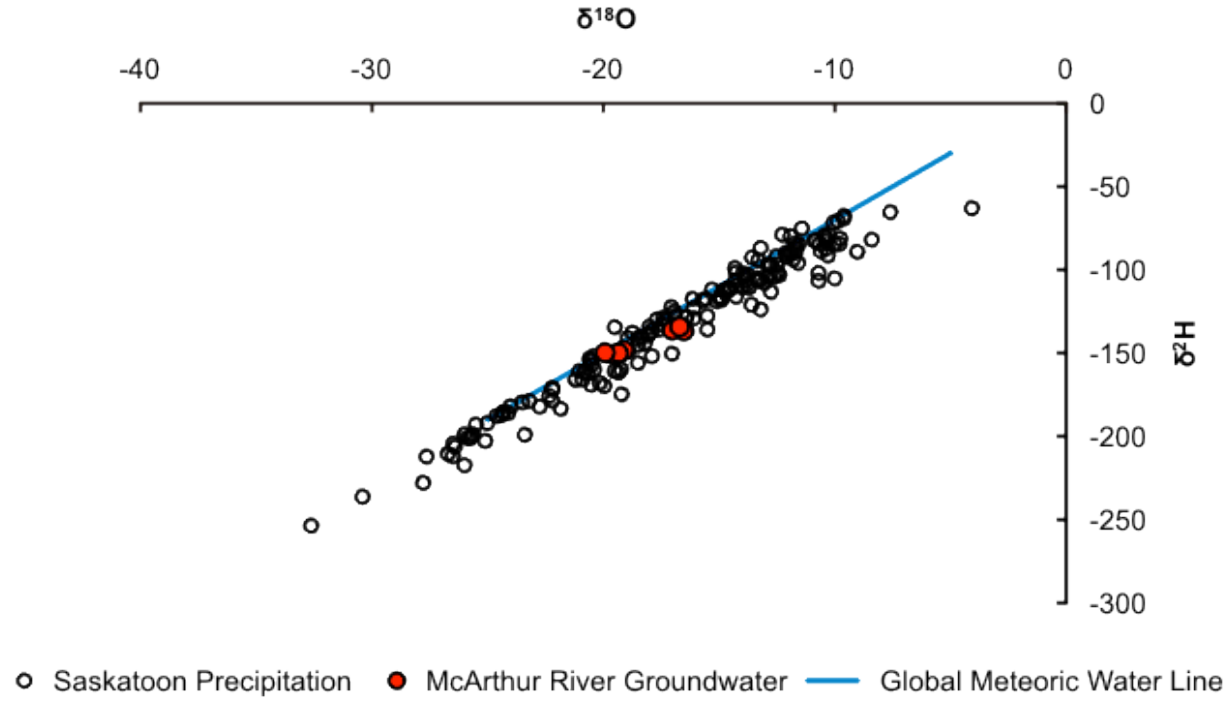

Figure 46: Scatter plot of $\delta^{18}O$ and $\delta^{2}H$ values from 14 shallow groundwater samples from McArthur River, Saskatoon precipitation (IAEA GNIP) and the Global Meteoric Water Line (Craig, 1961).

Table 21: $\delta^{2}H$- $\delta^{18}O$ values (‰) reported in $^{2}H/^{1}H$ and $^{18}O/^{16}O$ relative to Vienna Standard Mean Ocean Water (VSMOW).

Sample ID	$\delta\,^{2}H$ (VSMOW)	$\delta\,^{18}O$ (VSMOW)
MC-389	-151	-19.4
MC-393	-137	-16.5
MC-399	-148	-19.1
MC-403	-150	-19.9
MC-430	-136	-17.0
MC-434	-150	-19.3
Swamp Lake	-134	-16.7
Min	-151	-19.9
Max	-134	-16.5
Mean	-144	-18.3
Uncertainty	0.3	0.09

Uncertainty determined by analysis of a blind standard (n=6).

Dissolved C in groundwater above McArthur River is predominantly inorganic (Figure 47); DIC concentrations range from 1.17 – 7.59 mg/L C and DOC concentrations range from

0.65 – 198 mg/L (max. is 2.79 mg/L with outlier MC-430 removed) mg/L C. The $\delta^{13}C$ DIC data range from -23.0 to -10.1 ‰ and $\delta^{13}C$ DOC data range from -28.7‰ to -24.2‰ C (Table 22). $\delta^{13}C$ DIC values correspond to the oxidation of DOC, soil-derived CO_2, and the dissolution of non-marine carbonate, and $\delta^{13}C$ DOC values correspond to organic plant-derived C (Table 6).

Table 22: Concentration of dissolved organic carbon (DOC) and dissolved inorganic carbon (DIC), and their $\delta^{13}C$ (‰) values. Swamp Lake is a nearby fresh water lake (Figure 2), shown for reference to local surface water.

DDH	DIC (mg/L C)	$\delta^{13}C$ (DIC)	DOC (mg/L C)	$\delta^{13}C$ (DOC)
MC-399	2.99	-16.6	2.79	-25.4
MC-393	4.73	-13.0	1.14	-25.9
MC-389	7.59	-19.4	2.00	-24.2
MC-434	2.53	-15.3	0.65	-26.0
MC-403	2.47	-11.0	2.01	-26.1
MC-430	2.30	-23.0	198	-28.7
Swamp Lake	1.77	-10.1	2.77	-25.2
Min	1.77	-23.0	0.65	-28.7
Max	7.59	-10.1	198	-24.2
Mean	3.48	-15.5	29.8	-25.9

The ratio of dissolved inorganic carbon to dissolved organic carbon in groundwater ranges from near 0 to 4 throughout the six samples (Figure 47). MC-403 and MC-399 are most similar to surface water from nearby Swamp Lake (Figure 2), and MC-389, MC-393 and MC-434 have more dissolved inorganic carbon. MC-430 has roughly 100 times more DOC than DIC, further indicating that the groundwater from MC-430 is different from the other samples, and not comparable.

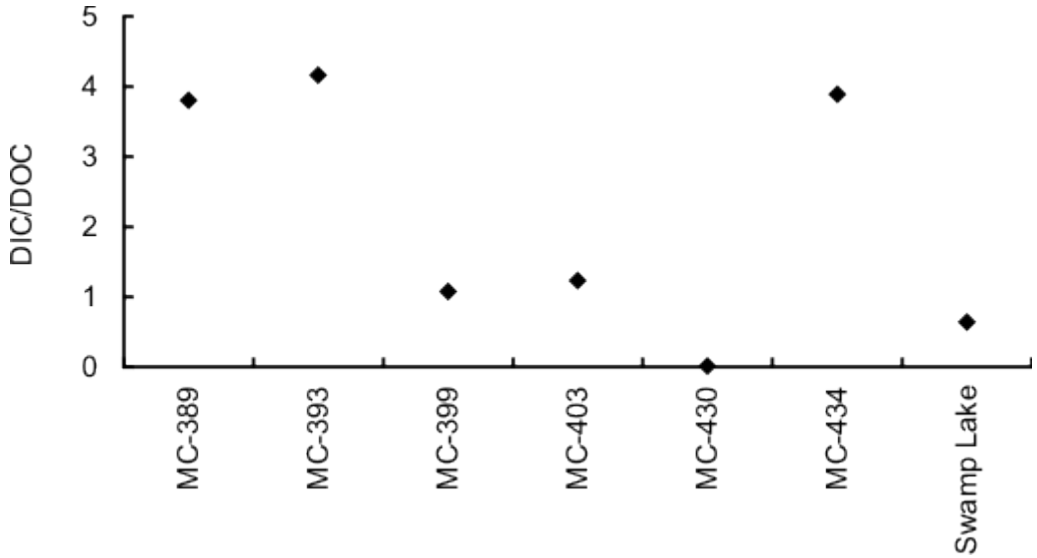

Figure 47: Ratio of dissolved inorganic carbon (DIC) and dissolved organic carbon (DOC) by sample site.

5.3.4 Tritium

Tritium in groundwater at the McArthur site ranges from 7.9 to 20.4 TU, with a mean value of 13.9 TU (Figure 48). ^{3}He data were not collected for these samples, so groundwater ages are approximate and assumed to be modern precipitation, <20 years old (Figure 100) because precipitation in northern Canada has had ^{3}H concentrations consistently below 20 TU since 1993. Figure 48 shows precise tritium values, after electrolytic enrichment and distillation, with error ranging from 1.69 – 2.54 TU. Northern latitudes have higher ^{3}H content in precipitation than mid-range latitudes, and continental areas have higher ^{3}H than coastal areas (Brown, 1970). However, McArthur River ^{3}H values are similar to that of present day northern Canada precipitation (Figure 100).

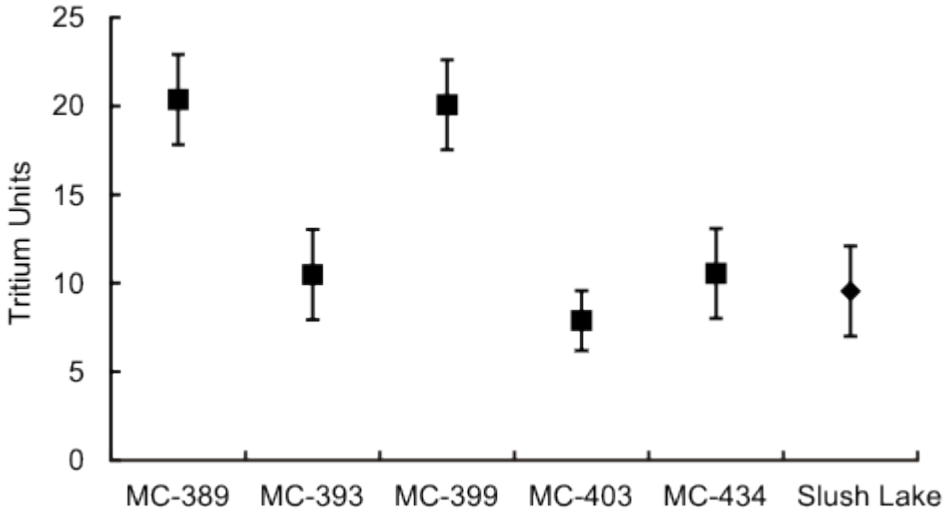

Figure 48: Tritum contents (in tritium units) of DDH groundwater at McArthur River and a nearby fresh water source (Slush Lake) in 2014. Error bars represent 1 standard deviation. X-axis labels correspond to the DDH number.

5.3.5 Rn in groundwater

Groundwater sampled at McArthur River was taken 1 m below the water level, all within the casing except for MC-4343 that was sampled from 4m below the casing depth. Radon activity ranged from 44 cpm – 5342 cpm (approximately 2 – 232 Bq/L), detected by a Perkin Elmer 1220 Quantulus Ultra Low Level Liquid Scintillation Spectrometer, throughout the six locations (Table 23). The highest Rn radioactivity within McArthur River groundwater was in MC-393, and the lowest Rn radioactivity was in MC-403 (Figure 49).

Table 23: Rn activity (counts per minute) from groundwater at 6 locations above the McArthur River deposit. Drill fence corresponds to the location of the drill-hole sampled relative to ore bodies at McArthur River.

DDH	Drill Fence	Easting	Northing	Rn Activity (cpm)	σ1
MC-389	SW	494941	6400249	703	31
MC-399	SW	495081	6400489	84	5
MC-403	SW	495736	6400986	44	14
MC-434	Between Zones 1: A	497478	6401540	4584	156
MC-393	SW	495522	6400773	5342	101

GPS coordinates are in Universal Transverse Mercator system, North American Datum 83, Zone 13 North.

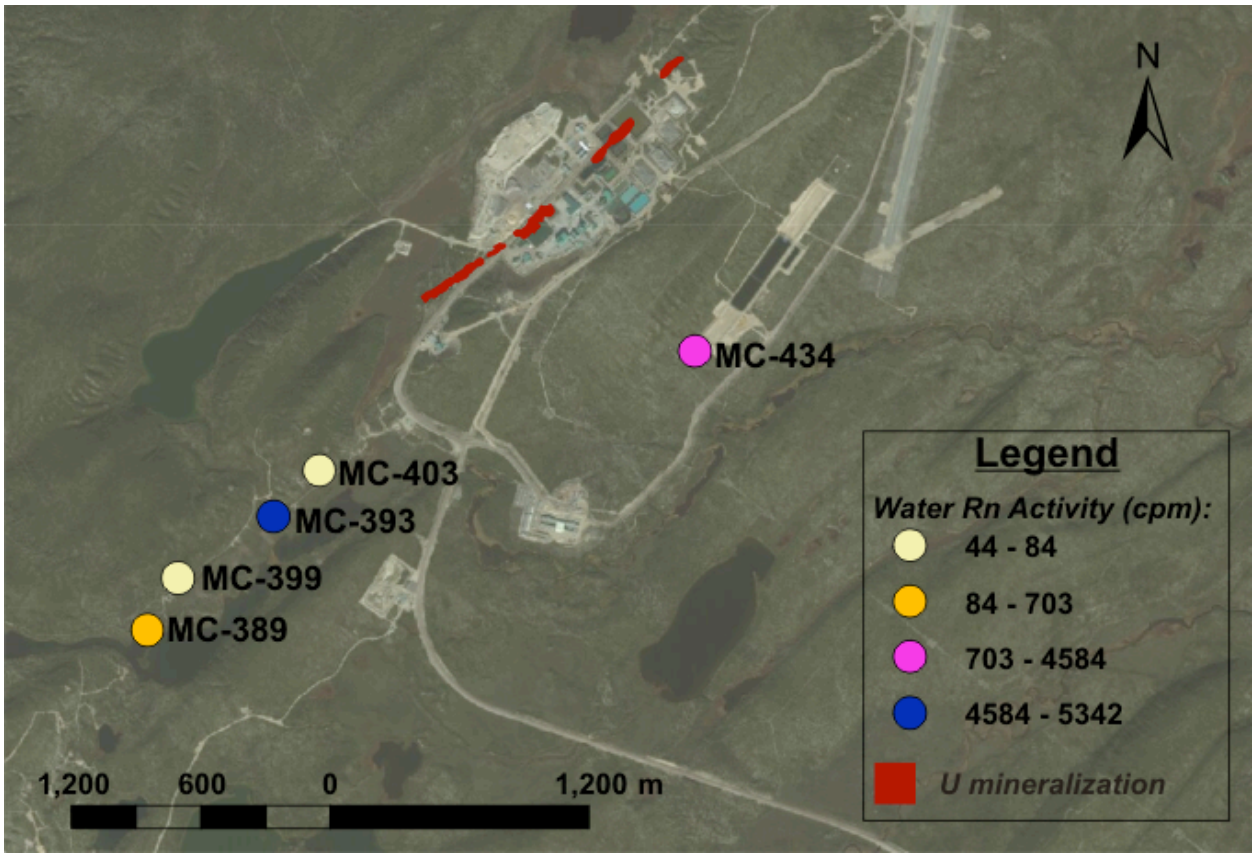

Figure 49: Plan view map of DDH sampled for Rn in groundwater at McArthur River. The red shapes represent surface projection of ore bodies, and Rn radioactivity increases from pale yellow to blue.

Overburden thickness varies throughout the McArthur River area due to several episodes of glaciation and it may impact the circulation of groundwater near the locations sampled for Rn. Table 24 compares Rn radioactivity in the groundwater to the depth of overburden in that particular drill-hole. In all cases the water was sampled at the water table. The main observation to note is that MC-434 has the highest Rn radioactivity, and is the only sample taken from a depth below the overburden and from below the casing depth. This may be an indication of a higher concentration of Rn-parent radionuclides (e.g. ^{226}Ra) in the upper sandstones compared to the till. Considering it was sampled below the casing it is also a true indication of the Rn

radioactivity at that specific depth in the DDH. For this study water samples taken within the casing are likely a mix of water from varying depths, flowing throughout the bedrock and up into the DDH.

Table 24: Groundwater Rn radioactivity and the depth to overburden in six McArthur River drill-holes. All depths are in meters below surface.

DDH	Depth to Overburden	Casing Depth	Sample Depth	Rn (cpm)
MC-389	23	23	0	703
MC-393	15	15	5	5342
MC-399	18	18	3	84
MC-403	16	16	10	44
MC-434	8	8	12	4584

Radiogenic ^{4}He was also measured from groundwater in several McArthur River drill-holes to determine if they would show the same pattern as Rn, because ^{4}He is produced during the alpha decay of several ^{238}U-series decay products. The first set of 8 diffusion samplers collected by Devine were not sufficiently crimped, which caused the sample gas to equilibrate with atmospheric air. Re-sampling for ^{4}He was arranged by Tom Kotzer, of Cameco Corporation in June of 2015, and 4 of 7 samples were also improperly crimped. Thus, out of 15 samples, only 3 yielded results of He dissolved in the groundwater (Table 25). All successful samples yielded ^{4}He levels that are in equilibrium with the atmosphere (Sample/ASW = 1), possible due to the absence of faults and fractures that are suspected to be conduits for ^{4}He to travel from mineralization to the surface (e.g. Hattori et al., 2014). All He samples were collected at depths below the casing, within sandstones.

Table 25: Noble gas abundance data from three McArthur River drill-holes, including depth of the water table, depth of sampling, and $^{4}He/^{20}Ne$ normalized to air saturated water (ASW). All samples had ^{4}He levels in equilibrium with the atmosphere.

DDH	Easting	Northing	Water Table Depth (m)	Sample Depth (m)	$[^{4}He/^{20}Ne]$ in sample / $[^{4}He/^{20}Ne]$ in ASW

MC-399	6400489	495081	1	60	1.07
MC-393	6400773	495522	1	60	1.10
MC-403	6400986	495736	10	60	1.03

GPS coordinates are in Universal Transverse Mercator system, North American Datum 83, Zone 13 North. Air saturated water has 8.6 mg O_2/L at 25ºC, and at sea level.

5.3.6 Rn in Soil

Rn in soil was collected near drill-holes sampled for groundwater, as well as areas to the north and west of the deposit (Figure 50). Reported results are an average of 5 repeated measurements from the same location (Table 26). Samples with replicate values greater than 2 times the standard deviation were not included. Depths ranged from 30-50 cm below the surface and activity ranged from 1.1-6.3 kBq/m^3. Rn radioactivity was highest at MC-251; the DDH closest to mineralization of the locations sampled, and was low near the DDH with the highest Rn-in-water radioactivity (MC-393). Rn in soil within the McArthur River footprint is low compared to background levels in non-mineralized areas within Canada (Gascoyne et al., 1993).

Table 26: Rn activity in soil with GPS coordinates and depth in meters. Activity is the average of five repeated measurements.

Proximal DDH	Easting	Northing	Depth (cm)	Activity (kBq/m^3)
MC-389	494956	6400269	31	1.1
MC-399	495091	6400474	55	2.7
MC-399	495064	6400490	55	1.5
MC-393	495522	6400772	53	1.8
MC-393	495523	6400773	37	2.4
MC-393	495520	6400771	53	1.5
MC-403	495731	6400976	26	4.1
MC-403	495729	6400991	31	4.6
MC-403	495733	6400962	54	3.1
MC-403	495765	6400971	40	2
MC-403	495712	6400984	50	3.4
MC-430	497253	6401807	30	2.5
MC-430	497242	6401772	30	2.7
MC-430	497286	6401751	50	3.7
MC-434	497425	6401538	40	1.3
MC-434	497486	6401546	40	4.4

MC-434	497458	6401568	40	3.1
MC-434	497464	6401526	50	2.5
MC-434	497512	6401520	40	1.9
MC-415	497762	6402979	40	2.8
MC-415	497791	6403032	30	2.5
MC-415	497727	6403008	40	3.2
MC-415	497740	6403059	40	2.4
MC-251	496359	6402015	40	4.3
MC-251	496351	6402020	30	5.1
MC-251	496342	6401994	35	6.3
MC-251	496371	6402011	35	5.5
MC-251	496396	6401996	40	5
MC-252	496069	6402111	30	2.9
MC-252	496096	6402127	30	1.9

GPS coordinates are in Universal Transverse Mercator system, North American Datum 83, Zone 13 North. Detection limit = 1 kBq/m^3.

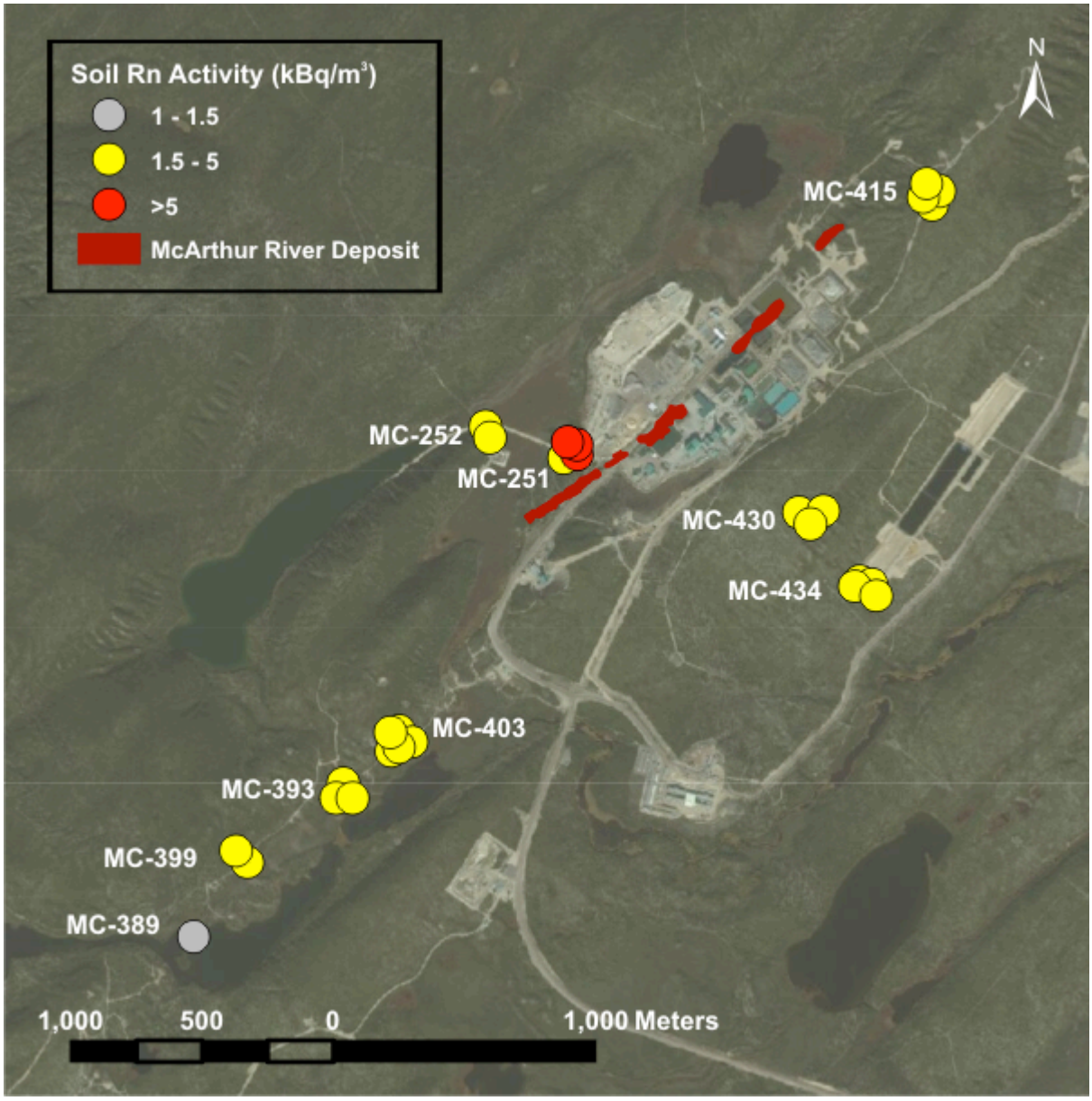

Figure 50: Plan view map of Rn radioactivity in soil at McArthur River. Activity increases from grey to red. Surface projections of U deposit lenses are illustrated in red.

5.3.7 Soil Geochemistry

B-horizon soil samples were collected from relatively undisturbed locations near drill-holes that were also sampled for Rn-soil gas (Figure 51) and, where possible, for water.

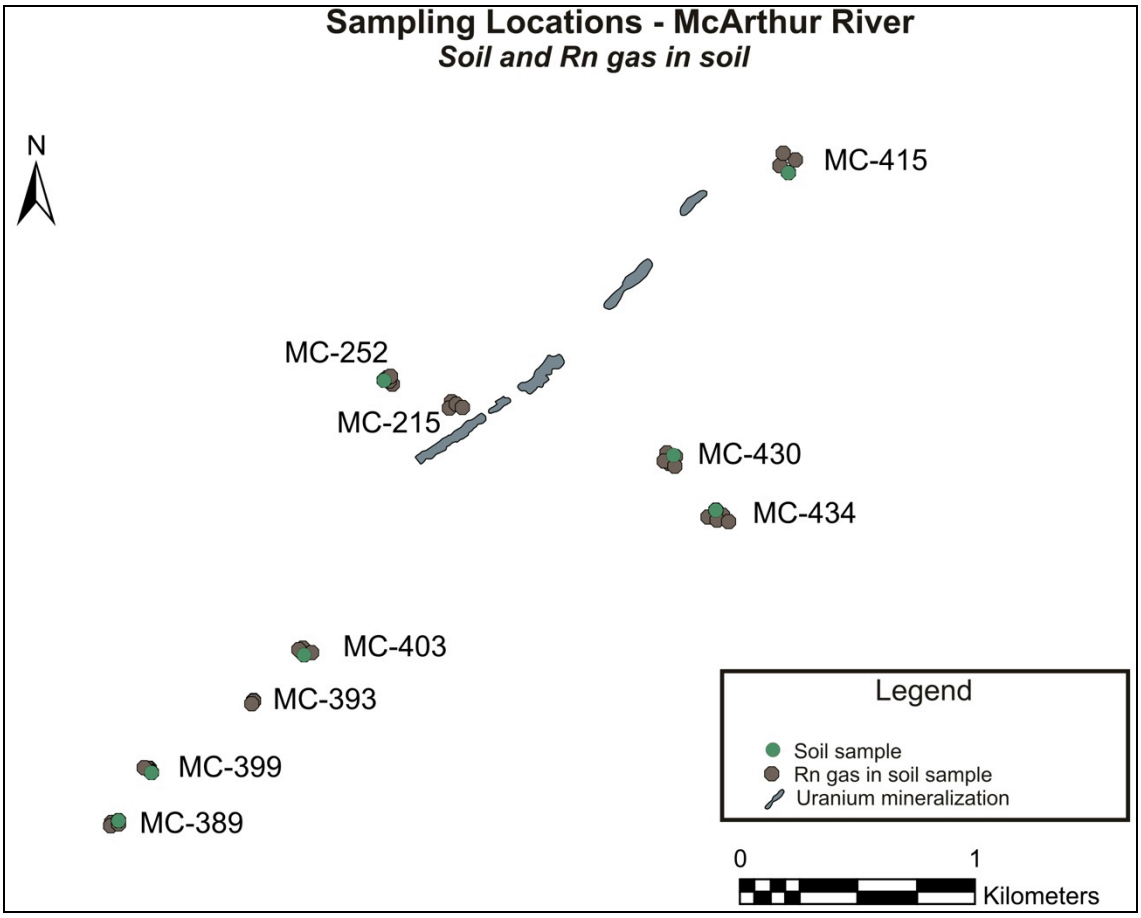

Figure 51: Plan view map indicating the surficial expression of the McArthur River uranium deposit in grey, soil sample locations in green dots and Rn-soil gas sampling locations in brown dots.

Soils were leached with ammonium acetate at pH=5 (AA5) and analysed for major and trace elements. Major element chemistry (Table 27) shows that Al > Ca > Fe are leached by ammonium acetate, and Mg, K, P and Ti are less soluble.

Table 27: Concentration of major elements leached by ammonium acetate from B-horizon soils at McArthur River. DL = detection limit.

Majors (ppm)	DL	MC251	MC252	MC389	MC393	MC399	MC403	MC415	MC430	MC434
Al	1	157	169	203	302	290	177	143	156	189
Ca	5	<5	8	33	44	29	<5	<5	<5	<5
Fe	5	8	39	17	12	14	11	13	11	13
Mg	1	1	3	4	4	5	2	1	1	<1

All values for K, P and Ti were below detections of 5 ppm, 5 ppm, and 1 ppm, respectively.

In order to determine the proportion of major, trace and REE that are weakly adsorbed, the AA5 leach results were compared to near-total digestion results of the same soils (Figure 52). The most abundant major element leached by AA5 was Al, with 143 – 302 ppm throughout nine B-horizon soil samples above the McArthur River deposit. The next most abundant major element was Fe with a concentration range of 8-39 ppm throughout the same nine samples. Ca concentrations were low and ranged from below detection (5 ppm) in four samples to 8-29 ppm in the remaining five samples. Mg concentrations within B-horizon soils at McArthur were all less than 5 ppm. K, P and Ti were all below detection within the same nine samples.

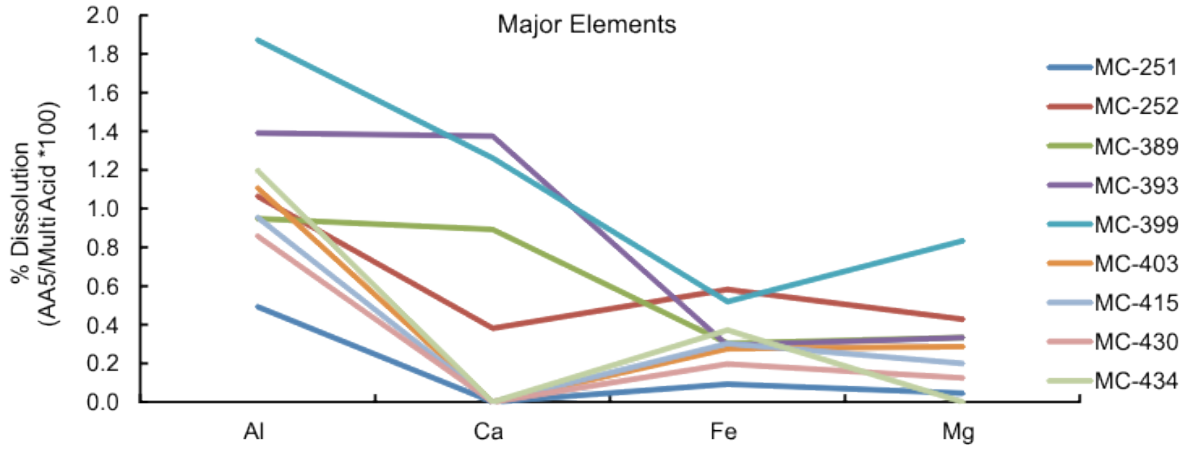

Figure 52: Line graph of major element chemistry of B-horizon soil samples from McArthur River collected in 2014. Ammonium acetate leach (pH = 5) chemistry, normalized with multi acid leach chemistry, and converted to percent.

As is evident from Figure 52, the percent dissolution of Ca is less than 2% for all samples, and therefore the Ca within the soil is not primarily hosted in carbonates, but rather less soluble minerals (apatite, feldspars).

Trace element concentrations of B-horizon soils weakly leached by AA5 (Table 28) are at ppb levels. The elements with the highest concentrations are Ba (1821 ppb – 10491 ppb), Mn (85 ppb – 8396 ppb), and Sr (55 ppb – 939 ppb). Ba and Sr are both alkali earth elements that

can replace Ca within minerals and are likely to adsorb onto Mn and Fe oxyhydroxides. Ra (the parent of Rn) also has similar chemical behaviours as Ba, Sr and Ca, however it is less well studied due to its radioactivity.

Table 28: Concentration of trace elements leached by ammonium acetate from B-horizon soils at McArthur River. DL = detection limit.

Element (ppb)	DL	MC251	MC252	MC389	MC393	MC399	MC403	MC415	MC430	MC434
Ba	50	7697	1678	5249	10491	5092	3970	4676	1821	2968
Cs	5	29	6	12	22	29	24	6	7	17
Cu	20	45	45	33	23	56	28	<20	62	42
Mn	50	85	687	1632	603	8396	455	901	795	6532
Ni	50	<50	59	125	125	204	<50	57	<50	93
Pb	20	<20	137	75	200	162	96	71	35	50
Sr	20	84	143	370	939	389	148	145	55	159
Th	20	100	30	60	43	31	69	40	67	27
U	5	62	21	27	32	23	20	15	55	9
Zn	100	<100	255	460	<100	558	281	<100	<100	<100
Zr	20	64	42	51	58	53	52	81	115	33

*All analyses were near or below detection limit for Sn (20), W (10), Cd (20), Au (1) and Ag (3), Be (20), Li (20), Co (20), Bi (5), Mo (10). Detection limit (ppb) written in brackets.

Typically, U provides the best indication of buried mineralization for shallow U deposits (Leybourne and Cameron, 2007). To determine the amount of mobile U in soils relative to the surface projection of the deep McArthur River deposit, it was plotted in quartiles (Figure 53). The small sample set does not allow for more robust geochemical statistics, and therefore single soil samples are treated as single locations. Figure 53 shows that U ranges from 9-62 ppb (AA5) within B-horizon soils at McArthur River. One of the upper quartile U values (near MC-251) occurs closest to the surface projection of the ore deposit. However, the other upper quartile U value (near MC-430) occurs south of the deposit near two un-mineralized DDH.

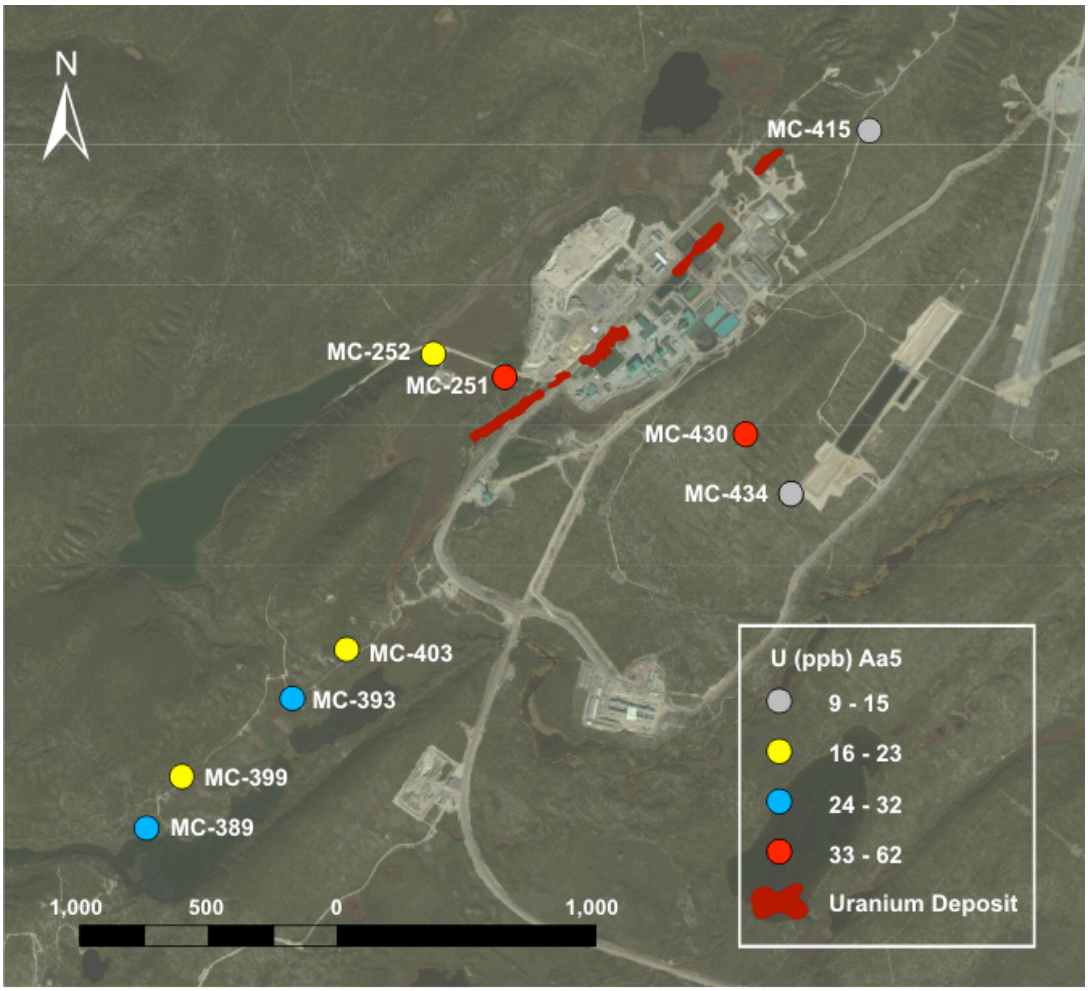

Figure 53: Plan view map of uranium concentrations leached from B-horizon soils near McArthur River. Values are divided into quartiles, and given in parts per billion (ppb).

The proportion of trace elements that are weakly adsorbed to clays, Fe-Mn-oxy-hydroxides or carbonates is determined by the percent of the element dissolved by AA5 divided by its total bulk chemistry. B-horizon soils taken at McArthur River show different % dissolution patterns, and therefore must be composed of different secondary minerals. MC-251 shows the greatest proportion of Cu, Mn, Ni and Pb compared to any other soil tested (Figure 54). MC-434 also shows high percent dissolution for Cu, Mn, Ni and Zn (Figure 54). All samples except MC-403 and MC-430 show between 2% and 13 % dissolution of Ni, and between 2% and 7% of U within the soils is hosted within secondary minerals. Overall, these B-horizon soils have a larger

portion of trace elements hosted within secondary minerals than the soils from the Millennium site.

The partial leach geochemistry of B-horizon soils at McArthur River indicates that typical indicator elements (Se, Mo, As, V, Cu and Pb) are not the most abundant on Fe-Mn oxides, co-precipitating with carbonates, nor adsorbed to clays. Rather, Mn, Sr, Ba and Zr appear to be the most abundant weakly adsorbed elements.

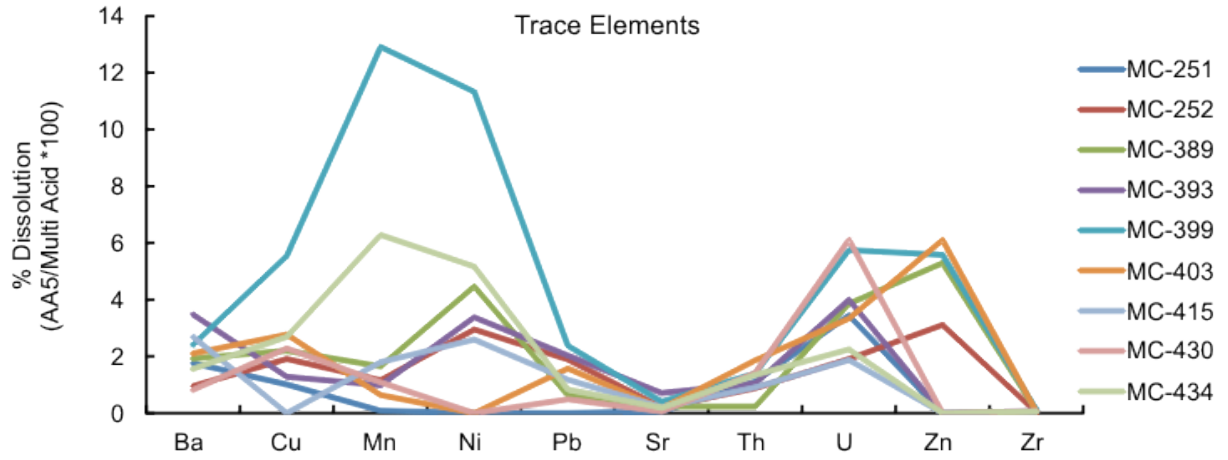

Figure 54: Line graph of trace element chemistry of B-horizon soil samples from McArthur River collected in 2014. Ammonium acetate leach (pH = 5) chemistry, normalized with multi acid leach chemistry, and converted to percent.

The portion of weakly adsorbed REE in B-horizon soils at is represented by the data from the % dissolution AA5 leach (Table 29 and Figure 55). Overall, less than 3.5 % of REE within the soil are leached, indicating that the majority are likely present within primary minerals present within sandstones such as aluminum phosphate-sulphate minerals (APS) (Adlakha and Hattori, 2015), xenotime and/or monazite (Quirt, 2005; Chen et al., 2015). Figure 55 shows that within each soil sample, the LREE (La, Ce, Pr, Nd) show very similar % dissolution, and the heavier REEs (Sm, Gd, Dy) and Y show more variable % dissolution.

Table 29: Concentration of rare earth elements and Y leached by ammonium acetate from B-horizon soils at McArthur River. DL = detection limit.

Element (ppb)	DL	MC251	MC252	MC389	MC393	MC399	MC403	MC415	MC430	MC434
La	5	199	14	56	37	78	63	77	60	21
Ce	5	316	20	96	84	125	118	145	162	60
Pr	5	46	<5	15	5	14	19	19	19	<5
Nd	5	169	19	77	28	58	56	59	85	23
Sm	5	33	<5	16	<5	14	13	17	23	<5
Gd	5	30	<5	8	<5	9	<5	11	9	5
Dy	5	45	<5	13	9	7	6	10	22	<5
Y	5	167	5	37	28	36	28	42	60	15

The % dissolution for all B-horizon soils does not follow the same pattern for each sample tested. This suggests that the secondary mineral phases contain varying amounts of REEs. The soil sample MC-399 contained the highest concentration of REEs (from AA5 leach) except for Dy.

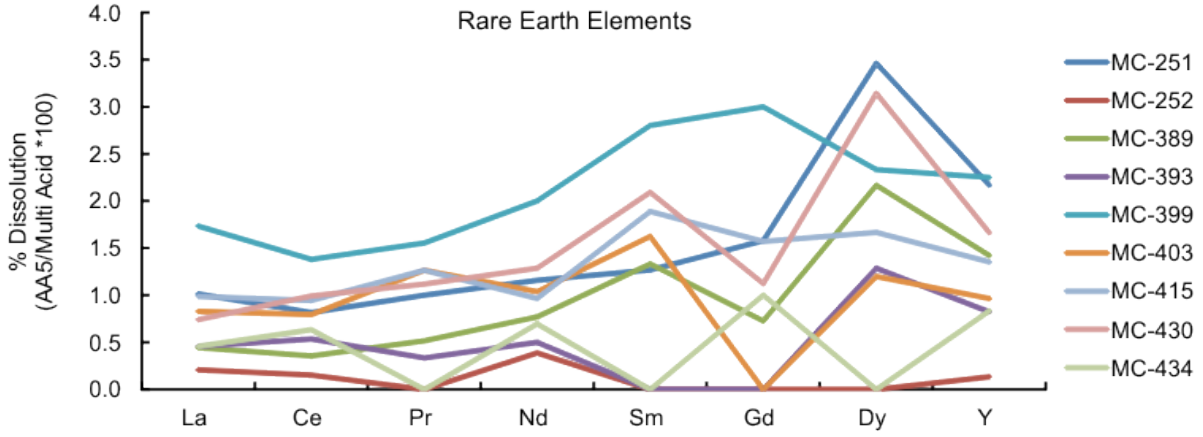

Figure 55: Line graph of rare earth element chemistry of B-horizon soil samples from McArthur River collected in 2014. Ammonium acetate leach (pH = 5) chemistry, normalized with multi acid leach chemistry, and converted to percent.

A multi-acid digestion was performed on a separate of the same soil samples. It reveals greater concentrations of elements because more elements are dissolved than by AA5. The major element chemistry of B-horizon soils near nine drill-holes at McArthur River (Table 30 and

Figure 56) represents the near total digestion of the soils the chemistry of the minerals within the till and soil. As was the case with partial digestion, Al (kaolin minerals, smectite), Ca (calcite) and Fe (iron-oxides) are strong components of the till. Unlike the partial digestion, Na and K are also large components of soil because they are contained within less soluble minerals such as illite and feldspars.

Table 30: Major element concentrations of McArthur River B-horizon soils after multi-acid digestion. DL = detection limit.

Element (%)	DL	MC251	MC252	MC389	MC393	MC399	MC403	MC415	MC430	MC434
Fe	0.02	0.87	0.67	0.56	0.41	0.27	0.4	0.43	0.56	0.35
Ca	0.01	0.41	0.21	0.37	0.32	0.23	0.23	0.19	0.26	0.21
P	0.001	0.045	0.054	0.015	0.015	0.025	0.013	0.016	0.029	0.018
Mg	0.01	0.22	0.07	0.12	0.12	0.06	0.07	0.05	0.08	0.05
Ti	0.001	0.149	0.084	0.078	0.069	0.04	0.051	0.077	0.095	0.052
Al	0.01	3.19	1.59	2.14	2.17	1.55	1.6	1.5	1.82	1.58
Na	0.002	1.16	0.53	0.96	0.95	0.66	0.62	0.49	0.65	0.59
K	0.01	1.44	0.56	0.92	0.97	0.71	0.64	0.54	0.69	0.62

*All sulfur values were below detection (<0.04)

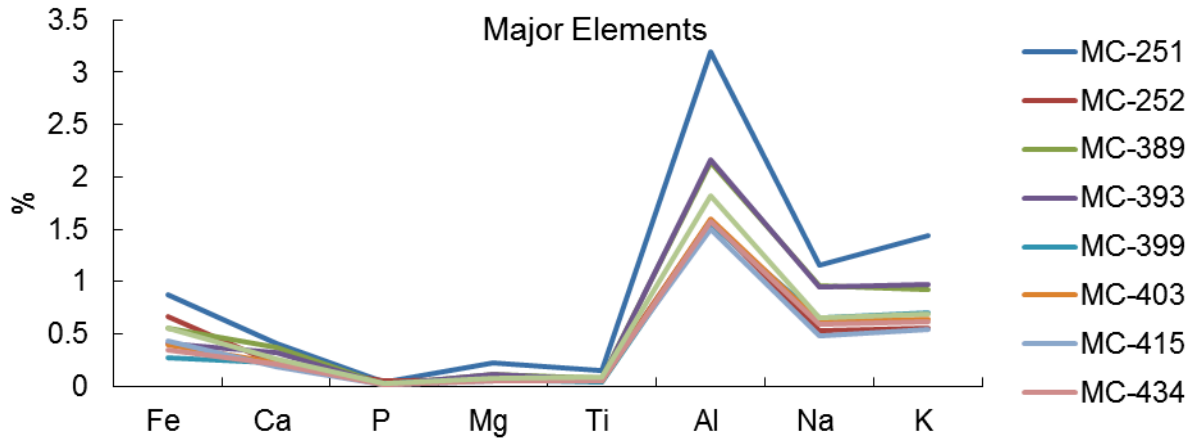

Figure 56: Major elements dissolved by multi-acid digestion of McArthur River soil samples; concentrations are in percent.

Multi-acid leach trace element concentrations in McArthur River soils are presented below (Table 31 and Figure 57). In each soil sample there are high concentrations of Pb, Cu, Ni, V, and and As relative to Co, Mo, Sn, U and Se. The most abundant trace elements are Pb, V and Zn.

Table 31: Trace element concentrations in ppm (Ag in ppb) of McArthur River B-horizon soils dissolved by multi-acid digestion. DL = detection limit.

Element (ppm)	DL	MC251	MC-252	MC389	MC393	MC399	MC403	MC415	MC430	MC434
Mo	0.05	0.16	0.2	0.1	0.12	<0.05	0.07	0.13	0.12	<0.05
Cu	0.02	4.44	2.35	1.5	1.79	1.01	1.01	1.19	2.71	1.56
Pb	0.02	12.59	7.24	11.88	9.84	6.8	6.1	6.03	7.2	6.02
Zn	0.2	10.7	8.2	8.7	9.1	10	4.6	4.4	8.3	15
Ag (ppb)	20	83	68	41	50	26	46	52	68	39
Ni	0.1	4.9	2	2.8	3.7	1.8	1.9	2.2	2.7	1.8
Co	0.2	1.9	0.5	1.3	1	0.7	0.8	0.9	1.2	0.5
Mn	2	98	59	99	61	65	71	50	73	104
As	0.2	2	1.4	1.2	1.1	1.2	1.4	1.6	1	1.1
U	0.1	1.8	1.1	0.7	0.8	0.4	0.6	0.8	0.9	0.4
Th	0.1	9	3.4	25.1	4.1	2.2	3.7	4.4	4.7	2
Sr	1	141	74	160	131	96	87	69	93	84
Cd	0.02	0.1	0.08	0.05	0.04	<0.02	0.05	0.06	0.07	0.03
Sb	0.02	0.1	0.09	0.05	0.09	0.06	0.06	0.1	0.08	0.05
Bi	0.04	0.12	0.08	<0.04	0.08	<0.04	<0.04	<0.04	<0.04	<0.04
V	1	20	15	10	10	5	8	9	12	7
Cr	1	10	7	6	5	3	3	4	6	3
Ba	1	436	176	272	302	211	188	174	221	190
W	0.1	0.5	0.3	0.2	0.3	0.2	0.2	0.2	0.3	-
Zr	0.2	200.1	158.9	59.7	92.2	42.7	97.4	154.8	162.8	62.9
Sn	0.1	1.1	0.5	0.4	0.5	0.2	0.2	0.4	0.4	0.2

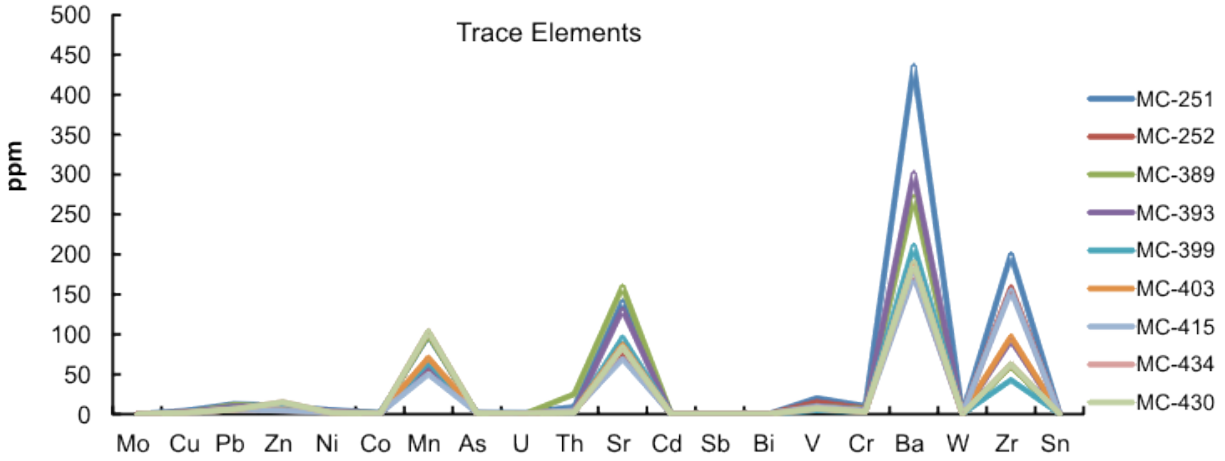

Figure 57: Scatterplot of trace elements dissolved by multi-acid digestion of McArthur River soil samples; concentrations are in parts per million.

Bulk concentrations of rare earth elements (Table 32) were normalized using the North American Shale Composite (NASC) (Condie, 1993). Normalized REE patterns show a declining slope from LREE to HREE (Figure 58). McArthur River B-horizon soils are depleted in REEs relative to both NASC due to the ratio <1. Soil sample MC-251 has the highest concentration of REEs relative to NASC, and MC-434 has the lowest REE concentration.

Table 32: Rare earth element (REE) concentrations in ppm of McArthur River B-horizon soils dissolved by multi-acid digestion. DL = detection limit.

Element (ppm)	DL	MC251	MC252	MC389	MC393	MC399	MC403	MC415	MC430	MC434
La	0.1	19.6	6.7	12.6	8.1	4.5	7.6	7.8	8.1	4.6
Ce	0.01	38.7	13.2	27.0	15.7	9.06	14.9	15.3	16.3	9.47
Pr	0.1	4.6	1.3	2.9	1.5	0.9	1.5	1.5	1.7	0.8
Nd	0.1	14.6	4.9	10	5.6	2.9	5.4	6.1	6.6	3.3
Sm	0.1	2.6	0.8	1.2	0.9	0.5	0.8	0.9	1.1	0.5
Eu	0.1	0.5	0.2	0.2	0.2	0.2	0.05	0.2	0.2	0.05
Gd	0.1	1.9	0.8	1.1	0.9	0.3	0.7	0.7	0.8	0.5
Tb	0.1	0.2	<0.1	<0.1	<0.1	<0.1	<0.1	<0.1	<0.1	<0.1
Dy	0.1	1.3	0.6	0.6	0.7	0.3	0.5	0.6	0.7	0.3
Ho	0.1	0.3	<0.1	<0.1	<0.1	<0.1	<0.1	<0.1	<0.1	<0.1
Er	0.1	0.8	0.4	0.3	0.4	0.2	0.3	0.4	0.4	0.2
Yb	0.1	0.8	0.5	0.3	0.4	0.2	0.3	0.3	0.5	0.2
Lu	0.1	0.2	<0.1	<0.1	<0.1	<0.1	<0.1	<0.1	<0.1	<0.1-
Hf	0.01	5.8	4.24	1.76	2.63	1.1	2.78	4.16	4.27	1.67

Sc	0.1	2.6	1.2	1.2	1.3	0.6	1	1	1.3	0.8
Y	0.1	7.7	3.7	2.6	3.4	1.6	2.9	3.1	3.6	1.8

Tm is below detection limits (0.1 ppm).

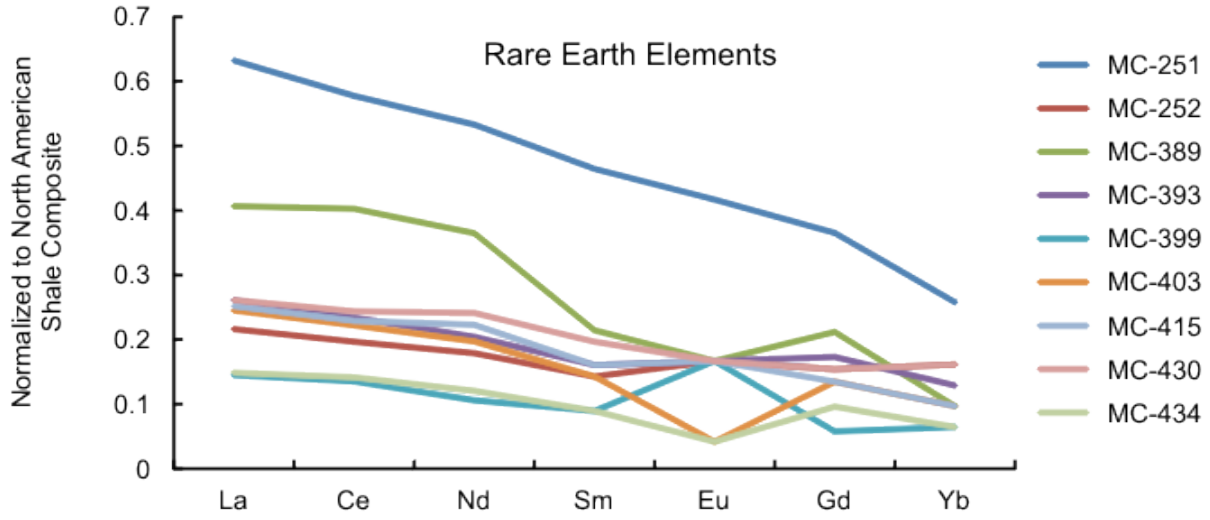

Figure 58: Line graph of REE from multi-acid digestion of B-horizon soils. Concentrations are normalized to North American Shale Composite (Condie, 1993).

Rare earth element patterns show a general trend of LREE-enrichment when normalized to the NASC. Some B-horizon soils show Eu anomalies, most likely reflecting the presence or absence of feldspars within the till. Major element chemistry aligns with the XRD results indicating that the major components of the soil are likely illite, kaolin minerals, with lesser calcium and Fe-bearing minerals which are discussed in more detail throughout the sequential leach section 4.2.8.

5.3.8 Fracture Sequential Leach

Drill-holes (n=13) at McArthur River were sampled in the top 100 m of MFd sandstones for open fractures with mineral coatings on their surfaces (Figure 59). Several analyses were completed to determine if fractures were potential conduits for radiogenic elements throughout the sandstones. The interaction of groundwater and fracture surfaces could be the cause of

radiogenic elements in the groundwater within the McArthur River footprint area. Core fracture material was leached by water and four different concentrations of HNO_3. Secondly, X-ray diffraction was used to identify end-member fracture samples for minerals that are present along common fracture surfaces. Lastly, γ-ray spectrometry of these samples was performed to determine the amount of Ra within the core fracture material. Table 33 lists the location, depth, angles of fracture coatings in sampled drill holes.

Table 33: McArthur River fracture coating samples listed by drill-hole ID and sample depth.

Fracture Sample ID	Easting	Northing	Fracture α-angle (relative to core axis)	Drill Hole Dip
MC-208-13.4	496851	6402266	Low	-90
MC-208-86.2	496851	6402266	low (~10º)	-90
MC-208-86.5	496851	6402266	high (~90º)	-90
MC-246-53.0	496419	6401950	long, low	-90
MC-246-71.8	496419	6401950	low and high	-90
MC-252-21.7	496198	6402117	low (~10º)	-90
MC-253-70.4	496989	6402119	high (~45º)	-55
MC-253-78.0	496989	6402119	Low	-55
MC-255-101.7	496473	6401896	Low	-90
MC-255-24.1	496473	6401896	Low	-90
MC-255-37.0	496473	6401896	wavy, low	-90
MC-255-47.2	496473	6401896	Low	-90
MC-338-19.0	495524	6400771	Low	-82
MC-338-64.6	495524	6400771	High	-82
MC-413-73.6	497719	6403037	Low	-73
MC-415-80.4	497762	6403008	Low	-76
MC-415-82.9	497762	6403008	High	-76
MC-434-24.2	497458	6401568	high (75)	-70
MC-434-9.0	497458	6401568	high (80)	-70

The α-angle (fracture angle relative to the core axis) was estimated at time of sampling. Low refers to an angle <45º, and high refers to an angle >45º.

Of the fractures sampled, 6 were high angle fractures (greater than 45 degrees relative to core axis) and 13 were low angle fractures. Of the drill-holes sampled for fractures, 11 were from DDH that intersected mineralization at depth, and two were from DDH that did not intersect

mineralization. MC-434 was at the time the most recent hole drilled in 2015 and did not intersect mineralization.

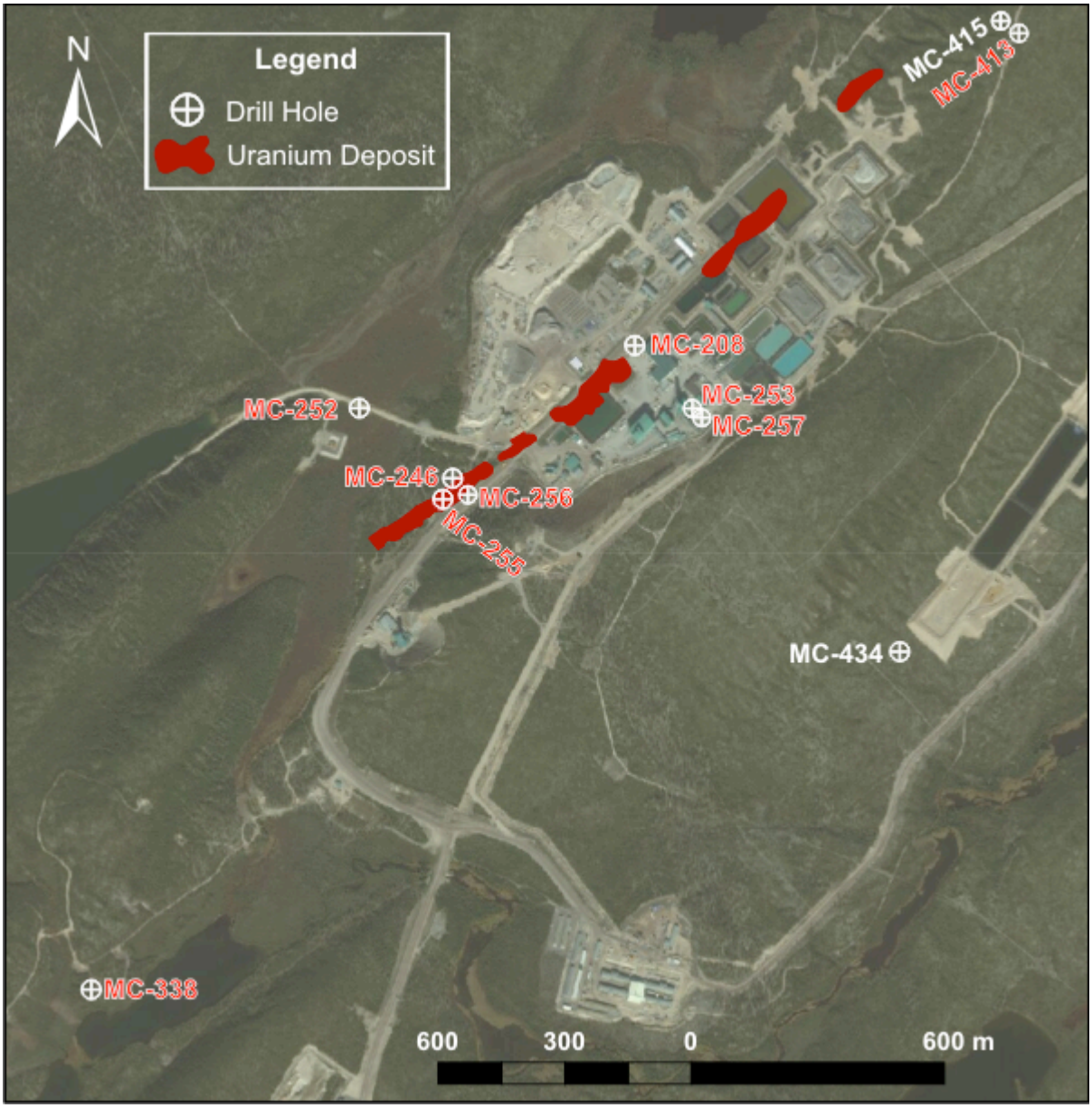

Figure 59: Plan view map illustrating the location of the McArthur River U deposit in red, and the location of drill-holes sampled for core fracture samples. Drill-holes that intersect mineralization are labelled in red and background holes are labelled in white.

Leachates were analysed for P, Mn, Fe, Ni, Cu, As, Zr, Ba, Pb, Th, U and Ca by ICP-MS. The water leach (Figure 60-65) was predicted to dissolve elements that are water-soluble and/or

weakly adsorbed to the surface of mineral grains. Results show that Fe (0.86 – 31.1 ppm) and Ca (1.27 – 21.3 ppm) were the main elements leached by water. Two samples, 415-82.9 and 255-102, showed higher concentrations of Mn; 6.07 ppm and 6.77 ppm of Mn, respectively, compared to an average of 1.27 ppm of the 19 samples. These results are evidence for water-soluble Fe-Mn-oxy-hydroxides. It is also evidence for water-soluble Ca bearing minerals in which other alkali earth metals such as Ra could substitute and be dissolved by water. Other potential sources of Ca and Fe, Mn are elements adsorbed to the surfaces of clay minerals. The following six figures illustrate the water-leach results from eight DDH. Proximal DDH were grouped together for comparison.

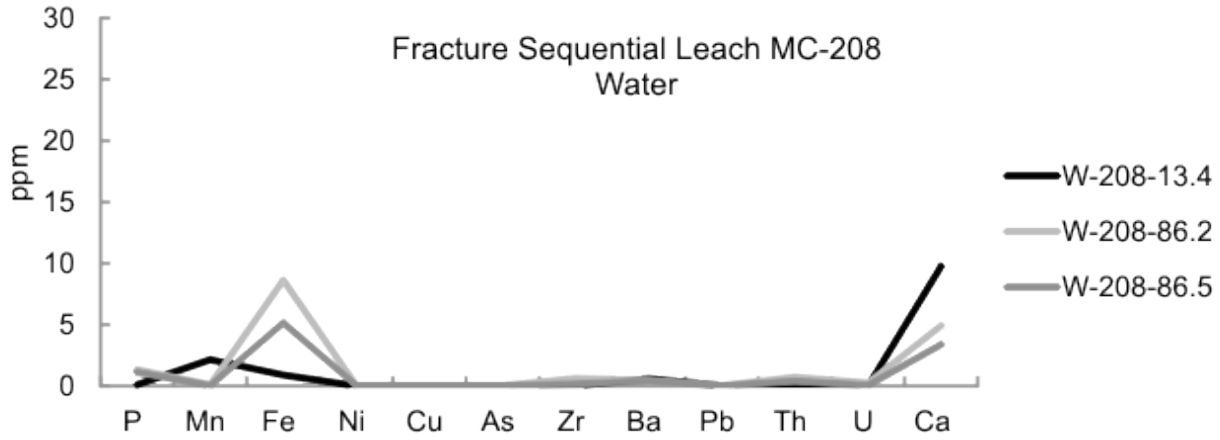

Figure 60: Concentrations (ppm) of water-leached elements from three fractures taken at 13.4 m (black), 86.2 m (light grey) and 86.5 m (dark grey) within drill-hole MC-208.

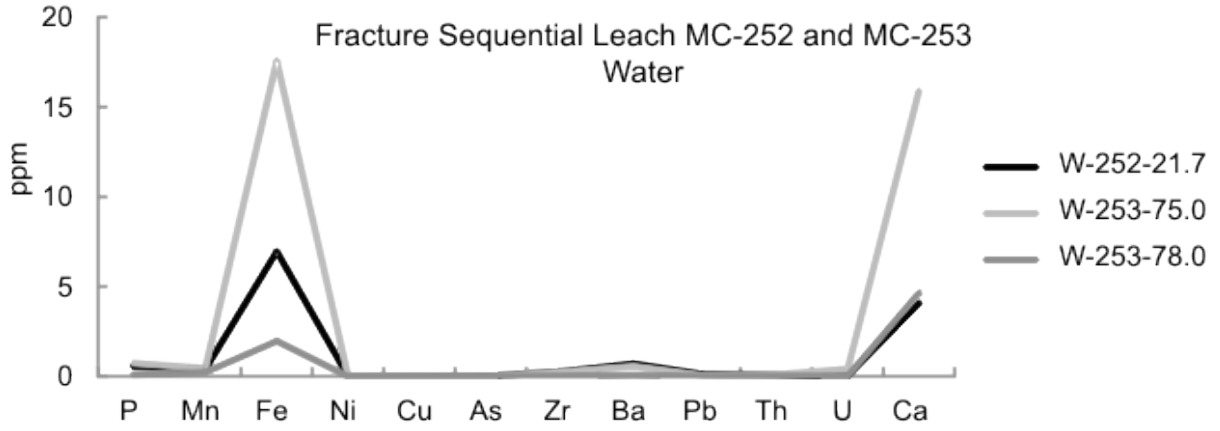

Figure 61: Concentrations (ppm) of water-leached elements from three fractures taken at 21.7 m (black) within drill-hole MC-252, and at 75 m (light grey) and 78 m (dark grey) within drill-hole MC-253.

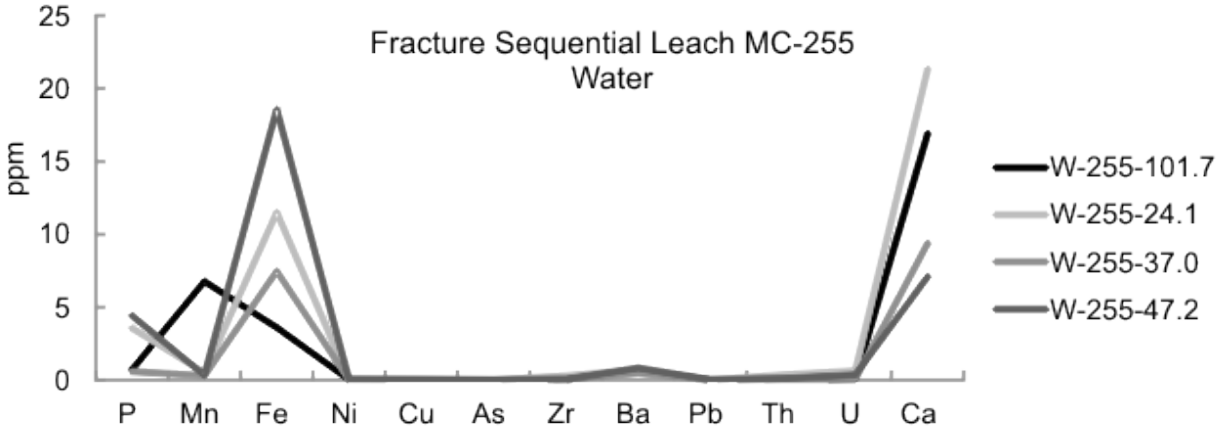

Figure 62: Concentrations (ppm) of water-leached elements from four fractures taken at 101.7 m (black), 24.1 m (light grey) and 37.0 m (medium grey), and 47.2 m (dark grey) within drill-hole MC-255.

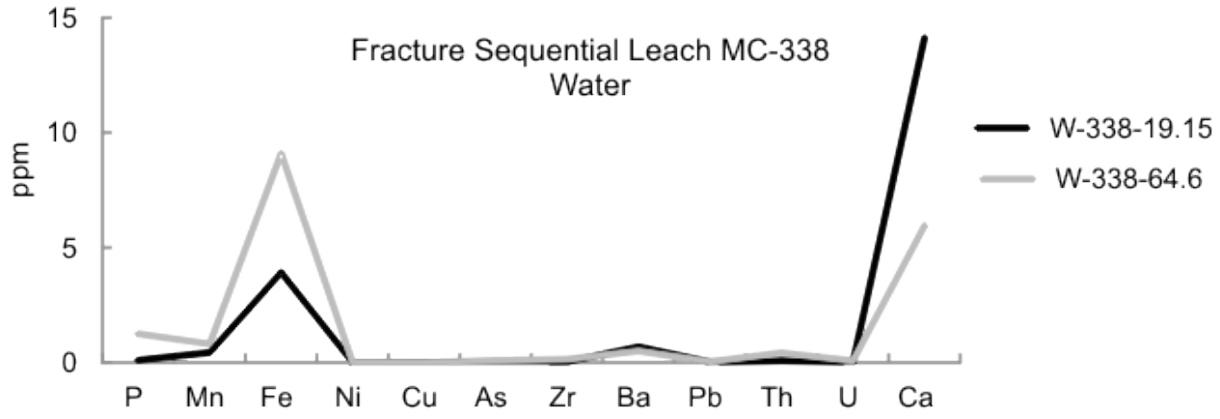

Figure 63: Concentrations (ppm) of water-leached elements from two fractures taken at 19.15 m (black), 64.6 m (light grey) within drill-hole MC-338.

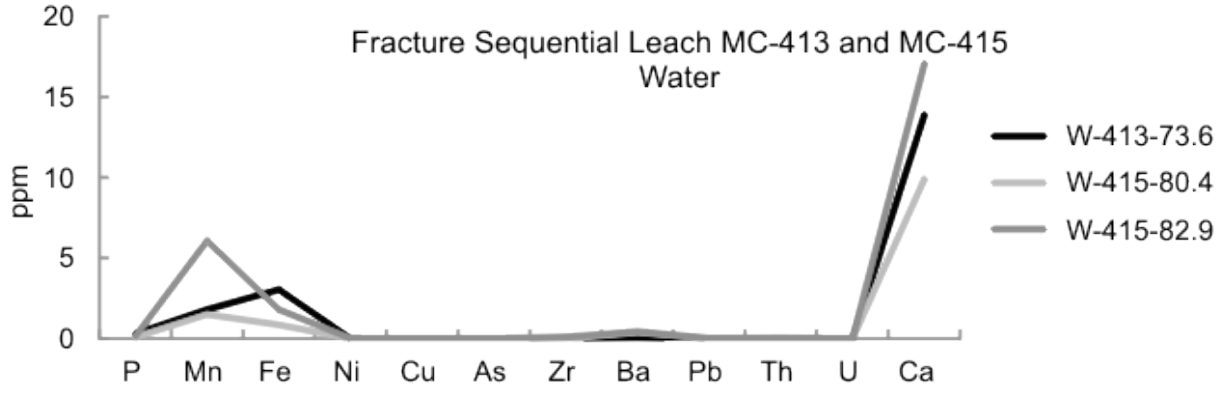

Figure 64: Concentrations (ppm) of water-leached elements from three fractures taken at 73.6 m (black) from drill-hole MC-413, and two fractures at 80.4 m (light grey) and 82.9 m (dark grey) within drill-hole MC-415.

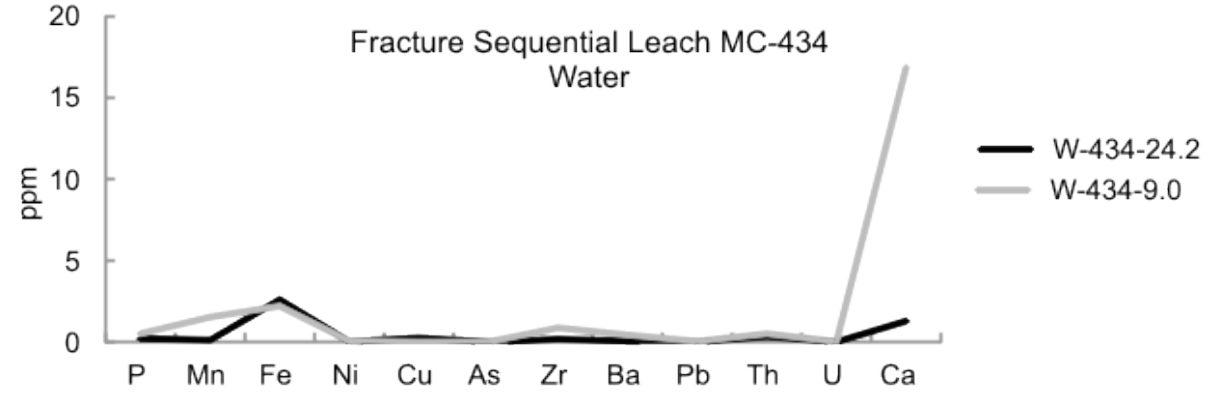

Figure 65: Concentrations (ppm) of water-leached elements from two fractures taken at 24.2 m (black) and 9.0 m (light grey) within drill-hole MC-434.

The first acidic leach (A1) (Figure 66-72) used 0.05 N HNO_3 and was predicted to leach elements weakly adsorbed on the surface of minerals and oxyhydroxides into solution. We see the same elements leached as with the water leach, but at higher concentrations; Fe (151 – 6.84 $x10^3$ ppm), Ca (55 – 1.51 x 10^3 ppm) and Mn (5.9 – 1.44 $x10^3$ ppm). The same samples that had relatively higher levels of Mn with the water leach are also the samples with higher levels of Mn with the A1 (255, 413, 415 and 434). Concentrations (ppm) indicate the elements dissolved by the water leach and the 0.5 N HNO_3 leach.

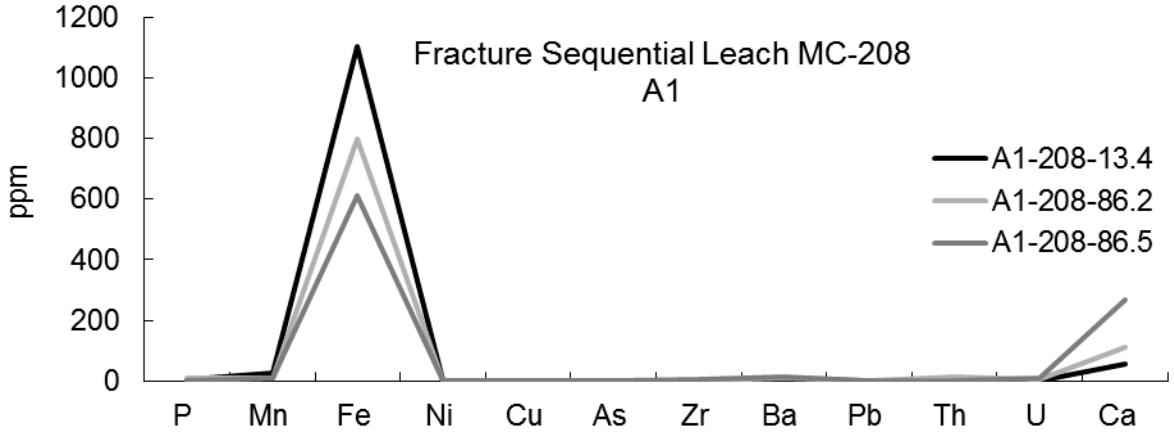

Figure 66: Concentrations (ppm) of elements leached in 0.05 N HNO3 from three fractures taken at 13.4 m (black), 86.2 m (light grey) and 86.5 m (dark grey) within drill-hole MC-208.

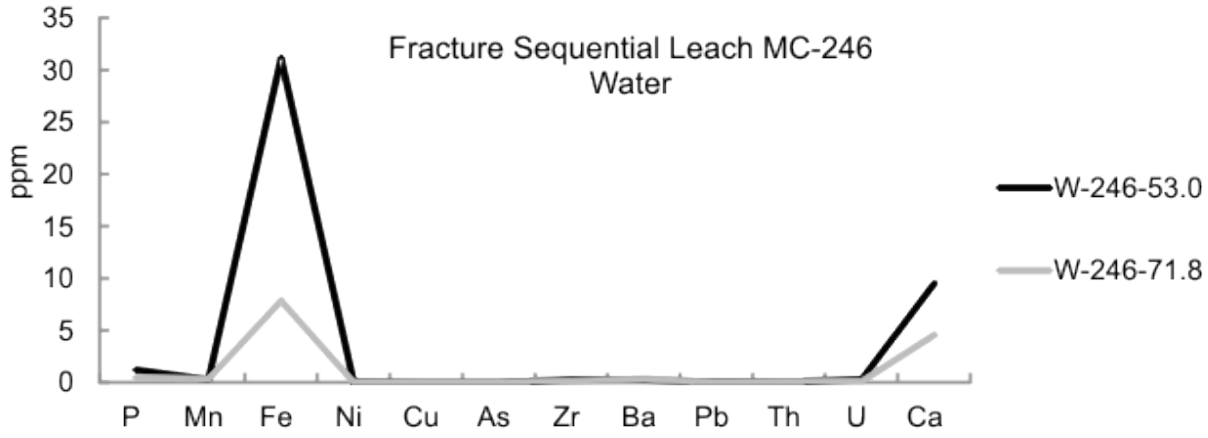

Figure 67: Concentrations (ppm) of elements leached in 0.05 N HNO_3 from two fractures taken at 53 m (black) and at 71.8 m (light grey) within drill-hole MC-246.

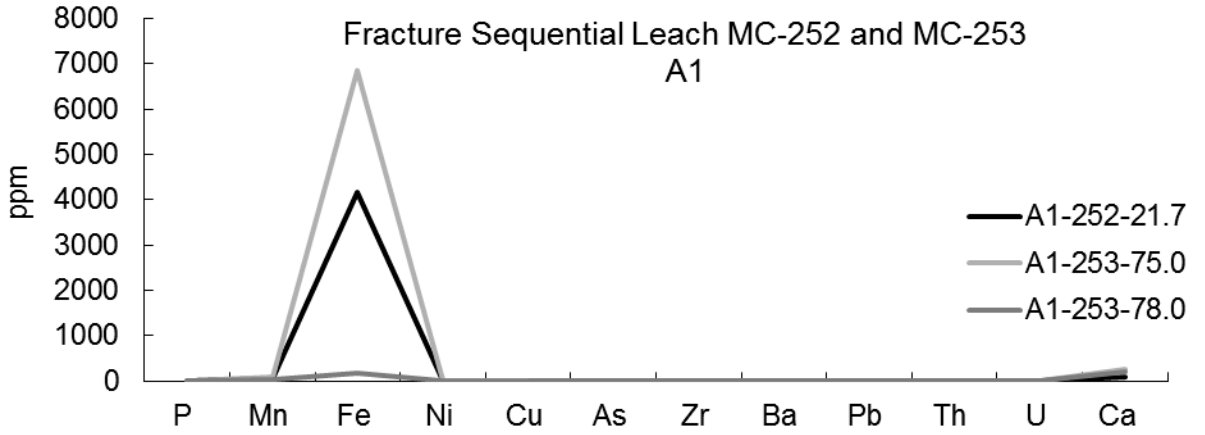

Figure 68: Concentrations (ppm) of elements leached in 0.05 N HNO_3 from three fractures taken at 21.7 m (black) within drill-hole MC-252, and at 75 m (light grey) and 78 m (dark grey) within drill-hole MC-253.

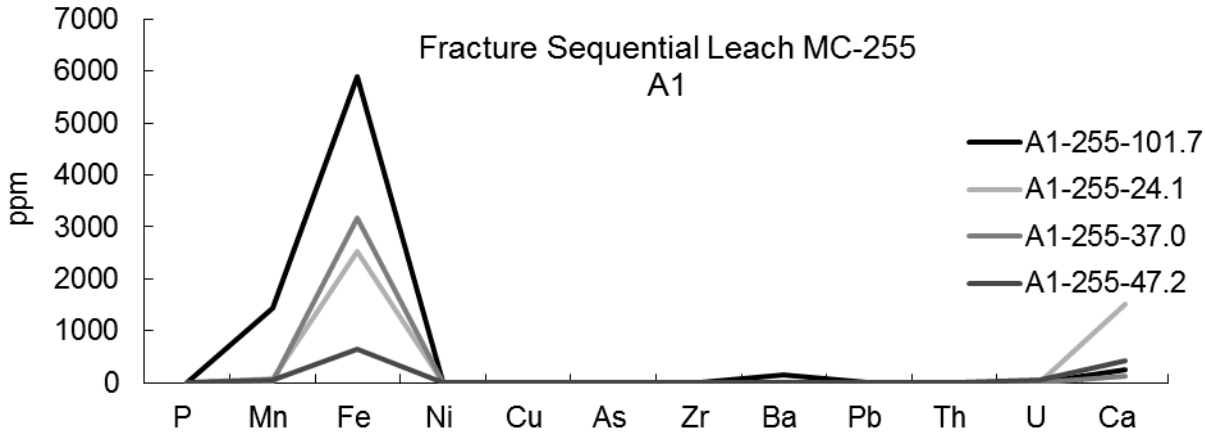

Figure 69: Concentrations (ppm) of elements leached in 0.05 N HNO_3 from four fractures taken at 101.7 m (black), 24.1 m (light grey) and 37.0 m (medium grey), and 47.2 m (dark grey) within drill-hole MC-255.

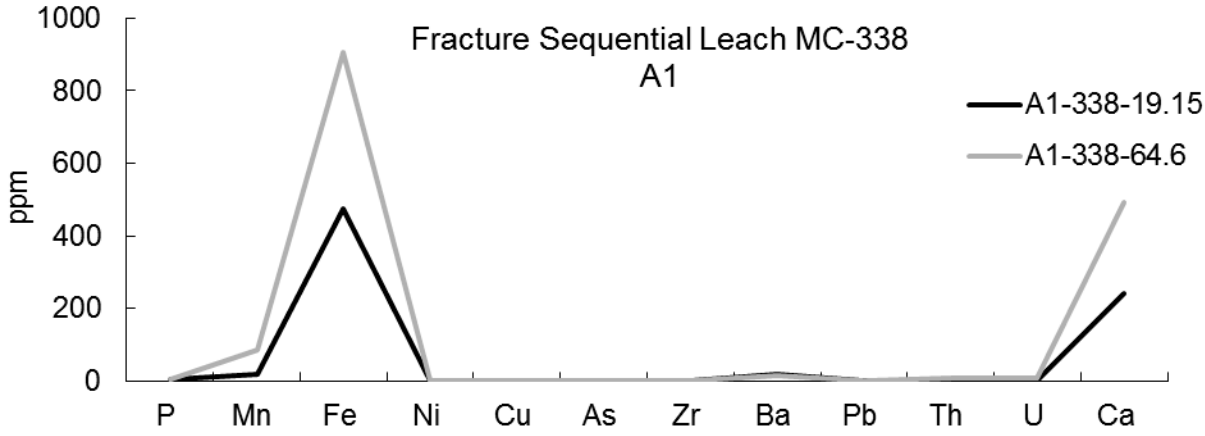

Figure 70: Concentrations (ppm) of elements leached in 0.05 N HNO_3 from two fractures taken at 19.15 m (black), 64.6 m (light grey) within drill-hole MC-338.

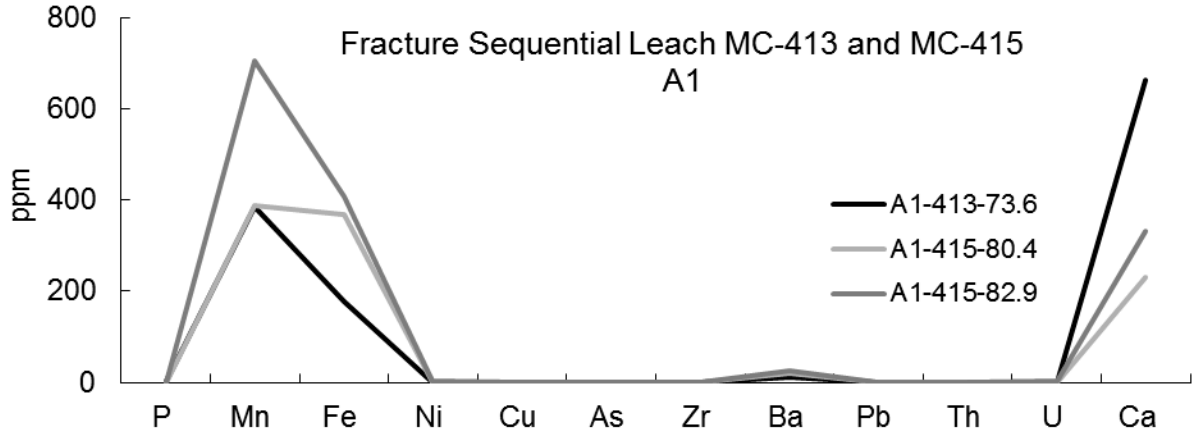

Figure 71: Concentrations (ppm) of elements leached in 0.05 N HNO_3 from three fractures taken at 73.6 m (black) from drill-hole MC-413, and two fractures at 80.4 m (light grey) and 82.9 m (dark grey) within drill-hole MC-415.

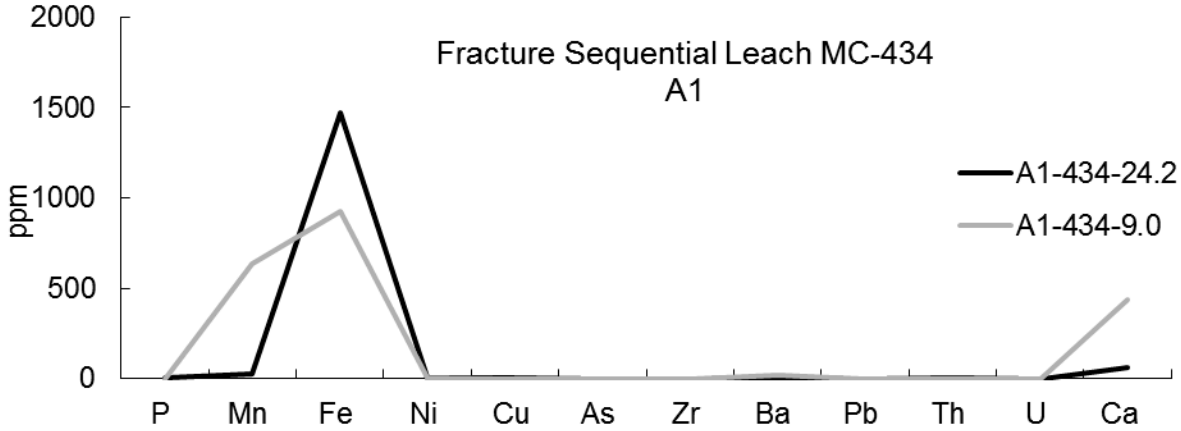

Figure 72: Concentrations (ppm) of elements leached in 0.05 N HNO_3 from two fractures taken at 24.2 m (black) and 9.0 m (light grey) within drill-hole MC-434.

The second acid leach in the sequence (A2) (Figure 73-79) used 0.1 N HNO_3, and was once again expected to dissolve the lesser-soluble elements than the previous A1 and water leaches. Again we see Fe (218 – 9.84 x 10^3 ppm), Ca (70 – 2.01 x 10^3 ppm), Mn (6.8 – 2.5 x 10^3 ppm) in higher leachate concentrations than the two previous leaches, and the dignificant dissolution of soluble Ba (3.5 – 314 ppm). The mean Ba concentration dissolved in A2 is 32.5 ppm, with sample 255-101.7 having by far the highest Ba concentration at 3x the mean (314 ppm), followed by sample 415-82.9 with 40 ppm Ba. Results reported below indicate the

concentration of elements dissolved by the sequential water, A1 (0.5 N HNO_3) and A2 (0.1 N HNO_3) leaches.

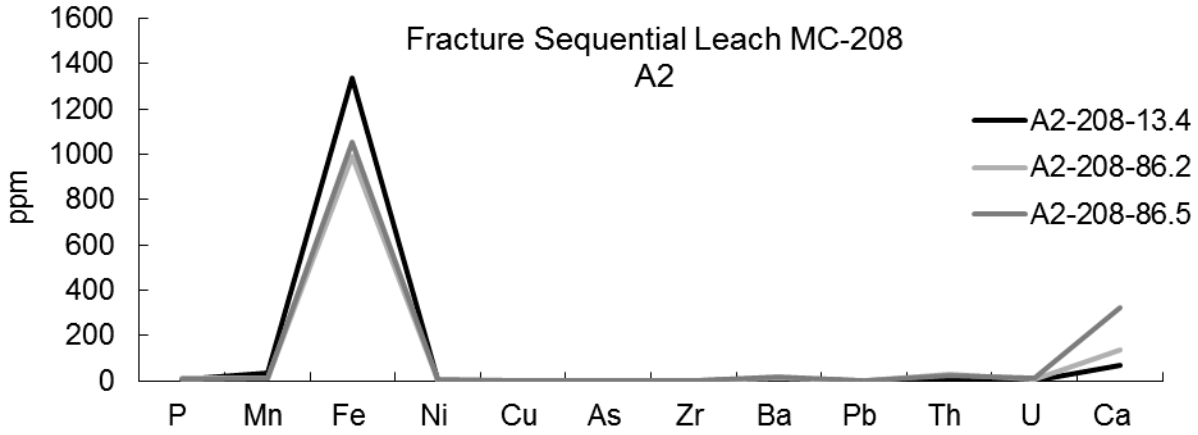

Figure 73: Concentrations (ppm) of elements leached in 0.1 N HNO_3 from three fractures taken at 13.4 m (black), 86.2 m (light grey) and 86.5 m (dark grey) within drill-hole MC-208.

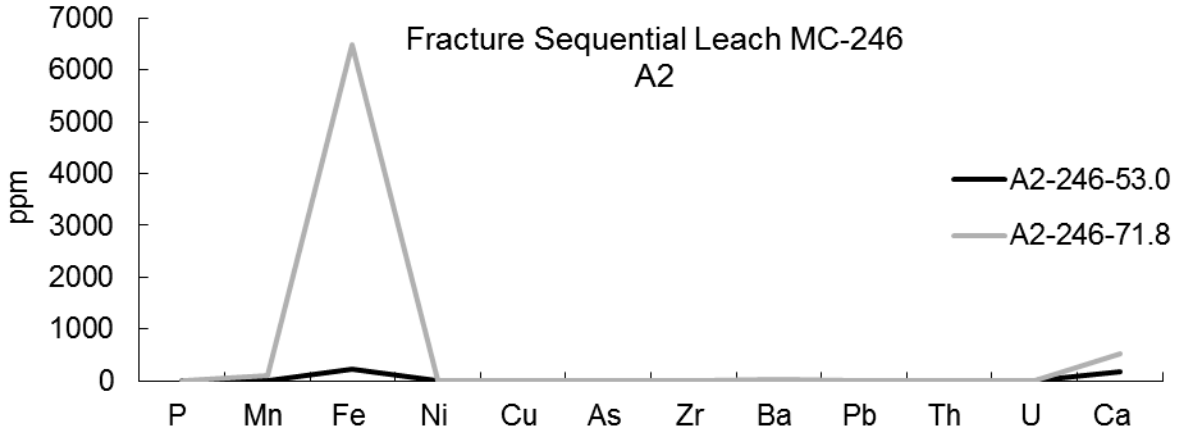

Figure 74: Concentrations (ppm) of elements leached in 0.1 N HNO_3 from two fractures taken at 53 m (black) and at 71.8 m (light grey) within drill-hole MC-246.

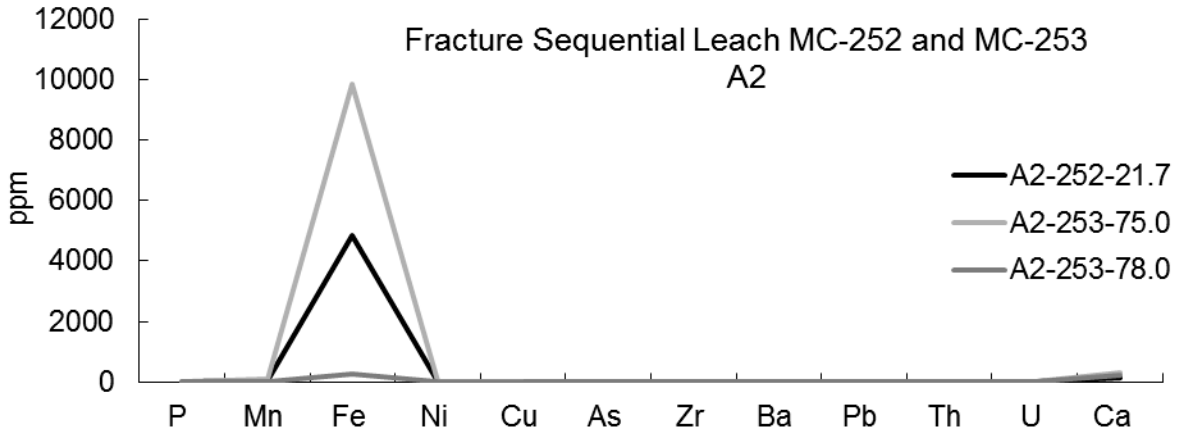

Figure 75: Concentrations (ppm) of elements leached in 0.1 N HNO_3 from three fractures taken at 21.7 m (black) within drill-hole MC-252, and at 75 m (light grey) and 78 m (dark grey) within drill-hole MC-253.

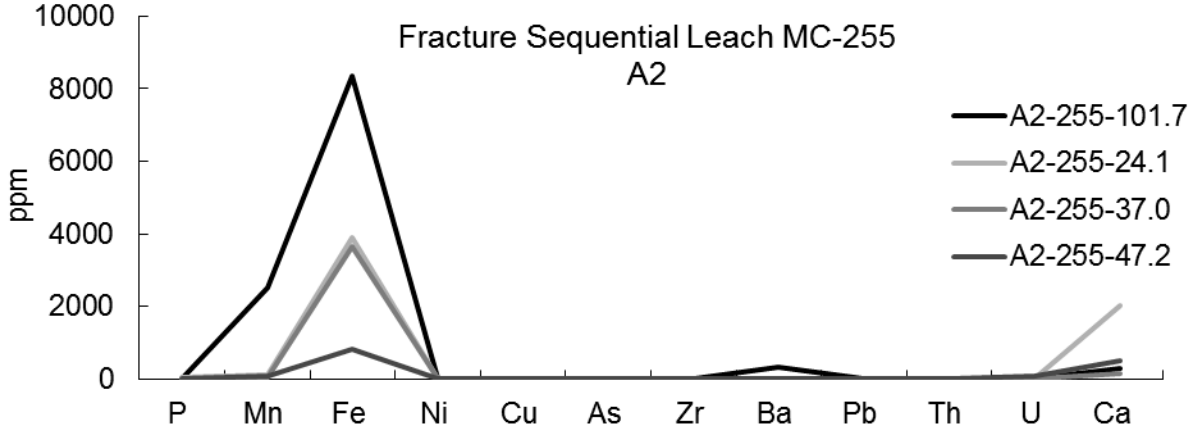

Figure 76: Concentrations (ppm) of elements leached in 0.1 N HNO_3 from four fractures taken at 101.7 m (black), 24.1 m (light grey) and 37.0 m (medium grey), and 47.2 m (dark grey) within drill-hole MC-255.

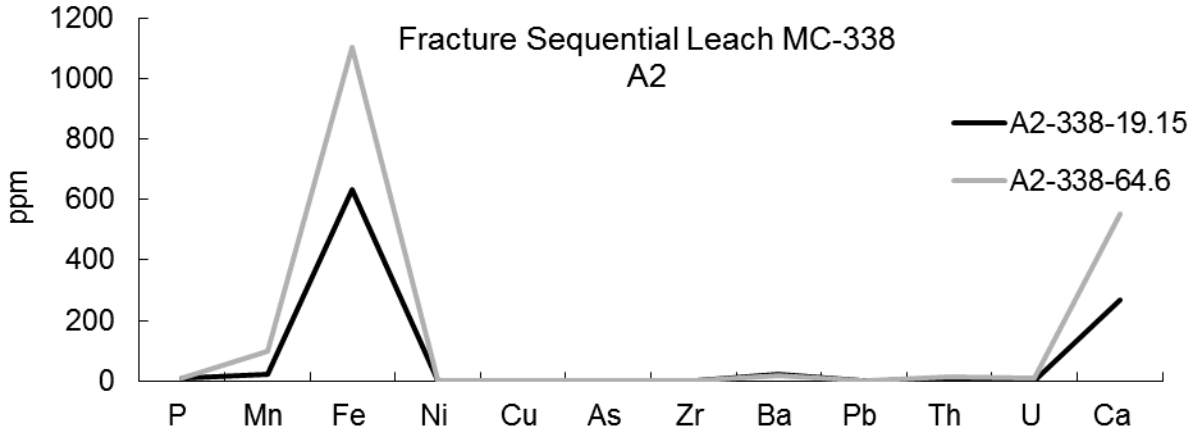

Figure 77: Concentrations (ppm) of elements leached in 0.1 N HNO_3 from two fractures taken at 19.15 m (black) and 64.6 m (light grey) within drill-hole MC-338.

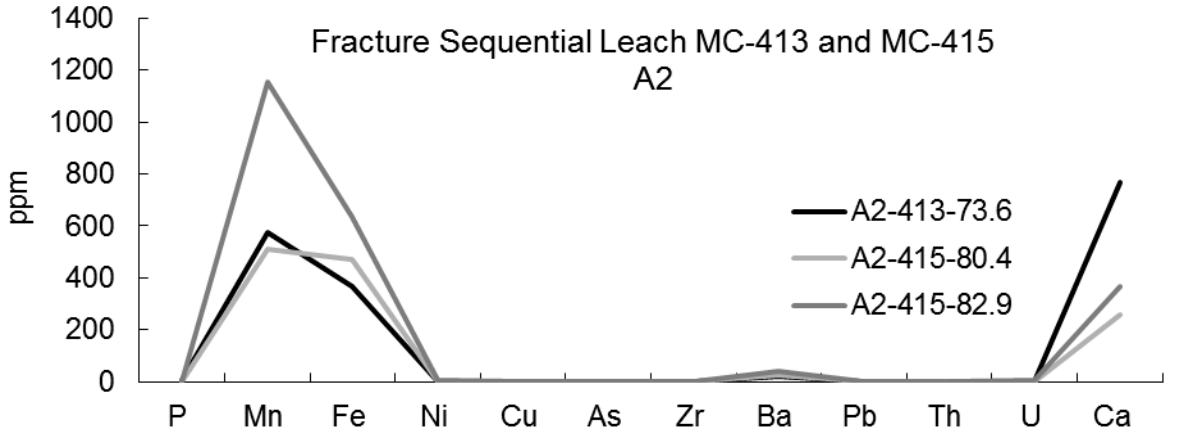

Figure 78: Concentrations (ppm) of elements leached in 0.1 N HNO_3 from three fractures taken at 73.6 m (black) from drill-hole MC-413, and two fractures at 80.4 m (light grey) and 82.9 m (dark grey) within drill-hole MC-415.

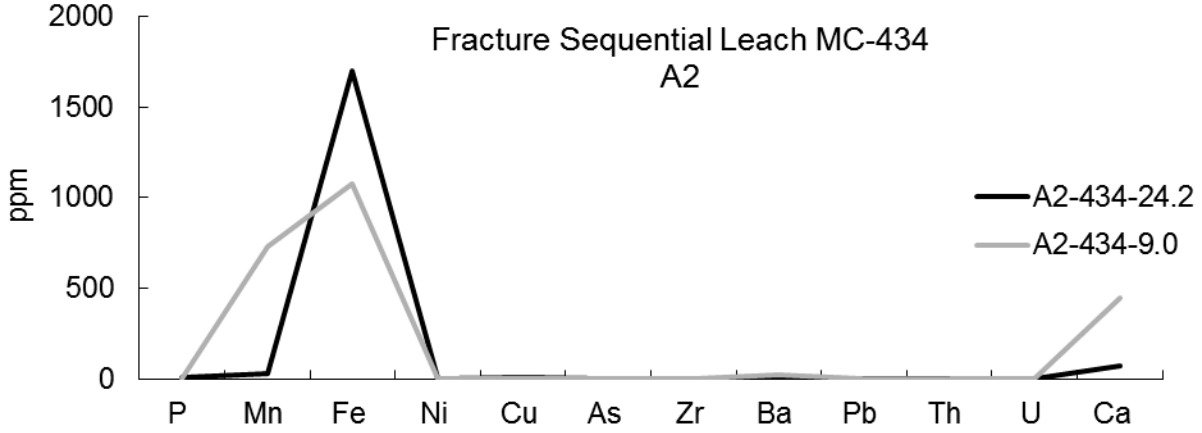

Figure 79: Concentrations (ppm) of elements leached in 0.1 N HNO_3 from two fractures taken at 24.2 m (black) and 9.0 m (light grey) within drill-hole MC-434.

The third sequential acid leach (A3) (Figure 80-86) used 0.5 N HNO_3 and dissolved higher concentrations of Fe (312 ppm – 1.2 %), Ca (73 – 2.36 x 10^3 ppm), Mn (7.3 – 3 x 10^3 ppm) and Ba (3.8 – 363 ppm) from the core fracture material than the previous 3 leaches. Results reported below indicate the total concentration of elements dissolved by the water, A1 (0.5 N HNO_3), A2 (0.1N HNO_3) and A3 (0.5 N HNO_3) sequential leaches.

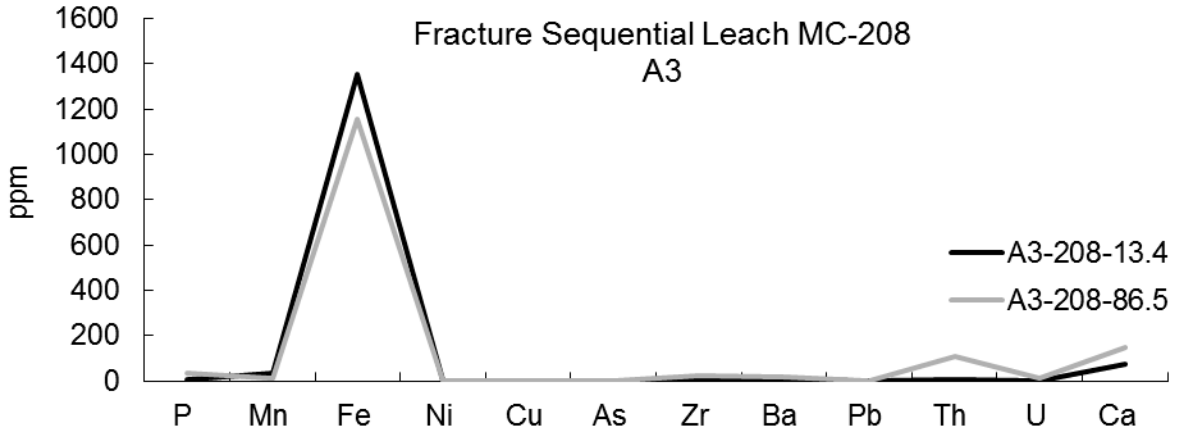

Figure 80: Concentrations (ppm) of elements leached in 0.5 N HNO_3 from two fractures taken at 13.4 m (black), 86.2 m (light grey) and 86.5 m (dark grey) within drill-hole MC-208.

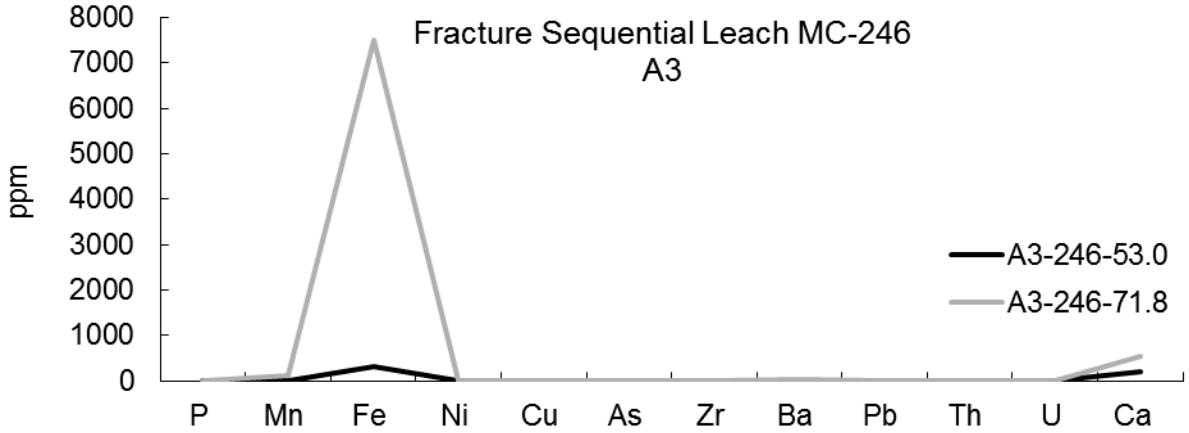

Figure 81: Concentrations (ppm) of elements leached in 0.5 N HNO_3 from two fractures taken at 53 m (black) and at 71.8 m (light grey) within drill-hole MC-246.

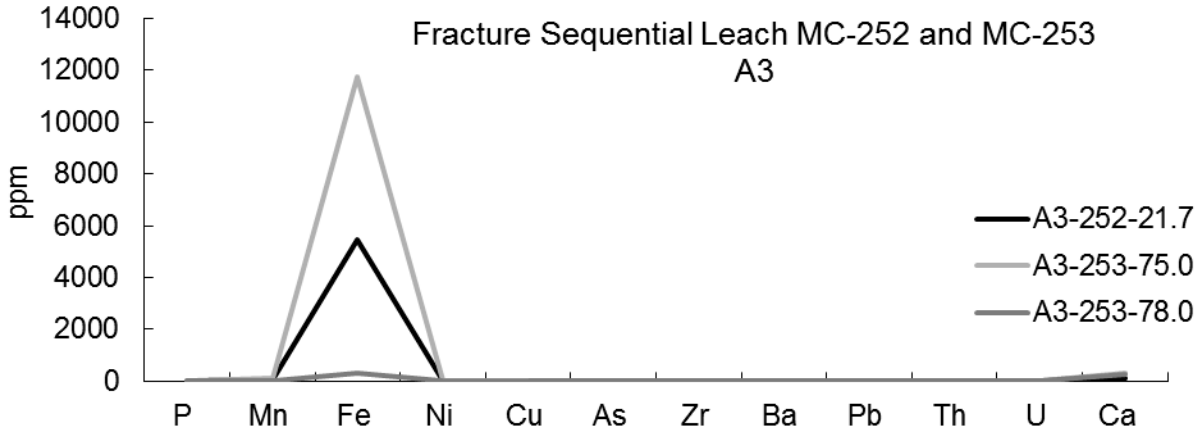

Figure 82: Concentrations (ppm) of elements leached in 0.5 N HNO_3 from three fractures taken at 21.7 m (black) within drill-hole MC-252, and at 75 m (light grey) and 78 m (dark grey) within drill-hole MC-253.

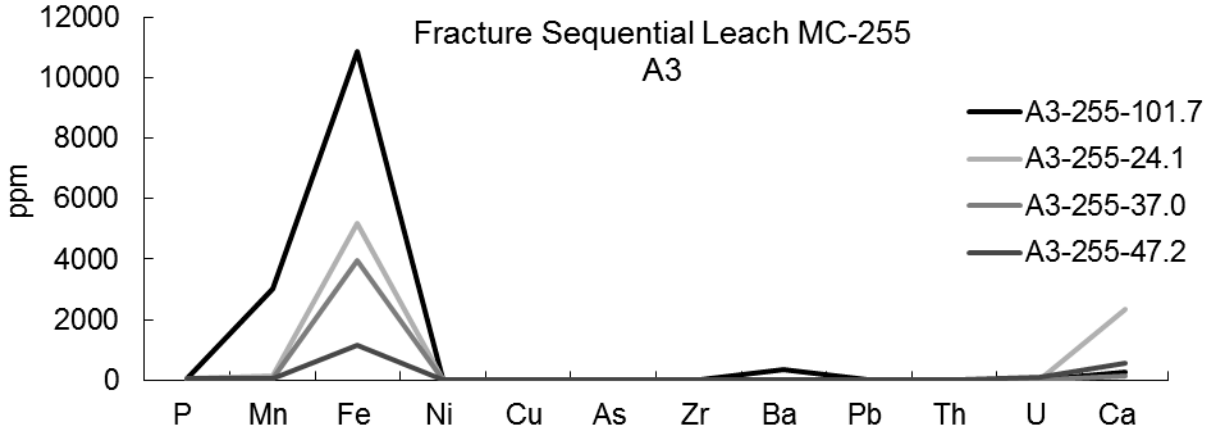

Figure 83: Concentrations (ppm) of elements leached in 0.5 N HNO_3 from four fractures taken at 101.7 m (black), 24.1 m (light grey) and 37.0 m (medium grey), and 47.2 m (dark grey) within drill-hole MC-255.

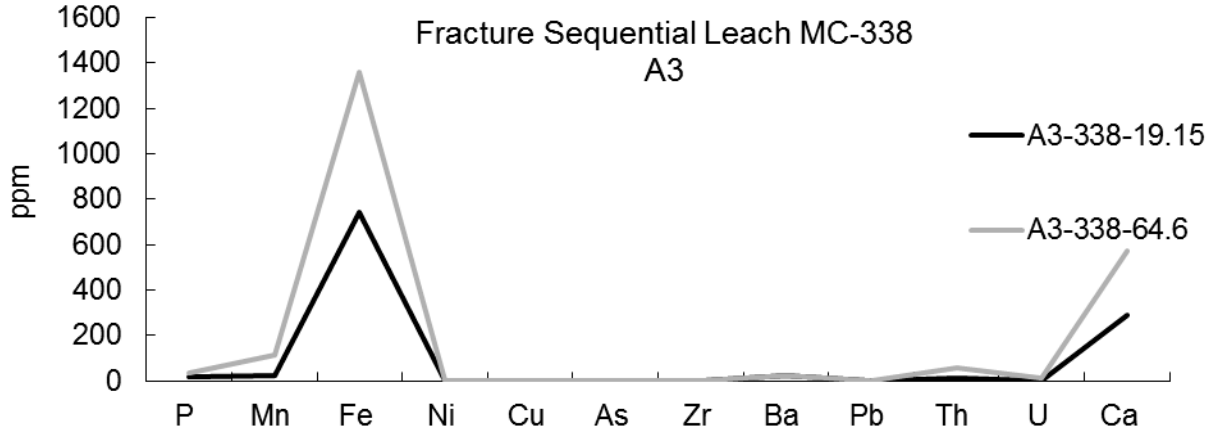

Figure 84: Concentrations (ppm) of elements leached in 0.5 N HNO_3 from two fractures taken at 19.15 m (black), 64.6 m (light grey) within drill-hole MC-338.

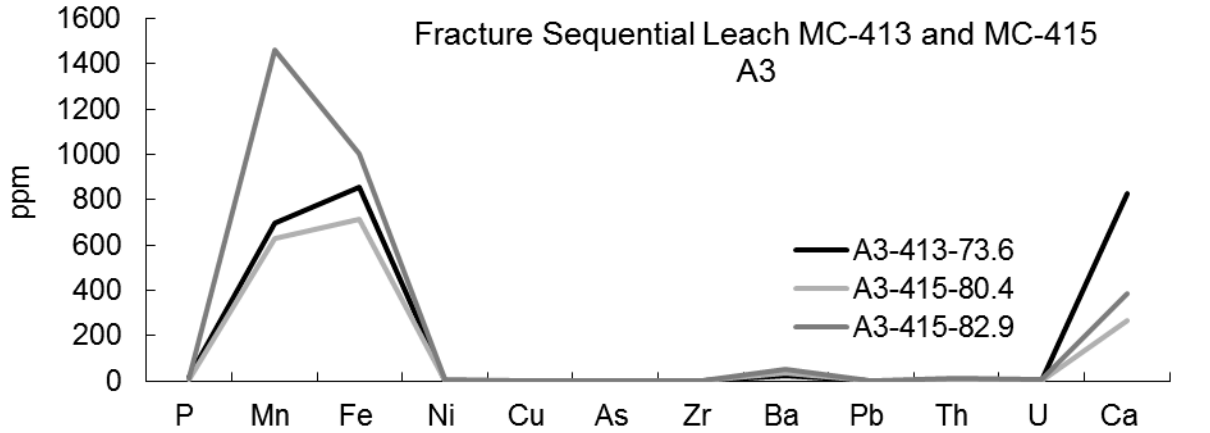

Figure 85: Concentrations (ppm) of elements leached in 0.5 N HNO_3 from three fracture taken at 73.6 m (black) from drill-hole MC-413, and two fractures at 80.4 m (light grey) and 82.9 m (dark grey) within drill-hole MC-415.

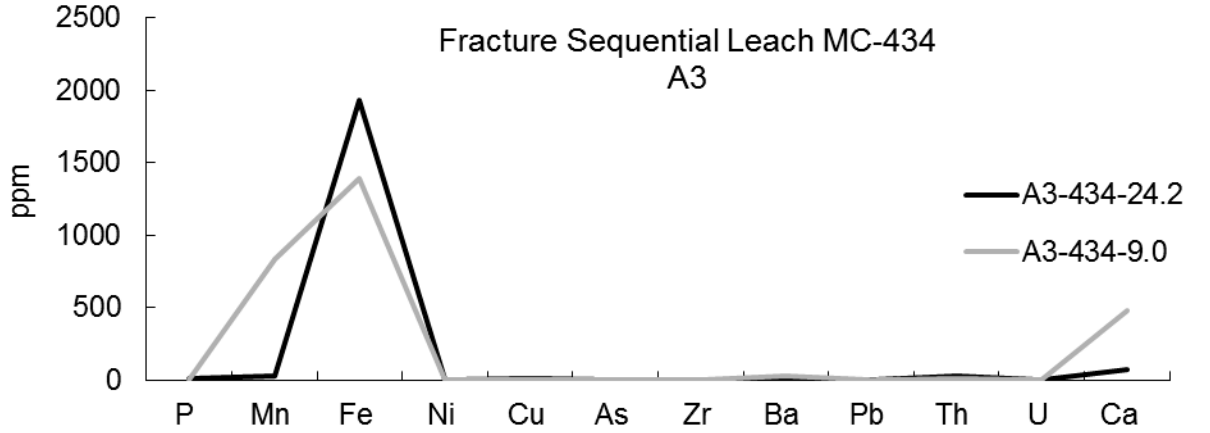

Figure 86: Concentrations (ppm) of elements leached in 0.5 N HNO_3 from two fractures taken at 24.2 m (black) and 9.0 m (light grey) within drill-hole MC-434.

The fourth sequential acid leach (A4) (Figures 87-93) used 2 N HNO_3^- and leached increased concentrations of Fe (562 – 1.5%), Ca (91 – 2.83 x 10^3 ppm), Mn (9.2 – 4.6 x 10^3 ppm), and Ba (5.3 – 521). P was also leached at this acidity and leachate concentrations ranged from 11.9 – 265 ppm, with a mean concentration of 69 ppm from all 19 samples, indicating the presence of phosphates. Results reported below are the elements dissolved by the water, A1 (0.5 N HNO_3), A2 (0.1N HNO_3), A3 (0.5 N HNO_3) and A4 (2N HNO_3) sequential leaches.

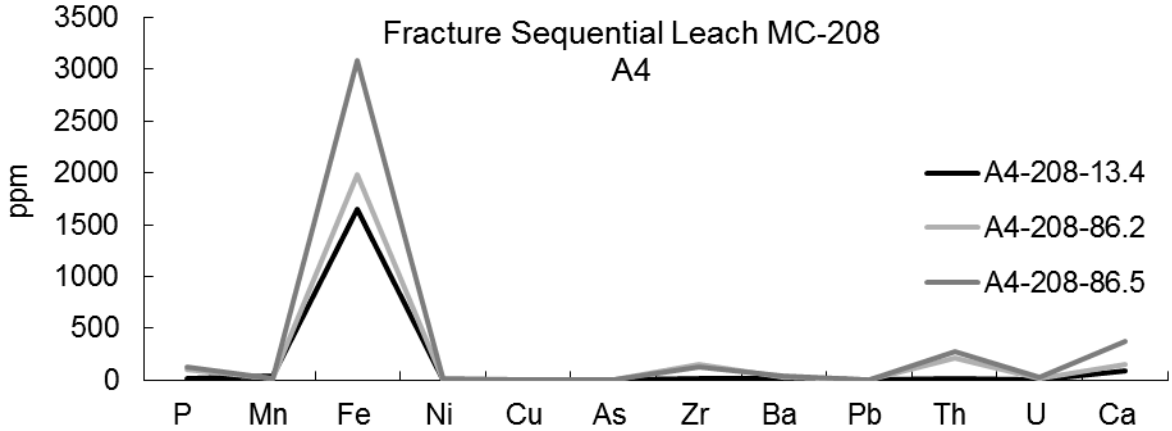

Figure 87: Concentrations (ppm) of elements leached in 2 N HNO_3 from three fractures taken at 13.4 m (black), 86.2 m (light grey) and 86.5 m (dark grey) within drill-hole MC-208.

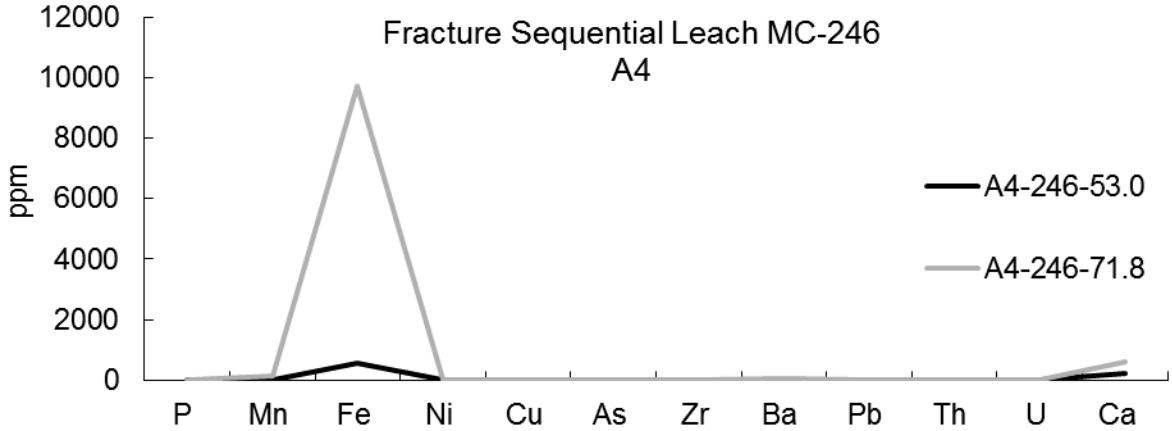

Figure 88: Concentrations (ppm) of elements leached in 2 N HNO_3 from two fractures taken at 53 m (black) and at 71.8 m (light grey) within drill-hole MC-246.

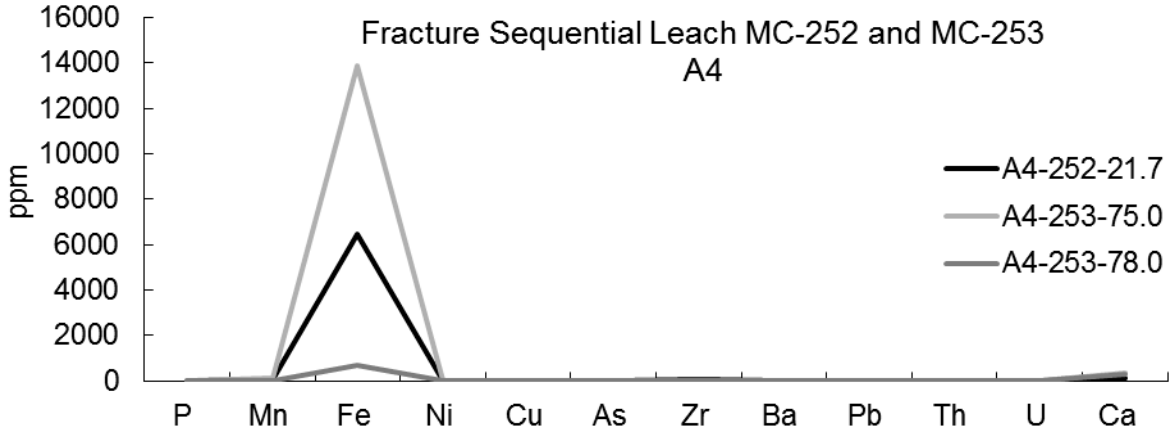

Figure 89: Concentrations (ppm) of elements leached in 2 N HNO_3 from three fractures taken at 21.7 m (black) within drill-hole MC-252, and at 75 m (light grey) and 78 m (dark grey) within drill-hole MC-253.

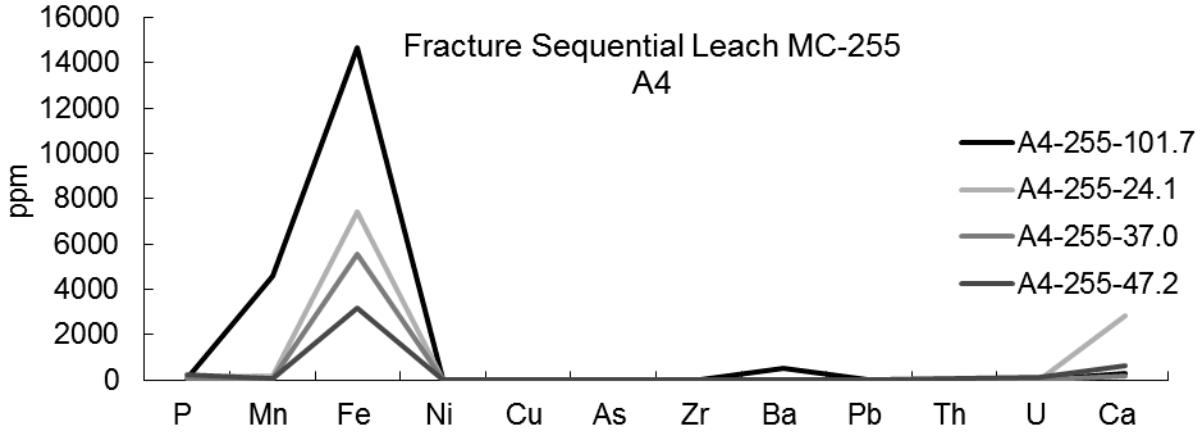

Figure 90: Concentrations (ppm) of elements leached in 2 N HNO_3 from four fractures taken at 101.7 m (black), 24.1 m (light grey) and 37.0 m (medium grey), and 47.2 m (dark grey) within drill-hole MC-255.

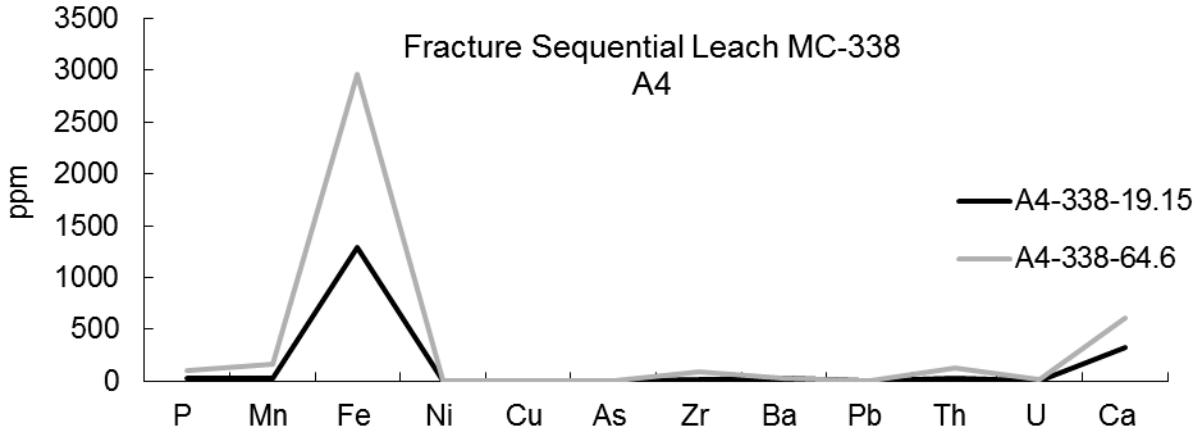

Figure 91: Concentrations (ppm) of elements leached in 2 N HNO_3 from two fractures taken at 19.15 m (black), 64.6 m (light grey) within drill-hole MC-338.

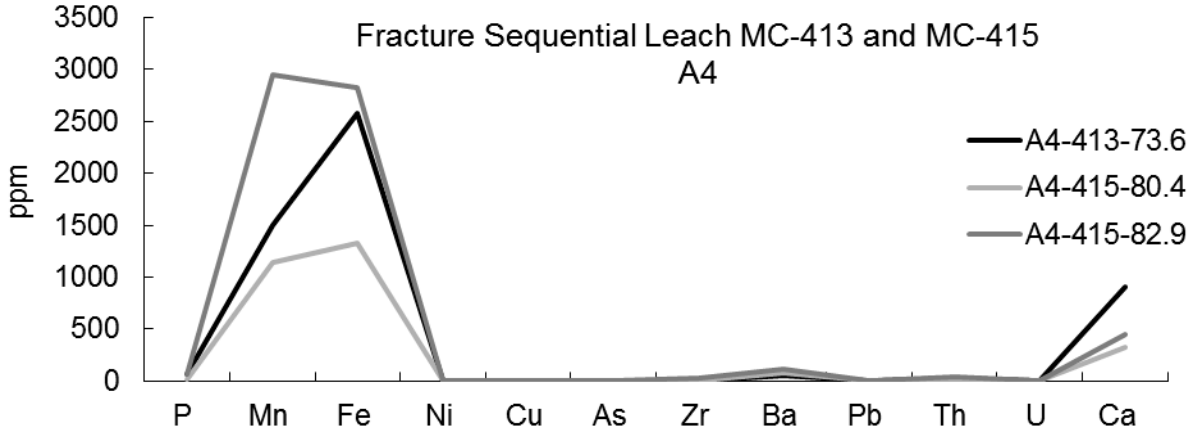

Figure 92: Concentrations (ppm) of elements leached in 2 N HNO_3 from three fractures taken at 73.6 m (black) from drill-hole MC-413, and two fractures at 80.4 m (light grey) and 82.9 m (dark grey) within drill-hole MC-415.

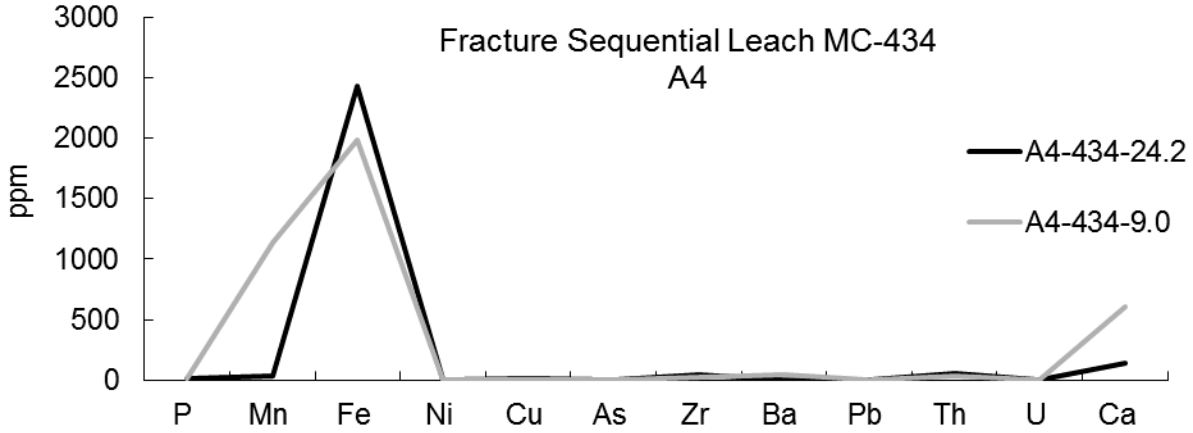

Figure 93: Concentrations (ppm) of elements leached in 2 N HNO_3 from two fractures taken at 24.2 m (black) and 9.0 m (light grey) within drill-hole MC-434.

It is also noteworthy that sample MC-255-47.2 yielded the highest concentration of U in each acid leach solution; ranging from A1 = 47 ppm, A2 = 74 ppm, A3 = 95 ppm, to A4 = 150 ppm U. As well, Th concentrations are highest in drill hole MC-208 at depths 86.2 m and 86.5 m. The A4 leachate concentrations of Th are 206 ppm and 270 ppm, respectively, with a mean concentration of 55 ppm from all 19 core fracture samples.

Box and whisker plots of individual elements throughout the 5 leaches (water, A1= 0.05 N, A2 = 0.1 N, A3 = 0.5 N and A4 = 2 N) are presented in Figures 94-95 to display the proportion of elements that were cumulatively leached with every step. For example, P, As, Zr,

Pb and Th were leached mostly by the final step of the sequence with 2 N HNO_3^-. Contrastingly, Fe, Ca, Ba, Ni, Mn and U were leached equally by each step of the leach and there is a gradual linear increase of these elements from A1 to A4. Cu shows an intermediate pattern of dissolution, whereby the dissolution is gradual as acidity increases from A1-A3, but the A4 leach increases dissolution by nearly double A3.

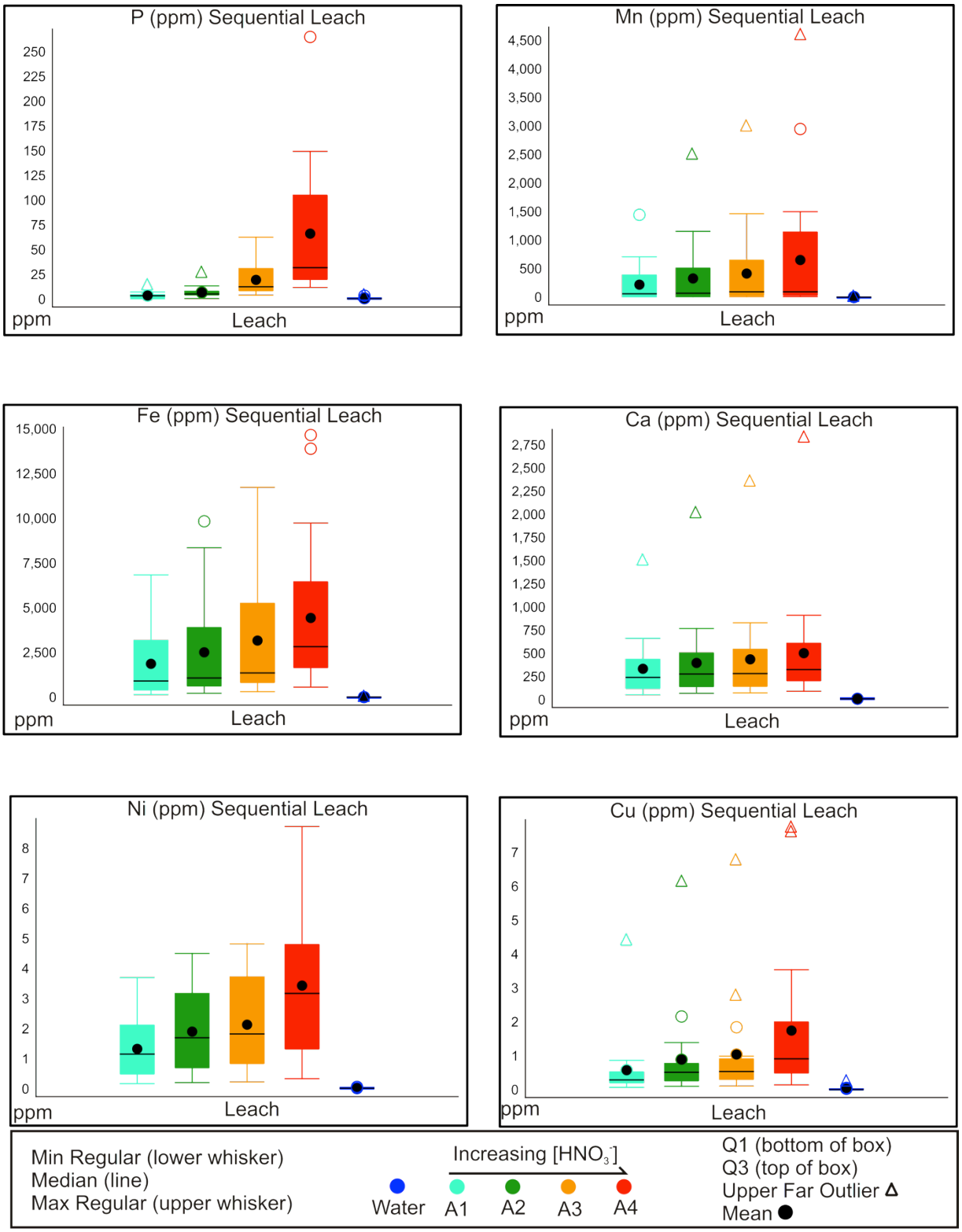

Figure 94: Box and whisker plots of P, Mn, Fe, Ca, Ni and Cu sequential leach results. Element concentrations in ppm, and leach intensity increases from blue to red.

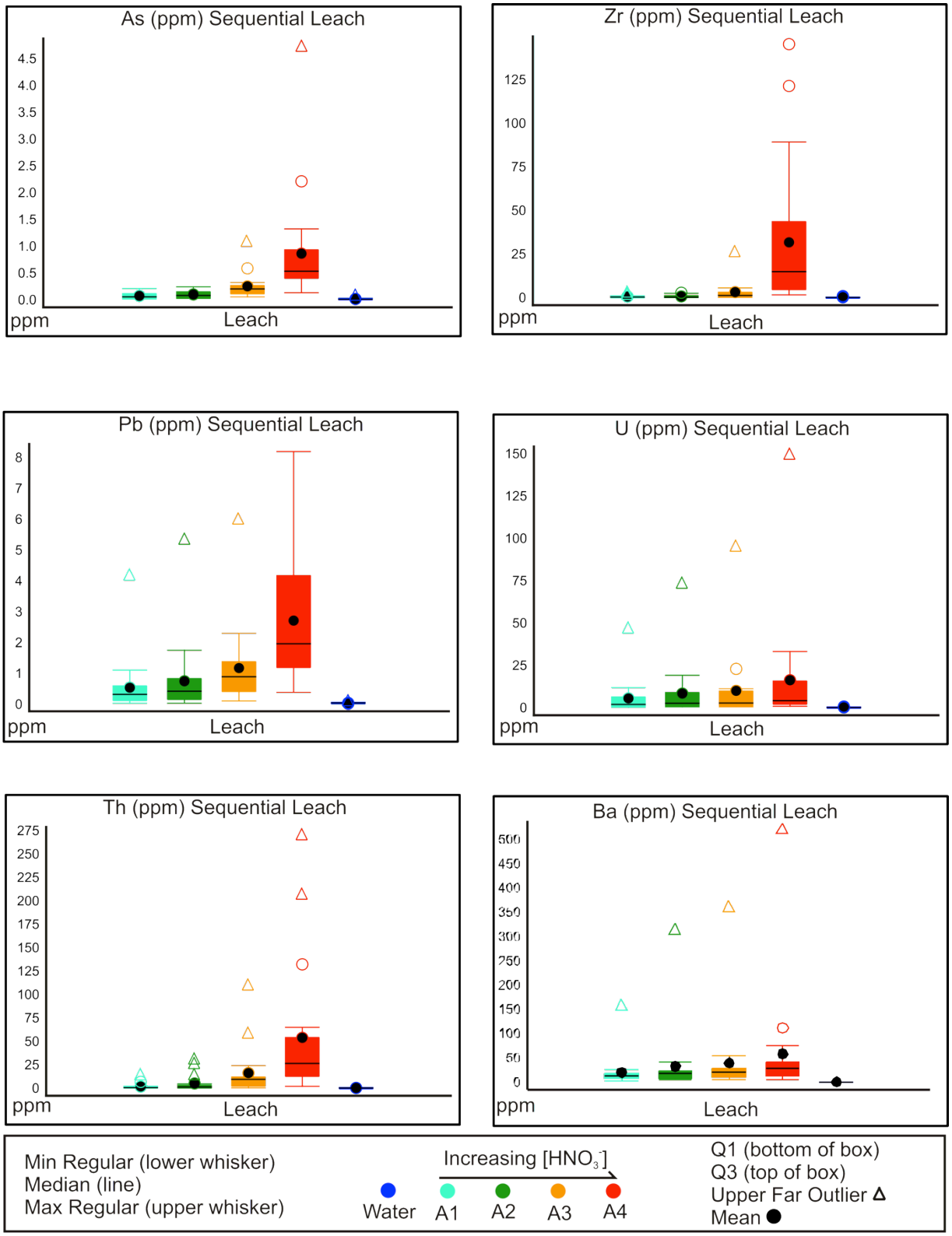

Figure 95: Box and whisker plots of As, Zr, Pb, U, Th and Ba sequential leach results. Element concentrations in ppm, and leach intensity increase from blue to red.

Overall the sequential leach provides evidence for the dissolution of Fe-Mn oxy-hydroxides due to the presence of Fe and Mn at the water-soluble phase and throughout all three nitric acid concentrations. There is also evidence for the dissolution of Ca-bearing minerals such as carbonate, as well as less soluble Ca –bearing minerals such as apatite (evident from P) that remained un-dissolved until the A4 step. Both Fe-Mn oxy-hydroxides (Sajih et al., 2014, Ames et al., 1983 and water-soluble Ca-bearing minerals are potential hosts for Ra on fracture surfaces due to their electronegativity and chemical affinity, respectively. Results of the sequential leach indicate that there are minerals present along fracture surfaces that Ra can adsorb to or incorporate with.

5.3.9 X-ray Diffraction: Fracture Minerals

X-ray diffraction was completed on core fracture samples to identify minerals present in the core fracture coatings. XRD spectra of three end member samples are presented below (Figures 96-98). Phases identified include quartz, illite, dravitic tourmaline, anatase and kaolin-group minerals. Amorphous phases of Fe and Mn oxy-hydroxides were not identified by XRD.

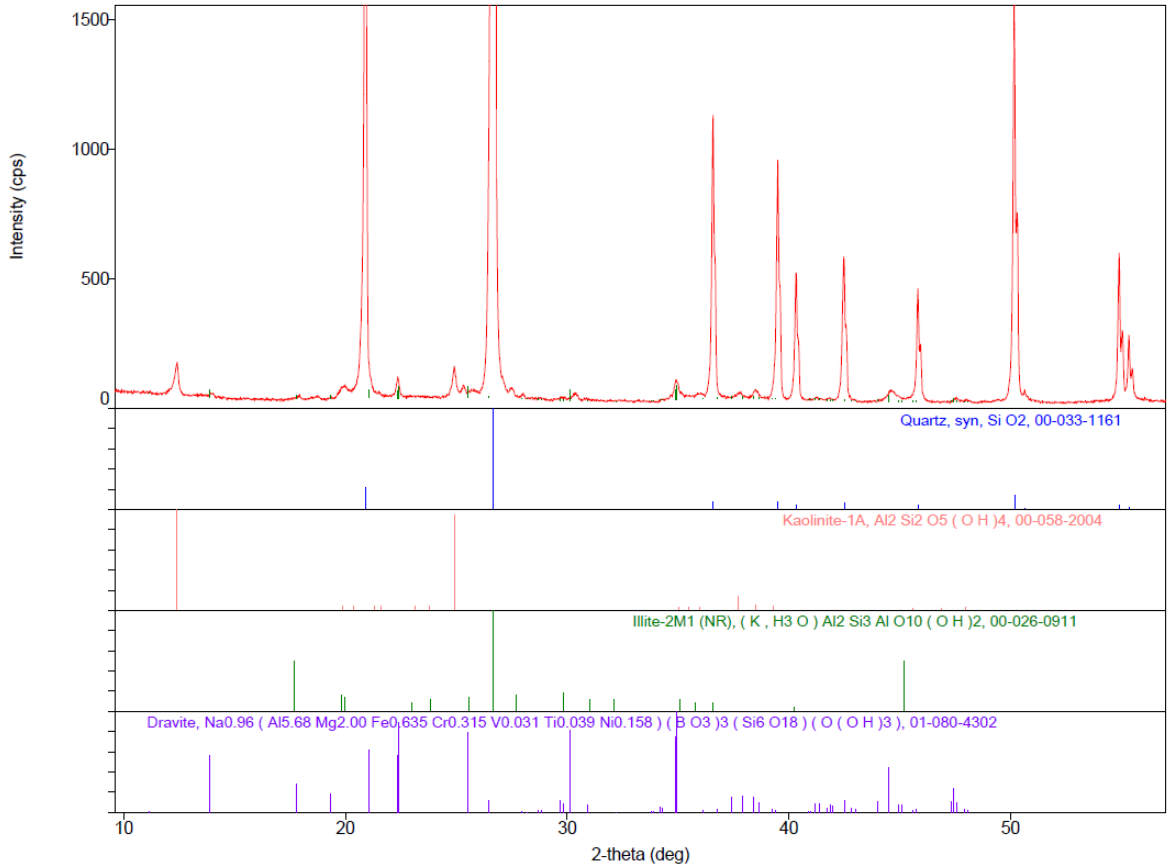

Figure 96: X-ray diffraction spectra of core fracture material at 85 m depth from drill-hole MC-415 at McArthur River. Lines at specific degrees identify characteristic peaks of quartz (blue), illite (green), kaolinite (red) and dravite (purple) as the phases along this fracture surface. Scan speed of 0.25 deg/min.

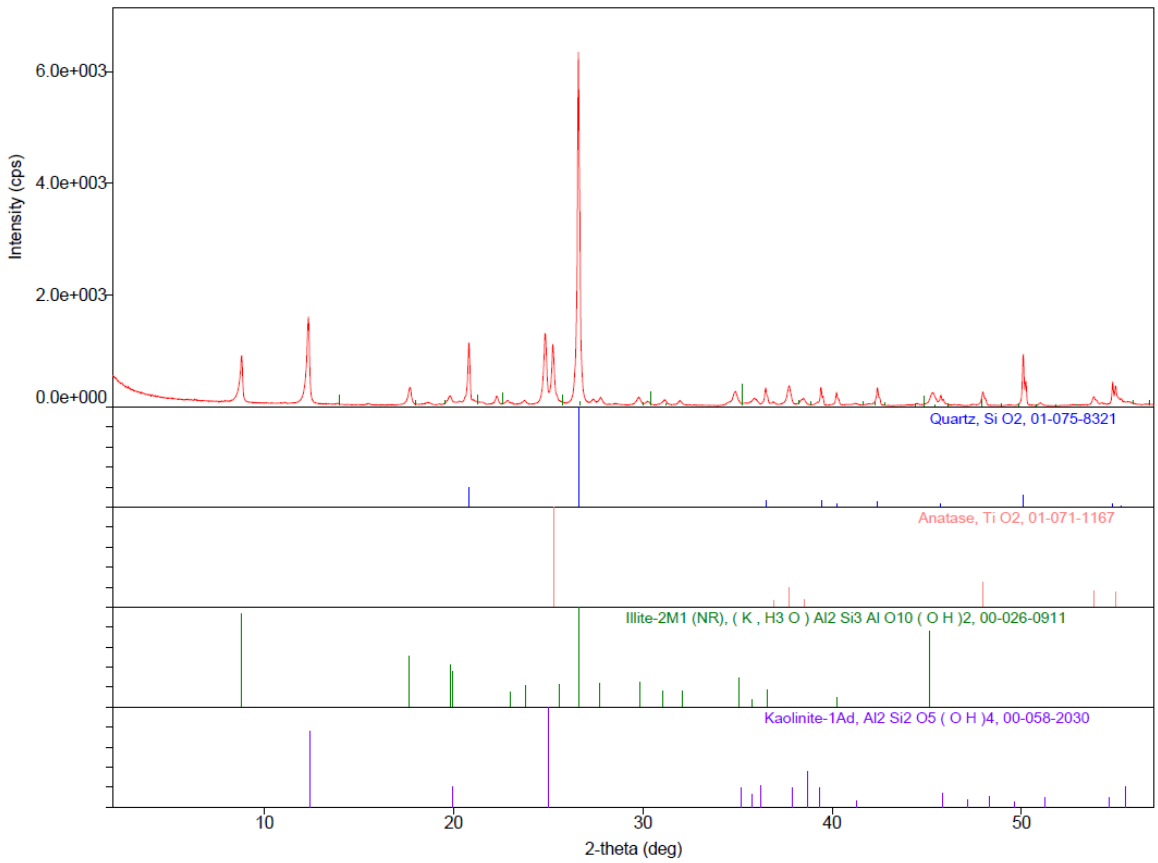

Figure 97: X-ray diffraction spectra of core fracture material at 82.9 m depth in drill-hole MC-415 at McArthur River. Lines at specific degrees identify characteristic peaks of quartz (blue), illite (green), kaolinite (purple) and anatase (red) as the phases along this fracture surface. Scan speed was 0.3 deg/min.

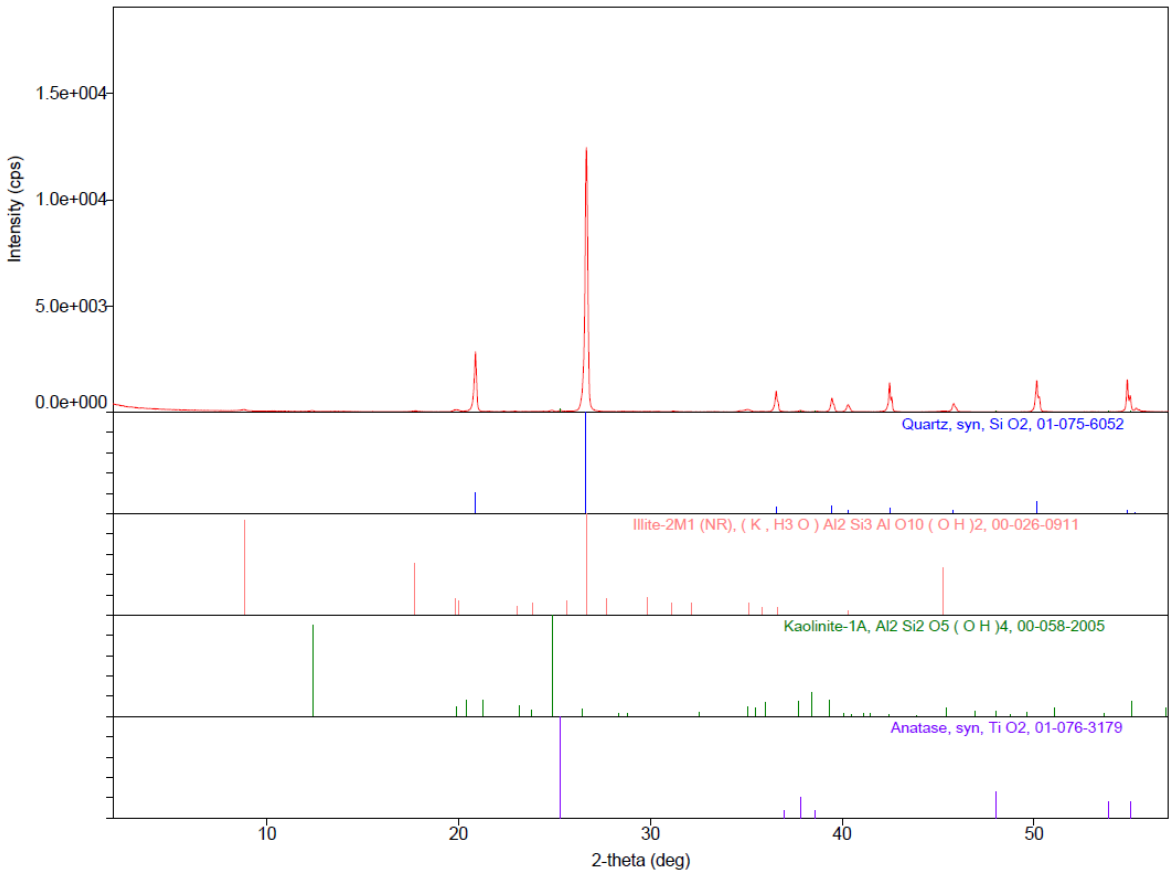

Figure 98: X-ray diffraction spectra of core fracture material at 24 m depth in drill-hole MC-434 at McArthur River. Lines at specific degrees identify characteristic peaks of quartz (blue), illite (red), kaolinite (green) and anatase (purple) as the phases along this fracture surface. Scan speed was 0.4 deg/min.

5.3.10 Radium

To determine the radioactivity of fracture coatings along sandstone fractures and soils, samples were analyzed by γ–ray spectroscopy. γ-ray energies of ^{214}Pb (295 Kev and 352 Kev) were counted to proxy for ^{226}Ra because γ-rays from ^{226}Ra cannot be used as they interfere with the energy from ^{235}U (186 Kev). The results (Table 34) represent the mass of Ra per one gram of fracture material. Radium contents of fracture coatings range from 0.789 – 32.3 pg (1 x 10^{-12} g) per gram of sample, with an average concentration of 6.58 pg/g.

Table 34: γ-ray spectroscopy results of Ra activity of fracture coating material in DDH, and location based on mineralized zones.

Core Fracture	Ra (pg/g)	Drill Fence
MC-208-13.4	1.15	Zones 1:A
MC-208-86.2	3.46	Zones 1:A
MC-208-86.5	3.25	Zones 1:A
MC-246-53.0	2.63	Zone 4
MC-246-71.8	2.59	Zone 4
MC-252-21.7	0.835	Zone 4
MC-253-78	2.29	Zones 1:A
MC-255-37.0	1.73	Zone 4
MC-255-47.2	11.5	Zone 4
MC-338-19.15	2.59	SW-Distal Zone
MC-338-64.6	3.12	SW-Distal Zone
MC-413-73.6	32.3	Zone C
MC-413-82.9	23.2	Zone C
MC-434-24.2	0.789	Outside
MC-434-9.0	7.26	Outside

Soil samples from undisturbed areas near 8 DDH at McArthur River were also analyzed by γ-ray spectroscopy and revealed much lower Ra concentrations than core fracture materials (Table 35). Radium concentrations ranged from 0.058-0.220 pg/g, and soils are relatively more similar in radioactivity than core fracture coatings.

Table 35: Radium concentration of 8 soil samples taken near DDH at McArthur River. Concentration is reported in pg per gram of soil.

Soil Sample	Ra (pg/g)
MC-251	0.220
MC-389	0.067
MC-393	0.065
MC-399	0.058
MC-403	0.068
MC-415	0.082
MC-430	0.094
MC-434	0.082

The soil with the highest Ra concentration (MC-251) is also the soil with the highest Rn radioactivity in soil pores, and the location closest to the surface projection of the deposit (Figure

99). All other soil samples taken from McArthur River for this study have low Rn radioactivity in soil pores and have between 0.058-0.094 pg/g Ra. In this case, the amount of Ra within soil is reflected by the amount of Rn in the pore space of soils, and also is an indication of U mineralization beneath. Gascoyne et al. (1993) also found that the source of Rn soil gas was mostly in-situ Ra, and more distal sources were a smaller contributor.

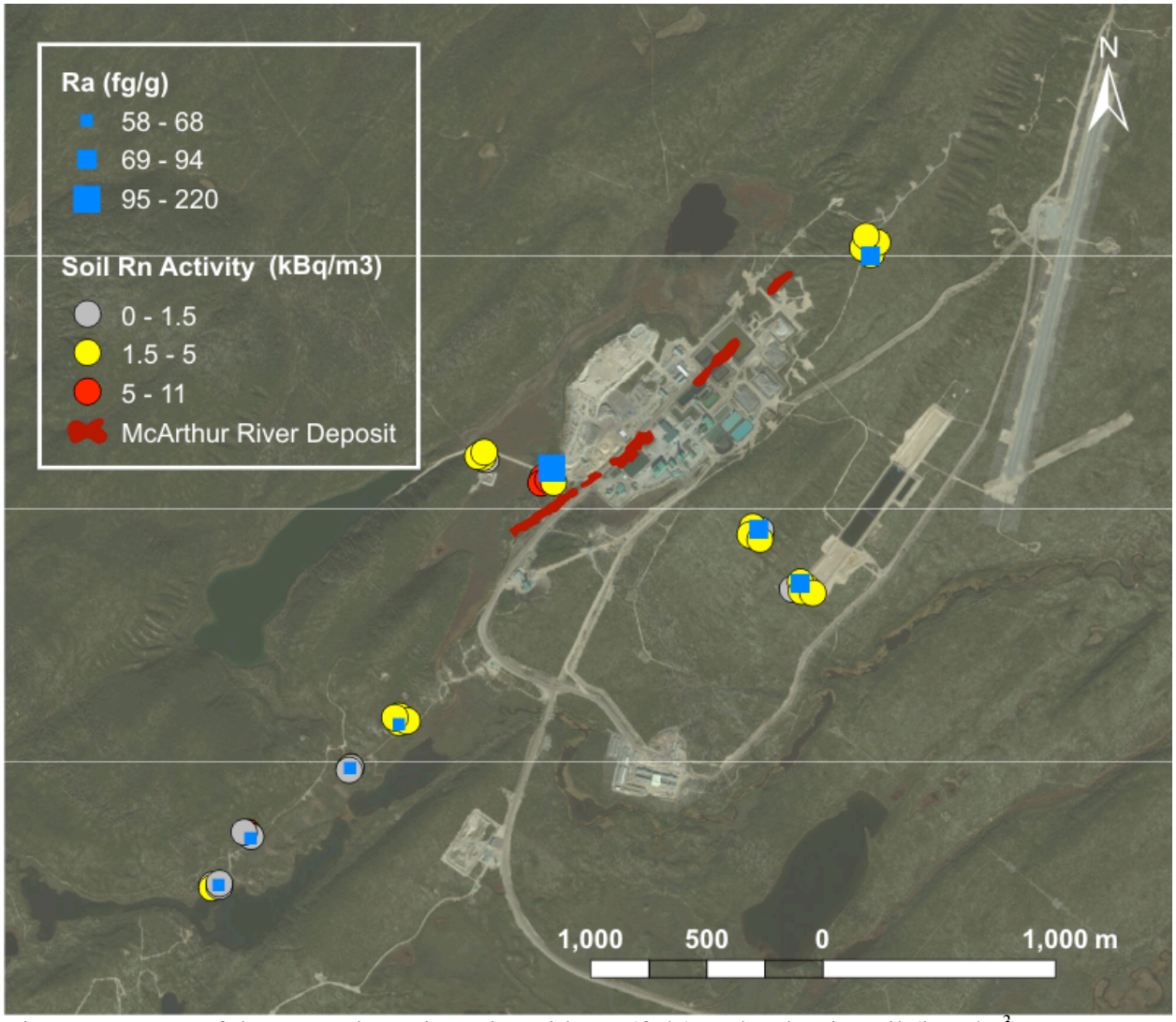

Figure 99: Map of the McArthur River site with Ra (fg/g) and radon in soil (kBq/m^3) content. Radium concentration increases as blue squares increase in size. Rn in soil gas radioactivity increases from grey to red.

5.4 Discussion

The near neutral pH and atmospheric temperature of groundwater indicates that only water-soluble elements would be able to leach from the surrounding rock and till into the ground water. Oxygen and H isotopes are within the range of Saskatchewan precipitation and have a slightly evaporated signature compared to the global meteoric water line.

Atomic bomb testing caused an increase of ^{3}H in precipitation throughout the world. Peak ^{3}H levels occurred before the Limited Nuclear Test Ban Treaty was signed in 1963 to ban atomic bomb testing above ground. Since 1963, ^{3}H in the atmosphere has gradually decreased to background levels and the "bomb peak" provides a marker for the age of groundwater throughout the world. In Figure 100 it is evident that groundwater from McArthur River and Millennium is recent meteoric because it has ^{3}H values of northern Canadian precipitation in 2013-2014. ^{3}H content in northern Canadian precipitation has been <20 TU since 1993, and therefore a general conclusion must be made that groundwater at McArthur and Millennium is <20 years old.

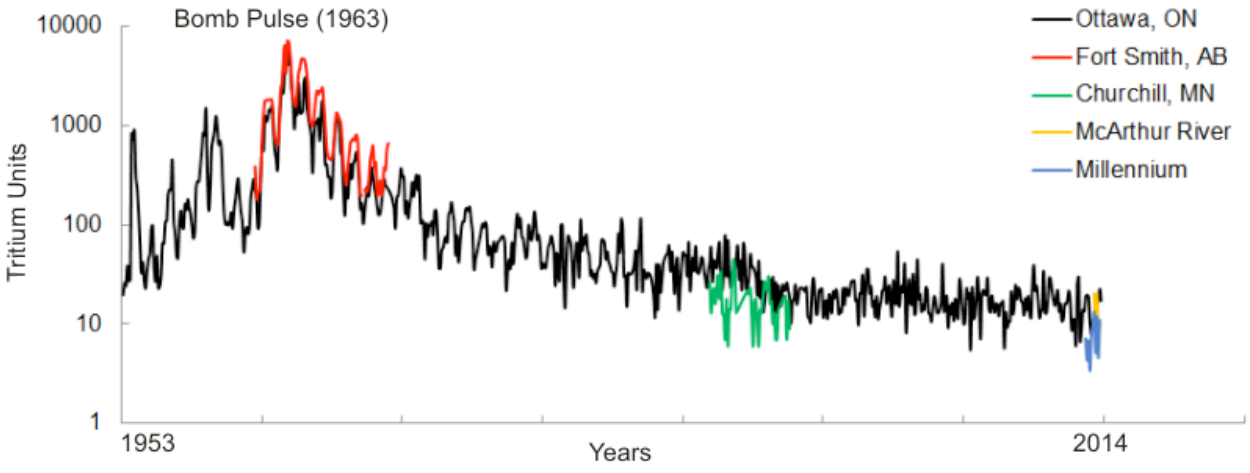

Figure 100: Tritium values from 1953 to 2014 from Ottawa, ON, Fort Smith, AB, Churchill, MB, McArthur River and Millennium (IAEA GNIP).

Dissolved carbon at McArthur River has a more negative $\delta^{13}C$ signature than groundwater at Millennium. Its C source is likely organic carbon that was oxidized into bicarbonate within the groundwater, and soil-derived CO_2. There is a higher concentration of inorganic C than organic carbon.

Radon was compared to dissolved ions within groundwater at McArthur River (Figure 101). U, SO_4^{2-}, NO_3^-, Br^-, Cl^- and F^- do not correlate with Rn radioactivity with R^2 values </=0.2. The absence of a relationship between dissolved U and Rn in groundwater at McArthur River indicates that the source for Rn in groundwater is not dissolved U within the groundwater.

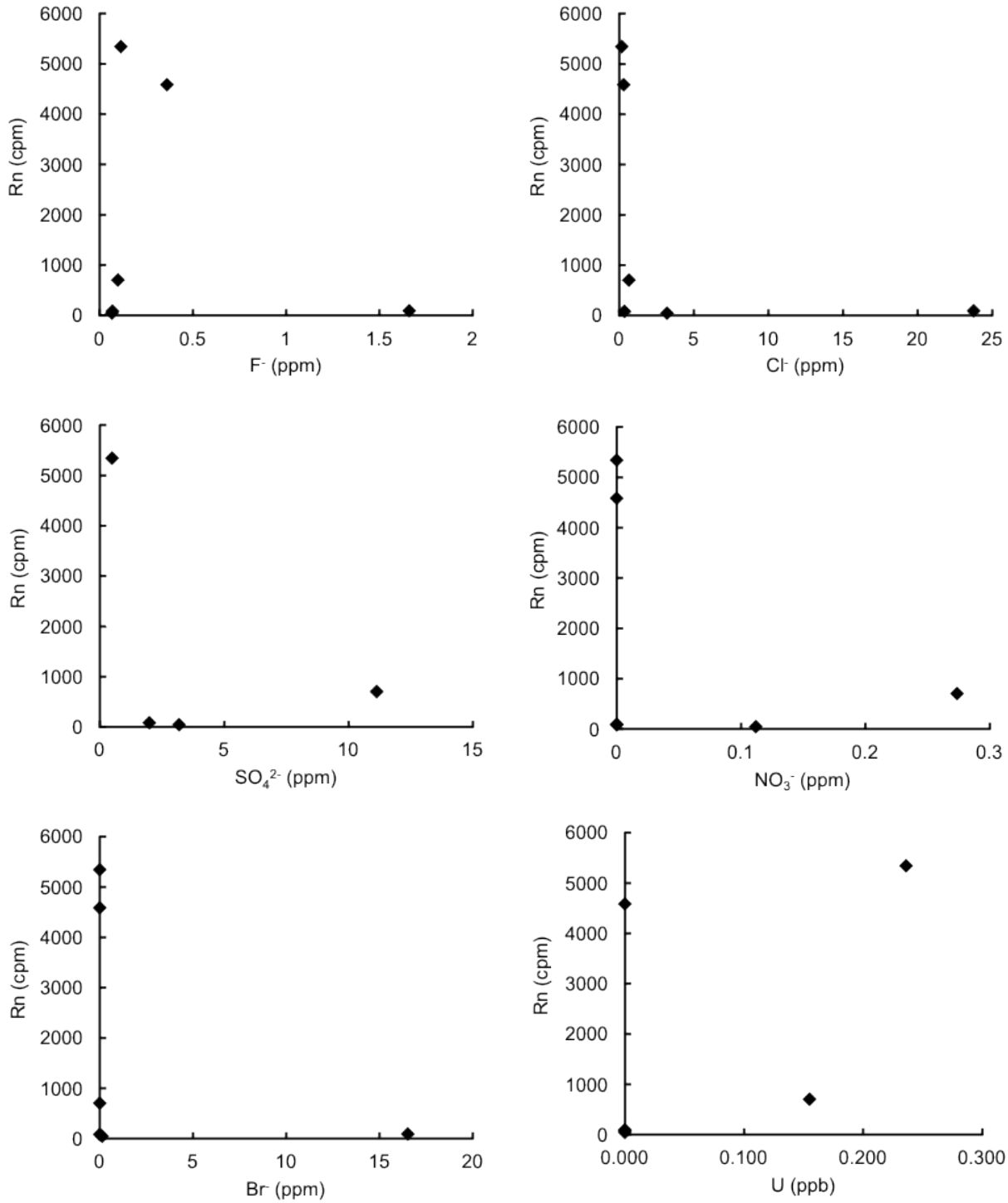

Figure 101: Rn activity (counts per minute) and dissolved ions in groundwater at McArthur River. Limits of detection: U = 0.002 ppb, SO_4^{2-} = 0.0021 ppm, NO_3^- = 0.0317 ppm, Br^- = 0.0011 ppm, F^- = 0.0016 ppm, Cl^- = 0071 ppm.

Radon content in groundwater at McArthur River ranged from 44 cpm to over 100 times that at 5342 cpm using Perkin Elmer 1220 Quantulus Ultra Low Level Liquid Scintillation Spectrometer. Accessible drill-holes (n=6) were only available to the south of the deposit, and therefore it is not possible to statistically determine how Rn radioactivity ranges throughout the full surficial footprint. However, based on the available data, the groundwater with the highest Rn radioactivity is from a DDH that intersects >100 ppm U at >500 m depth, and there are anomalous concentrations of U throughout the DDH (Figure 102) and the bedrock is heavily fractured and faulted. The next highest Rn radioactivity occurs in MC-434, a background hole that does not intersect mineralization, but has 1-100 ppm U in upper sandstone less than 200 m north from the DDH. The drill-hole (MC-403) with the lowest Rn activity (44 cpm) intersects >100 ppm U at approximately 600 m depth, has low U (< 1 ppm) in the upper sandstones, and has minor faults and fractures.

Figure 102 (1-6) are cross sections looking NE that illustrate the delineation of drilling, the concentration of U (0 to >100 ppm) and the Rn radioactivity of shallow groundwater within drill-holes. Groundwater from DDH MC-389 (Figure 102-1), MC-399 (Figure 102-3), MC-403 (Figure 102-4) and MC-430 (Figure 102-5) has low Rn radioactivity. In contrast, two drill-holes have high Rn radioactivity in groundwater at McArthur River; MC-434 (Figure 102-6) and MC-393 (Figure 102-5). MC-434 has > 0.5 ppm U in the bedrock surrounding the DDH (Figure 102-6), does not intersect mineralization at depth; it was tested as a background hole. However, proximal sandstones have 1-100 ppm U, and could be the source for radioactivity in the groundwater in MC-434. The second drill-hole with high Rn radioactivity in groundwater is MC-393. It intersects >100 ppm U at depth of approximately 550 m and has a range of U (0.5 - >100 ppm) throughout the DDH (Figure 102-2), and the surrounding bedrock is intensely fractured

and faulted. It is likely that U throughout local sandstones has decayed to Ra, which then circulated throughout fractured bedrock, and adsorbed onto fracture coatings. Over time, the Ra decayed to Rn, and the Rn emanated from the solid phase into the groundwater.

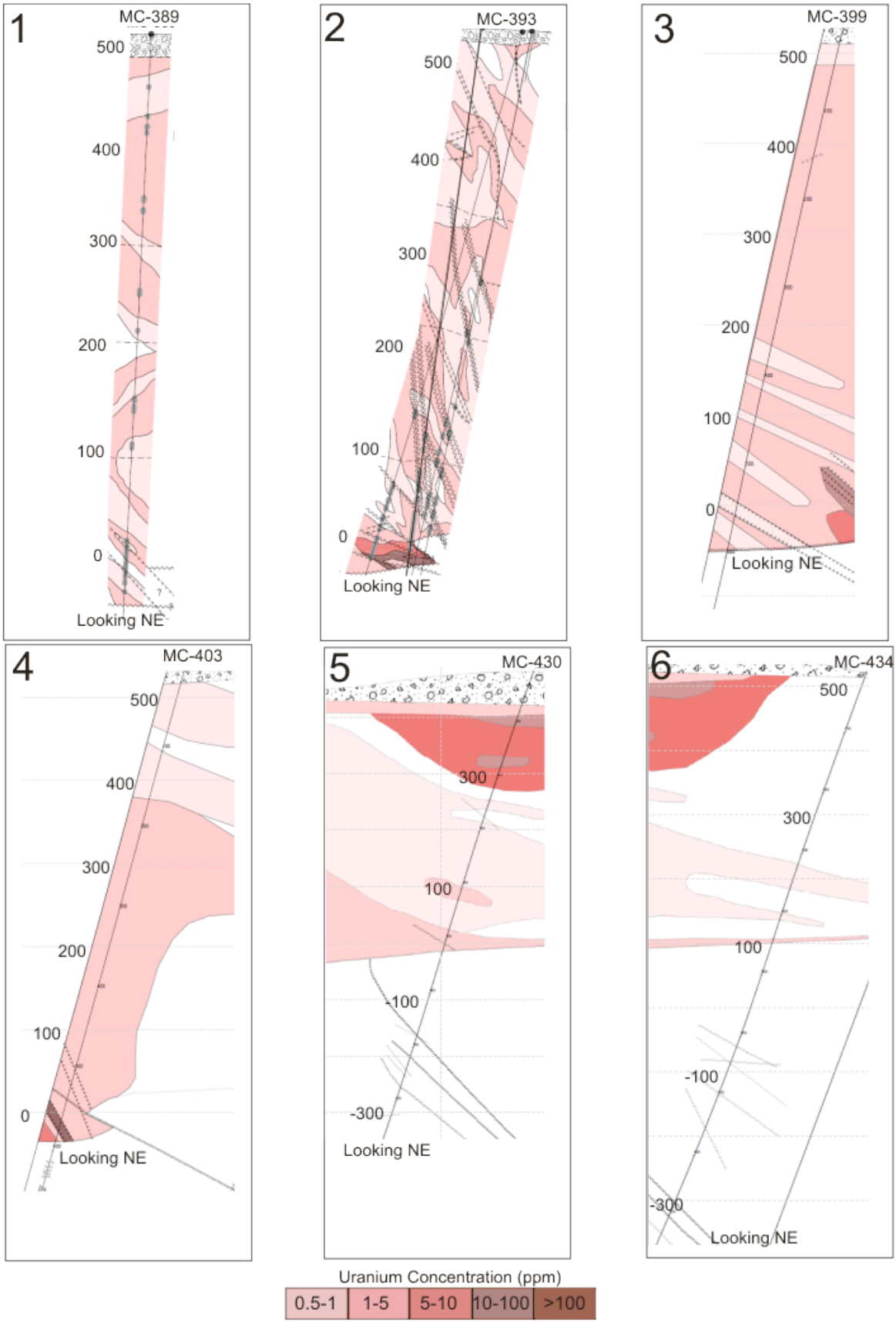
1
MC-389
500
400
300
200
100
0
Looking NE
2
MC-393
500
400
300
200
100
0
Looking NE
3
MC-399
500
400
300
200
100
0
Looking NE
4
MC-403
500
400
300
200
100
0
Looking NE
5
MC-430
300
100
-100
-300
Looking NE
6
MC-434
500
300
100
-100
-300
Looking NE
Uranium Concentration (ppm)
0.5-1
1-5
5-10
10-100
>100

Figure 102: Geological cross section of six McArthur River diamond drill-holes (DDH) with partial uranium concentration indicated in shades of pink from 0.5 – 100 ppm U, adapted from Cameco, 2012. Approximate depths are written along drill-hole delineations in meters above sea level. Smaller jagged lines represent faults and fractures. Pebbly infill represents unconsolidated overburden above the sandstone.

Ra in natural waters is controlled by its production from U and Th, and is removed from solution by adsorption and cation exchange (Herczeg et al., 1998; Langmuir and Melchoir, 1984). Typically, Ra is in such small concentrations in groundwater it does not reach saturation to form pure Ra mineral phases (Goulden et al., 1998). Generally, the average concentration of Ra dissolved in groundwater is less than 0.037 Bq/L (1.0 pCi/L) and in most groundwaters throughout the world there is more dissolved U than Ra (Hem, 1985). Radon concentration in groundwater is substantially higher than that of Ra, and is mostly derived from the solid Ra within an aquifer (Hem, 1985). Rogers (1985) calculated that an aquifer with 1 ppm dissolved U would have Rn activity of at least 29 Bq/L in secular equilibrium. The concentration of dissolved U in groundwater at McArthur River is less than 1 ppb, and therefore the source of Rn in the groundwater is likely due to the presence of Ra in rocks and soils.

Radiogenic ^{4}He was measured in 3 locations at 60 m depth below the water table and all results revealed levels of ^{4}He in equilibrium with the atmosphere: $[^{4}He/^{20}Ne]$ sample / $[^{4}He/^{20}Ne]$ in ASW range from 1.03 -1.10. MC-393 had the highest Rn radioactivity of the six holes analyzed but has atmospheric levels of radiogenic He. The other two drill-holes (MC-399 and MC-403) had < 85 cpm Rn, indicating that Rn and He content do not always correlate, likely because He does not decay and can therefore travel farther away from its original source. It should be noted that with a small sample set (n=3) it is difficult to draw quantitative conclusions, and in this case, ^{4}He does not provide a vector for mineralization.

In order to determine the host for Ra within soils, Ra was compared to near total digestion Ca and Ba concentrations of B-horizon soils (Figure 103). Ca and Ra weakly correlate ($R^2 = 0.4$) and Ba and Ra moderately correlate ($R^2 = 0.6$), suggesting that Ra is co-precipitating with Ca- and Ba-bearing minerals. Radium's ability to co-precipitate with barite was researched by Goulden et al. (1998) within fresh tailings from the Cluff Lake mine in the Athabasca Basin. Typical tailing solids have similar grain size as soil and till, and include quartz, illite, Fe-oxides and chlorite (Goulden et al., 1998). Goulden et al. (1998) determined by sequential leach and SEM that barite within the clay size fraction of tailings soilds was the primary host of Ra, as (Ra,Ba) SO_4. However, the moderate correlation between Ba/Ra and Ca/Ra in our samples suggests that some Ra within B-horizon soils does not co-precipitate with Ca- and Ba-bearing minerals. Barite is not soluble in HNO_3 and therefore, any Ba existing as barite is not represented by this correlation.

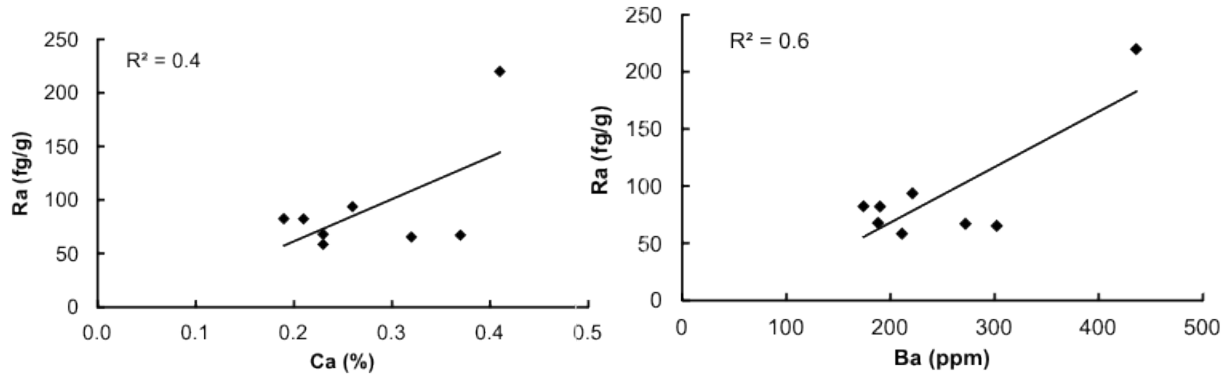

Figure 103: XY plots of alkali earth metals Ba (ppm) and Ca (%) compared to Ra (fg/g).

Figure 104 and 105 illustrate that Ca/Ba, K/Ca, and K/Ba have strong Pearson correlations. This indicates that Ca, Ba, and K have similar proportional abundances in soil samples, and that Ca-, Ba- and K-bearing minerals (calcite, and illite respectively) within B-horizon soils occur in the same abundances throughout the 9 soils analysed. The most abundant

element is K, which coincides with the common occurrence of illite as an alteration mineral throughout the Athabasca Basin.

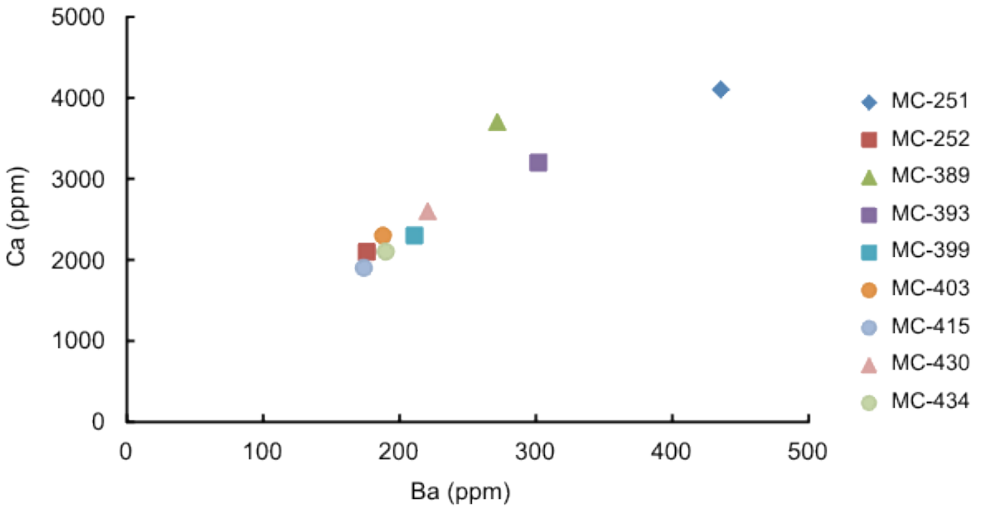

Figure 104: XY plot showing the correlation between total Ca (ppm) and Ba (ppm) within soils at McArthur River, $R^2 = 0.85$.

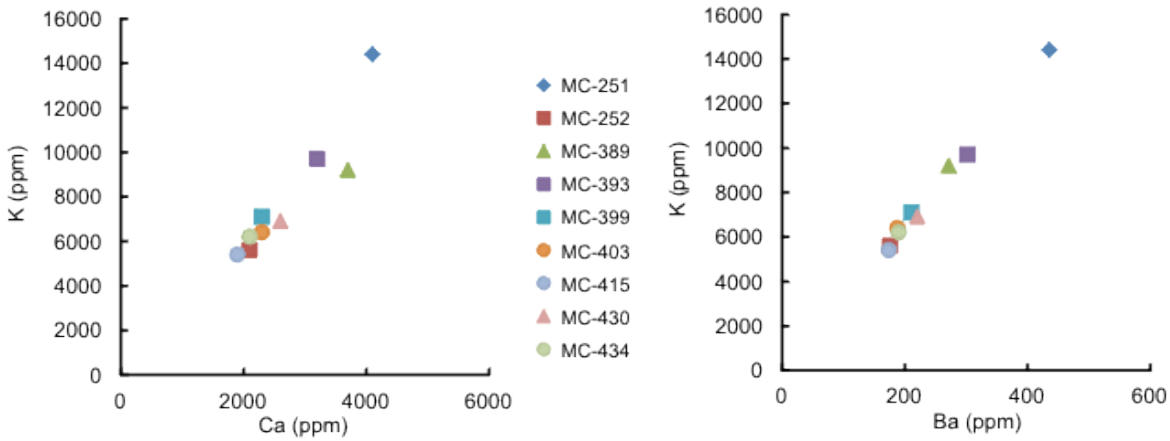

Figure 105: XY plot of calcium and barium against potassium concentration (ppm) after a multi acid leach of B-horizon soils from McArthur River. Pearson correlations: $R^2 = 0.99$ for K/Ba and $R^2=0.87$ for K/Ca.

The complete sequential leach of fracture material dissolved 0.98 – 33 ppm U (Avg = 8.0 ppm, n= 14). Ra concentration on fractures determiend by γ-ray spectrometry ranges from 0.789 – 32.2 x 101 pg/g (Avg = 6.58 x 10^3, n=14). The amount of Ra and U on core fracture material does not correlate, suggesting that Ra is not locally supported by U on fractures. A likely

explanation for this is the different redox behaviors of Ra and U which do not behave similarily in aqueous environments. U occurs in its reduced +4 state in rock-forming minerals, and is insoluble in that state. However, U readily oxidizes to its +6 state, whereby it becomes more soluble and typically forms carbonate, phosphate and chloride complexes in natural waters (Herczeg et al., 1988). Ra always exists in the +2 state, and its mobility is more likely a result of the presence of other elements that it can easily adsorb to (Mn-oxides) than its own chemical affinity (Heczeg et al., 1988). Mn is commonly used to extract Ra from seawater, and due to the immobility of Mn in oxygenated environments it is not easily weathered from rocks into the hydrosphere (Herczeg et al., 1988). Therefore, a potential cause for increased Ra on core fractures may be the existence of Mn-oxides/hydroxides along fracture surfaces that Ra from groundwater adsorbs onto. Both Fe and Mn-oxides are known for scavenging metal ions out of solution (Chao and Theobald, 1976). Fe most often occurs as ferrihydrite, hematite and goethite under low temperature conditions, and is typically more abundant than Mn-oxy-hydroxides. However, we do not see a correlation between Ra and Fe on fracture surfaces at McArthur River. Valentino et al. (2016) identified 7 common fracture types from 76 fractures from MFd to MFa at McArthur River. Mineral phases identified by optical microscopy, SEM, XRD and SWIR include hematite, goethite, magnetite, Mn-oxides, dravite, kaolin, illite and quartz (Valentino et al., 2016). This confirms the mineralogy deduced from sequential leach experiments and XRD of this study that identified Fe-Mn oxides, dravitic tourmaline, kaolin, illite and quartz as the mineral phases on fracture surfaces.

Ra was also compared to metals (Fe, Th, Mn, U) and U pathfinder elements (Pb, Cu, Ni, As) (Rose and Wright, 1980) dissolved by the sequential leach in order to determine if it is associated with other elements within the core fracture material (Figures 106-107). Pb, Ni, Cu,

Fe, As, and Th do not correlate to Ra concentration (R^2<0.1), and Ra and Mn have a moderate positive correlation (R^2 = 0.7). The moderate correlation of Ra and Mn is likely due to radium's ability to be adsorbed with Mn-oxyhydroxides (Herczeg et al, 1988).

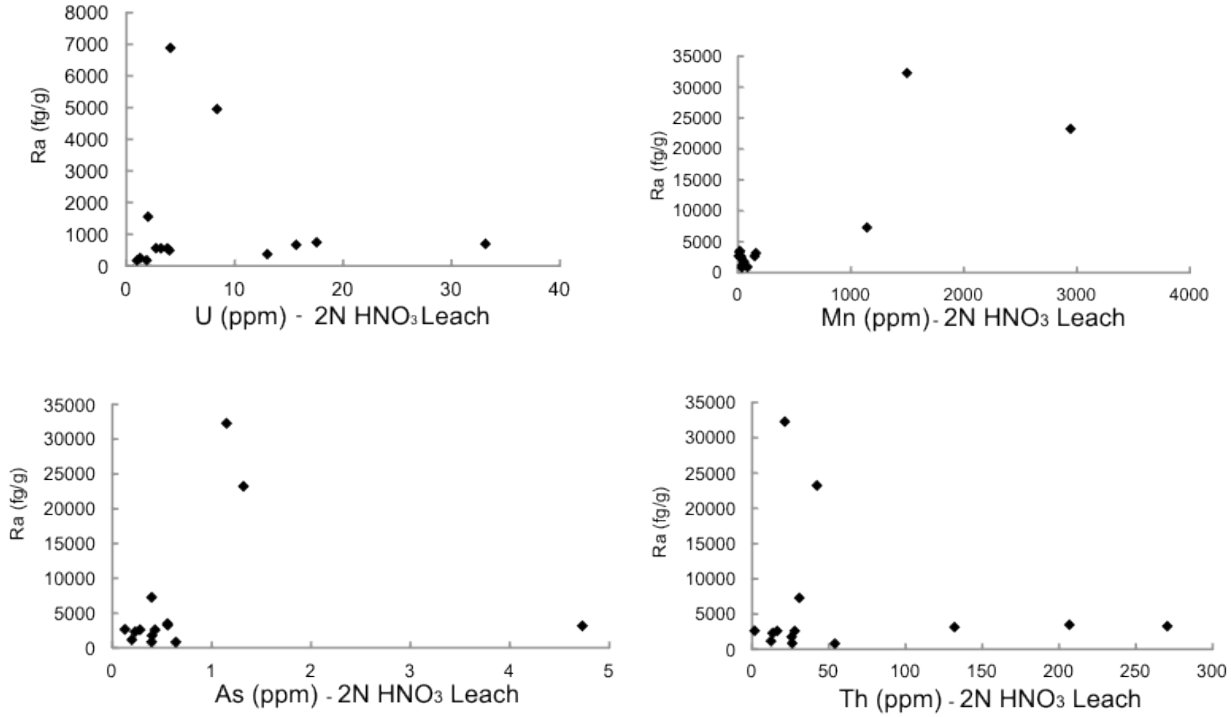

Figure 106: XY plot of radium concentration (fg/g) compared to trace element partial concentrations (ppm) after the sequential leach.

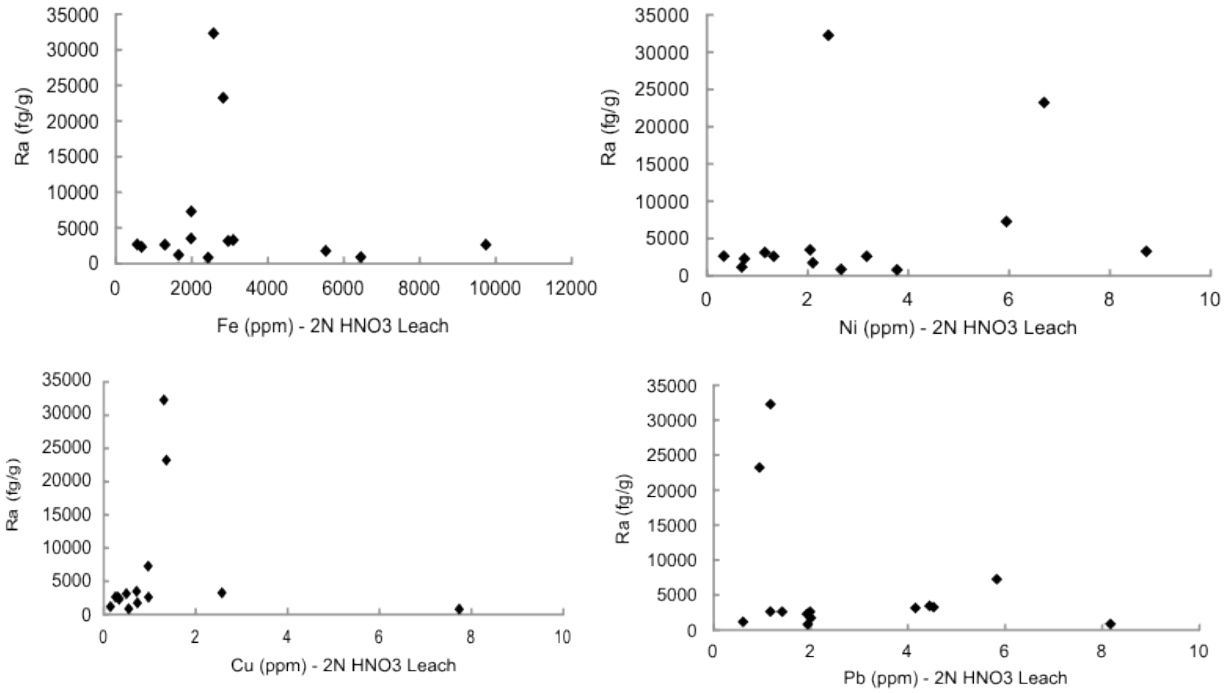

Figure 107: XY plot of radium concentration (fg/g) compared to trace element partial concentrations (ppm) after the sequential leach.

5.5 Conclusions

Groundwater above the McArthur River deposit is <20 years old, based on its ^{3}H content compared to ^{3}H in precipitation in northern Canada in 2014 (IAEA GNIP). The groundwater chemistry is typical of groundwater in the Athabasca Basin (Cramer and Nesbitt, 1994), and is meteoric based on its stable isotope compositions (O, H) compared to that of Saskatoon precipitation. Dissolved C isotope ratios and concentrations indicate mostly inorganic C and negative $\delta^{13}C$ values that are typical of soil CO_2.

Rn content varies greatly throughout the groundwater at McArthur River, which is likely caused by the varying Ra concentrations within the soil and on shallow sandstone fractures. No direct link was seen between groundwater Rn radioactivity and Ra along fractures due to

sampling limitations, however given the higher Ra concentration of the fracture surfaces than the soil, fractures are a more likely source for Rn in groundwater. Furthermore, dissolved U in groundwater is not the cause for elevated Rn in groundwater, and U content in soil and fractures does not correlate to Ra. Therefore, Rn in groundwater better reflects the Ra content than the U content of near-by solid materials such as soil and open fractures.

Additionally, drill-holes with high Rn were either heavily faulted/fractured or had anomalous (>2.5 ppm) U within nearby sandstones (<200 m away). This suggests that Ra decaying from U in sandstones travels away from its source throughout the groundwater, and adsorbing onto fracture surfaces. When comparing Ra concentration of fracture materials with sequentially leached elements from fracture materials, the only correlation was Mn, suggesting that Ra is likely absorbed to Mn-oxy-hydroxides, and less-so replacing Ba and Ca.

CHAPTER 6: Recommendations for future work

The sample set for this research was restricted by drill-hole location and accessibility; however, it provides the most recent look into the hydro-geochemistry of shallow groundwater, and the geochemistry and radiochemistry of soil and core fracture coatings within the eastern Athabasca Basin. Earlier studies of this kind, in this area, include (Earle and Drever (1983), Campbell (1995), Coker and Dunn (1983), Dyck and Tan, (1978), Cramer and Nesbitt (1994), and Simpson and Sopuck (1983), and more recently, Power (2014), Power et al. (2012), Hattori et al. (2014), Krahenbil (2014), Krahenbil et al. (2014) and Dudek and Hattori (2015). This study compares the data and methodologies from these studies to the surficial geochemistry at Millennium and McArthur River in 2013 and 2014.

This study experimented with different water collection methods and analyses of Rn in water. For precise and accurate collection of groundwater from DDH for use in any analysis, the Solinst point source bailer is recommended over the Waterra Inertial Pump method. It allows for incremental measurements without disturbing the sediments and drilling residue along the side of the drill-hole walls, and its incremented tug-line is much more precise for measuring specific depths. With the Waterra Inertial Pump, a pumping action is required and therefore water is collected from an approximate depth as the Nalgene tubing rises up and down within the DDH to create the flow of water. However, if large volumes of water are required (>1 L) the Waterra pump is much more efficient and greatly reduces sampling time. Additionally, the most accurate method for DDH water collection at specific depths is the packer method (Earle and Drever, 1983) however this method requires extensive time and resources which were beyond the scale of this research project.

The two Rn extraction and analytical procedures discussed in Chapter 3 each have their benefits. The author recommends the Rn-in-water method described by Lefebvre et al. (2013) when sampling close to the laboratory where the liquid scintillation counting will occur, and transportation and/or time before counting are minimal. Lefebvre's method allows for simple water collection without any additional steps or scintillation oil in the field, because the extraction process is completed in the laboratory. However, the field extraction method described by Leaney and Herczeg (2006) is much more robust and convenient when travelling by all-terrain vehicle, plane, and when samples are shipped to a laboratory from a remote location. The volume of sample is reduced by roughly 10-times with the Leaney and Herczeg (2006) method because Rn is extracted from 350 ml of water into 30 ml of scintillation oil immediately after collection. Additionally, plastic scintillation vials were compared to glass vials and they were equally impermeable for Rn; this reduces the risk of breakage during transit, and enables the samples to be counted immediately after they arrive at the laboratory.

To elaborate on the work completed in this thesis, it would be worthwhile to complete analyses of additional major ions dissolved in groundwater (Mg, Ca, Ba, Fe, Na, K, Mn) in order to better correlate the till and fracture geochemistry to the groundwater chemistry. Additionally, it would be useful to determine the Rn radioactivity, chemistry, isotope composition, and ^{3}H content of deeper groundwater at the same depths as fractures analysed for Ra to assess their relationships. As well, a more in-depth mineralogical study of fracture coatings by SEM would be beneficial to further evaluate hosts for Ra adsorption and co-precipitation such as Mn-Fe-oxy-hydroxides, clays, carbonate, and barite. Lastly, it would be beneficial to determine more precise hydrogeology of the groundwater system in order to better trace the movement of elements throughout the groundwater, bedrock and soil.

REFERENCES

ADLAKHA, E.E. AND HATTORI, K., 2015. Compositional variation and timing of aluminum phosphate-sulfate minerals in the basement rocks along the P2 fault and in association with the McArthur River uranium deposit, Athabasca Basin, Saskatchewan, Canada. *American Mineralogist*, **100(7)**,1386-1399.

AMES, L. L., MCGARRAH, J. E., WALKER, B. A., AND SALTER, P. F., 1983. Uranium and radium sorption on amorphous ferric oxyhydroxide. *Chemical Geology*, **40(1)**, 135-148.

ANNESLEY, I.R., MADORE, C. AND PORTELLA, P., 2005. Geology and thermotectonic evolution of the western margin of the Trans-Hudson Orogen: evidence from the eastern sub-Athabasca basement, Saskatchewan. *Canadian Journal of Earth Sciences,* **42.4**, 573-597.

BALL, T.K., CAMERON, D.G., COLMAN T.B. AND ROBERTS P. D., 1991. Behaviour of radon in the geological environment: a review. British Geological Survey, Keyworth, Nottingham. *Quarterly Journal of Engineering Geology*, **24**, 169-182.

BEATTIE, D., BASHIR, R. AND HATLEY, J., 2008. Impact of Geotechnical and Hydrogeological Parameters upon Shaft Sinking Performance in the Athabasca Basin Canada. Proceedings: IMWA 2008.

BISSET, A., 2003. Detecting unconformity related alteration using Tempest - an example from Arnhem Land, Australia; in *Uranium Geochemistry, International Conference, April 13-16, 2003, Proceedings*, Edited by M. Cuney, 75-78.

BONHAM-CARTER, G. AND HALL, G., 2010. Exploration Division Project 08E01: Phase III, Unpublished Final Report on Results of Soil Geochemistry Using Selective Leaches. Canadian Mining Industry Research Organization (CAMIRO).

BROWN, R.M., 1970. Distribution of hydrogen isotopes in Canadian waters. In *Isotope Hydrology 1970. Proceedings of a sympo*sium, International Atomic Energy Association, Vienna, 3-21.

Bureau Veritas Mineral Laboratories. Soil, Till and Sediment Analytical Services., 2014. World Wide Web Address: acmelab.com/services/method-descriptions/soil-till-and-sediment.

Cameco Corporation., 2014. World Wide Web Address: www.cameco.com/businesses/uranium-operations.

CAMERON, E.M., BECKZ, L.S. AND DARNLEYL, A.G., 1983. Introduction in *Uranium Exploration in Athabasca Basin Saskatchewan, Canada*, *Edited by EM Cameron, Geological Survey of Canada,* **82-11,** vii-x**.**

CAMERON, E. M., 1977. Geochemical dispersion in lake waters and sediments from massive sulphide mineralization, Agricola Lake, Northwest Territories. *Journal of Geochemical Exploration,* **7**, 327-348.

CAMERON, E. M., 1978. Hydrogeochemical methods for base metal exploration in the northern Canadian Shield. Jo*urnal of Geochemical Exploration,* **10**, 219-243.

CAMERON, E. M., LEYBOURNE, M. I. & KELLEY, D. L. 2002. Exploring for deeply covered mineral deposits: Formation of geochemical anomalies in northern Chile by earthquake-induced surface flooding of mineralized groundwaters. *Geology*, **30**, 1007–1010.

CAMERON, E. M., HAMILTON, S. M., LEYBOURNE, M. I., HALL, G. E., AND MCCLENAGHAN, M. B., 2004. Finding deeply buried deposits using geochemistry. *Geochemistry: Exploration, Environment, Analysis*, **4(1)**, 7-32.

CAMPBELL, J.E., 1995. The surficial geology of the Virgin Lake project area, Saskatchewan and recommendations for future work; in *Saskatchewan Industry and Resources Mineral Assessment*, **74G14-0012**, 9.

CAMPBELL, J.E., 2007. Quaternary geology of the eastern Athabasca Basin, Saskatchewan. *Bulletin-Geological Survey of Canada*, **588**, 211.

CHAO, T.T. AND THEOBALD, P.K., 1976. The significance of secondary iron and manganese oxides in geochemical exploration. *Economic Geology*, **71(8)**, 1560-1569.

CHEN, S., HATTORI, K. AND GRUNSKY, E.C., 2016. Multivariate statistical analysis of the REE-mineralization of the Maw Zone, Athabasca Basin, Canada. *Journal of Geochemical Exploration*, **161**, 98-111.

CLARK, A.M., 1984. Mineralogy of the rare earth elements. *Rare Earth Element Geochemistry*, **2**, 33-61.

CLARKE, W.B., TOP, Z. AND EISMONT, W.C., 1983. Helium isotope and tritium content of lakes, and uranium exploration in the NEA/IAEA Athabasca Test Area, in *Uranium Exploration in Athabasca Basin Saskatchewan, Canada*, *Edited by EM Cameron, Geological Survey of Canada,* **82-11**, 139-146.

COKER, W.B. AND DUNN, C.E., 1983. Lake water and lake sediment geochemistry, NEA/IAEA Athabasca Test Area; in *Uranium Exploration in Athabasca Basin, Saskatchewan, Canada, Edited by EM Cameron, Geological Survey of Canada*, **82-11**, 117-125.

CONDIE, K.C., 1993. Chemical composition and evolution of the upper continental crust: contrasting results from surface samples and shales. *Chemical Geology,* **104**, 1-37.

CRAIG, H., 1961. Isotopic Variations in Meteoric Waters. *Science New Series*, **133**, 1702-1703.

CRAMER, J.J. AND NESBITT, H.W., 1994. Groundwater evolution and redox geochemistry. *Final Report of the AECL/SKB Cigar Lake Analog Study*, 191-207.

DUDEK, N. AND HATTORI, K., 2015. Radon and helium distribution and concentrations above buried uranium ore: The Phoenix deposits, Saskatchewan; Geological Survey of Canada, Scientific Presentation 33, 1 poster. doi:10.4095/2965155/296515

DUNN, C. E., 1983.Uranium biogeochemistry of the NEA/IAEA Athabasca test area in *Uranium Exploration in Athabasca Basin, Saskatchewan, Canada, Edited by EM Cameron. Geological Survey of Canada,* **82-11**, 127-132.

DYCK, W., 1969. *Radon determination apparatus for geochemical prospecting for uranium* in *Uranium Exploration in Athabasca Basin, Saskatchewan, Canada, Edited by EM Cameron. Geological Survey of Canada*, **68-21**, 13.

DYCK, W. AND MCCORKELL, R.H., 1983. A study of uranium-rich reduction spheroids in sandstones from Pugwash Harbour, Nova Scotia. *Canadian Journal of Earth Sciences*, **20(11)**, 1738-1746.

DYCK, W. AND TAN, B., 1978. Seasonal variations of helium, radon, and uranium in lake waters near the Key Lake uranium deposit, Saskatchewan. *Journal of Geochemical Exploration*, **10**, 153–167.

EARLE, S. A. M. AND DREVER, G. L., 1983. Hydrogeochemical exploration for uranium within the Athabasca Basin, northern Saskatchewan. *Journal of Geochemical Exploration*, **19**, 57–73.

EARLE, S., MCGILL, B. AND MURPHY, J., 1989. Glacial boulder lithogeochemistry: an effective new uranium exploration technique in the Athabasca Basin, Saskatchewan. *Saskatchewan Geological Society Special Publication Number 10: modern exploration techniques,* Proceedings of a Symposium Held in Regina, Saskatchewan *20 - 21* November, 1989. Uranium Exploration, 94-114.

EARLE, S.A.M. AND SOPUCK, V.J., 1989. Regional lithogeochemistry of the eastern part of the Athabasca Basin uranium province, Saskatchewan, Canada. In *Uranium Resources and Geology of North America Proceedings of a Technical Committee Meeting Organized by the International Atomic Energy Agency* and held in Saskatoon, Canada, 1-3 September 1987.

ENVIRONMENTAL CANADA, 2016. World Wide Web Address: http://climate.weather.gc.ca/climate_normals/results_1981_2010_e.html?searchType=stnProv&lstProvince=SK&txtCentralLatMin=0&txtCentralLatSec=0&txtCentralLongMin=0&txtCentralLongSec=0&stnID=3377&dispBack=0

FAURE, G., 1998. *Principles and applications of geochemistry: a comprehensive textbook for geology students, second edition*. Prentice Hall, NJ, 315-316.

KYSER, T.K. AND FAYEK, M., 1997. Characterization of multiple fluid-flow events and rare-earth-element mobility associated with formation of unconformity-type uranium deposits in the Athabasca Basin. Saskatchewan. Canadian Mineralogist, **35**, 627-658.

FLEET, A. J., 1984. Aqueous and sedimentary geochemistry of the rare earth elements. *Rare earth element geochemistry*, **2**, 343-369.

FRAPE, S.K., FRITZ, P. AND MCNUTT, R.H., 1984. Water-rock interaction and chemistry of groundwaters from the Candian Shield. *Geochemica et Cosmochimica Acta*, **48**, 1617-1627.

FREEZE, R.A. AND CHERRY, J.A., 1979. Groundwater, Englewood Cliffs, N.J., Prentice Hall, 604.

GASCOYNE, M., WUSCHKE, D.M. AND DURRANCE, E.M., 1993. Fracture detection and groundwater flow characterization using He and Rn in soil gases, Manitoba, Canada. *Applied geochemistry*, ***8*(3)**, 223-233.

GOULDEN, W.D., HENDRY, M.J., CLIFTON, A.W. AND BARBOUR, S.L., 1998. Characterization of radium-226 in uranium mill tailings. In *Tailings and mine waste*, **98**, 561-570.

Government of Canada Agriculture and Agri-Food Canada, Chapter 2: Soil, Pedon, Control Section and Soil Horizons, World Wide Web Address: http://sis.agr.gc.ca/cansis/taxa/cssc3/chpt02_a.html#mineralhorizons

Government of Canada, Agriculture and Agri-food Canada, Soils of Canada. World Wide Web Address: www.agr.gc.ca/atlas/agpv?webmap=c225cc78d5b142d58eacefae91cc535b.

GAY, P. AND ROY, N.N., 1968. The mineralogy of the potassium-barium feldspar series III: Subsolidus relationships. *Mineralogical Magazine*, **36**, 914-932.

HAMILTON, S.M., HATTORI, K.H., CLARK, I.D., 2005. Investigation into the source of forest-ring-related natural gas in northern Ontario; Ontario Geological Survey Open File Report **6172**, 19-1–19-4.

HATTORI, K., POWER, M.J., KRAHENBIL, A., SORBA, C., KOTZER, T. AND POTTER, E.G., 2014. Surficial geochemical surveys over concealed uranium ore of the Phoenix and Millennium deposits in the Athabasca Basin, Saskatchewan. *Geological Survey of Canada Open File Report,* **7791**, 32- 42.

HEM, J.D., 1985. Study and interpretation of the chemical characteristics of natural water. *Department of the Interior, US Geological Survey*, **2254.**

HERCZEG, A.L., SIMPSON, H.J., ANDERSON, R.F., TRIER, R.M., MATHIEU, G.G. AND DECK, B.L., 1988. Uranium and radium mobility in groundwaters and brines within the Delaware Basin, southeastern New Mexico, USA. *Chemical Geology: Isotope Geoscience section*, **72**(2), 181-196.

HOFFMAN, S. J., 1983. Geochemical exploration for unconformity-type uranium deposits in permafrost terrain, Hornby Bay Basin, Northwest Territories, Canada. In: G.R. Parslow (Editor), Geochemical Exploration, 1982. *Journal of Geochemical Exploration*, **19**, 11–32.

INTERNATIONAL ATOMIC ENERGY ASSOCIATION, 1989. *Uranium Resources and Geology of North America*, Technical Document No. 500, IAEA, Vienna.

International Atomic Energy Association Global Network of Isotopes in Precipitation (IAEA GNIP), World Wide Web Address: www-naweb.iaea.org/napc/ih/IHS_resources_gnip.html

JEFFERSON, C.W., THOMAS, D.J., GANDHI, S.S., RAMAEKERS, P., DELANEY, G., BRISBIN, D., CUTTS, C., QUIRT, D., PORTELLA, P., AND OLSON, R.A., 2007. Unconformity associated uranium deposits of the Athabasca Basin, Saskatchewan and Alberta, in Goodfellow, W.D., ed., Mineral Deposits of Canada: A Synthesis of Major Deposit-Types, District Metallogeny, the Evolution of Geological Provinces, and Exploration Methods: *Geological Association of Canada, Mineral Deposits Division, Special Publication,* **5**, 273-305.

JOHNSON., 2007. Ecological Framework of Canada, Ecoregions of Canada, Athabasca Plain. World Wide Web Address: http://ecozones.ca/english/region/87.html.

JONES, M.J., BUTCHINS, L.J., CHARNOCK, J.M., PATTRICK, R.A., SMALL, J.S., VAUGHAN, D.J., WINCOTT, P.L. AND LIVENS, F.R., 2011. Reactions of radium and barium with the surfaces of carbonate minerals. *Applied geochemistry*, ***26*(7)**, 1231-1238.

JUHOJUNTTI, N., WOOD, G., JUHLIN, C., O'DOWD, C., DUECK, P. AND COSMA, C., 2012. 3D seismic survey at the Millennium uranium deposit, Saskatchewan, Canada: Mapping Depth to Basement and Imaging Post-Athabasca Structure Near the Orebody. *Geophysics*, **77(5)**. WC245-WC258.

KISH H.J., 1983. Mineralogy and petrology of burial diagenesis (Burial Metamorphism) and incipient metamorphism in clastic rocks. In *Developments in Sedimentology #25B: Diagenesis in Sediments and Sedimentary Rocks*, Elsevier, Amsterdam, **2**, 189-493.

KRAHENBIL, A., HATTORI, K., POWER, M. AND KOTZER, T., 2014. Surficial Geochemistry associated with the deeply buried Millennium and Phoenix Uranium Deposits, Athabasca Basin, Northern Saskatchewan. Geological Survey of Canada, Open File 7611, 1, Poster originally presented at the *Prospectors and Developers Association*

of Canada, Society of Economic Geologists Student Minerals Colloquium, Toronto, Ontario.

LANGMUIR, D. AND MELCHIOR, D., 1985. The geochemistry of Ca, Sr, Ba and Ra sulfates in some deep brines from the Palo Duro Basin, Texas. *Geochimica et Cosmochimica Acta*, **49(11)**, 2423-2432.

LEANEY, F. W. AND HERCZEG, A.L., 2006. A rapid field extraction method for determination of radon-222 in natural waters by liquid scintillation counting. *Limnology and Oceanography: Methods,* **4.7,** 254-259.

LEFEBVRE, K., BARBECOT, F., GHALEB, B., LAROCQUE, M. AND GAGNÉ, S., 2013. Full range determination of 222 Rn at the watershed scale by liquid scintillation counting. *Applied Radiation and Isotopes*, ***75***, 71-76.

LEWRY, J.F. AND SIBBALD, T., 1980. Thermotectonic evolution of the Churchill province in northern Saskatchewan; Tectonophysics, **68**, 45–82.

LEYBOURNE, M., 2007. Aqueous geochemistry in mineral exploration. *Mineral Resources of Canada: A Synthesis of Major Deposit-types, District Metallogeny, the Evolution of Geological Provinces, and Exploration Methods*, 1007-1034.

LEYBOURNE, M. I., AND E. M. CAMERON., 2007. Groundwaters in geochemical exploration: methods, applications, and future directions in *Proceedings of Exploration 07: Fifth Decennial International Conference on Mineral Exploration*, Edited by B. Milkereit, Prospectors and Developers Association of Canada, Toronto, Ontario, 201-221.

LEYBOURNE, M. I., AND W. D. GOODFELLOW., 2003. Processes of metal solution and transport in ground waters interacting with undisturbed massive sulfide deposits, Bathurst Mining Camp, New Brunswick. Massive Sulfide Deposits of the Bathurst Mining Camp, New Brunswick, and Northern Maine. *Economic Geology Monograph,* **11**, 723-739.

MACDONALD, C. C., 1980. Mineralogy and geochemistry of a Precambrian regolith in the Athabasca Basin. *M. Sc. Thesis, University of Saskatchewan, Saskatoon*, 151.

MARLATT, J., MCGILL, B., MATTHEWS, R., SOPUCK, V. AND POLLOCK G., 1992. The discovery of the McArthur River Uranium deposit, Saskarchewan, Canada. *In* The Geological Society of CIM; first annual field conference, Edited by I.A. Homeniuke, 18-127.

MCGILL, B.D., MARLATT, J.L., MATTHEWS, R.B., SOPUCK, V.J., HOMENIUK, L.A. AND HUBREGTSE, J.J., 1993. The P2 North uranium deposit, Saskatchewan, Canada. *Exploration and Mining geology*, ***2***, 321-331.

MILLER W. R., FICKLIN W. H., AND LEARNED R. E., 1982. Hydrogeochemical prospecting for porphyry copper deposits in the tropical-marine climate of Puerto Rico. *Journal of Geochemical Exploration,* **16**, 217-233.

MOORE, W. S., 1984. Mechanism of transport of U-Th series radioisotopes from solids into groundwater. *Geochimica et Cosmochimica Acta,* **48.2**, 395-399.

MURPHY, S.E., 2009. Characterization of a TCE-contaminated aquifer using tritium-helium dating and geochemical tracers, Valcartier, Quebec, Canada. *PhD Thesis University of Ottawa*, 33-38.

Ottawa Hydro, 2014. https://hydroottawa.com/about/our-company/our-reports

PALMER, S.M., HOPE, D., BILLETT, M.F., DAWSON, J.J. AND BRYANT, C.L., 2001. Sources of organic and inorganic carbon in a headwater stream: evidence from carbon isotope studies. *Biogeochemistry*, ***52*(3)**, 321-338.

PLASTINO, W., CHEREJI, I., CUNA, S., KAIHOLA, L., DE FELICE, P., LUPSA, N., BALAS, G., MIREL, V., BERDEA, P. AND BACIU, C., 2007. Tritium in water electrolytic enrichment and liquid scintillation counting. *Radiation measurements*, ***42*(1)**, 68-73.

POWER, M.J., 2014. Geochemical Surface Expression of the Phoenix and Millennium Uranium Deposits, Athabasca Basin, Saskatchewan. *M.Sc. Thesis, University of Ottawa*, 78-114.

POWER, M.J., HATTORI, K., SORBA, C., POTTER, E., 2012. Geochemical anomalies in the soil and uppermost sandstones overlying the Phoenix uranium deposit, Athabasca Basin, Saskatchewan, Canada. Geological Survey of Canada Open File Report **7257,** 36 doi:10.4095/291981

QUIRT, D. H., 1985. Lithogeochemistry of the Athabasca Group: Summary of sandstone data, in *Summary of Investigations 1985 Saskatchewan Geological Survey, Saskatchewan Energy and Mines, Miscellaneous Report*, **85(4)**, 123-132.

Radonex, 2013. *Patterson Lake South Project*. World Wide Web Address: http://radonex.com/pls/

RAMAEKERS, P., 1981. Hudsonian and Helikian basins of the Athabasca region, northern Saskatchewan. *Proterozoic basins of Canada. Edited by FHA Campbell. Geological Survey of Canada, Paper*, 81-10.

RAMAEKERS, P., JEFFERSON, C.W., YEO, G.M., COLLIER, B., LONG, D.G.F., DREVER, G., MCHARDY, S., JIRICKA, D., CUTTS, C. AND WHEATLEY, K., 2007. Revised geological map and stratigraphy of the Athabasca Group, Saskatchewan and Alberta. *Bulletin-Geological Survey of Canada*, **588**,155.

ROBERTSON, R., 2006b. Millennium: Cameco's newest uranium discovery: The Northern Miner, **91**, 1-14

ROLLINSON, H.R., 1993. Using Geochemical Data: Evaluation, Presentation, Interpretation. Pearson Education Limited, Harlow, England, 133-141.

ROSE, A. W. AND WRIGHT, R. J., 1980. Geochemical exploration models for sedimentary uranium deposits. *Journal of Geochemical Exploration*, **13.2**, 153-179.

SADER, J. A., HATTORI, K. H., KONG, J. M., HAMILTON, S. M. & BRAUNEDER, K. 2011.Geochemical responses in peat groundwater over Attawapiskat kimberlites, James Bay Lowlands, Canada and their application to diamond exploration. *Geochemistry: Exploration, Environment, Analysis*, **11**, 193-210.

SAJIH, M., BRYAN, N.D., LIVENS, F.R., VAUGHAN, D.J., DESCOSTES, M., PHROMMAVANH, V., NOS, J. AND MORRIS, K., 2014. Adsorption of radium and barium on goethite and ferrihydrite: A kinetic and surface complexation modelling study. *Geochimica et Cosmochimica Acta*, **146**,150-163.

SANDERS, L.L., 1998. A Manual of Field Hydrogeology: Prentice-Hall, NJ, 381.

SANFORD, W.E., SHROPSHIRE, R.G. AND SOLOMON, D.K., 1996. Dissolved gas tracers in groundwater: Simplified injection, sampling, and analysis. *Water Resources Research*, **32(6)**,1635-1642.

SCHREINER, B. T., 1983. Quaternary geology of the NEA/IAE test area. In *Uranium exploration in Athabasca Basin, Saskatchewan, Canada*, *Edited by EM Cameron, Geological Survey of Canada*, **82-11**, 27-32.

SCOTT, A.G., 1983. Radon daughter deposition velocities estimated from field measurements. *Health physics*, **45(2)**, 481-485.

SECOY, D., 2007. The Encyclopedia of Saskatchewan, Ecozones and Ecoregions. World Wide Web Address: http://esask.uregina.ca/entry/ecozones_and_ecoregions.html

SHAW, D.M., CRAMER, J.J., HIGGINS, M.D., AND TRUSCOTT, M.G., 1986. Composition of the Canadian Precambrian shield and the continental crust of the earth. In: Dawson JB, Carswell DA, Hall J, Wedepohl KH *The nature of the lower continental crust, Geological Society Special Publication,* **24**, 275–282.

SHELDON, A. L., SOLOMON, D. K., POREDA, R. J. AND HUNT, A., 2003. Radiogenic helium in shallow groundwater within a clay till, southwestern Ontario. *Water Resources Research*, **39**,1331.

SIBBALD, T.I.I., QUIRT, D.H. AND GRACIE, A.J., 1990. Uranium deposits of the Athabasca Basin, Saskatchewan Geological Survey, Open File, 2166, 56.

SIBBALD, T.I.I., 1983. Geology of the crystalline basement, NEA/IAEA Athabasca test area. *Uranium exploration in Athabasca Basin, Saskatchewan, Canada. Edited by EM Cameron. Geological Survey of Canada,* **82-11**, 1-14.

SIMPSON, M. A., AND SOPUCK, V. J., 1983. Till geochemistry near the Midwest uranium deposit. In *Uranium Exploration in Athabasca Basin, Saskatchewan, Canada, Edited by EM Cameron. Geological Survey of Canada,* **82-11**, 207-214.

SMEE, B. W. 1998. A new theory to explain the formation of soil geochemical responses

over deeply covered gold mineralization in arid environments. *Journal of Geochemical Exploration*, **61**, 149–172.

SUN, H. AND SEMKOW, T. M., 1998. Mobilization of thorium, radium and radon radionuclides in ground water by successive alpha-recoils. *Journal of Hydrology,* **205.1**, 126-136.

TREMBLAY, L. P., 1983. Some chemical aspects of the regolithic and hydrothermal alterations associated with the uranium mineralization in the Athabasca Basin, Saskatchewan. Geological Survey of Canada, **83-1A**, 1-14.

TUNCER, V., UNSWORTH, M.J., SIRIPUNVARAPORN, W. AND CRAVEN, J.A., 2006. Audio-magnetotelluric exploration for unconformity uranium deposits in the Athabasca Basin, Saskatachewan, Canada. In *Extended Abstract, SEG/New Orleans 2006 Annual Meeting*.

VALENTINO, M., KYSER, K., LEYBOURNE, M., KOTZER, T. AND QUIRT, D., 2016. Analysis of Fractures in Sandstone of the Athabasca Basin as Records of Primary and Secondary Dispersion. Poster originally presented at the *Prospectors and Developers Association of Canada, Society of Economic Geologists Student Minerals Colloquium*, Toronto, Ontario.

WOOD, G., O'DOWD, C., COSMA, C. AND ENESCU, N., 2012. An interpretation of surface and borehole seismic surveys for mine planning at the Millennium uranium deposit, northern Saskatchewan, Canada. *Geophysics*, **77(5)**, WC203-WC212.

WOOD, W.W., KRAEMER, T.F. AND SHAPIRO, A., 2004. Radon (^{222}Rn) in ground water of fractured rocks: A diffusion/ion exchange model. *Groundwater,* **42.4**, 552-567.

World Nuclear Association, 2015. Nuclear Power in Canada. World Wide Web Address: www.world-nuclear.org/info/Country-Profiles/Countries-A-F/Canada--Nuclear-Power.

YEO, G. M., AND DELANEY, G., 2007. EXTECH IV: Geology and Uranium Exploration TECH-nology of the Proterozoic Athabasca Basin, Saskatchewan and Alberta, 89-117.